INSTRUMENT DEVELOPMENT FOR THE ANALYSIS OF LOW ABUNDANCE ANALYTES IN SINGLE CELLS AND SMALL VOLUME SAMPLES

BY

CHRISTINE CECALA

DISSERTATION

Submitted in partial fulfillment of the requirements
for the degree of Doctor of Philosophy in Chemistry
in the Graduate College of the
University of Illinois at Urbana-Champaign, 2011

Urbana, Illinois

Doctoral Committee:

Professor Jonathan V. Sweedler, Chair
Professor Robert B. Gennis
Professor Chad M. Rienstra
Professor Alexander Scheeline

Abstract

Understanding the cell-to-cell differences between cells is important for both fundamental biology and in identifying normal and pathological functioning. Biogenic amines, which include catecholamines and indolamines, are of particular interest due to their presence throughout the central and peripheral nervous systems in many species, as well as their association with a wide variety of higher order behaviors such as sleep, memory formation, feeding, and mood; however, they are low abundance analytes since they are present in localized regions of the nervous system in femtomole to attomole quantities. Also, when sampling from the nervous system, the amines are often present within a complex matrix of proteins, salts, lipids, and other common biological compounds, which can complicate the detection and identification of trace levels of amines. This combination prompts the use of technologies that enable single cell measurements. Single cell measurements also provide insight into cell-specific metabolism, as different cell types are both quantitatively and qualitatively unique. Cell-specific metabolism distinguishes a cell that is morphologically similar to its neighbors but has a different molecular complement, which may result in a different function or indicate a difference in cell status. Differences in metabolism could also indicate potentially pathological behavior. The goal has been the design, construction, and validation of analytical instruments to enable single cell characterization.

The high sensitivity and low sample consumption of capillary electrophoresis (CE) combined with the selectivity and sensitivity of laser-induced native fluorescence detection (LINF) makes CE-LINF well suited to study single cells and even subcellular organelles; however, the isolation and loading of such small samples into the CE system is challenging. This issue is addressed by designing, constructing, and interfacing a single beam optical trap with a laboratory-built CE system that uses multi-channel LINF detection, which has been optimized for single cell analyses. The optical trap is formed by tightly focusing the output of a Nd:YAG laser with a high numerical aperture objective. Once the cell is localized within the trap, the capillary inlet is moved adjacent to the trapped cell using a combination of a

computer-controlled micromanipulator and a microscope stage. The cell is then released from the trap and pressure injected into the capillary. Cell lysis occurs within the capillary and the cellular constituents are subsequently separated and detected. Detection takes place using multi-channel LINF, which has been optimized for selective excitation and detection of biogenic amines. Briefly, a 224 nm HeAg hollow cathode ion laser is used in combination with a sheath-flow cuvette; the fluorescence emission is collected and measured using three channel detection with each photomultiplier tube having its own wavelength range selected with the appropriate dichroic mirror. This instrument allows unambiguous identification of a variety of catecholamines and indolamines based on differences in both their fluorescence emission profiles and migration times.

This system, both as a hyphenated instrument and as individual components, has been used for several neurochemical applications, including detecting trace levels of indolamines in microdialysis samples and in single pinealocytes, the indolamine-containing cells of the pineal gland. These analyses highlight the ability of the system to isolate and manipulate single cells and perform injections and separate and detect low abundance analytes in samples with high concentrations of salts.

Design is not just what it looks like and feels like. Design is how it works. – Steve Jobs

Designs of purely arbitrary nature cannot be expected to last long. – Kenzo Tange

I mean, if you decided to go out today and get you an instrument and do whatever it is that you do, no one can tell you how you're going to do it but when you do it. – Ornette Coleman

At last a dream come true. The Instrument of Instruments. – Mick Fleetwood

Acknowledgments

There are a number of people who have helped me before and during my graduate work who deserve recognition for their contributions. My advisor, Prof. Jonathan Sweedler, has given me opportunities that I wouldn't have otherwise had. His advice, encouragement, and management style have allowed me to develop into an independent scientist, for which I am profoundly grateful. I would also like to thank the members of my committee, Prof. Robert Gennis, Prof. Chad Rientra, and Prof. Alexander Scheeline, for their insight, advice, and support.

I have collaborated over the years with several people, without whom I wouldn't have been able to perform these measurements. Dr. Stanislav Rubhakin has provided advice, encouragement, and an untold number of animal parts. His willingness to tinker and try new ideas is inspiring. I would like to thank my collaborators in the Gillette group, Jennifer Arnold, Dr. Jennifer Miller, and Prof. Martha Gillette, for their work on two of the projects covered in this dissertation. They provided samples, animals, helpful advice, and a place to perform dissections under red light. Without their assistance, Chapters 4 and 6 would not have been possible.

The Sweedler group, as a whole, has been unfailingly kind and supportive throughout my tenure in the group. Dr. Ted Lapainis and Dr. Cory Scanlan were instrumental to my success. In particular, I'd like to thank Jordan Aerts, Stephanie Baker, Chris Dailey, Dr. Michael Heien, Dr. Ann Knolhoff, Dr. Chang Young Lee, Dr. Peter Nemes, Nobutoshi Ota, Ting Shi, and Dr. Kevin Tucker for their friendship, advice, discussions, edits, and help throughout the years. The Sweedler group would have been a lonely place without them.

Julie Sides is a one-woman wonder, and has been one of the most kindhearted, helpful, and genuinely nice people that I have had the pleasure to know while I have been here. The secretaries in the IMP office have always been the most accommodating, supportive, and knowledgeable people, and I am grateful for their assistance.

The SCS Machine shop has put in countless hours of work in the pursuit of my PhD. They are an incredible resource and I appreciate all of the times that they looked at my designs and made them better. They also have provided me with a limitless number of screws, nuts, and bolts every time that I broke or lost one, without ever appearing irritated, and have always loaned me tools when disaster struck. If it wasn't for them, much of the custom work described in this dissertation could not have been made.

Bill Hug, Ray Reid, and Prashant Oswal at Photon Systems Inc. have been a great resource, and their help is always appreciated.

My friends and family have been a source of support and happiness throughout my time here, and I am grateful for their continued presence in my life. My husband has surrounded me with love and patience, for which I am thankful. I would also like to acknowledge my pets, because at the end of the day, they are always happy to see me and have never cared when I fail.

Table of contents

1 Introduction

1.1 Research motivation

Cells contain tens of thousands of compounds spread amongst numerous analyte classes with concentrations that can range across more than nine orders of magnitude. These concentrations can vary widely depending on the time of day, the animal's age, and the season, among other factors. When working with average values across a tissue sample or homogenate, much of this important information is lost. This also places a large demand on the dynamic range of the detection system, since analyte levels can range from mole to yoctomole amounts within a tissue.

In order to retain this information content single cell analysis is critical. It provides insight into cell-to-cell heterogeneity; for tissue samples with a mixture of different cell types (such as neurons and glia), performing bulk chemical analysis would only result in determining average values for the region and would be unsuitable for analysis of defined cell types. Dilution of trace analytes by constituents common to all cells can also occur, which can mask the effects of cells that appear morphologically similar but in fact have distinctly different contents and therefore a different function. Differences in metabolism could also indicate potentially pathological behavior. Performing single cell analysis bypasses these issues by reducing analyte dilution, potentially decreasing the sample complexity, and lowering the dynamic range necessary to detect the components present within the cell.

There are a variety of methods that have been used to probe single cells, such as electrophysiology and optical microscopy, and although they provide a plethora of useful information, accurate quantitation of analytes within single cells is less common. One method that has proven itself useful is for quantitating cellular contents is electrophoresis. Electrophoresis involves the application of an electric field to a background matrix containing ionized species of interest. Within the electric field, the molecules can be spatially and temporally separated based on their effective charge. This analyte separation reduces the complexity of the data and can assist in the identification of molecules that possess similar characteristics. Also, electrophoretic methods can be paired with a variety of

sensitive detection methods such as fluorescence to enable analyses of low abundance analytes.

Despite the number of techniques available for single cell analysis, effective sampling can still be a challenge. The possibility of damaging the cell during handling or sampling can be high, which can produce inaccurate data. Also, isolating and manipulating single cells typically requires a skilled physiologist. The development of sampling techniques to enable analytical measurements of single cells has broadened this topic beyond biology to encompass several different fields, including analytical chemistry and physics. Combining a sample handling instrument with a separation step and a sensitive, selective detection method allows for effective and robust analysis of single cells.

1.2 Thesis overview

The remainder of this chapter will briefly cover the history of electrophoresis for single cell analysis as well as an overview of catecholamines and indolamines, the analyte classes that are studied using the techniques and instrumentation presented throughout this thesis. Chapter 2 is a review of sampling techniques for single cell electrophoresis for the time period 2008 to 2011. Chapter 3 covers the redesigning of and improvements to a laboratory-built capillary electrophoresis-laser-induced native fluorescence instrument, to increase reliability and robustness as well as to enable hyphenation to sampling instrumentation. Chapter 4 details several capillary electrophoresis techniques that are tested and optimized for analyzing low abundance indolamines within high salt-containing sample matrices, specifically artificial cerebral spinal fluid used in microdialysis. Chapter 5 covers the design, construction, and testing of an optical trap with biological and non-biological samples, and its hyphenation with the capillary electrophoresis-laser-induced native fluorescence instrument mentioned in Chapter 3. Chapter 6 describes the analysis of single pinealocytes, the cells of the pineal gland, using the hyphenated system detailed in Chapter 5.

1.3 Historical review of electrophoresis for single cell analysis

Some of the earliest work done on electrophoresis for biological sample analysis was in the late 1930s, primarily on mammalian sera and erythrocytes.[1, 2] The band boundaries were identified optically, by measuring refractive index changes using the schlieren method.[3] The idea behind much of this research was to see if different biological states could be determined, categorized, and even induced based on separation profiles obtained from electrophoretic experiments. For example, research was done on skin-sensitizing antibodies which involved electrophoretically separating the components, using a Tiselius apparatus, in the sera of allergic individuals and applying the isolated fractions to non-allergic test subjects, to see if the proteins could sensitize their skin.[4] Another research area that electrophoresis played a role in was identifying the physical characteristics of various proteins. Work from as early as 1924 was done to determine the pI and mobility of sera proteins and their interaction with quartz beads.[5-7]

In the 1950s and 1960s, electrophoretic methods and instrumentation were developed to isolate cellular components from lower volume samples. Microdisc electrophoresis, paper electrophoresis, and starch-zone electrophoresis were techniques commonly used to separate proteins from cell suspensions, small cell clusters, and individual cells. In 1955 Smithies reported investigating sera proteins using starch-zone electrophoresis and was able to identify three different classes of sera based on the presence or absence of various unidentified compounds.[8] Hydén, Bjurstam, and McEwen reported the electrophoretic separation of 10^{-7} to 10^{-9} grams of proteins from individual neurons and cell clusters in 1966 using microdisc electrophoresis coupled with a laboratory-built microdensiometer to record the protein bands.[9] Five 200 µm-diameter glass capillaries filled with polyacrylamide gel were used in parallel to separate a total of 17 protein bands from 60 Deiters' neurons. Sample isolation and manipulation was done by hand for this work. Matioli and coworkers realized that instrumentation and analyses needed to be scaled down to the single cell level for effective sampling; they performed polyacrylamide gel electrophoresis on a single fiber to separate hemoglobin fractions from a single blood

cell.[10] Rüchel used a postage stamp-sized, ultrathin slab gel to isolate proteins from an individual bag cell neuron from *Aplysia*.[11]

Interest in single cell electrophoresis intensified as new methods for analysis were developed. Pioneering research by several groups began in the late 1980s to create and use microelectrophoretic techniques such as capillary electrophoresis and microfluidic electrophoretic devices to look quantitatively at the contents of single cells. Kennedy, Jorgenson, and co-workers were among the first to perform microcolumn separations on individual cells.[12-14] The Ewing research group used 2 and 5 µm inner diameter capillaries and electrochemical detection to analyze cytoplasm from *Planorbis corneus* by inserting one end of an etched electrophoresis capillary directly into a single nerve cell,[15, 16] among other single cell studies.[17-19] Sweedler and co-workers have studied signaling molecules such as nitric oxide[20-23] and indolamines[24-27] in single neurons using capillary electrophoresis with laser-induced fluorescence detection. Dovichi and co-workers pioneered the used of the sheath flow cell for post-column detection in capillary electrophoresis,[28] coined the term "chemical cytometry" to describe the analysis of the chemical contents of single cells, and have performed a variety of single cell studies on cancer cells.[29-31] The Yeung research group has contributed a number of papers in this field, using capillary electrophoresis paired with native fluorescence to selectively detect biogenic amines, in addition to derivatized fluorescence detection.[32-35] The Arriaga research group has focused on analysis of subcellular components such as mitochondria[36, 37] and other organelles.[38-41]

Sampling techniques to improve single cell analysis have become more necessary as the sizes of the cells of interest decreased and as detection methods became more sensitive, enabling trace analyte levels to be detected. There is still a need today to further improve sampling methods, to facilitate high throughput analysis so that statistical information can be more easily gathered and to allow a wider range of research to be conducted. Manual, mechanical, and microfluidic manipulation are popular and effective choices for sampling from single cells, as are optical methods such as laser lysis and optical traps. Chapter 2 details recent progress in this field.

1.4 Catecholamines and indolamines in single cells

Among the analytes that are of interest in single cell research are the biogenic amines, specifically catecholamines and indolamines. Catecholamines are derived from tyrosine (*e.g.*, epinephrine and dopamine) and indolamines from tryptophan (*e.g.*, serotonin and melatonin). They play roles in numerous physiological functions, including but not limited to cardiac regulation,[42-44] memory formation,[45-47] mood,[48, 49] behavior,[50] satiation,[51, 52] sleep,[53-55] and reproduction.[56-60] Catecholamines and indolamines are also implicated in several degenerative[61, 62] and pathological diseases, such as Parkinson's disease,[63-67] and in tumor inhibition and growth.[68, 65, 66, 69-73] Their presence and functions are well conserved throughout the animal kingdom, from insects to mollusks to mammals.

Their widespread functions make catecholamines and indolamines the subject of much research, although they are considered low abundance analytes and are typically synthesized and localized in specific areas or cell types, especially catecholamines. These factors make catecholamines and indolamines ideal candidates for analysis in single cells. In particular, capillary electrophoresis has been used to study single cell levels of catecholamines and indolamines in a variety of animal models and cell types, such as the sea hare metacerebral cells,[27, 74, 25] sea hare R2 neurons,[74] sea hare cerebral ganglion neurons,[75] pond snail giant dopamine neurons,[15, 16, 76, 77, 19] fresh water snail RPeD1 and LPeD1 neurons,[26] bovine adrenal medullary cells,[32] and rat mast cells.[33] A variety of schemes have been used to detect catecholamines and indolamines in single cells, including fluorescence, electrochemical, and mass spectrometric detection. In this work, native fluorescence is used to detect these analytes, since it simplifies sample preparation, provides information about analyte identity, and allows for selective excitation, which reduces the complexity of analysis.

1.5 Conclusions

Instrumentation for small volume samples and single cell analysis has been designed, built, and optimized, employing a novel hyphenated optical trap-capillary electrophoresis-laser induced native fluorescence system. This instrument isolates and manipulates single cells, performs cell introduction into a capillary for lysing and separation

of analytes, and uses sensitive and selective native fluorescence detection specific for catecholamines and indolamines to analyze the contents of single cells. Single pinealocytes, the cells of the pineal gland, were analyzed for indolamine content under a variety of conditions. Small volume samples were also analyzed for trace levels of indolamines under high salt, physiological conditions, which required testing and optimization of a variety of capillary electrophoretic methods. This work allows for the routine analysis of single cells and small volume samples under physiological conditions.

1.6 References

(1) Luetscher, J. *J Am Chem Soc*. **1939**, *61*, 2888–2890.

(2) Longsworth, L. *Chem. Rev.* **1942**, *30*, 323–340.

(3) Longsworth, L. *Ind. Eng. Chem. Anal. Ed.* **1946**, *18*, 219–229.

(4) Newell, J. M.; Sterling, A.; Oxman, M. F.; Burden, S. S.; Krejci, L. E. *The Journal of Allergy*. **1939**, *10*, 513–520.

(5) Sherman, H.; Caldwell, M.; Naylor, N. *J Am Chem Soc*. **1925**, *47*, 1702–1709.

(6) Sherman, H.; Thomas, A.; Caldwell, M. *J Am Chem Soc*. **1924**, *46*, 1711–1717.

(7) Abramson, H. *J Am Chem Soc*. **1928**, *50*, 390–393.

(8) Smithies, O. *Biochem J*. **1955**, *61*, 629–641.

(9) Hydén, H.; Bjurstam, K.; McEwen, B. *Anal Biochem*. **1966**, *17*, 1–15.

(10) Matioli, G. T.; Niewisch, H. B. *Science*. **1965**, *150*, 1824–1826.

(11) Rüchel, R. *J. Chrom.* **1977**, *132*, 451–468.

(12) Kennedy, R. T.; Jorgenson, J. W. *Anal Chem*. **1988**, *60*, 1521–1524.

(13) Kennedy, R. T.; Oates, M. D.; Cooper, B. R.; Nickerson, B.; Jorgenson, J. W. *Science*. **1989**, *246*, 57–63.

(14) Oates, M. D.; Cooper, B. R.; Jorgenson, J. W. *Anal Chem*. **1990**, *62*, 1573–1577.

(15) Olefirowicz, T. M.; Ewing, A. G. *Anal Chem*. **1990**, *62*, 1872–1876.

(16) Olefirowicz, T.; Ewing, A. *J. Neurosci. Methods*. **1990**, *34*, 11–15.

(17) Ewing, A. *J. Neurosci. Methods*. **1993**, *48*, 215–224.

(18) Woods, L. A.; Roddy, T.; Ewing, A. G. *Electrophoresis*. **2004**, *25*, 1181–1187.

(19) Anderson, B. B.; Ewing, A. G. *J Pharm Biomed Anal*. **1999**, *19*, 15–32.

(20) Floyd, P. D.; Moroz, L. L.; Gillette, R.; Sweedler, J. V. *Anal Chem*. **1998**, *70*, 2243–2247.

(21) Ye, X.; Rubahkin, S. S.; Sweedler, J. V. *Analyst*. **2008**, *133*, 423–433.

(22) Ye, X.; Kim, W.-S.; Rubakhin, S. S.; Sweedler, J. V. *J Neurochem*. **2006**, *101*, 632–640.

(23) Kim, W.-S.; Ye, X.; Sweedler, J. V. *Anal Chem*. **2006**, *78*, 1859–1865.

(24) Fuller, R. R.; Moroz, L. L.; Gillette, R.; Sweedler, J. V. *Neuron*. **1998**, *20*, 173–181.

(25) Hatcher, N. G.; Zhang, X.; Stuart, J. N.; Moroz, L. L.; Sweedler, J. V.; Gillette, R. *J Neurochem*. **2008**, *104*, 1358–1363.

(26) Lapainis, T.; Scanlan, C.; Rubahkin, S. S. *Anal Bioanal Chem*. **2007**, *387*, 97–105.

(27) Miao, H.; Rubahkin, S. S.; Sweedler, J. V. *Anal Bioanal Chem*. **2003**, *377*, 1007–1013.

(28) Zarrin, F.; Dovichi, N. J. *Anal Chem*. **1985**, *57*, 2690–2692.

(29) Hu, S.; Zhang, L.; Krylov, S. N.; Dovichi, N. J. *Anal Chem*. **2003**, *75*, 3495–3501.

(30) Fazal, M. A.; Palmer, V. R.; Dovichi, N. J. *J. Chrom. A*. **2006**, *1130*, 182–189.

(31) Krylov, S. N.; Zhang, Z.; Chan, N. W.; Arriaga, E. A.; Palcic, M. M.; Dovichi, N. J. *Cytometry*. **1999**, *37*, 14–20.

(32) Chang, H.; Yeung, E. *Anal Chem*. **1995**, *67*, 1079–1083.

(33) Ho, A.; Yeung, E. *J. Chrom. A*. **1998**, *817*, 377–382.

(34) Aspinwall, C. A.; Yeung, E. S. *Anal Bioanal Chem*. **2005**, *381*, 660–666.

(35) Yeung, E. S. *J. Chrom. A*. **1999**, *830*, 243–262.

(36) Johnson, R. D.; Navratil, M.; Poe, B. G.; Xiong, G.; Olson, K. J.; Ahmadzadeh, H.; Andreyev, D.; Duffy, C. F.; Arriaga, E. A. *Anal Bioanal Chem*. **2007**, *387*, 107–118.

(37) Wolken, G. G.; Kostal, V.; Arriaga, E. A. *Anal Chem*. **2011**, *83*, 612–618.

(38) Xu, X.; Arriaga, E. A. *Free Radical Biology and Medicine*. **2009**, *46*, 905–913.

(39) Xu, X.; Thompson, L. V.; Navratil, M.; Arriaga, E. A. *Anal Chem*. **2010**, *82*, 4570–4576.

(40) Gunasekera, N.; Olson, K. J.; Musier-Forsyth, K.; Arriaga, E. A. *Anal Chem*. **2004**, *76*, 655–662.

(41) Olson, K. J.; Ahmadzadeh, H.; Arriaga, E. A. *Anal Bioanal Chem*. **2005**, *382*, 906–917.

(42) Matsushita, T.; Kuwasawa, K.; Uchimura, K.; Ai, H.; Kurokawa, M. *Comp. Biochem. Physiol., Part A Mol. Integr. Physiol.* **2002**, *133*, 625–636.

(43) Mialet-Perez, J.; Bianchi, P.; Kunduzova, O.; Parini, A. *J Neural Transm*. **2007**, *114*,

823–827.

(44) Frascarelli, S.; Ghelardoni, S.; Chiellini, G.; Vargiu, R.; Ronca-Testoni, S.; Scanlan, T. S.; Grandy, D. K.; Zucchi, R. *Eur J Pharmacol*. **2008**, *587*, 231–236.

(45) Sitaraman, D.; Zars, M.; Laferriere, H.; Chen, Y.-C.; Sable-Smith, A.; Kitamoto, T.; Rottinghaus, G. E.; Zars, T. *Proceedings of the National Academy of Sciences*. **2008**, *105*, 5579–5584.

(46) Kaczer, L.; Klappenbach, M.; Maldonado, H. *European Journal of Neuroscience*. **2011**, *34*, 1170–1178.

(47) Agarwal, M.; Giannoni Guzmán, M.; Morales-Matos, C.; Del Valle Díaz, R. A.; Abramson, C. I.; Giray, T. *PLoS ONE*. **2011**, *6*, e25371.

(48) Xu, Y.; Li, S.; Chen, R.; Li, G.; Barish, P. A.; You, W.; Chen, L.; Lin, M.; Ku, B.; Pan, J.; Ogle, W. O. *Pharmacology, Biochemistry and Behavior*. **2010**, *94*, 447–453.

(49) Pezze, M.; Feldon, J. *Prog Neurobiol*. **2004**, *74*, 301–320.

(50) Wada-Katsumata, A.; Yamaoka, R.; Aonuma, H. *Journal of Experimental Biology*. **2011**, *214*, 1707–1713.

(51) Martínez-Rubio, C.; Serrano, G. E.; Miller, M. W. *J Comp Neurol*. **2009**, *514*, 329–342.

(52) Lemierre, S.; Rouch, C.; Nicolaidis, S.; Orosco, M. *Int. J. Obes. Relat. Metab. Disord.* **1998**, *22*, 993–999.

(53) Arendt, J.; Skene, D. J. *Sleep Medicine Reviews*. **2005**, *9*, 25–39.

(54) Gooneratne, N. S.; Gehrman, P.; Gurubhagavatula, I.; Al-Shehabi, E.; Marie, E.; Schwab, R. *J Clin Sleep Med*. **2010**, *6*, 572–580.

(55) Waldhauser, F.; Kovács, J.; Reiter, E. *Exp. Gerontol.* **1998**, *33*, 759–772.

(56) Yamane, T.; Miyatake, T. *Journal of Insect Physiology*. **2010**, *56*, 271–276.

(57) Hirashima, A.; Yamaji, H.; Yoshizawa, T.; Kuwano, E.; Eto, M. *Journal of Insect Physiology*. **2007**, *53*, 1242–1249.

(58) Harano, K.-I.; Sasaki, K.; Nagao, T.; Sasaki, M. *Journal of Insect Physiology*. **2008**, *54*, 848–853.

(59) Hernandez-Rauda, R.; Aldegunde, M. *Mar Biol*. **2002**, *141*, 209–216.

(60) Petterborg, L. J.; Reiter, R. J. *J Neural Transm*. **1982**, *55*, 149–155.

(61) Catena-Dell'Osso, M.; Bellantuono, C.; Consoli, G.; Baroni, S.; Rotella, F.; Marazziti, D. *Curr. Med. Chem.* **2011**, *18*, 245–255.

(62) Terry, A. V., Jr.; Buccafusco, J. J.; Wilson, C. *Behav Brain Res*. **2008**, *195*, 30–38.

(63) Tong, Y.; Pisani, A.; Martella, G.; Karouani, M.; Yamaguchi, H.; Pothos, E. N.; Shen, J. *Proceedings of the National Academy of Sciences*. **2009**, *106*, 14622–14627.

(64) Calon, F.; Morissette, M.; Rajput, A. H.; Hornykiewicz, O.; Bédard, P. J.; Di Paolo, T. *Mov. Disord.* **2003**, *18*, 241–253.

(65) Goldstein, D. S.; Sullivan, P.; Holmes, C.; Kopin, I. J.; Basile, M. J.; Mash, D. C. *European Journal of Neurology*. **2010**, *18*, 703–710.

(66) Alberio, T.; Colapinto, M.; Natale, M.; Ravizza, R.; Gariboldi, M. B.; Bucci, E. M.; Lopiano, L.; Fasano, M. *IUBMB Life*. **2010**, *62*, 688–692.

(67) Goldstein, D. S.; Holmes, C.; Kopin, I. J.; Sharabi, Y. *J. Clin. Invest.* **2011**, *121*, 3320–3330.

(68) Martin, V. *Cancer Research*. **2006**, *66*, 1081–1088.

(69) Casado-Zapico, S.; Martín, V.; García-Santos, G.; Rodríguez-Blanco, J.; Sánchez-Sánchez, A. M.; Luño, E.; Suárez, C.; García-Pedrero, J. M.; Menendez, S. T.; Antolín, I.; Rodriguez, C. *J Pineal Res*. **2011**, *50*, 345–355.

(70) Coufal, M.; Invernizzi, P.; Gaudio, E.; Bernuzzi, F.; Frampton, G. A.; Onori, P.; Franchitto, A.; Carpino, G.; Ramirez, J. C.; Alvaro, D.; Marzioni, M.; Battisti, G.; Benedetti, A.; DeMorrow, S. *Int. J. Cancer*. **2009**, *126*, 2112–2122.

(71) Germano, P. M.; Lieu, S. N.; Xue, J.; Cooke, H. J.; Christofi, F. L.; Lu, Y.; Pisegna, J. R. *J Mol Neurosci*. **2009**, *39*, 391–401.

(72) Kao, Y.-Y.; Liu, K.-T.; Huang, M.-F.; Chiu, T.-C.; Chang, H.-T. *J. Chrom.* **2010**, *1217*, 582–587.

(73) Li, Z. J.; Cho, C. H. *Eur J Pharmacol*. **2011**, *667*, 17–22.

(74) Lapainis, T.; Rubahkin, S. S.; Sweedler, J. V. *Anal Chem*. **2009**, *81*, 5858–5864.

(75) Park, Y. H.; Zhang, X.; Rubakhin, S. S.; Sweedler, J. V. *Anal Chem*. **1999**, *71*, 4997–5002.

(76) Kristensen, H. K.; Lau, Y. Y.; Ewing, A. G. *J. Neurosci. Methods*. **1994**, *51*, 183–188.

(77) Chen, G.; Ewing, A. *Brain Res*. **1995**, *701*, 167–174.

2 Sampling techniques for single cell electrophoresis

Notes and Acknowledgments

This work is being prepared for publication as "Sampling techniques for single cell electrophoresis", Christine Cecala and Jonathan V. Sweedler, in the *Analyst* special issue theme "Single" in April 2012. I would like to thank Prof. Jonathan V. Sweedler for his advice and edits. This work was supported by the National Institute on Drug Abuse under award number P30 DA018310 and by the National Institute of Dental and Craniofacial Research under award number R01 DE018866. The content is solely the responsibility of the authors and does not necessarily represent the official views of the National Institute on Drug Abuse or the National Institute of Dental and Craniofacial Research.

2.1 Introduction

Cells contain hundreds of different compounds belonging to many analyte classes: amino acids, proteins, lipids and sugars, among others. The concentration range of these analytes can span from the millimolar to the picomolar, and can vary based on a number of factors, such as an animal's physiological state, season, and even the time of day. While chemical differences between cell types are expected, even for so-called homogenous cell populations, a surprising cell-to-cell heterogeneity exists. When working with measurements that report average values for larger numbers of cells, much of this critical information is lost.

Single cell analysis provides insight into cellular heterogeneity and oftentimes retains the unique information present within individual cells. For example, if only one cell out of 100 possesses an analyte of interest, assaying 100 cells dilutes the analyte of interest, likely complicates detection due to signals from constituents common to all cells, and therefore makes the measurements more challenging. This also places a large demand on the dynamic range of the detection system, since analyte levels can range from millimole to zeptomole amounts within a tissue. What types of samples are used for such measurements? As examples, adjacent neurons can have different complements of signaling molecules[1] and there is large stochastic variance in protein expression from

supposedly identical bacterial cells.[2] Obviously, for heterogeneous samples where multiple cell types are intertwined (like neurons and glia), performing bulk chemical analysis results in average values for the region and does not provide information on defined cell types. Performing single cell analysis bypasses these issues by reducing analyte dilution, potentially decreasing the sample complexity, and lowering the dynamic range necessary to detect the components present within the cell. While there are numerous potential applications, the need for individual cell measurements in neuroscience, cancer research, and stem cell biology have driven many studies.[3, 4]

There are different parameters used to describe a cell, including its morphology, electrophysiology, transcriptome, and chemical constituents. Thus, numerous methods are used to probe single cells, from optical microscopy, next generation sequencing, electrophysiology, and a host of chemical characterization approaches. For small molecules (e.g., the metabolome), separations such as electrophoresis have become widely employed.[5] This analyte separation reduces the complexity of the data and can assist in the identification of molecules that possess similar characteristics. The physical scaling laws for electrophoresis favor miniaturization, and it has been applied to a broad range of single cell experiments.[6] This review focuses on the recent applications of capillary electrophoresis to single cell measurements.

While the separation and detection figures of merit are important, perhaps no area determines the success of such measurements more than isolating and sampling the cells. Hence, approaches for sampling cells and introducing them to the separation channel are highlighted, with an emphasis on sampling strategies for single cell electrophoresis developed from 2008-2011. The descriptions are not meant to be comprehensive, but to highlight recent results, improvements and trends in single cell sampling applied to capillary electrophoresis. Why highlight sampling? One of the challenges and unique aspects of single cell analysis is effective sample handling. Selecting and isolating specific cells, especially when rare, without affecting the cell contents requires either a skilled physiologist or technologies for automated cell manipulations. Recent progress in isolating and sampling cells, including optical traps, improved cell sorting, and microfluidic

manipulations, are enabling a number of studies. The development of sampling techniques to enable analytical measurements of single cells encompasses multiple different fields, including analytical chemistry, biology and physics.

2.2 Historical overview of electrophoresis for single cell analysis

While electrophoresis has a long history,[7] applying it to individual cells is more recent. In the 1950s and 1960s, electrophoretic methods and instrumentation were developed to isolate cellular components from lower volume samples. Microdisc electrophoresis, paper electrophoresis, and starch-zone electrophoresis were techniques commonly used to separate proteins from cell suspensions, small cell clusters, and individual cells. In 1955 Smithies reported investigating sera proteins using starch-zone electrophoresis and was able to identify three different classes of sera based on the presence or absence of various unidentified compounds.[8] Hydén, Bjurstam, and McEwen reported the electrophoretic separation of 10^{-7} to 10^{-9} grams of proteins from individual brain stem neurons and cortical cells, as well as low numbers of Deiters' neurons and cell clusters in 1966 using microdisc electrophoresis coupled with a laboratory-built microdensiometer to record the protein bands.[9] Five 200 μm-diameter glass capillaries filled with polyacrylamide gel were used in parallel to separate a total of 17 protein bands from 60 Deiters' neurons. Sample isolation and manipulation was done by hand for this work. The importance of downscaling the electrophoresis apparatus to match the scale of the cells was recognized early; even before the advent of capillary electrophoresis, Matioli and coworkers separations the hemoglobin fractions in an individual red blood cell via polyacrylamide gel electrophoresis on a fiber[10] and Rüchel used a postage stamp-sized, ultrathin slab gel to isolate proteins from an individual bag cell neuron from *Aplysia*.[11]

Interest in single cell electrophoresis intensified as the figures of merit for small-scale electrophoresis improved to allow a greater range of measurements. Pioneering research done by the Jorgenson, Yeung, and Ewing groups as well as the Dovichi, Arriaga, and Sweedler groups created and used microelectrophoretic techniques to look quantitatively at the contents of single cells and organelles, including neurotransmitters,[12-19] amino acids,[20, 21] enzymes and proteins,[22-26] sugars,[27, 28] and other small molecules.[29-31]

Improved and more flexible cell sampling approaches continue to evolve as the sizes of the cells of interest decrease, detection methods become more sensitive, and separation throughput increases. There is still a need today to further improve sampling methods to facilitate high throughput analysis so that statistical information can be more easily gathered and to allow a wider range of research to be conducted.

2.3 Present strategies for single cell separations

The development of capillary electrophoresis (CE), described by Jorgenson and Lukacs in 1981,[32, 33] has enabled many groups to perform single cell research. The components can be relatively inexpensive and a basic instrument is fairly simple to set up, compared with the first electrophoresis work described previously. There are several benefits associated with using CE for single cell analysis, such as its low sample volume requirements, spatial dimensions, fast and efficient separations, and its versatility. These attributes combine to make CE a popular choice for the analytical separation of the contents within single cells.[20, 21, 29, 34-37]

Microfluidic chips coupled with CE have also been used for single cell electrophoresis.[36, 38-41] The development of lab-on-a-chip techniques has broadened the scope of the single cell studies and has impacted biology, chemistry, physics, and engineering. The benefits of microfluidics as a basis for analytical platforms are numerous. The small volumes, low cost of fabrication, portability, and design versatility all contribute to the use of microfluidics for single cell analysis. Also, the ability to integrate multiple experiment components (like sample preparation, separation, and detection) on one device and potentially automate them is a main benefit especially for rapid, high-throughput analysis. Finally, the typical materials used for devices are optically transparent in the visible and ultraviolet region, which allows for hyphenation with a variety of optical instruments and components like microscopes and detectors.

When analyzing samples whose content may be in the femtomole to zeptomole range or lower, sensitive detection methods are necessary. For capillary electrophoresis, a number of detection systems have been developed, including fluorescence, electrochemical, mass spectrometric, radionuclide, NMR, and others.[42] The first three

(fluorescence, electrochemical, and mass spectrometric) are by far the most common . The figures of merit of these detection systems impact the cell samples and sampling approaches used for single cell applications, and so the detection systems are briefly described within the context of single cell measurements.

Fluorescence is often used for single cell analysis due to its sensitivity to analyte concentration, large linear dynamic range (10^9 orders of magnitude), low detection limits (yoctomole amounts), and selectivity. The combination of these factors allows for both common and trace analyte levels to be detected and quantitated. Laser-induced native fluorescence (LINF) is a highly selective detection method, as relatively few biological analytes are natively fluorescent. This selectivity can reduce the complexity of electropherograms and wavelength-resolved information can provide additional information about the analyte identity. In contrast, derivatization reagents are used to bind a fluorophore to a non-fluorescent molecule (laser-induced fluorescence (LIF)). Although there is a loss in selectivity and information content when using derivatization, there are a wide variety of reagents available, which allows for detection to occur with a range of instrumentation. Another benefit is the extremely low detection limits (zeptomole to yoctomole) that are achievable due to the high quantum yields (typically > 0.9) of the fluorophores. CE-LIF[25, 31, 43, 44] and CE-LINF[16, 45, 46] have been used extensively to profile the contents of single cells and organelles.

Electrochemistry (EC) is a popular alternative to fluorescence detection for single cell analysis.[47-49] Instrumentation for EC measurements is relatively simple and low cost, and no derivatization is necessary, which reduces sample preparation. The limits of detection for EC are sub-attomole, comparable to fluorescence measurements. Three main types of EC detection are used: amperometry, voltammetry, and conductivity. Amperometry is the most commonly used EC detection technique, as it is highly sensitive but not selective. Voltammetry is roughly 100-fold less sensitive than amperometry but can be more selective. Finally conductivity is the least selective as it can measure signal generated by any charged compound, but is the most universal of the three electrochemical approaches.

Mass spectrometry (MS) has increasingly been used to profile the contents of single cells.[50-55] There are several characteristics of MS that make it a valuable detection method for single cell analysis. One is the large variety of analyte classes that are amenable to MS detection, including small molecules, peptides, proteins, and sugars, as the main requirement is that the analyte can be ionized in the gas phase. Another is the ability to detect many different analytes simultaneously, providing data with high information content for each sample that is analyzed. Structural information can be obtained which aids in analyte identification and no derivatization or modification to the analytes is necessary for detection. Mass detection limits are appropriate for single cell analysis, in the range of nanograms to femtograms, and the low sample volumes typically encountered in CE and microfluidics can readily be analyzed.

2.4 Sampling techniques

In the context of single cell measurements, one of the greatest benefits of CE is its cell-sized sample volumes. On the surface, injecting picoliters to nanoliters of sample appears well-matched to the needs of single cell analysis using additional sample handling; however, typically only 0.03 to 1% percent of a given sample is usually injected into the capillary for analysis. This low percentage provokes the question of whether an analyte is not detected because it is not present in the cell or because it is present in too low an amount so that injecting only a small fraction of the sample creates a measurement below the instrumental detection limits. One way to increase the analyte concentration present within the portion of the sample that is injected while retaining the low sampling volume is to inject the entire cell. There are numerous sample manipulation strategies that have been interfaced to CE and microfluidic instruments, some of which are detailed below.

It would be remiss not to mention the importance of flow cytometry in single cell analysis.[56-62] It is the classical method used for single cell measurements and uses characteristics of cells such as morphology or fluorescence to sort cells for further measurements. Many of the sampling strategies discussed in this review, regardless of their heading, use modified forms of flow cytometry to automate the isolation of single cells or cytometry-inspired detection cells for sensitive detection post-capillary. Given this

widespread use, flow cytometry does not have a heading of its own, but its use is noted where appropriate throughout the descriptions that follow.

2.4.1 Manual manipulation

Manual manipulations have enabled a variety of single cell studies to be performed. In general, a number of optical, electrical, chemical, and physical tools have been used to remove cells from an organ or organism,[63-65] isolate organelles from a cell,[25, 26, 29, 66] and sample directly from the cytoplasm,[13, 67] among other things. Although manual manipulations may take time and skill, advantages include flexibility and compatibility with classical physiological and immunohistochemical approaches, which can allow studies to be performed on cells that are not amenable to culturing or other handling procedures. Representative examples of such applications are highlighted.

The Sweedler group has profiled single cell and subcellular metabolites using CE coupled to MS.[53, 54] In the first report, two different cell types from *Aplysia californica* were individually isolated and disrupted using sharpened needles and contents were extracted for analysis. The contents of a single R2 cell soma were also compared with the contents from the same R2 cell's neurite, and it was determined that different subcellular regions contain different relative amounts of several metabolites. Nemes, Knolhoff, and others profiled 50 *Aplysia* cells belonging to six different neuron types.[54] More than 300 distinct ion signals from endogenous metabolites were detected from a single neuron, 140 of which were selected for chemometric data analysis. This profiling revealed quantitative and qualitative chemical differences between individual neurons and neuronal types (Figure 1).

Lantz and co-workers have used whole-cell fluorescence *in situ* hybridization with CE-LIF to rapidly identify microbial cells within heterogeneous populations of other microbial cells[68] and within whole blood.[69] Using this technique, as few as three injected cells of *Salmonella* Typhimurium were detected against a background of 300 injected *Escherichia coli* cells, approaching the detection of single pathogens. This procedure and analysis was rapid, did not experience band broadening, and is particularly useful for identifying microbial cells that are similar and physiologically unable to be separated. In the second report, single *Candida albicans* cells were detected and quantitated in lysed whole

blood samples. The lysis of blood cells has a two-fold use: to remove potentially interfering cells and to promote the natural aggregation of yeast cells. The stacked cells show a strong correlation between cell concentration and signal, enabling quantitation. This sample preparation and analysis technique has potential use in the food and pharmaceutical industry.

Detection of nitric oxide in a variety of single cells was accomplished by Yang *et al*.[70] Single cells from four model cell systems for studying nitric oxide biochemistry and release (*Lymnaea stagnalis* neurons, human ECV-304 cells, rat PC12 cells, and MDCK cells infected with the highly pathogenic avian influenza virus (H5N1)) were analyzed by trapping nitric oxide *in vivo* using fluorescent probes. Cells were incubated in proteolytic enzymes and the connective cells were removed and dispersed manually. Prior to cell injection, a plug of surfactant was introduced into the capillary to lyse the cell. A micromanipulator was used to position the capillary above a single cell and negative pressure was applied to inject the cell. Limits of detection were 42 amol for nitric oxide and the separation time was under three minutes.

The Yeung group has developed a CE method that can quantitate attomole levels of both NAD^+ and NADH within a single rat myoblast.[71] Individual cells are contained within an area on a microscope slide, injected into the capillary via pressure, and lysed using a Tesla coil. After separation of NAD^+ and NADH, they were exposed to a cycling buffer and quantitated using fluorescence. Concentrations were determined for cells exposed to oxidative stress induced by peroxide and for non-stressed cells.

Overall, manual manipulation strategies are among the most used approach for single cell sampling, as this term can encompass many different methods and its flexibility. An important function of manual manipulation is the removal of the cells of interest from the organism, as many of the sampling techniques described below are used only after the cells are in suspension.

2.4.2 Mechanical manipulation

Automated mechanical manipulations reduce user handling. In many cases one of the slowest, more error-prone areas of analysis is sample handling, and mechanical manipulation can reduce the time it takes to isolate and introduce cells to the separation channel.

Parallel separation of the ganglioside metabolites of AtT-20 cells was performed by Boardman and co-workers.[72] An array of five capillaries was used to inject single cells from etched nanoliter wells on a poly(2-hydroxyethyl methacrylate)-coated glass substrate with a minimal amount of manual manipulation. A cell suspension was placed on the surface and the cells were allowed to settle into the wells. The cell concentration and settling time were chosen to ensure that approximately one cell was loaded per well, according to Poisson statistics. The capillaries were held in place by an alignment block and the outlets were threaded into a five-channel sheath flow cuvette for fluorescence detection. The capillary array was controlled by a micromanipulator which, when coupled with the alignment block, allowed for precise positioning of the array with respect to the cell-containing wells. Cells were aspirated into the capillary by hydrodynamic pressure and the contents separated. Approximately one nanoliter was injected into each capillary, and the single cell results correspond well with bulk measurements.

Another advance in this field made by the Dovichi group uses an indium-tin oxide-coated microfabricated device to isolate and capture individual NG-108 cells for analysis.[73] The device has 512, 500 μm-diameter wells with 2 μm high apertures that connect to a central channel that is used for applying a vacuum (Figure 1). Cells within a suspension are allowed to settle in each well under a vacuum, and once a cell has been drawn and trapped at the 2 μm high aperture, a rinsing step is employed to remove non-trapped cells. The dimensions of the aperture prevent multiple cells from being trapped. A micromanipulator was used to bring the capillary as close as possible to a trapped cell, and both hydrodynamic and electrokinetic injections were performed simultaneously to lyse and inject the cell into the capillary for analysis by LIF using a sheath flow cuvette for post-column detection.

Future work for this device is to use multiple capillaries for simultaneous analysis of a large number of single cells.

Marc and co-workers developed fast-lysis traps for single adherent cell analysis.[74] Rat basophilic leukemic cells, a mast cell tumor line, were loaded with Oregon Green and fluorescein, introduced into the chambers, and allowed to settle into wells and incubate for 12 hours before analysis. To sample from a cell, the capillary inlet was positioned 10-40 μm above a cell prior to lysis. A physiologic buffer was flowed across the cell, and simultaneously a voltage is applied below the cell for lysis, and to the capillary to initiate injection. After two minutes, the capillary inlet is moved to the next cell location and the process is repeated. This is one of the few technologies that is applicable for analyzing adherent cells.

2.4.3 Microfluidic manipulation

The use of microfluidics for single cell analysis has gained momentum in the past few years, due to its low cost and ability to be hyphenated to other instrumentation.

The Ramsey group has made several advances in using microfluidic electrophoretic devices for single cell analysis. They created a high-throughput, monolithically integrated device and interfaced it to ESI-MS detection to continuously analyze the protein content of single human erythrocytes.[75] Cells were loaded into a reservoir and moved by applying potentials to the four fluid reservoirs. Individual erythrocytes were manipulated into an intersection where they were lysed by rapid buffer exchange and an increase in electric field strength. The lysate was then directed into the separation channel and analytes (the dissociated heme group and heme protein subunits) were subsequently separated and detected. The average analysis rate was 12 cells per minute. This is the first time continuous analysis of individual cells integrated with electrophoretic separation and MS detection has been reported.

Omiatek and co-workers developed a capillary-based microfluidic platform to isolate subcellular vesicles and then lyse them as they exit the capillary using a detergent-containing sheath-flow interface. The lysate components were then detected using amperometric EC detection.[49] Results were reported for large unilamellar vesicles, a model

system for secretory vesicles, which were loaded with the neurotransmitter dopamine. Both analyte quantitation and liposome size were determined, with zeptomole amounts of dopamine detected for each individual lysis event encapsulated within a mean liposome radius of 80 ± 18 nm.

Secretion of insulin from individual islets of Langerhans has been continuously monitored and quantified by fluorescence on a microfluidic chip with 15 parallel electrophoresis channels by Dishinger and co-workers (Figure 2).[76] Multiplexed detection is possible due to a radial microchannel design where all of the outlets converge at a shared location. Islets were contained in perfusion chambers on-chip and different amounts of glucose were introduced into the chamber. Insulin released from the islets was introduced into the assay portion of the chip and reacted with FITC-insulin and human insulin antibody. Small plugs of this mixture were introduced into the electrophoresis channels in 10 second intervals. A total of 5400 serial immunoassays per hour can be performed, providing insight into insulin secretion dynamics for single islets. This device was used to determine that chronic fatty acid exposure eliminates pulsatile insulin secretion.

The Zare group has developed a microfluidic chip that can simultaneously perform whole gene amplification and protein separation from approximately 10 cells (Figure 3).[77] In particular, the content and composition of light-harvesting proteins from cyanobacterial cells and their corresponding genes were analysed. Cell suspension was loaded into the device and cell capture was performed by manipulating valves until the requisite number of cells was contained in the lysing chamber. After lysis, the proteins were collected into an injection plug for electrophoretic separation while the remaining cell lysate was directed into another chamber for denaturing and subsequent gene analysis. Separation and denaturing occur simultaneously on-chip. Native fluorescence detection was used to identify the protein complexes. This is the first system that performs both of these analyses on a single chip.

Xu and Yin have created a microfluidic chip that combines continuous cell introduction, rapid dynamic lysis, and CE-LIF with a throughput of 38 cells/minute for the analysis of reduced glutathione and reactive oxygen species in single erythrocytes.[78] Cells

were directed via sheath flow streams to the cross of the chip, where the cells were driven into the separation channel by the application of voltage. Cells were rapidly lysed within 33 milliseconds at the entry of the separation channel by surfactant and the fluorescent content separated and detected within a few seconds. The rate for introducing individual cells into the separation channel is determined by the components' electrophoretic resolution, as the maximum rate of introduction (~150 cells/minute) can cause overlap of the signals from individual cells and complicate analysis.

2.4.4 Laser lysis

Laser lysis, in combination with micromanipulation or microfluidics, represents a strategy to lyse cells without detergent and quickly inject the lysate with a minimum of sample dilution. Laser lysis employs a high intensity, short pulse length laser to generate a cavitation bubble that mechanically lyses the cell in under 1 millisecond.[79] This rapidity prevents the cell from responding to the stress of lysis, which could lead to analyte degredation or additional analytes present that are normally not in the day-to-day functioning of the cell.

Brown and co-workers performed CE-LIF analysis on the enzymatic activity of single live TF-1 cells and confirmed their results using bulk measurements from liquid chromatography coupled to MS detection.[80] Cell suspension was placed on a glass microscope coverslip and a cell was selected. The capillary inlet was manipulated over the cell and run buffer was deposited around the physiological buffer droplet surrounding the cell. A high numerical aperture objective focused a single nanosecond laser pulse onto the cell for lysis. The firing of the laser pulse triggered the high voltage power supply and the lysate was immediately electrokinetically injected into the separation capillary for analysis. Three different proteolytic fragments (~ 10^7 fragments/cell) from the β-amyloid precursor protein were separated and detected in addition to the native β-amyloid precursor peptide peak in single cells.

Jiang, Sims, and Allbritton developed a capillary-based microelectrophoresis platform using laser lysis to serially analyze single rat basophilic leukemia cells that were loaded with fluorescein diacetate and Oregon green.[81] The chip contains two channels, one

for electrophoresis buffer and one for physiological buffer, and an array of microwells where each cell resides once they are loaded onto the chip. The microwells provide an address for the automatic positioning of the capillary for injection and separation of the intercellular dyes following laser lysis. The capillary location remains constant and the chip is translated so that the capillary inlet is positioned within the electrophoresis buffer channel. Once analysis is complete, the chip is translated so that the next cell can be lysed and injected. The throughput for this device was 1.8 cells per minute.

Allen and co-workers conducted high-throughput analysis of single B cell mitochondria by labeling the acidic components prior to lysis with Oregon Green diacetate succinimidyl ester, a membrane-permeable dye, and using a membrane-permeable base to raise the intramitochondrial pH (Figure 4).[82] Laser lysis on a glass microfluidic chip coupled with fluorescence detection was used to lyse the mitochondria and separate and detect the derivatized contents while preventing dilution of the sample. The targeted organelle was selected from a group of mitochondria and centered in the focus region for lysis. After lysis by a nanosecond UV laser pulse, the contents diffuse and are separated by on-chip electrophoresis. Analyzed volumes were calculated to be one attoliter.

2.4.5 Optical trapping

Optical traps are a popular tool for cell manipulation. First used for biological work in 1987 by Ashkin *et al*.,[83, 84] the use of optical traps for cellular and subcellular manipulation has grown. Samples that have been studied using optical traps include yeast,[63, 85] bacteria,[83, 86] neurons,[87] and spermatozoa.[88, 89] Optical traps make use of the forces generated by light interacting with a dielectric object through scattering and refraction.

Although optical traps are a widespread technique for single cell manipulation, interfacing a trap to an electrophoresis instrument is less common. Prior to 2008, there are only a few papers that demonstrate this for a capillary electrophoresis instrument, although hyphenating a trap to a microfluidic device is more prevalent.[39, 90-93] Cecala and Sweedler have created a hyphenated optical trap-CE-LINF instrument and have used it for the manipulation and analysis of single pinealocytes, which are the cells of the pineal gland. Several indolamines have been identified and quantified within single pinealocytes,

including serotonin and N-acetylserotonin. The capillary is directed using a computer-controlled micromanipulator toward the trap location, and a pinealocyte is located and immobilized within the trap. External debris and other cells can be removed by using a second capillary to remove untrapped objects or by using "outflow" from the separation capillary prior to injection. Once the area around the trapped cell is clear, the cell is released and injection into the separation capillary is performed hydrodynamically. The capillary is moved to a grounded buffer vial, the cell is lysed within the capillary, and the cellular contents are separated and detected using a three channel native fluorescence detection system optimized for catecholamines and indolamines.

2.5 Conclusions and future work

Single cell electrophoretic analyses have expanded our knowledge of cell-to-cell heterogeneity, allowed for the determination of statistically significant differences between cells exposed to different environments, and enabled the physiological functions of several compounds to be determined. Tracking cell-to-cell variability also promotes a deeper understanding of biological function and has the potential to elucidate not only intercellular information but also interactions within a local network.

Future developments in single cell measurements will focus on technological aspects such as expanding the number of detectable compounds per sample by using multiple fluorescent reagents to derivatize a larger variety of analyte types, or employing a complimentary multiple detection method scheme on-chip, either in series or in parallel (such as LIF coupled to MS). In terms of sampling, we expect more robust and automated approaches to be developed. Hyphenation of microelectrophoretic techniques with a number of other technologies, such as cell-sorting or manipulation techniques that rely on magnetophoretic properties,[94-96] optically-induced dielectrophoresis,[97-99] optoelectronic traps,[100] microvortices,[101-103] or digital microfluidics[104, 105] will enable a number of exciting studies. These technologies have already been paired with microfluidic devices for cell manipulation and mechanical studies, and adding a separation step could further enhance the information content gathered and allow for increased automation. These enhanced

sampling approaches will be applied to a greater range of applications in neuroscience, development and disease research.

2.6 Figures

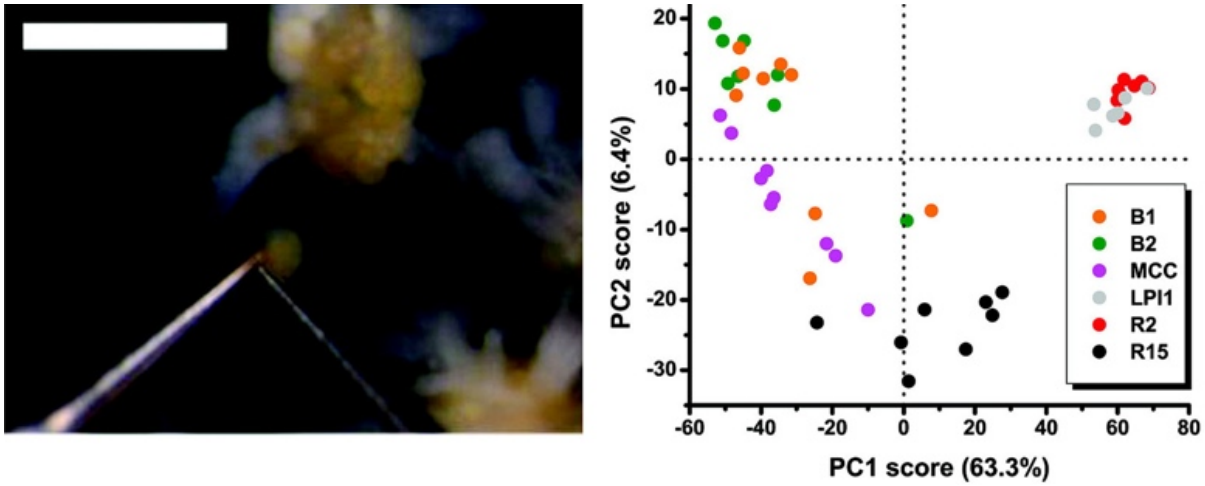

Figure 2.1 (Left) A single R2 neuron removed from the abdominal ganglia of *Aplysia californica*. Scale bar is 1 mm. (Right) Principle component analysis score plot revealed chemical differences between individual neurons and neuron types. Each data point corresponds to a different single cell. Adapted with permission from (54). Copyright 2011 American Chemical Society.

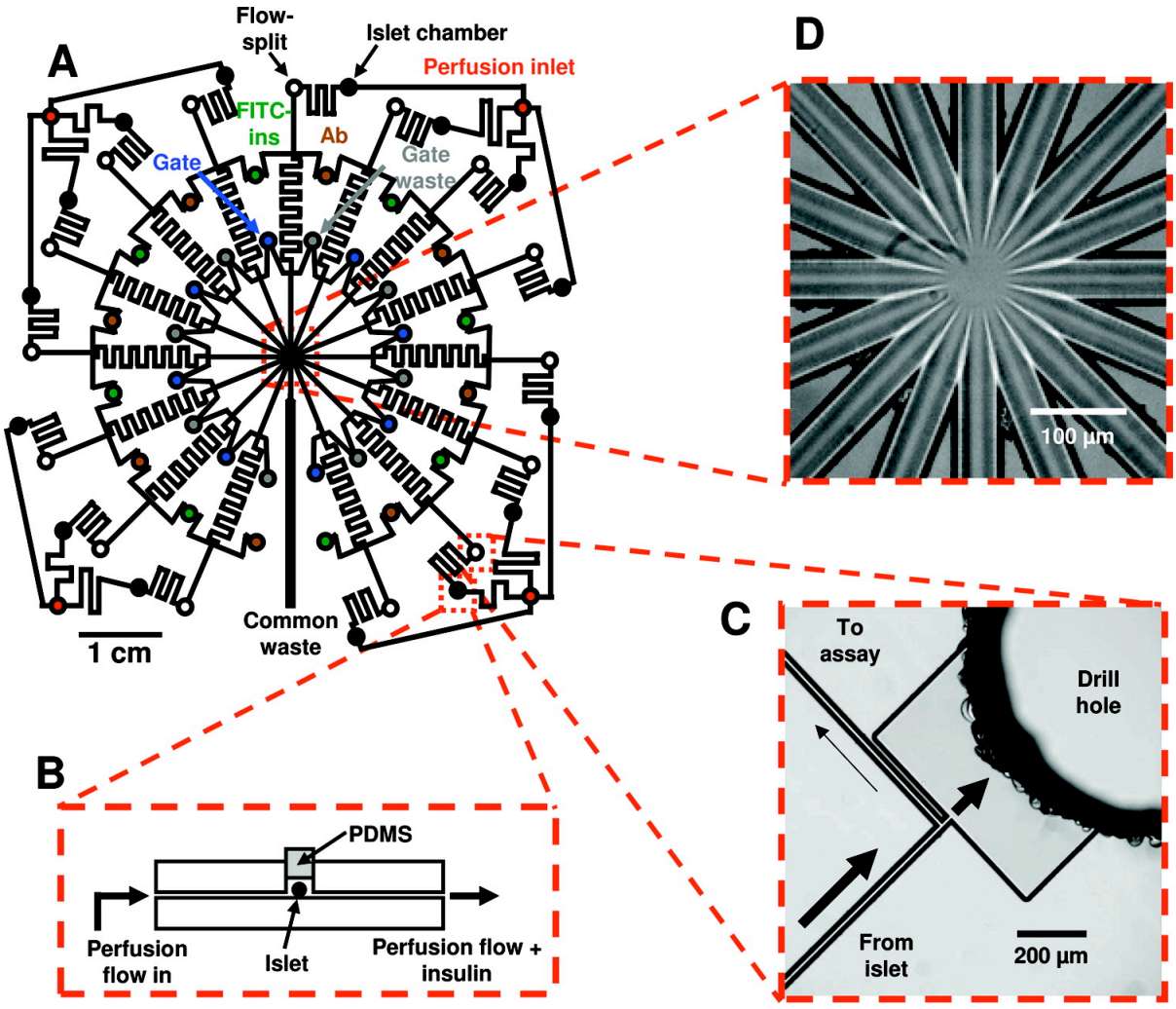

Figure 2.2 Channel layout and images of detailed portions of a microfluidic chip for monitoring insulin secretion from 15 independent islets. (A) The channel network of the entire device. Microfluidic channels are indicated by solid black lines, and circles represent the fluidic reservoirs. Each type of fluidic reservoir (holding a different solution) is color-coded for clarity. (B) Side-view representation (not to scale) of an islet perfusion chamber. (C) CCD image of an on-chip flow-split that allows the fast flowing insulin sampling stream to be compatible with the slower flow of the EOF-driven immunoassay reagents. Arrows indicate direction and estimated magnitude of flow. (D) Brightfield image of the detection area taken with the CCD camera. Flow from 15 separation channels enter the center portion of the chip before flowing out through a single waste channel (bottom center in photograph). Reprinted with permission from (76).

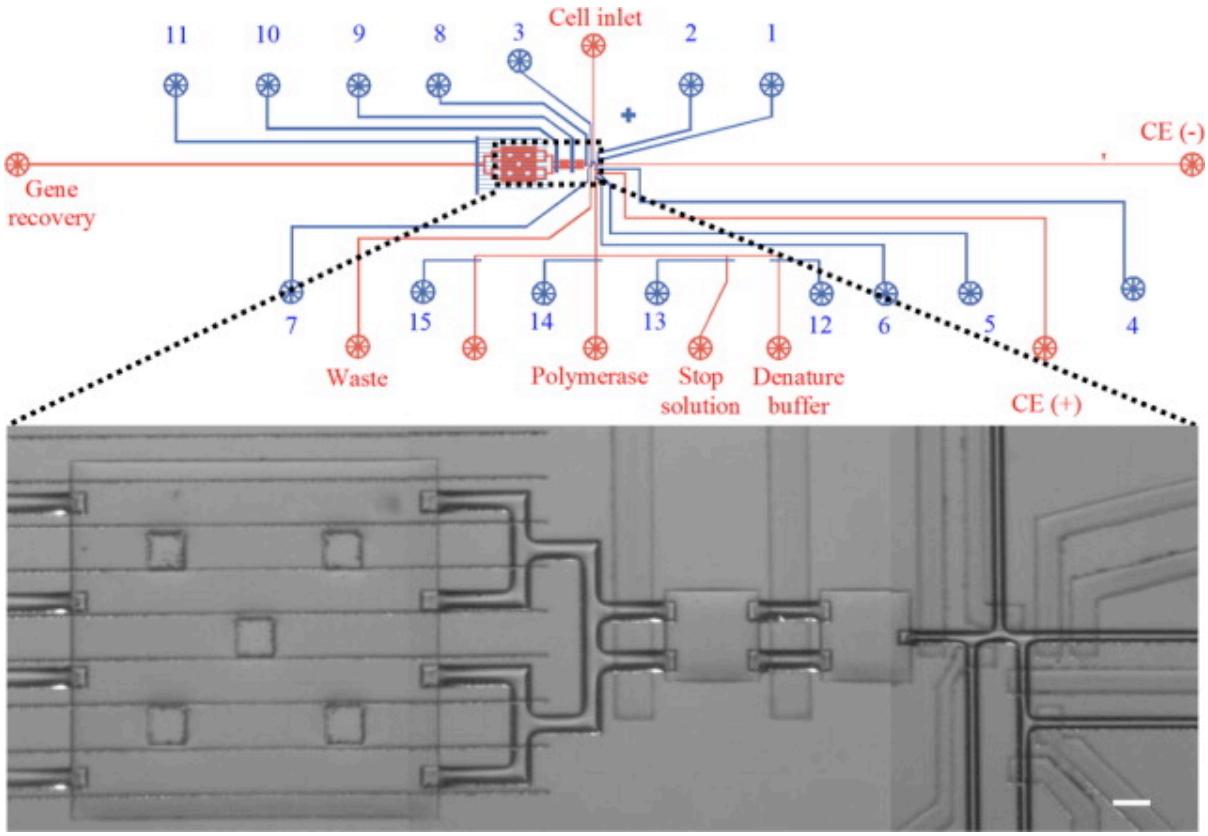

Figure 2.3 Mask design of the integrated microfluidic device. The channel and control layers are depicted in red and blue, respectively. Reservoirs of the channel layer were opened for reagent/cell access while reservoirs of the control layer (1–15) were connected to a pressure controller for valve actuation. For laser-induced fluorescence detection, a 532-nm laser beam was focused in the separation channel with position indicated by a red arrow near the CE (–) reservoir. A zoom-in confocal micrograph shows the details of the core microstructures in this microdevice. (For interpretation of the references to color in this figure legend and the description in the text, the reader is referred to the Web version of this article.). Reprinted from (77) with permission from Elsevier.

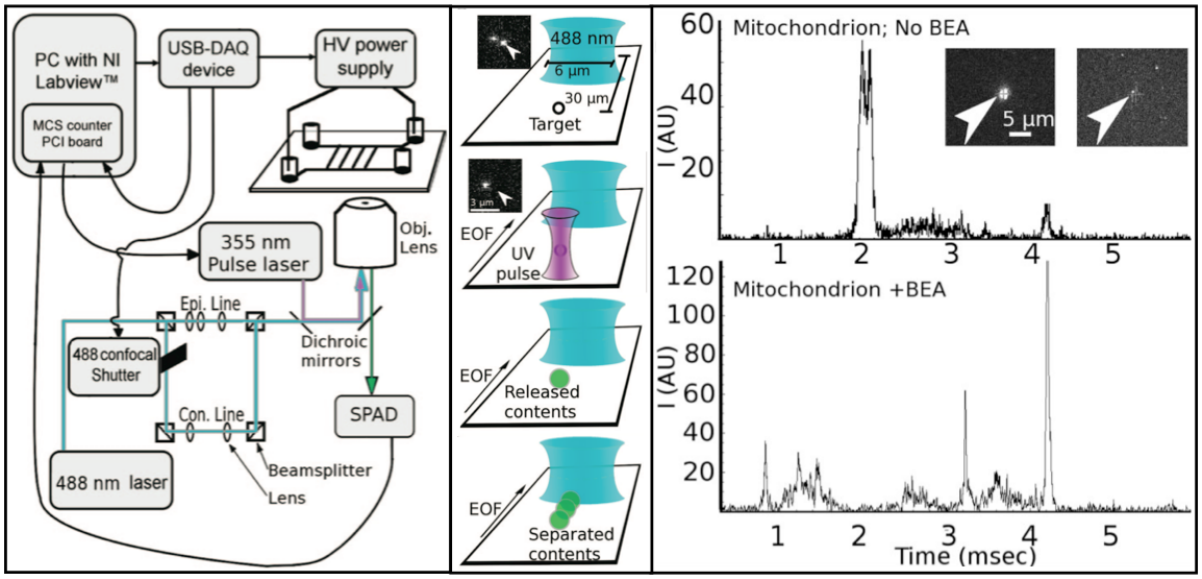

Figure 2.4 (Left) A schematic diagram of the CE-LIF instrument, including the connections among the modules and essential optics. Epi. indicates epifluorescence optics, Con. indicates confocal optics, Obj. indicates objective lens. (Center) Schematics showing the sequence of events in a capillary electrophoresis experiment, starting with a target aligned in the UV laser focus, which caused the target to be lysed with a single nanosecond UV laser pulse; the insets show the target (arrow) before and after lysis. The released components are separated as they travel toward and across the probe volume (blue elliptical focus). (Right) Single-mitochondrion electropherograms obtained without the use of benzylethanolamine (BEA) (top trace) and with BEA (bottom trace). Inset shows before and after photolysis of a mitochondrion prior to capillary electrophoresis separation. Adapted with permission from (82). Copyright 2011 American Chemical Society.

2.7 References

1. T. Lapainis and J. V. Sweedler, *Journal Of Chromatography A*, 2008, **1184**, 144-158.
2. G.-W. Li and X. S. Xie, *Nature*, 2011, **475**, 308-315.
3. N. de Souza, *Nature Publishing Group*, 2011, **8**, 307-307.
4. M. Leslie, *Science*, 2011, **331**, 24-26.
5. S. S. Rubakhin, E. V. Romanova, P. Nemes and J. V. Sweedler, *Nature Publishing Group*, 2011, **8**, S20-S29.
6. Y. Lin, R. l. Trouillon, G. Safina and A. G. Ewing, *Analytical Chemistry*, 2011, **83**, 4369-4392.
7. O. Vesterberg, *Journal Of Chromatography A*, 1989, **480**, 3-19.
8. O. Smithies, *The Biochemical journal*, 1955, **61**, 629-641.
9. H. Hydén, K. Bjurstam and B. McEwen, *Analytical Biochemistry*, 1966, **17**, 1-15.
10. G. T. Matioli and H. B. Niewisch, *Science*, 1965, **150**, 1824-1826.
11. R. Rüchel, *Journal of Chromatography*, 1977, **132**, 451-468.
12. B. B. Anderson, G. Chen, D. A. Gutman and A. G. Ewing, *Journal of Neuroscience Methods*, 1999, **88**, 153-161.
13. B. B. Anderson and A. G. Ewing, *Journal of pharmaceutical and biomedical analysis*, 1999, **19**, 15-32.
14. B. B. Anderson, S. E. Zerby and A. G. Ewing, *Journal of Neuroscience Methods*, 1999, **88**, 163-170.
15. G. Chen and A. Ewing, *Brain Research*, 1995, **701**, 167-174.
16. R. R. Fuller, L. L. Moroz, R. Gillette and J. V. Sweedler, *Neuron*, 1998, **20**, 173-181.
17. H. Miao, S. S. Rubahkin and J. V. Sweedler, *Analytical And Bioanalytical Chemistry*, 2003, **377**, 1007-1013.
18. T. Olefirowicz and A. Ewing, *Journal of Neuroscience Methods*, 1990, **34**, 11-15.
19. R. A. Wallingford and A. G. Ewing, *Analytical Chemistry*, 2001, **60**, 1972-1975.
20. R. T. Kennedy, M. D. Oates, B. R. Cooper, B. Nickerson and J. W. Jorgenson, *Science*, 1989, **246**, 57-63.

21. M. D. Oates, B. R. Cooper and J. W. Jorgenson, *Analytical Chemistry*, 1990, **62**, 1573-1577.
22. S. Hu, L. Zhang, S. N. Krylov and N. J. Dovichi, *Analytical Chemistry*, 2003, **75**, 3495-3501.
23. S. Lillard, E. Yeung and M. McCloskey, *Analytical Chemistry*, 1996, **68**, 2897-2904.
24. Q. Xue and E. S. Yeung, *Analytical Chemistry*, 1994, **66**, 1175-1178.
25. N. Gunasekera, K. J. Olson, K. Musier-Forsyth and E. A. Arriaga, *Analytical Chemistry*, 2004, **76**, 655-662.
26. R. D. Johnson, M. Navratil, B. G. Poe, G. Xiong, K. J. Olson, H. Ahmadzadeh, D. Andreyev, C. F. Duffy and E. A. Arriaga, *Analytical And Bioanalytical Chemistry*, 2007, **387**, 107-118.
27. S. N. Krylov and N. J. Dovichi, *Electrophoresis*, 2000, **21**, 767-773.
28. S. N. Krylov, Z. Zhang, N. W. Chan, E. A. Arriaga, M. M. Palcic and N. J. Dovichi, *Cytometry*, 1999, **37**, 14-20.
29. Y. Chen, G. Xiong and E. A. Arriaga, *Electrophoresis*, 2007, **28**, 2406-2415.
30. L. Cruz, L. L. Moroz, R. Gillette and J. V. Sweedler, *Journal Of Neurochemistry*, 1997, **69**, 110-115.
31. P. D. Floyd, L. L. Moroz, R. Gillette and J. V. Sweedler, *Analytical Chemistry*, 1998, **70**, 2243-2247.
32. J. W. Jorgenson and K. D. Lukacs, *Clinical Chemistry*, 1981, **27**, 1551-1553.
33. J. W. Jorgenson and K. D. Lukacs, *Analytical Chemistry*, 1981, **53**, 1298-1302.
34. I. G. Arcibal, M. F. Santillo and A. G. Ewing, *Analytical And Bioanalytical Chemistry*, 2007, **387**, 51-57.
35. S. Ge, S. Koseoglu and C. L. Haynes, *Analytical And Bioanalytical Chemistry*, 2010, **397**, 3281-3304.
36. W. Huang, F. Ai, Z. Wang and J. Cheng, *Journal of Chromatography B*, 2008, **866**, 104-122.
37. K. J. Olson, H. Ahmadzadeh and E. A. Arriaga, *Analytical And Bioanalytical Chemistry*, 2005, **382**, 906-917.

38. S. M. Kenyon, M. M. Meighan and M. A. Hayes, *Electrophoresis*, 2011, **32**, 482-493.
39. A. Ros, W. Hellmich, J. Regtmeier, T. T. Duong and D. Anselmetti, *Electrophoresis*, 2006, **27**, 2651-2658.
40. C. E. Sims and N. L. Allbritton, *Lab On A Chip*, 2007, **7**, 423-440.
41. R. N. Zare and S. Kim, *Annual Review of Biomedical Engineering*, 2010, **12**, 187-201.
42. J. Landers, ed., *Handbook of Capillary and Microchip Electrophoresis and Associated Microtechniques*, CRC Press, 2007.
43. P. B. Hietpas and A. G. Ewing, *Journal of Liquid Chromatograpy and Related Technologies*, 1995, **18**, 3557-3576.
44. W.-S. Kim, R. L. Dahlgren, L. L. Moroz and J. V. Sweedler, *Analytical Chemistry*, 2007, **74**, 5641-5620.
45. W. Hellmich, D. Greif, C. Pelargus, D. Anselmetti and A. Ros, *Journal of Chromatography*, 2006, **1130**, 195-200.
46. T. Lapainis, C. Scanlan, S. S. Rubahkin and J. V. Sweedler, *Analytical And Bioanalytical Chemistry*, 2007, **387**, 97-105.
47. H. Fang, T. L. Vickrey and B. J. Venton, *Analytical Chemistry*, 2011, **83**, 2258-2264.
48. H. K. Kristensen, Y. Y. Lau and A. G. Ewing, *Journal of Neuroscience Methods*, 1994, **51**, 183-188.
49. D. M. Omiatek, M. F. Santillo, M. L. Heien and A. G. Ewing, *Analytical Chemistry*, 2009, **81**, 2294-2302.
50. A. Amantonico, P. L. Urban and R. Zenobi, *Analytical And Bioanalytical Chemistry*, 2010, **398**, 2493-2504.
51. H. B. Gutstein, J. S. Morris, S. P. Annangudi and J. V. Sweedler, *Mass Spectrometry Reviews*, 2008, **27**, 316-330.
52. R. Haselberg, G. J. de Jong and G. W. Somsen, *Electrophoresis*, 2010, **32**, 66-82.
53. T. Lapainis, S. S. Rubahkin and J. V. Sweedler, *Analytical Chemistry*, 2009, **81**, 5858-5864.
54. P. Nemes, A. M. Knolhoff, S. S. Rubakhin and J. V. Sweedler, *Analytical Chemistry*, 2011, **83**, 6810-6817.

55. M. Perry, Q. Li and R. T. Kennedy, *Analytica Chimica Acta*, 2009, **653**, 1-22.

56. D. A. Bass, J. W. Parce, L. R. Dechatelet, P. Szejda, M. C. Seeds and M. Thomas, *Journal of immunology (Baltimore, Md. : 1950)*, 1983, **130**, 1910-1917.

57. P. Dalerba, S. J. Dylla, I.-K. Park, R. Liu, X. Wang, R. W. Cho, T. Hoey, A. Gurney, E. H. Huang, D. M. Simeone, A. A. Shelton, G. Parmiani, C. Castelli and M. F. Clarke, *Proceedings of the National Academy of Sciences of the United States of America*, 2007, **104**, 10158-10163.

58. H. M. Davey and D. B. Kell, *Microbiological reviews*, 1996, **60**, 641-696.

59. R. L. Fernandes, M. Nierychlo, L. Lundin, A. E. Pedersen, P. E. P. Tellez, A. Dutta, M. Carlquist, A. Bolic, D. Schäpper, A. C. Brunetti, S. Helmark, A. L. Heins, A. D. Jensen, I. Nopens, K. Rottwitt, N. Szita, J. D. van Elsas, P. H. Nielsen, J. Martinussen, S. J. Sørensen, A. E. Lantz and K. V. Gernaey, *Biotechnology Advances*, 2011, **29**, 575-599.

60. S. Müller and G. Nebe-von-Caron, *FEMS Microbiology Reviews*, 2010.

61. J. R. S. Newman, S. Ghaemmaghami, J. Ihmels, D. K. Breslow, M. Noble, J. L. DeRisi and J. S. Weissman, *Nature*, 2006, **441**, 840-846.

62. E. Quintana, M. Shackleton, M. S. Sabel, D. R. Fullen, T. M. Johnson and S. J. Morrison, *Nature*, 2008, **456**, 593-598.

63. J. Ando, G. Bautista, N. Smith, K. Fujita and V. R. Daria, *Review of Scientific Instruments*, 2008, **79**, 103705.

64. N. Maghelli and I. M. Tolić-Nørrelykke, *Methods in Cell Biology: Volume 95*, 2010, **97**, 173-183.

65. K. Schuetze, Y. Niyaz, M. Stich and A. Buchstaller, *Methods in Cell Biology*, 2007, **82**, 649-673.

66. G. D. M. Jeffries, J. S. Edgar, Y. Zhao, J. P. Shelby, C. Fong and D. T. Chiu, *Nano Letters*, 2007, **7**, 415-420.

67. A. Ewing, *Journal of Neuroscience Methods*, 1993, **48**, 215-224.

68. A. W. Lantz, B. F. Brehm-Stecher and D. W. Armstrong, *Electrophoresis*, 2008, **29**, 2477-2484.

69. A. W. Lantz, B. Bisha, M.-Y. Tong, R. E. Nelson, B. F. Brehm-Stecher and D. W. Armstrong, *Electrophoresis*, 2010, **31**, 2849-2853.

70. Q. Yang, X. Zhang, X. Bao, H. Lu, W. Zhang, W. Wu, H. Miao and B. Jiao, *Journal of Chromatography*, 2008, **1201**, 120-127.

71. W. Xie, A. Xu and E. S. Yeung, *Analytical Chemistry*, 2009, **81**, 1280-1284.

72. A. K. Boardman, S. C. McQuaide, C. Zhu, C. D. Whitmore, M. E. Lidstrom and N. J. Dovichi, *Analytical Chemistry*, 2008, **80**, 7631-7634.

73. A. Boardman, T. Chang, A. Folch and N. J. Dovichi, *Analytical Chemistry*, 2010, **82**, 9959-9961.

74. P. J. Marc, C. E. Sims, M. Bachman, G. P. Li and N. L. Allbritton, *Lab On A Chip*, 2008, **8**, 710.

75. J. S. Mellors, K. Jorabchi, L. M. Smith and J. M. Ramsey, *Analytical Chemistry*, 2010, **82**, 967-973.

76. J. F. Dishinger, K. R. Reid and R. T. Kennedy, *Analytical Chemistry*, 2009, **81**, 3119-3127.

77. B.-h. Chueh, C.-W. Li, H. Wu, M. Davison, H. Wei, D. Bhaya and R. N. Zare, *Analytical Biochemistry*, 2011, **411**, 64-70.

78. C.-X. Xu and X.-F. Yin, *Journal Of Chromatography A*, 2011, **1218**, 726-732.

79. P. A. Quinto-Su, H. H. Lai, H. H. Yoon, C. E. Sims, N. L. Allbritton and V. Venugopalan, *Lab On A Chip*, 2008, **8**, 408.

80. R. B. Brown, J. A. Hewel, A. Emili and J. Audet, *Cytometry*, 2010, **77A**, 347-355.

81. D. Jiang, C. E. Sims and N. L. Allbritton, *Electrophoresis*, 2010, **31**, 2558-2565.

82. P. B. Allen, B. R. Doepker and D. T. Chiu, *Analytical Chemistry*, 2009, **81**, 3784-3791.

83. A. Ashkin and J. M. Dziedzic, *Science*, 1987, **235**, 1517-1520.

84. A. Ashkin, J. M. Dziedzic and T. Yamane, *Nature*, 1987, **330**, 769-771.

85. G. Volpe, G. P. Singh and D. Petrov, *Applied Physics Letters*, 2006, **88**, 231106.

86. T. Alexander, P. Pellegrino and J. Gillespie, *Applied Spectroscopy*, 2003, **57**, 1340-1345.

87. D. J. Carnegie, D. J. Stevenson, M. Mazilu, F. Gunn-Moore and K. Dholakia, *Optics Express*, 2008, **16**, 10507-10517.

88. J. L. Nascimento, E. L. Botvinick, L. Z. Shi, B. Durrant and M. W. Berns, *Journal Of Biomedical Optics*, 2006, **11**, 044001.

89. B. Shao, L. Z. Shi, J. M. Nascimento, E. L. Botvinick, M. Ozkan, M. W. Berns and S. C. Esener, *Biomedical Microdevices*, 2007, **9**, 361-369.

90. W. Hellmich, C. Pelargus, K. Leffhalm, A. Ros and D. Anselmetti, *Electrophoresis*, 2005, **26**, 3689-3696.

91. N. R. Munce, J. Li, P. R. Herman and L. Lilge, *Analytical Chemistry*, 2004, **76**, 4983-4989.

92. J. K. Valley, A. T. Ohta, H.-Y. Hsu, S. L. Neale, A. Jamshidi and M. C. Wu, *IEEE Transactions on Biomedical Circuits and Systems*, 2009, **3**, 424-431.

93. H. Wu, A. Wheeler and R. N. Zare, *Proceedings of the National Academy of Sciences of the United States of America*, 2004, **101**, 12809-12813.

94. J. D. Adams, U. Kim and H. T. Soh, *Proceedings of the National Academy of Sciences of the United States of America*, 2008, **105**, 18165-18170.

95. C.-L. Chen, K.-C. Chen, Y.-C. Pan, T.-P. Lee, L.-C. Hsiung, C.-M. Lin, C.-Y. Chen, C.-H. Lin, B.-L. Chiang and A. M. Wo, *Lab On A Chip*, 2011, **11**, 474.

96. S.-H. Song, H.-L. Lee, Y. H. Min and H.-I. Jung, *Sensors And Actuators B-Chemical*, 2009, **141**, 210-216.

97. P. Y. Chiou, A. T. Ohta and M. C. Wu, *Nature*, 2005, **436**, 370-372.

98. Y.-H. Lin and G.-B. Lee, *Sensors And Actuators B-Chemical*, 2010, **145**, 854-860.

99. Y.-H. Lin, W.-Y. Lin and G.-B. Lee, *IEEE Nanotechnology Magazine*, 2009, **3**, 6-11.

100. S. Kühn, B. S. Phillips, E. J. Lunt, A. R. Hawkins and H. Schmidt, *Lab On A Chip*, 2009, **10**, 189.

101. D. T. Chiu, *Analytical And Bioanalytical Chemistry*, 2006, **387**, 17-20.

102. C.-M. Lin, Y. S. Lai, H. P. Liu, C.-Y. Chen and A. M. Wo, *Analytical Chemistry*, 2008, **80**, 8937-8945.

103. S. L. Stott, C.-H. Hsu, D. I. Tsukrov, M. Yu, D. T. Miyamoto, B. A. Waltman, S. M. Rothenberg, A. M. Shah, M. E. Smas, G. K. Korir, F. P. Floyd, A. J. Gilman, J. B. Lord, D. Winokur, S. Springer, D. Irimia, S. Nagrath, L. V. Sequist, R. J. Lee, K. J. Isselbacher, S. Maheswaran, D. A. Haber and M. Toner, *Proceedings of the National Academy of Sciences of the United States of America*, 2010, **107**, 18392-18397.

104. S. H. Au, P. Kumar and A. R. Wheeler, *Langmuir : the ACS journal of surfaces and colloids*, 2011, **27**, 8586-8594.

105. M. J. Jebrail, H. Yang, J. M. Mudrik, N. M. Lafrenière, C. McRoberts, O. Y. Al-Dirbashi, L. Fisher, P. Chakraborty and A. R. Wheeler, *Lab On A Chip*, 2011, **11**, 3218.

3 Updates and improvements to the multi-channel capillary electrophoresis-laser-induced native fluorescence instrument

Notes and Acknowledgments

I would like to acknowledge Drs. Ted Lapainis and Cory Scalan for their initial work on designing and constructing the first-generation instrument[1] and for training me when I first joined the Sweedler laboratory. I would also like to thank Dr. Stanislav S. Rubhakin for providing samples and advice, Prof. Jonathan V. Sweedler for support, advice, and funding, and the SCS Machine Shop for their advice and work. I would also like to acknowledge Bill Hug, Ray Reid, and Prashant Oswal at Photon Systems Inc. for providing the hollow cathode ion laser and their help with troubleshooting. This work was supported by the National Institute of Neurological Disorders and Stroke under award number R01 NS031609 and the National Institutes of Health under award number R01 DK070285.

3.1 Introduction

Understanding cell-to-cell communication in the brain is important for identifying normal and pathological brain functioning. Biogenic amines, which include catecholamines (*e.g.*, dopamine) and indolamines (*e.g.,* serotonin), are of particular interest due to their presence throughout the central and peripheral nervous systems of many species and involvement in a range of vital biological functions such as sleep regulation, memory, and mood, as well as their significance in varied pathologies like Parkinson's disease and Irritable Bowel Syndrome.[2, 3] There are, however, several challenges involved in detecting and identifying these compounds. Within a given sample, the analytes of interest are typically both mass- and concentration-limited, with values generally in the femtogram (attomole) range or lower. Also, the analytes reside in a complicated matrix of proteins, lipids, salts, and other biological compounds, which can interfere with identification. Another concern is the relatively rapid degradation of catecholamines and indolamines compared to other biological molecules.[4] Several separation and detection techniques have been used to study biogenic amines, such as high pressure liquid chromatography with electrochemical detection[5-9] and gas chromatography with mass spectrometric detection.[10-

[12] One technique that alleviates the above concerns is capillary electrophoresis with laser-induced fluorescence detection (CE-LIF).

Capillary electrophoresis (CE) is a separation technique well suited for studying trace analytes such as biogenic amines.[13-15] CE is used to separate charged analytes, based on their mass-to-charge ratio, in the presence of an electric field (Figure 3.1). A typical CE set up involves a fused silica capillary with each end immersed in a buffered solution. On the inner walls of the fused silica capillary, ionized silanol groups attract positively charged buffer molecules and form an electrical double layer. When a voltage is applied to the capillary, a constant electric field is produced and bulk fluid flow is towards the cathode. This bulk flow enables both positively and negatively charged analytes to be separated since the electroosmotic flow should be greater than the molecules' electrophoretic velocity.[16]

There are several benefits associated with CE. It is amenable to mass- and volume-limited samples, as a sample injection is typically in the low nanoliter range. It affords high separation efficiencies and provides relatively rapid analysis times compared with chromatography. CE is also compatible with biological environments. Furthermore, there is a number of CE modes and methods that can be modified in order to separate a variety of analytes, such as micellar electrokinetic chromatography[17-19], sample stacking,[20, 21] and dynamic pH junction.[22, 23]

Detection after separation can be accomplished by a variety of methods; three of the most widely used are electrochemistry,[24-27] mass spectrometry,[28-32] and laser-induced fluorescence (LIF).[33-35] Fluorescence can be both a sensitive and selective technique that provides low limits of detection (LOD), with values in the nanomolar to picomolar (attomole to zeptomole) range. Also, several classes of biological molecules, such as catecholamines and indolamines, are natively fluorescent, which reduces sample preparation and allows for analyte identification based on the unique spectral characteristics of the analytes. For those molecules that are not natively fluorescent, many derivatization reactions exist that can be used to attach a fluorescent moiety to the analyte of interest.[36-39] Although there is a loss of selectivity and chemical information when derivatizing, the LODs can be in the femtomolar (yoctomole) range, due to the high quantum yields typical to synthetic

fluorophores.[40, 41] Interfaced with CE, fluorescence detection has been used to detect amino acids,[42, 43] peptides,[44] proteins,[45, 44] carbohydrates,[46] nucleotides,[47, 48] and pharmaceuticals[49] within complex samples.

In order to effectively detect and identify trace levels of biogenic amines within volume-limited samples, the Sweedler group has designed and constructed several generations of CE-LINF instruments, with the first systems designed around a charge coupled device detector and frequency-doubled lasers with their continuum sources.[50-55] A more recent instrument design built by Lapainis and Scanlan uses a metal vapor laser and a series of photomultiplier tubes.[1] The multi-channel capillary electrophoresis-laser-induced native fluorescence system (MC-CE-LINF) uses deep UV excitation to selectively excite catecholamines and indolamines and detects the fluorescence emission across three detectors, which provides wavelength-resolved information for analyte identification. This instrument has been modified and updated to improve performance and to interface with other instrumentation in order to enhance its sampling abilities, which are detailed in Chapter 5.

3.2 Materials and methods

A list of abbreviations can be found in the Appendix.

3.2.1 Chemicals

Chemicals, unless otherwise noted, were from Sigma Aldrich (St. Louis, MO) and were reagent grade or higher. Citric acid sheath buffer (25 mM, pH 2.25) was made by dissolving 5.25 g of $C_6H_8O_7 \cdot H_2O$ in 1 L of ultrapure deionized water (Elga Purelab Ultra, Siemens Water Technologies, Warrendale, PA). Electrophoresis buffers were made by diluting a stock solution of 50 mM borate buffer, pH 8.8, which was prepared by dissolving 9.2 g of $Na_2B_4O_7 \cdot 10H_2O$ and 3.0 g of $B(OH)_3$ in 1 L of ultrapure deionized water or by dilution and/or titrating the sheath buffer as noted. For surfactant-containing electrophoresis buffers, 0.72 g of sodium dodecyl sulfate (SDS) was added to 50 mL of diluted borate buffer, pH 8.8, sonicated for 2 min to dissolve, and filtered with a 0.22 μm syringe filter (Nalgene, Rochester, NY). Serotonin (5-HT) (Alfa Aesar, Ward Hill, MA), dopamine (DA), tyrosine (Tyr),

tyramine (TyrA), tryptamine (TrpA), octopamine (OA), norepinephrine (NE), and epinephrine (E) were dissolved in 2.5 mM citric acid, pH 5.5, and sonicated on ice for 30 min if needed. Tryptophan (Trp), N-acetylserotonin (NAS), 5-hydroxyindole acetic acid (HIAA), melatonin (MT), 5-hydroxytryptophan (HTP), 5-methoxytryptamine (MOT) (TCI America, Portland, OR), and tryptophol (TOL) (Research Organics, Inc., Cleveland, OH) were dissolved in 2.5 mM citric acid, pH 5.5, + 10% v/v acetone and sonicated on ice for 30-60 min. Standard buffers were prepared by diluting the sheath buffer 1:10 with ultrapure deionized water and titrating to pH 5.5 with 10 M NaOH (20 g of NaOH pellets dissolved in 0.05 L of ultrapure deionized water). Sulphorhodamine-101 and fluorescein were prepared in ultrapure deionized water. Standard stock solutions were diluted in either 1 mM borate buffer, pH 8.8 (1:50 dilution of stock borate electrophoresis buffer) or modified Grey's balanced salt solution (mGBSS), pH 7.2, which consisted of 1.5 mM $CaCl_2$ (0.22 g), 4.9 mM KCl (0.37 g), 0.2 mM KH_2PO_4 (0.03 g), 11 mM $MgCl_2$ (2.24 g), 0.3 mM $MgSO_4$ (0.04 g), 138 mM NaCl (8.06 g), 27.7 mM $NaHCO_3$ (2.33 g), 0.8 mM Na_2HPO_4 (0.11 g), 25 mM HEPES (5.95 g), and 10 mM glucose (1.80 g) dissolved in 1 L of ultrapure deionized water. All buffers were filtered by a 0.45 µm bottle-top filter system (Nalgene, Rochester, NY) and degassed under vacuum with stirring for 30-60 min. NaOH (~0.1 M) was prepared by dissolving one pellet (~0.0025 g) in 0.025 L of ultrapure deionized water.

3.2.2 Animals

Animals were housed and cared for as described in animal protocols in full compliance with NIH guidelines for the humane care and treatment of animals, approved by IACUC and supervised by the Division of Animal Resources at the University of Illinois at Urbana-Champaign.

The pineal glands were isolated from the central nervous systems of mice (YFPAG9B WT, 5-8 mo old) and 3-4 glands were pooled for analysis. Sacrifice occurred at 10:45 AM and pineal preparation and dissection was completed within 2 h. Glands were treated in 10% trypsin for 1 h before manual trituration and stored in acidified methanol (90:9:1 methanol:water:acetic acid) on ice until analysis.

3.2.3 Biological samples

Biological samples were extracted using a solution of 90:9:1 methanol:water:acetic acid and diluted 1:10 in 1 mM borate buffer, pH 8.8, + ~1900 nM sulphorhodamine-101.

3.2.4 Hydrofluoric acid etching

Hydrofluoric acid (HF) etching of the capillary inlet and outlet is used to shape the ends into sharply tapered tips with a 40° angle (Figure 3.2).[56] The fused silica capillary dimensions are 50 µm inner diameter, 360 µm outer diameter, and 85-120 cm in length (Polymicro Technologies, Phoenix, AZ). The ends are scored and snapped to provide a relatively even surface for etching. Approximately 1 cm of the capillary's polyimide coating is burned off of each end and the tips cleaned with methanol. A container is filled to 5 mm of depth with 48% HF and covered with isooctane to prevent HF fumes from rising. The capillary tip is pushed through a FEP sleeve (Upchurch Scientific, Oak Harbor, WA) held tightly in a customized Teflon holder, which maintains the tip position during etching, until the tip touches the bottom of the container. The capillary has isooctane continuously pumped through the non-submersed end via a syringe to prevent the inner walls of the submerged end from being etched. After two hours, the etched tip is rinsed with $Na_2B_4O_7 \cdot 10H_2O$ (Borax, Henkel Corp., Billerica, MA) and water and the process is repeated for the other end.

3.2.5 Instrument design and construction

Unless otherwise noted, all laboratory-built and custom-built components have been designed and fabricated in-house either within the laboratory or by the SCS Machine Shop. The injection port (Figure 3.3A) for the instrument is housed on a non-conductive breadboard platform on a microscope (AxioObserver A1, Carl Zeiss, Jena, Germany), contained in a clear Plexiglas box. The capillary inlet has PEEK fittings (Upchurch Scientific, Oak Harbor, WA) and a FEP sleeve attached to allow for fast and easy switching between syringes and the capillary holder. The injection port consists of a stainless steel disk with bored holes to hold the microvials used for sample injection and the buffer vials used for electrophoresis. This disk is mounted to the breadboard platform on a T-shaped Plexiglas

holder with a 2.5", ¼"-20 screw that connects the disk and holder to the platform. This allows the disk to rotate and the holder to translate a short distance, which is helpful for quickly injecting sample and placing the capillary inlet in the buffer vial. The disk is grounded to a copper grounding strap located above the optical table. The capillary is held in place during electrophoresis by a capillary holder that consists of an alligator clip mounted in an acetal resin block (Delrin, E. I. duPont de Nemours & Co., Wilmington, DE) which is held in place by a U-shaped slot with set screws for manipulation. This is mounted on a ¼'-20-tapped acetal resin post.

The capillary is held in place in the instrument by a custom-built acetal resin sheath flow cell (Figure 3.3B). It enters at the top of the cell and is held in place by liquid-tight fittings (Upchurch Scientific, Oak Harbor, WA). The sheath buffer enters the cuvette from the right side with respect to the optical table and exits from the bottom of the sheath flow cell. The quartz cuvette (Starna Cells, Atascadero, CA) used for excitation and detection of eluents is open on both ends and is attached to the top and bottom pieces of the sheath flow cell with Tra-Cast 3103 epoxy (Henkel Corp., Billerica, MA).

The current optical layout (Figures 3.4 and 3.5) was adapted from a previous version.[1] Deep UV radiation (224.6 nm) from a HeAg hollow cathode ion laser (HeAg70, Photon Systems Inc., Covina, CA) is spectrally filtered using a four-bounce mirror configuration, attached to the front of the laser head. The beam is directed via two UV-coated mirrors (Thorlabs, Newton, New Jersey) into a laboratory-built lightproof, non-conductive box and breadboard, which houses the detection optics and protects against spurious arcing. The collimated beam is nominally focused using a plano-convex lens (OptoSigma, Santa Ana, CA) to a 50 µm spot directly below the outlet of the capillary, which has been HF-etched to a cone-shaped tip and is housed in a custom-built sheath flow cell, as described above. As analytes elute from the capillary they are excited by the focused beam and emit fluorescence, which is collected and collimated by a 15x all-reflective objective (13596, Newport, Irvine, CA). The fluorescence is directed toward the three photomultiplier tube (PMT) detectors (H6780-06, Hamamatsu, Middlesex, NJ) by two dichroic mirrors (310dcxxr-haf #110258 and 400dcxru #111563, Chroma Technology, Rockingham, VT), with

transition points at 310 nm and 400 nm, respectively. The first detector (PMT "blue") measures emission from 250-310 nm, the second detector (PMT "green") measures emission from 310-400 nm, and the third detector (PMT "red") measures emission from 400 nm and above. The laser and PMTs are synchronized and controlled by software written in LABView and provided by Photon Systems Inc. Posts, post holders, and other optical mounts were purchased from Newport (Irvine, CA), Melles Griot (Albuquerque, NM), or custom-built. Optical mounts for the focusing optic and the collection optic are coated in Vinyl Liquid Electric Tape (Star Brite, Ft. Lauderdale, FL) and electrical tape (Scotch Super 88 electrical tape, 3M, St. Paul, MN) to reduce arcing from the capillary outlet and tubing to the mounts.

Negative voltage for electrophoresis is applied to the sheath flow waste by a stainless steel cylinder that is connected to a power supply (PS/MJ30N0400-11, Glassman High Voltage, High Bridge, NJ) and laboratory-built control box. A 10 kΩ resistor and a digital multimeter (Fluke 76, Fluke Corp., Everett, WA) are part of the circuit and are used to measure the current across the capillary.

Sheath buffer is gravity-driven and flow can be adjusted by a right angle switching valve (Upchurch Scientific, Oak Harbor, WA). High purity Teflon PFA Plus tubing and appropriate fittings were purchased from Upchurch Scientific. All tubing is further encased within FEP-lined polyethylene tubing (McMaster-Carr, Elmhurst, IL) to reduce static attraction and arcing during electrophoresis. Tubing between the optics box and the sheath box is also surrounded by four 16 oz. polyethylene containers and electrical tape (Scotch Super 88 electrical tape, 3M, St. Paul, MN).

3.2.6 Two power supplies

A goal was to increase the separation speed by increasing the voltage applied to the capillary using two power supplies. In order to use two power supplies simultaneously, the injection port ground is disconnected and high voltage wire with an eyelet on one end is attached by two nuts to the 2.5" ¼-20 screw that connects the disk and holder to the platform. This power supply (PS/MJ30P0400, Glassman High Voltage, High Bridge, NJ) and control box are configured similarly to the set up used at the sheath flow waste outlet,

except that the polarity is reversed from negative to positive so that the direction of electroosmotic flow remains toward the cathode.

3.2.7 Electrophoresis

The sheath flow buffer was 25 mM citric acid, pH 2.25, and the flow rate was 0.2 mm/s for all experiments. The electrophoresis buffers and sample buffers varied as stated in the text and figure captions. The voltage for all experiments was -30 kV unless otherwise stated. The injection volume was 14.7 nL for a 30 s hydrodynamic injection, which was performed by lowering the sheath flow waste outlet by 32.5 cm. The typical laser pulse energy was between 1.5 μJ/pulse and 3 μJ/pulse.

The capillary was conditioned at the beginning of the day with 0.1 M NaOH for 15-20 min, followed by water for 5 min, and then electrophoresis buffer for a minimum of 5 min.

3.2.8 Serial injections

Serial injections of four to six sample injections per electrophoretic run were performed. Each sample was injected for 30 s at 3 min intervals. The high voltage interlocks were disrupted during each injection.

3.2.9 Data analysis

Data analysis was performed in IgorPro 5.05A (WaveMetrics Inc., Lake Oswego, OR). An automated data analysis script was written that reduces the user input to a single command. Output consists of four tables of calculated values with four corresponding color-coded graphs displaying the raw data, 6-point boxcar averaged data, normalized (with respect to the laser pulse energy) data, and both normalized and boxcar averaged data. The baseline range (30 points, 10 s) with the lowest standard deviation is determined and used to calculate the limits of detection (LOD) for each PMT channel. Ratiometric analysis (calculating the intensity ratio between peak maxima in each of the PMT channels) is also automated to aid in analyte identification.

3.2.10 Limits of detection

LODs and concentration of analytes were determined by generating calibration curves for each analyte under the appropriate conditions. Analyte concentrations ranged from the micromolar to the low nanomolar, within physiological limits and at maximum an order of magnitude greater than LODs. The criterion for calculating the LODs was three times the standard deviation of the baseline.

3.3 Results and discussion

3.3.1 Improvements

The MC-CE-LINF instrument has a unique combination of features, and notable aspects include deep UV excitation, synchronization between the laser and PMTs, multiple detectors, a tapered outlet, post-column detection, and the ability to independently optimize the separation and detection conditions.

Deep UV excitation specific for exciting biogenic amines allows for selective excitation and reduces the complexity of electropherograms. Utilizing native fluorescence also reduces sample preparation since no derivatization is necessary. Better LODs are possible compared with similar instruments since the laser wavelength corresponds to an absorption maximum for catecholamines[57] and is near indolamine absorption maxima.[58, 59]

This excitation and detection system is unique in that the laser and PMTs are controlled through the proprietary circuit board design and control program provided by Photon Systems Inc. The laser pulse length and the PMT on-time can be synchronized, resulting in reduced dark noise and low background signal. The laser settings and each PMT setting can also be changed as a run progresses, allowing for adjustments to be made in real time.

Multiple detection channels enable unambiguous identification. The net intensity for a given peak is determined in each channel and used to calculate three different ratios (green/blue or G/B, blue/red or B/R, and green/red or G/R) (Figure 3.6). These ratios provide information on the unique spectral characteristics of the analytes and, when combined with migration time information, can allow for identification without using a

complimentary technique or sample spiking, as one would have to do with a traditional single channel system. Ratiometry is also useful for distinguishing between co-eluting peaks. For example, under certain conditions serotonin and dopamine co-elute, as does dopamine and octopamine. Determining the ratio of the signals can distinguish whether one, both, or neither analyte is present and provide the concentration of the analytes.

An HF-etched capillary outlet reduces background signal from scattering off of the edge of the capillary wall and changes the sheath flow profile around the outlet. This allows for the excitation beam to be focused closer to the outlet, which further improves the net signal since the analytes have not diffused as much into the sheath buffer.

Post-column detection has been used for CE-LIF since the 1980s.[60, 35] For deep UV excitation, post-column detection is critical for suitable detection levels as light scattering is proportional to λ^{-4}. Also, metal impurities within the fused silica capillary can luminesce in the UV, which can interfere with the detected signal. Another benefit of post-column detection is the ability to independently optimize the separation and detection conditions.[61] This is useful as maximal fluorescence for biogenic amines is under acidic conditions but the highest resolution separation conditions are typically neutral or basic.

Other miscellaneous improvements to the instrument include determining the appropriate adhesive for the sheath flow cell, redesigning some of the optical mounts and the sheath flow cell, and updating the electrical insulation.

Several adhesives were rigorously tested for chemical resistance (organic, aqueous, and acidic conditions) and longevity, and the only one that was found to be suitable was Tra-Cast 3103 epoxy, followed by Torr Seal (Varian, Lextington, MA). None of the cuvettes that have been sealed with Tra-Cast 3103 have leaked, even after three or more years of continuous use with acidic buffer. Previously, the cuvettes would begin leaking after 3-6 months of continuous use and would either have to be replaced or sealed, both of which require realignment of the instrument.

The first-generation MC-CE-LINF instrument experienced significant signal instability, primarily from the focusing optic and collection optic mounts, as well as the sheath flow cell mount. The xyz location of the mounts would shift over time due to compression of the

post holder pads from the combined weight and extended center-of-mass of the optics and mounts (both optics are mounted in 5-axis mounts and extend several inches along the optical axis). The optics would not only shift but also twist away from ideal alignment. The tip and tilt controls on the 5-axis mounts were another source of instability. Adjustments to these axes would not result in smooth angular motion but would require monitoring over the course of 30-60 min or more to ensure that the axes had reached a stable location. To resolve this, several designs were tested and the final solution was to update the mounts and replace the posts and post holders with x, y, and z translation stages and stainless steel mounting blocks. The translation stages provide a sturdy base for the optics and mounts and allow for finer control of the xyz location of the optics. Alignment of the optics is also easier due to the larger distances that can be traveled (1”-2” in the x, y, and z directions) without unscrewing the mounts and the stability of the translation stages can be greater than that of the xyz axes on the mounts.

The sheath flow cell was also redesigned to improve stability and ease of alignment. The original sheath flow cell was mounted on xy and z translation stages with a right angle adaptor bracket and four posts. Alignment of the sheath flow cell to the mount required using an Allen wrench and gently adjusting all four post set screws until the sheath flow cell was straight, which was time-consuming and unreliable. The cell was redesigned to mount to a magnetic kinematic base, providing repeatability of less than 100 μrad. It can be snapped into place and removed without requiring extensive optical realignment.

A significant change between the first-generation instrument and the current is the location of the high voltage line. The original instrument applied high voltage at the capillary inlet on the injection port. Given the desire to hyphenate the front end of the MC-CE-LINF to other instrumentation, the high voltage line was moved to the sheath flow waste outlet (Figure 3.4). An unforeseen consequence of this modification was that arcing occurred between the sheath flow tubing and nearby objects (including the optics). Several steps were taken to resolve this. All of the sheath flow tubing was encased in FEP-lined polyethylene tubing, which is characterized as an electrical insulator and can resist at minimum 500 V/0.001” of material thickness. As the wall thickness is 0.063”, this translates

into a breakdown voltage of 31.5 kV. Areas that were particularly prone to arcing or static build up were further enclosed by 16 oz. polyethylene cups and Scotch Super 88 electrical tape, which has a dielectric strength of 10 kV. Finally, several coats of Vinyl Liquid Electrical Tape (which has a dielectric strength of 1778 V/0.001" thickness) were painted on the stainless steel mounting blocks beneath the optics' translation stages. Areas that were unable to be painted were wrapped several times with Scotch Super 88 electrical tape. In combination, these steps reduced the likelihood of arcing during electrophoresis.

3.3.2 Performance

LODs for this instrument are either similar or improved compared to the first-generation system (Table 3.1). Improvements are primarily due to HF-etching the capillary outlet, more stable optical mounting, and a different alignment scheme. Compared to other instruments with similar excitation wavelengths, the MC-CE-LINF demonstrates superior performance, especially for catecholamines. This is primarily due to the close overlap between the laser wavelength (224.6 nm) and the $S_2 \rightarrow S_0$ transition in catecholamines, which has a larger absorption cross-section compared with the $S_1 \rightarrow S_0$ transition. Overall the best LODs obtained are 700-900 pM for serotonin and 2-4 nM for its metabolites. Typical LODs for serotonin are 1-3 nM. Typical catecholamine LODs are in the 10 nM to 45 nM range, which is a roughly 200-fold improvement over other instruments.

Representative electropherograms are shown in Figures 3.7 and 3.8. The instrument is capable of separating and detecting a wide range of indolamines and catecholamines in a single run. Within 30 min, 11 analytes of interest were well resolved without any overlap under these conditions, which mimic biological sample conditions. Table 3.2 lists the LODs and standard deviations for the standards in Figure 3.7. Notable are the physiologically relevant LODs (low nanomolar levels for most analytes) and relatively narrow peak widths (4-8 s full width at half maximum net intensity (FWHM)), given the conductivities of the sample matrix (19-21 mS/cm) versus the electrophoresis buffer (2.8 mS/cm). Typically, ideal conditions for trace analyte detection require that the sample have a lower conductivity than the background electrolyte, which enables field-amplified sample stacking (FASS)[21, 62] to occur. FASS makes use of differences in conductivity to effect concentration of analytes.

The sample is contained within a lower conductivity buffer (typically 10-fold lower), relative to the higher conductivity electrophoresis buffer. When voltage is applied, the sample plug experiences greater electric field strength compared to the electrophoresis buffer. The analytes' electrophoretic velocity is increased until the boundary between the lower conductivity sample plug and the higher conductivity BGE is reached. Here, the analytes experience a significant change in electric field strength and are slowed and concentrated into a narrow plug. This results in a net concentration or analytes and band narrowing during electrophoresis. This technique is demonstrated for a biological sample in Figure 3.8.

In order to reduce the sample run time and further improve LODs, another power supply and control box was added to the instrument. Typically, the breakdown voltage of air under ambient conditions is approximately 33 kV/cm, and many of the power supplies used for electrophoresis have an upper limit of ±30 kV. The unique design of the MC-CE-LINF is ideal for testing multiple high voltage sources on the same instrument. By combining positive polarity on the capillary inlet and negative polarity at the capillary outlet, the total voltage drop across the capillary was increased. A total of 42 kV was applied to the capillary without arcing and used to successfully perform a series of runs to compare migration time differences as a function of voltage (Figure 3.9). Compared with the usual separation voltage of -30 kV, a 55% reduction in migration time was observed when applying 42 kV, although the net intensity of the peak remained the same in all runs. For analytes that experience band broadening, using a higher voltage drop should also result in narrower peak widths and higher net intensities and therefore better LODs. The location of the second high voltage line also enables easy and quick removal to prevent interference with other sensitive instrumentation within the injection box.

Serial injections were also investigated as a means to reduce total run time. Figure 3.10 shows a series of four injections of 780 nM serotonin, run under field-amplified sample stacking conditions. Compared with single injection runs, the net intensity for the serially injected peaks increases for the later peaks relative to the first peak. Overall, the peak FWHMs for the serially injected samples are also ~24% larger compared with single sample injection. Peak areas were calculated by triangulation for easier comparison. Calculating the

net intensities and the peak areas result in a similar finding: the later peaks in the series have a higher intensity in spite of a larger FWHM and a larger peak area, compared with both earlier peaks in the series and peaks from single injection runs. This is unexpected as one would expect either that the serially injected peaks would have similar values as the singly injected peaks or have larger FWHM and lower intensity compared with the singly injected peaks. The average net intensity for singly injected peaks is in between the lowest and highest net intensities measured for serially injected peaks of the same concentration.

The average serotonin LODs for single runs is 2.63 ± 0.49 nM versus 2.64 ± 0.26 nM for serial injections, when normalized for differences in standard deviation of the background. The increase in net intensity for later peaks is possibly due to the number of previous injections experienced by the peaks in question. The voltage is disabled each time an injection is performed, so field-amplified sample stacking is halted for each peak that has already been injected. In this case, the first sample plug experiences three subsequent broadening periods and has an increased FWHM and the lowest intensity of the series. The increase in FWHM could also be ascribed to the significantly later migration times for the serially injected peaks, compared with single injection.

3.4 Conclusions and future work

The MC-CE-LINF instrument has been updated to increase robustness, improve performance, and enable front-end hyphenation to other instrumentation. Since the improvements have been completed, instrument failure requiring re-alignment of the optics has been reduced to zero. Instrument realignment now only occurs to replace the capillary. Performance has also been improved, which is beneficial for detecting trace analytes within complex sample matrixes. Hyphenation is now possible since the high voltage line has been moved to the sheath flow waste outlet, away from any sensitive equipment that would be near the injection port. Two methods for improving performance during electrophoresis were also tested, and both appear promising for reducing run time and acquiring lower LODs.

Future work on this instrument could include installing a second hollow cathode ion laser with a wavelength of 248.6 nm that uses the same PMTs and circuit boards (NeCu30,

Photon Systems Inc., Covina, CA), so that one could painlessly switch the excitation wavelength. This wavelength is more optimal for exciting indolamines compared to 224.6 nm, based on absorption spectra. Work could also be done to test and verify the PMT boards' performance, as there are several versions of the circuit boards available with different designs. Further improvements to the electrical insulation and design would be beneficial as well as potentially enabling higher voltages to be achieved using two power supplies.

3.5 Tables

analyte	revised MC-CE-LINF (224 nm) LOD, nM	original MC-CE-LINF (224 nm) LOD, nM[1]	CCD (257 nm) LOD, nM [61]	PMT (266 nm) LOD, nM[63]
serotonin	0.9	10	6	250
dopamine	46	40	120	N.D.
norepineprine	27	44	4500	N.D.
epinephrine	32	N.D.	64	N.D.
octopamine	9	11	42	N.D.
tryptamine	2	N.D.	4	60
tryptophan	0.9	N.D.	12	N.D.
tyrosine	2	N.D.	49	N.D.
N-acetyl serotonin	4	N.D.	9	N.D.
tyramine	10	N.D.	N.D.	N.D.

Table 3.1 This table compares the current MC-CE-LINF with the first-generation MC-CE-LINF, a similar system in our laboratory which uses a frequency doubled Ar^+ laser and a CCD detector, and a system from another group that uses a single PMT detector and a frequency quadrulpled Nd:YAG laser. All of the analyte LODs for the MC-CE-LINF are either similar or lower than what was reported for these instruments.

analyte	average LOD, nM	standard deviation, nM
epinephrine	61	16
norepinephrine	87	22
5-hydroxytryptophan	5.4	1.0
tryptophan	11	3.6
N-acetylserotonin	11	2.6
5-hydroxyindole acetic acid	6.3	1.5
tryptophol	4.6	1.2
melatonin	4.7	1.2
serotonin	10	2.9
5-methoxytryptamine	4.8	0.9

Table 3.2 LODs and standard deviations for the analytes separated in Figure 3.7. These conditions are typical of biological samples, where the sample matrix consists of a high salt solution. Note the physiologically relevant LODs for many of the analytes.

3.6 Figures

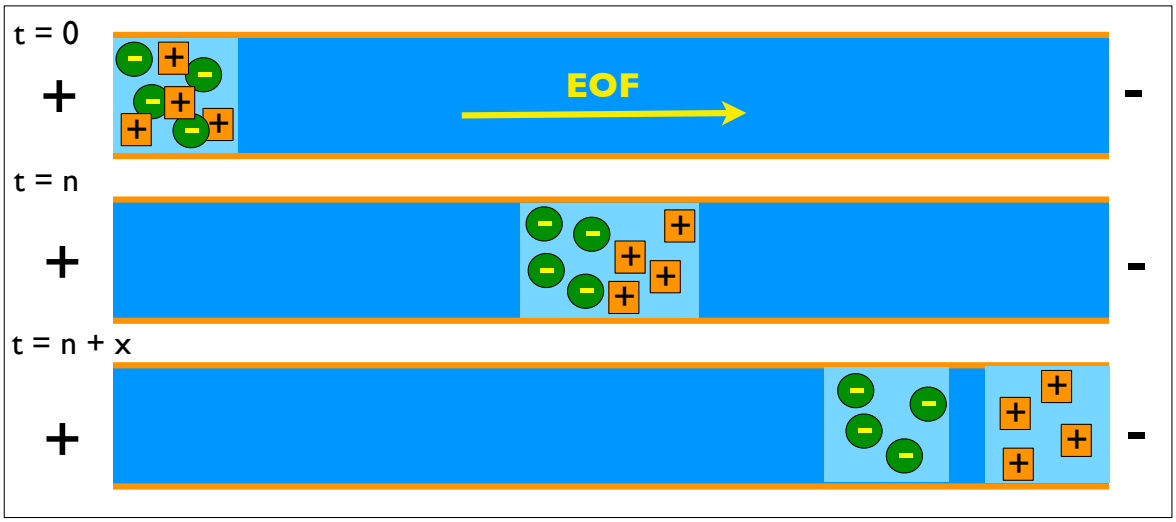

Figure 3.1 The separation capillary is filled with a uniform buffer solution and the application of a voltage in the longitudinal direction produces an electric field of constant strength. Analytes are separated according to differences in charge and size. Electroosmotic flow (EOF) is towards the cathode.

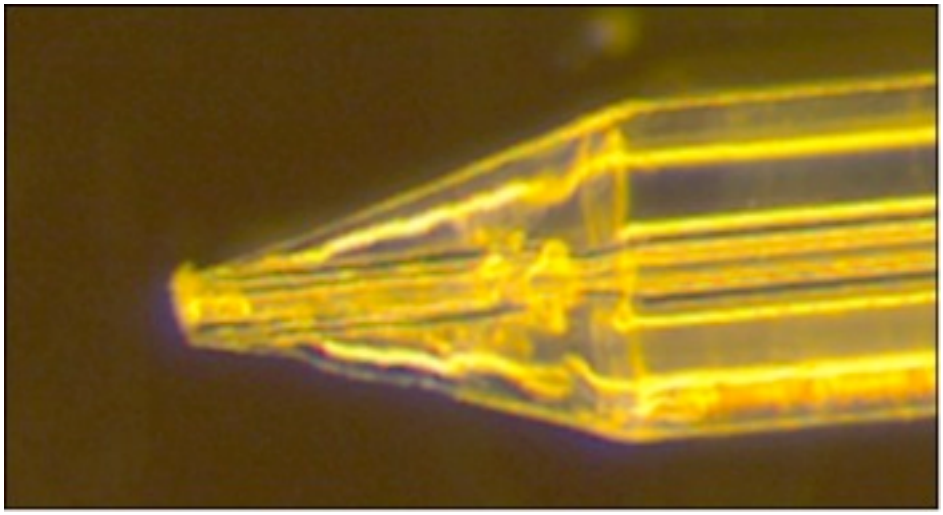

Figure 3.2 An HF-etched capillary tip with a 40° angle. The inner diameter is preserved to reduce the effects of a non-uniform electric field during electrophoresis.

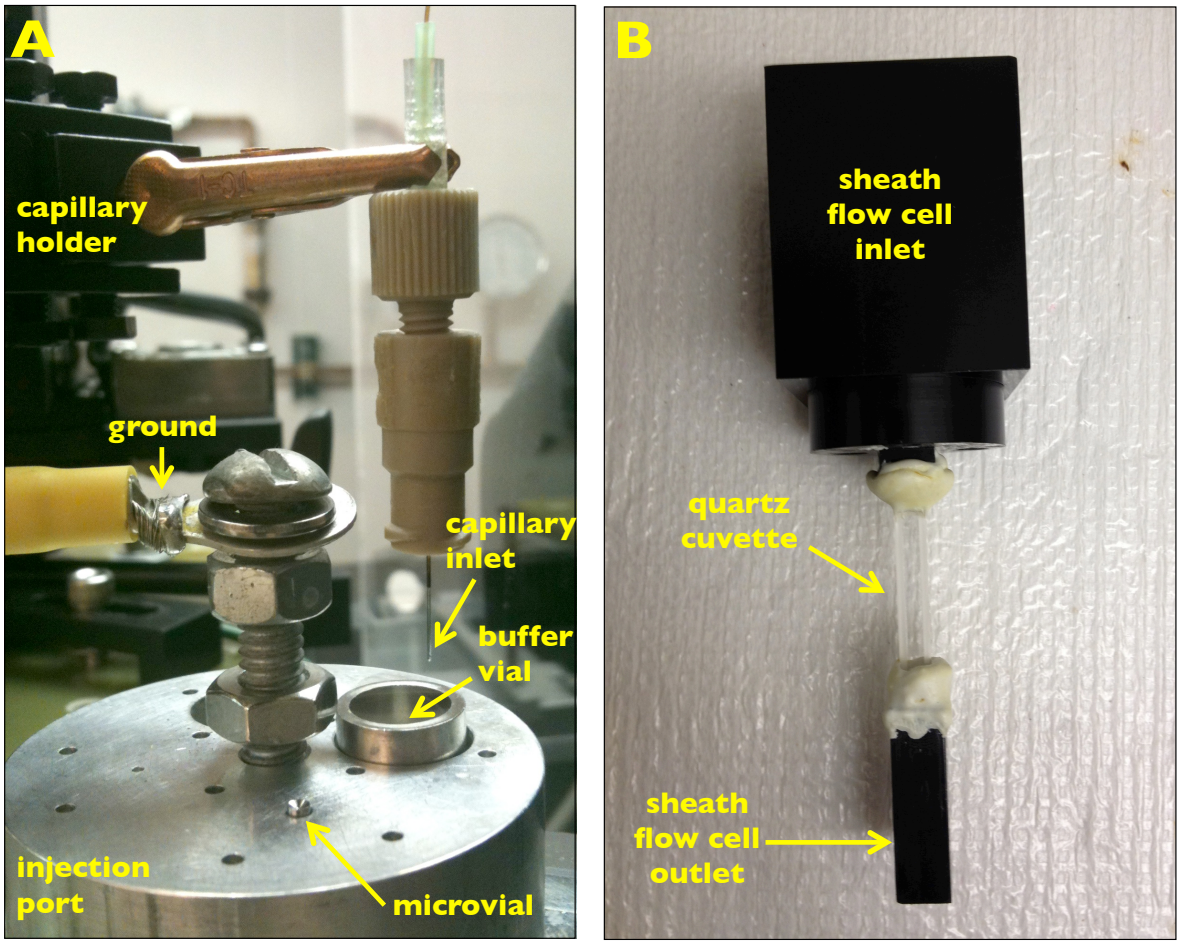

Figure 3.3 (A) The injection port, where the sample is introduced into the capillary. Samples are injected hydrodynamically from the microvial by lowering the sheath flow waste container. The capillary inlet is manually moved to the buffer vial to complete the circuit. (B) The sheath flow cell, which houses the capillary outlet.

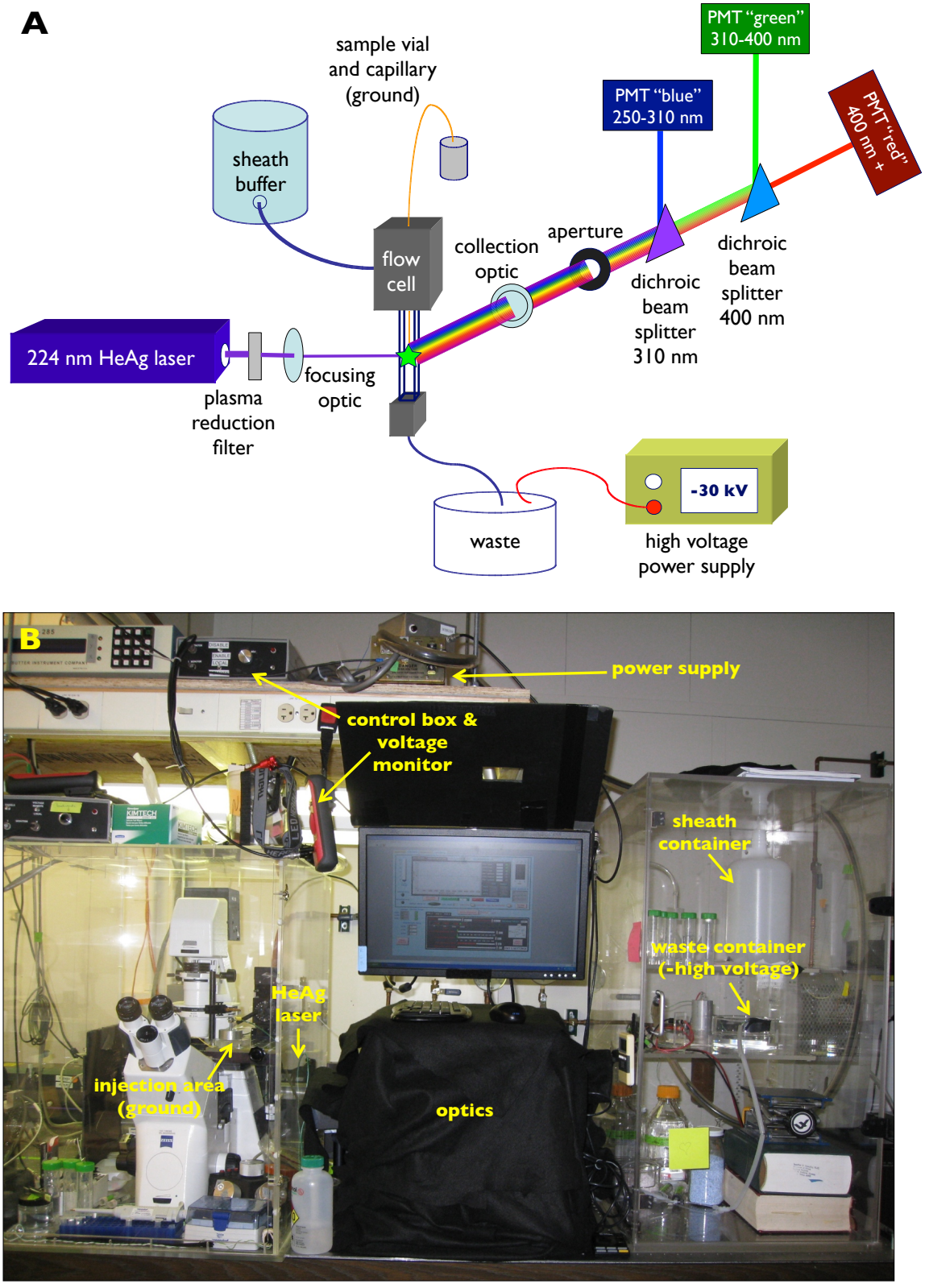
A
sample vial
and capillary
(ground)
PMT "green"
310-400 nm
PMT "blue"
250-310 nm
PMT "red"
400 nm +
sheath
buffer
flow
cell
collection
optic
aperture
dichroic
beam
splitter
310 nm
dichroic
beam
splitter
400 nm
224 nm HeAg laser
plasma
reduction
filter
focusing
optic
waste
-30 kV
high voltage
power supply
B
power supply
control box &
voltage
monitor
sheath
container
waste container
(-high voltage)
HeAg
laser
injection area
(ground)
optics

Figure 3.4

Figure 3.4 (cont.) (A) The current optical train schematic for the MC-CE-LINF. Emission from the HeAg laser is focused 0.5-1 mm below the outlet of the capillary. Fluorescence is collected orthogonal to excitation by an objective, which collimates and directs the emission to two dichroic beam splitters. The beam splitters separate the emission into three wavelength ranges: 250-310 nm, 310-400 nm, and 400 nm and above. Three detectors are used to collect the emission. (B) An image of the current instrument.

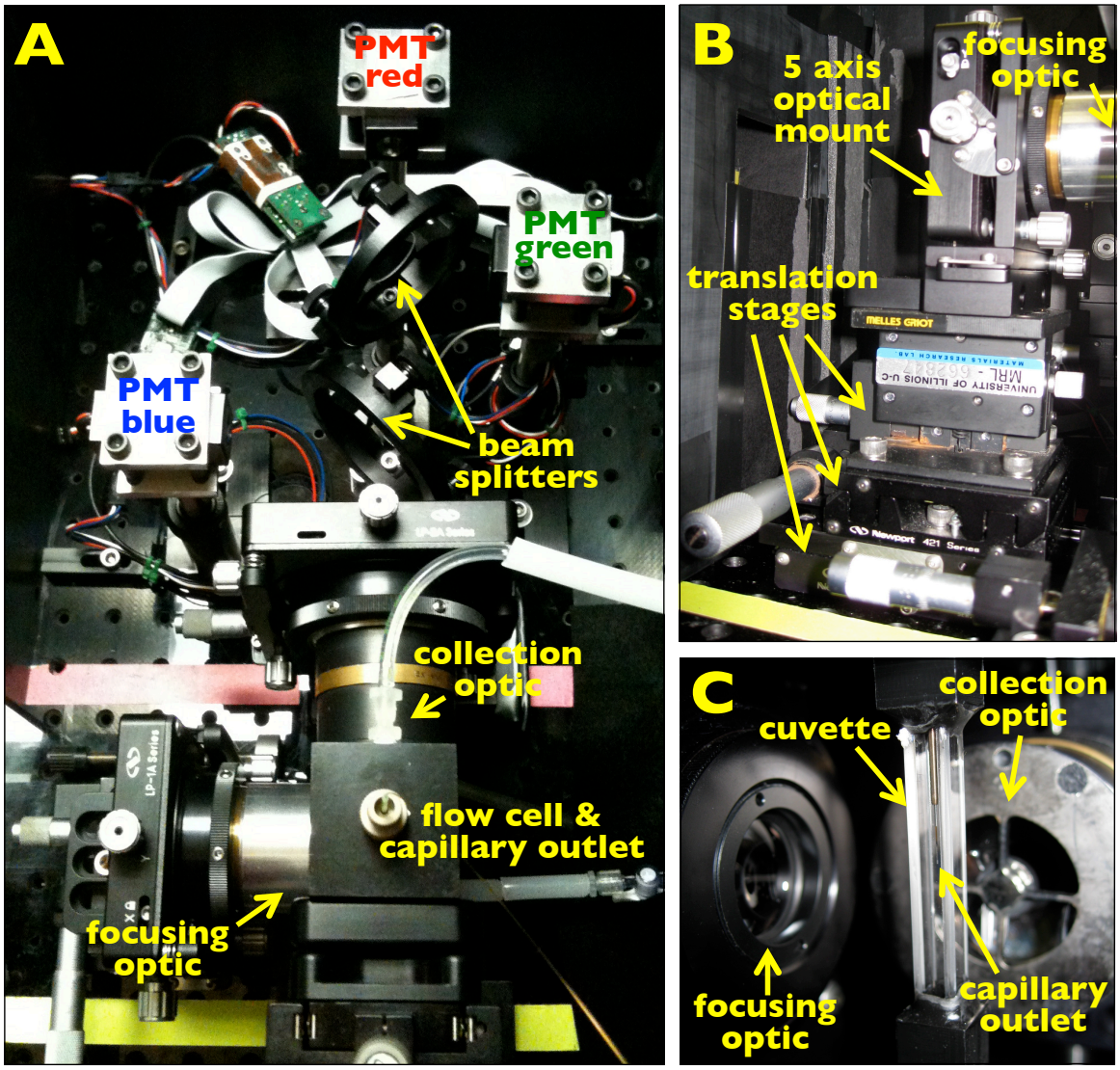

Figure 3.5 (A) An image of the detection optics. The laser enters the focusing optic on the left and fluorescence is detected orgothonal to excitation. (B) The mounting for the focusing optic. Translation stages provide increased stability and improve alignment. (C) A close-up image of the focusing optic, cuvette, and collection optic.

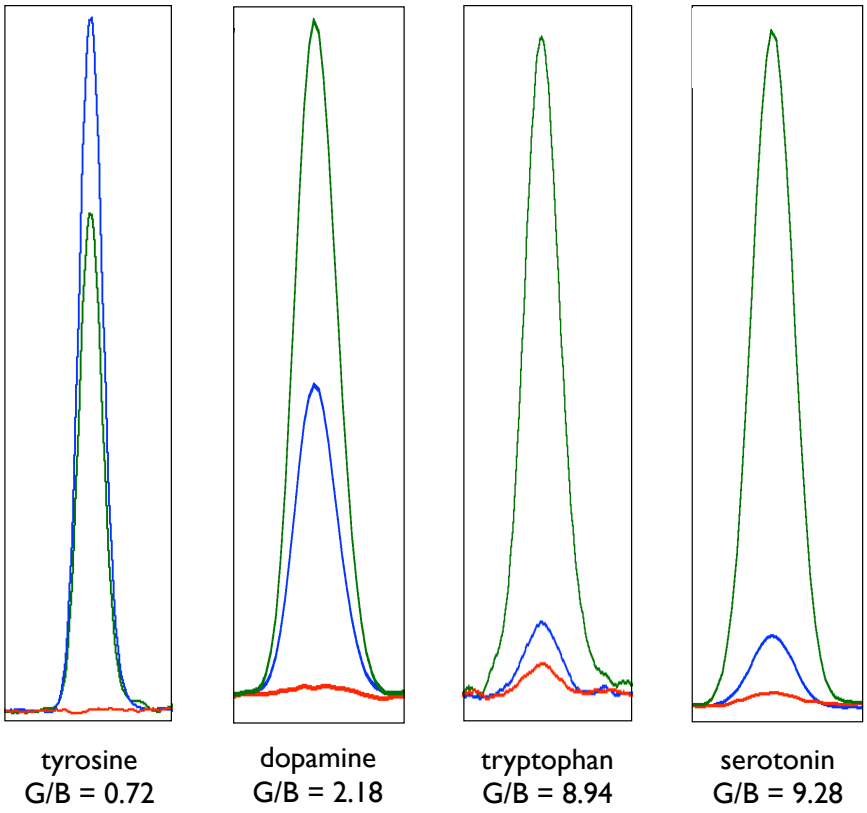

Figure 3.6 Shown are the green/blue (G/B) ratios for tyrosine, dopamine, tryptophan, and serotonin. These ratios, combined with migration time, allows for unambiguous identification of analytes of interest. Ratiometry is also useful for distinguishing between co-eluting peaks.

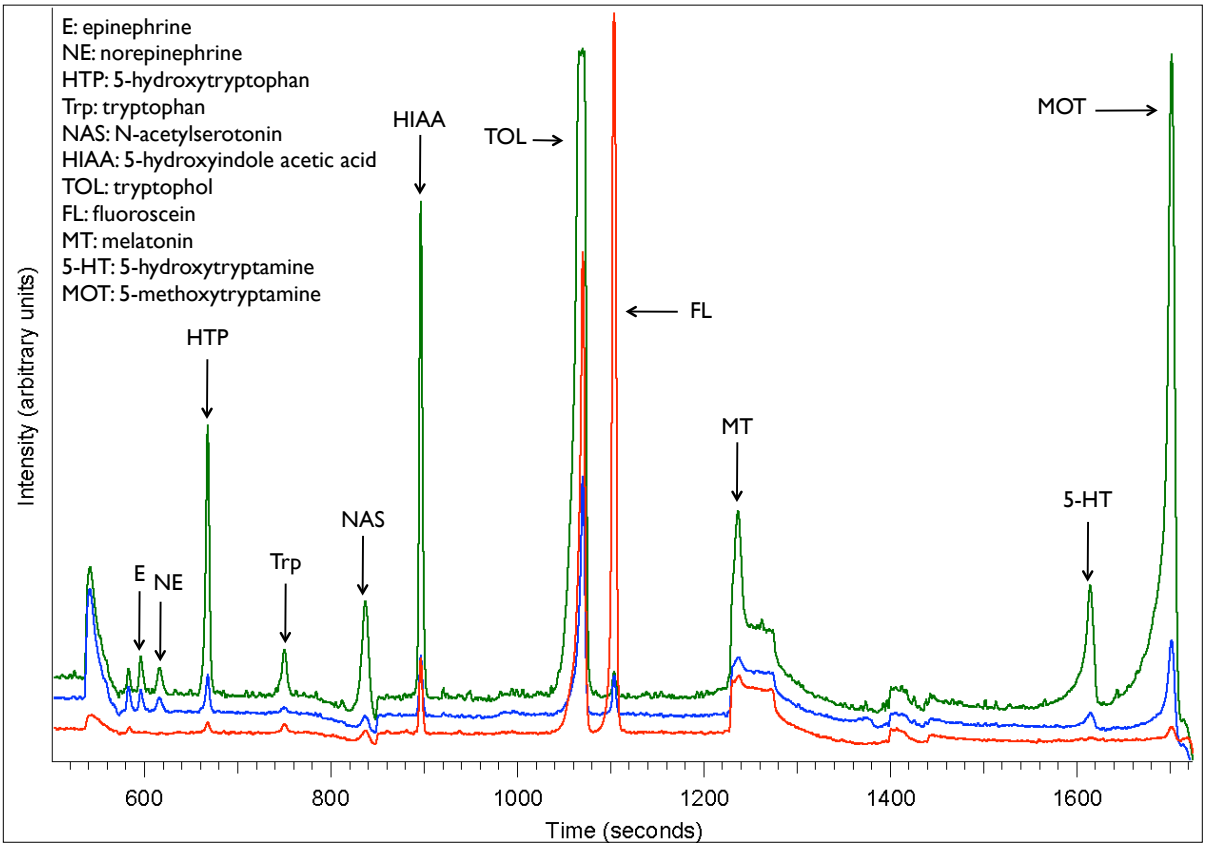

Figure 3.7 An example of a standard MC-CE-LINF run. Within 30 minutes, 11 analytes of interest can be separated and identified. Conditions are: 20 mM borate buffer, pH 8.8, + 50 mM SDS (electrophoresis buffer), mGBSS (sample buffer), 25 mM citric acid buffer, pH 2.25 (sheath buffer), -30 kV (separation voltage), 20 µA (current), 3 Hz (laser repetition rate), 100 µs (laser pulse length), 8 A (laser current), 420 V (laser BUSS voltage), 470 pF (PMT gain), 64% (gain voltage), 110 µs (PMT integration time).

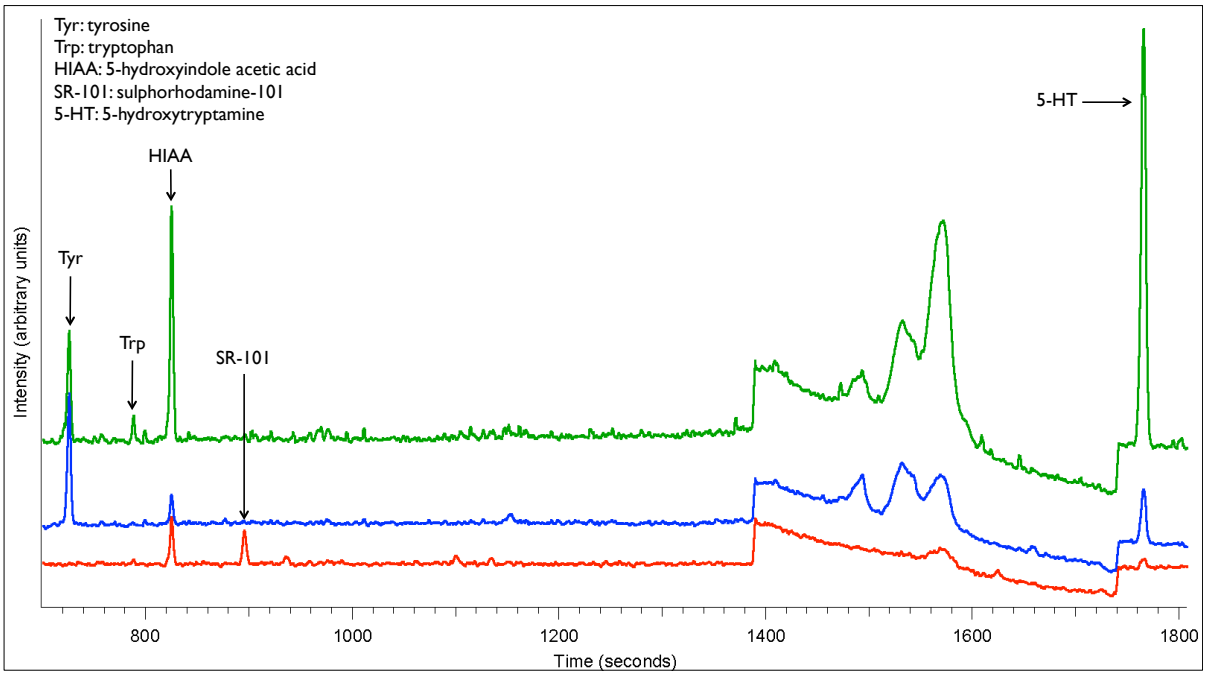

Figure 3.8 An example of a biological sample electropherogram. Sample was an extraction from four pooled pineal glands. Conditions are: 20 mM borate buffer, pH 8.8, + 50 mM SDS (electrophoresis buffer), 1:10 diluted extraction solution (sample solution), 25 mM citric acid buffer, pH 2.25 (sheath buffer), -30 kV (separation voltage), 17 µA (current), 3 Hz (laser repetition rate), 100 µs (laser pulse length), 8 A (laser current), 420 V (laser BUSS voltage), 470 pF (PMT gain), 64% (gain voltage), 110 µs (PMT integration time).

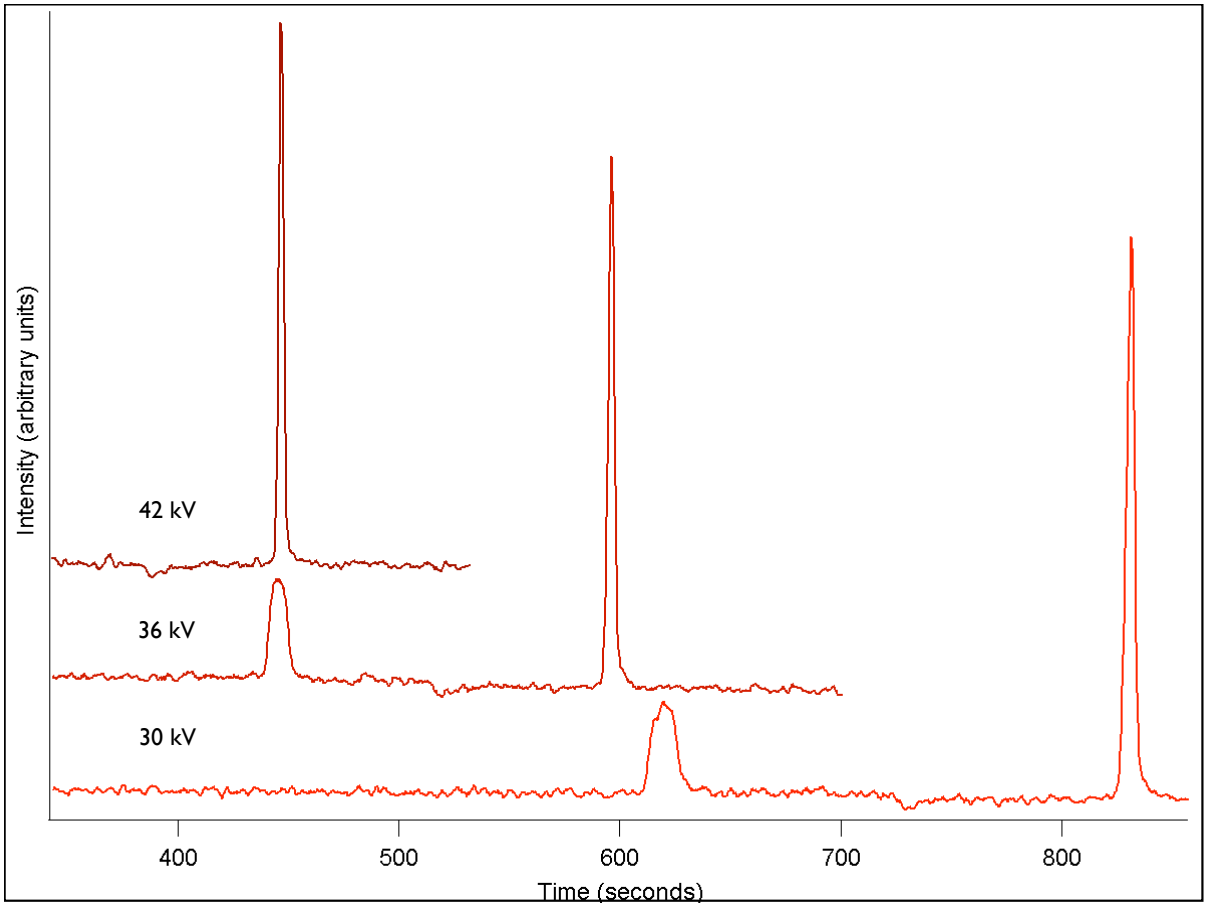

Figure 3.9 Three electropherograms of 4.4 µM sulphorhodamine-101, using two power supplies simultaneously to increase the voltage drop across the capillary. A 55% difference in migration time is observed between 42 kV and -30 kV. Conditions are: 50 mM borate buffer, pH 8.8 (electrophoresis buffer), water (sample solution), 25 mM citric acid buffer, pH 2.25 (sheath buffer), -30 kV (separation voltage), 30 µA (current), 3 Hz (laser repetition rate), 100 µs (laser pulse length), 8 A (laser current), 420 V (laser BUSS voltage), 470 pF (PMT gain), 64% (gain voltage), 110 µs (PMT integration time).

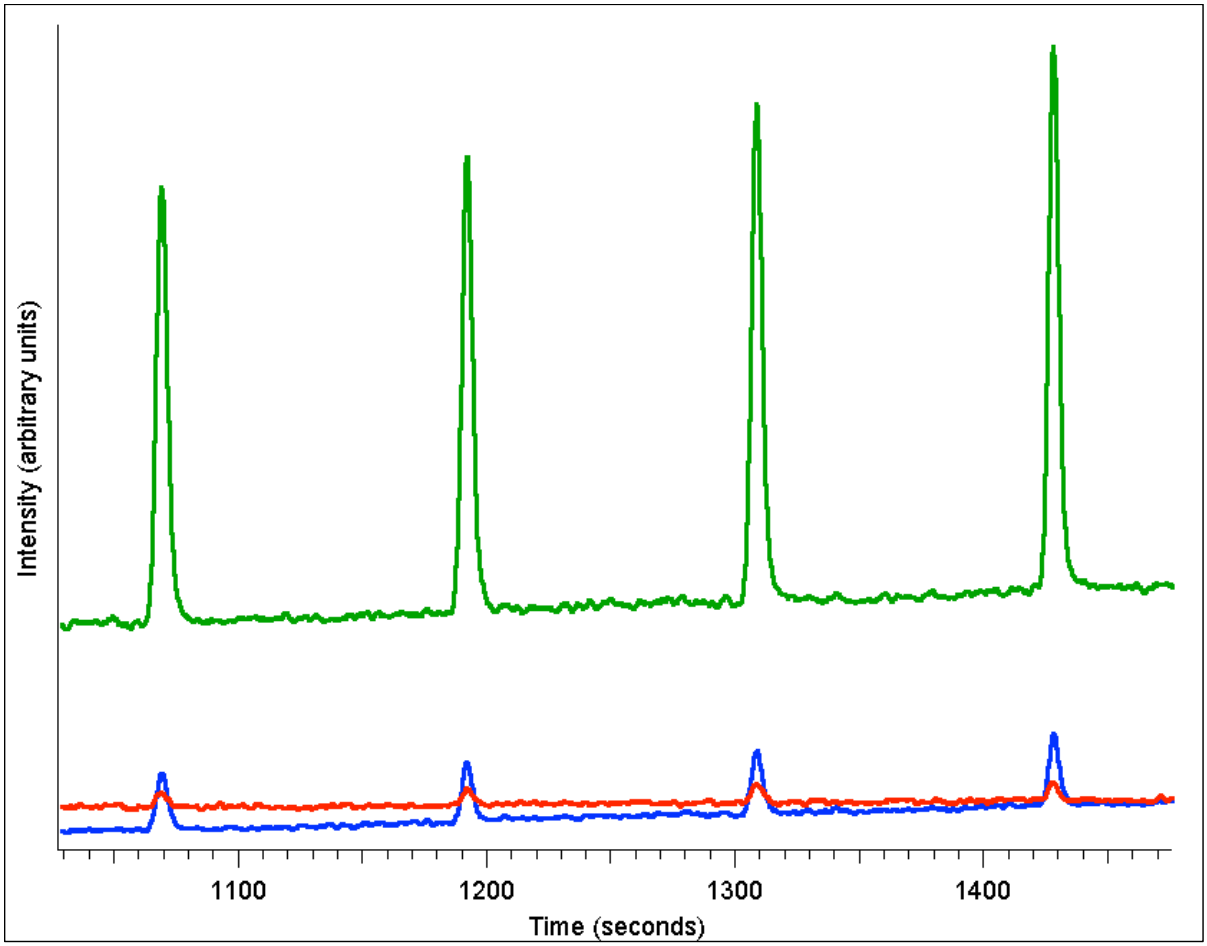

Figure 3.10 Four serial injections of 780 nM serotonin. Conditions are: 25 mM citric acid buffer, pH 5.5 (electrophoresis buffer), 2.5 mM citric acid buffer, pH 3.0 (sample buffer), 25 mM citric acid buffer, pH 2.25 (sheath buffer), -27 kV (separation voltage), 40 µA (current), 3 Hz (laser repetition rate), 100 µs (laser pulse length), 8 A (laser current), 420 V (laser BUSS voltage), 470 pF (PMT gain), 64% (gain voltage), 110 µs (PMT integration time).

3.7 References

(1) Lapainis, T.; Scanlan, C.; Rubahkin, S. S., Sweedler, J. V. *Anal Bioanal Chem*. **2007**, *387*, 97–105.

(2) Berry, M. D. *J Neurochem*. **2004**, *90*, 257–271.

(3) Giurfa, M. *Curr. Biol.* **2006**, *16*, R892–5.

(4) Zhang, X.; Fuller, R. R.; Dahlgren, R. L.; Potgieter, K.; Gillette, R.; Sweedler, J. V. *Fresen J Anal Chem*. **2001**, *369*, 206–211.

(5) Panayotis, N.; Ghata, A.; Villard, L.; Roux, J.-C. *BMC Neuroscience*. **2011**, *12*, 47.

(6) Senior, J.; Shah, A.; Monteux, C.; De Biasi, V. *J Pharm Biomed Anal*. **2001**, *24*, 843–848.

(7) Tekes, K. L.; Szegi, P.; Laufer, R.; Hantos, M.; Csaba, G. *International Journal of Developmental Neuroscience*. **2011**, *29*, 171–175.

(8) Chiu, A. S.; Godse, D. D.; Warsh, J. J. *Prog Neuropsychopharmacol*. **1981**, *5*, 559–563.

(9) Tusell, J.; Sunol, C.; Artigas, F.; Martinez, E.; Gelpi, E. *Chromatographia*. **1982**, *16*, 112–116.

(10) Andrew, R.; Best, S.; Watson, D.; Midgley, J.; Reid, J.; Squire, I. *Neurochem Res*. **1993**, *18*, 1179–1182.

(11) Pan, C.; Li, W.; Wang, Y.; Jiang, S. *Int J Mol Sci*. **2005**, *6*, 188–197.

(12) Eckstein, J. A.; Ammerman, G. M.; Reveles, J. M.; Ackermann, B. L. *J. Mass Spectrom.* **2008**, *43*, 782–790.

(13) Jorgenson, J. W.; Lukacs, K. D. *Clin. Chem.* **1981**, *27*, 1551–1553.

(14) Jorgenson, J. W.; Lukacs, K. D. *Anal Chem*. **1981**, *53*, 1298–1302.

(15) Chiu, T.-C.; Lin, Y.-W.; Huang, Y.-F.; Chang, H.-T. *Electrophoresis*. **2006**, *27*, 4792–4807.

(16) Monnig, C. A.; Kennedy, R. T. *Anal Chem*. **2001**, *66*, 280R–314R.

(17) Ryan, R.; Donegan, S.; Power, J.; Altria, K. *Electrophoresis*. **2010**, *31*, 755–767.

(18) Silva, M. *Electrophoresis*. **2010**, *32*, 149–165.

(19) Silva, M. *Electrophoresis*. **2009**, *30*, 50–64.

(20) Beckers, J. L.; Boček, P. *Electrophoresis*. **2000**, *21*, 2747–2767.

(21) Malá, Z.; Gebauer, P.; Boček, P. *Electrophoresis*. **2010**, *32*, 116–126.

(22) Britz-McKibbin, P.; Chen, D. D. Y. *Anal Chem*. **2007**, *72*, 1242–1252.

(23) Ptolemy, A. S.; Britz-McKibbin, P. *Analyst*. **2008**, *133*, 1643–1648.

(24) Wallingford, R. A.; Ewing, A. G. *Anal Chem*. **1987**, *59*, 1762–1766.

(25) Kubáň, P.; Hauser, P. C. *Electrophoresis*. **2009**, *30*, 3305–3314.

(26) Trojanowicz, M. *Anal Chim Acta*. **2009**, *653*, 36–58.

(27) Opekar, F.; Štulík, K. *Electrophoresis*. **2011**, *32*, 795–810.

(28) Haselberg, R.; de Jong, G. J.; Somsen, G. W. *Electrophoresis*. **2010**, *32*, 66–82.

(29) Nesbitt, C.; Zhang, H.; Yeung, K. *Anal Chim Acta*. **2008**, *627*, 3–24.

(30) Smith, R.; Olivares, J.; Nguyen, N. *Anal Chem*. **1988**, *60*, 436–441.

(31) Haselberg, R.; Dejung, G.; Somsen, G. *J. Chrom.* **2007**, *1159*, 81–109.

(32) Ramautar, R.; Mayboroda, O. A.; Somsen, G. W.; de Jong, G. J. *Electrophoresis*. **2010**, *32*, 52–65.

(33) Lowry, M.; Fakayode, S. O.; Geng, M. L.; Baker, G. A.; Wang, L.; McCarroll, M. E.; Patonay, G.; Warner, I. M. *Anal Chem*. **2008**, *80*, 4551–4574.

(34) Zhang, X.; Stuart, J. N.; Sweedler, J. V. *Anal Bioanal Chem*. **2002**, *373*, 332–343.

(35) Cheng, Y.; Wu, S.; Chen, D.; Dovichi, N. J. *Anal Chem*. **1990**, *62*, 496–503.

(36) Waterval, J. C.; Lingeman, H.; Bult, A.; Underberg, W. J. *Electrophoresis*. **2000**, *21*, 4029–4045.

(37) Udenfriend, S.; Stein, S.; Böhlen, P.; Dairman, W.; Leimgruber, W.; Weigele, M. *Science*. **1972**, *178*, 871–872.

(38) Kawauchi, H.; Tuzimura, K.; Maeda, H.; Ishida, N. *J Biochem-Tokyo*. **1969**, *66*, 783–789.

(39) de Montigny, P.; Stobaugh, J. F.; Givens, R. S.; Carlson, R. G.; Srinivasachar, K.; Sternson, L. A.; Higuchi, T. *Anal Chem*. **2002**, *59*, 1096–1101.

(40) Chen, D. D. Y.; Dovichi, N. J. *J. Chrom. B*. **2002**, *657*, 265–269.

(41) Whitmore, C. D.; Essaka, D.; Dovichi, N. J. *Talanta*. **2009**, *80*, 744–748.

(42) Chiu, T.-C.; Chang, H. *J. Chrom. A*. **2007**.

(43) Hietpas, P. B.; Ewing, A. G. *J. of Liquid Chromatography & Related Technologies*. **1995**, *18*, 3557–3576.

(44) Ye, M.; Hu, S.; Quigley, W.; Dovichi, N. J. *J. Chrom. A*. **2004**, *1022*, 201–206.

(45) Hu, S.; Michels, D. A.; Fazal, M. A.; Ratisoontorn, C.; Cunningham, M.; Dovichi, N. J. *Anal Chem*. **2004**, *76*, 4044–4049.

(46) Zhao, J. Y.; Diedrich, P.; Zhang, Y.; Hindsgaul, O.; Dovichi, N. J. *J. Chromatogr. B, Biomed. Appl.* **1994**, *657*, 307–313.

(47) Xiong, Y.; Park, S. R.; Swerdlow, H. *Anal Chem*. **1998**, *70*, 3605–3611.

(48) Tseng, H. C.; Dadoo, R.; Zare, R. N. *Anal Biochem*. **1994**, *222*, 55–58.

(49) Tolba, K.; Belder, D. *Electrophoresis*. **2007**, *28*, 2934–2941.

(50) Timperman, A. A.; Oldenburg, K.; Sweedler, J. V. *Anal Chem*. **1995**, *67*, 3421–3426.

(51) Timperman, A. A.; Khatib, K.; Sweedler, J. V. *Anal Chem*. **1995**, *67*, 139–144.

(52) Fuller, R. R.; Sweedler, J. V. *Cytometry*. **1996**, *25*, 144–155.

(53) Fuller, R. R.; Moroz, L. L.; Gillette, R.; Sweedler, J. V. *Neuron*. **1998**, *20*, 173–181.

(54) Stuart, J. N.; Zhang, X.; Jakubowski, J.; Romanova, E.; Sweedler, J. V. *J Neurochem*. **2003**, *84*, 1358–1366.

(55) Stuart, J. N.; Ebaugh, J.; Copes, A.; Hatcher, N. G.; Gillette, R.; Sweedler, J. V. *J Neurochem*. **2004**, *90*, 734–742.

(56) Hoffmann, P.; Dutoit, B.; Salathe, R. P. *Ultramicroscopy*. **1995**, *61*, 165–170.

(57) Li, L.; Lubman, D. *Anal Chem*. **1987**, *59*, 2538–2541.

(58) Gostkowski, M. L.; Allen, R.; Plenert, M. L.; Okerberg, E.; Gordon, M. J.; Shear, J. B. *Biophys. J.* **2004**, *86*, 3223–3229.

(59) Chattopadhyay, A.; Rukmini, R.; Mukherjee, S. *Biophys. J.* **2005**, *71*, 1952–1960.

(60) Zarrin, F.; Dovichi, N. J. *Anal Chem*. **1985**, *57*, 2690–2692.

(61) Park, Y. H.; Zhang, X.; Rubakhin, S. S.; Sweedler, J. V. *Anal Chem*. **1999**, *71*, 4997–

5002.

(62) Malá, Z.; Šlampová, A.; Gebauer, P.; Boček, P. *Electrophoresis*. **2009**, *30*, 215–229.

(63) Huhn, C.; Pütz, M.; Martin, N.; Dahlenburg, R.; Pyell, U. *Electrophoresis*. **2005**, *26*, 2391–2401.

4 Analyzing high salt samples for low abundance indolamines using capillary electrophoresis with laser-induced native fluorescence detection

Notes and Acknowledgments

I would like to acknowledge Jennifer M. Arnold and Prof. Martha U. Gillette for providing samples, and the SCS Machine Shop for their advice and work. I would also like to acknowledge Bill Hug, Ray Reid, and Prashant Oswal at Photon Systems Inc. for providing the hollow cathode ion laser and their help with troubleshooting. This work is part of a much larger body of work that is a collaboration between the Gillette, Gold, and Sweedler groups, including Hai Miao and Nobotoshi Ota in the Sweedler group. The overall work is titled "Signals from the brain sleep-wake system regulate behavioral timing via the circadian clock" and is under consideration at Neuron (Signals from the brain sleep-wake system regulate behavioral timing via the circadian clock, Sabra M. Abbott, Jennifer M. Arnold, Qing Chang, Hai Miao, Nobutoshi Ota, Christine Cecala, Paul E. Gold, Jonathan V. Sweedler, and Martha U. Gillette). My role in this complex research project was to determine the best conditions for analyzing microdialysis samples that contain trace levels of indolamines and then to identify and quantify the indolamines in these samples (e.g., separation, detection, identification, and quantitation). Of the work presented here, animal protocols, the samples that were analyzed, animal statistics, and Figure 4.16 were provided by the Gillette group. This work was supported by the National Institutes of Health and the National Science Foundation under awards P30 DA018310 and NSF CHE-1111705 to Jonathan V. Sweedler; GM07143 and NS47802 to Sabra M. Abbot; AG07648 and P30 DA16951 to Paul Gold; and HL092571Z and HL086870 to Martha U. Gillette.

4.1 Introduction

Indolamines (*e.g.* serotonin) are present throughout both the central and peripheral nervous systems. As a cell-to-cell signaling molecule, serotonin is involved in a range of biological functions such as sleep, memory formation, and feeding and its misregulation appears to be a part of diseases such as depression and Parkinson's disease. The detection and identification of these molecules is difficult because they are often both mass- and

concentration-limited (attomole to zeptomole range within specific cells) and present within a complex matrix of proteins, salts, and other biological compounds. As highlighted in Chapter 2, capillary electrophoresis with laser-induced native fluorescence possesses several characteristics that make it well suited for analyzing indolamines, such as low sample volume requirements, a selective and sensitive detection method, no required sample derivatization, and low limits of detection (LODs).

One of the challenges in directly analyzing biological samples with capillary electrophoresis is that the samples' matrix interferes with on-column concentration, separation, and identification, due to the high levels of inorganic salts present (typically 150 mM for mammalian samples).

4.1.1 Measuring trace levels of indolamines in high salt-containing samples

Numerous techniques have been developed within the analytical community to overcome the deleterious effects of high salt-containing samples, such as field-amplified sample stacking,[1-6] field-amplified sample injection,[7, 4, 5, 8-10] micellar electrokinetic chromatography,[11-19] dynamic pH junction,[20-25, 6] and pH-mediated sample stacking.[23, 21, 26-28, 4] These techniques make use of different electrolyte properties between the sample and the background electrolyte (BGE), such as conductivity, pH, and additive concentration and interactions, to enhance separations under both ideal and physiological conditions.

Field-amplified sample stacking (FASS) (Figure 4.1) makes use of differences in conductivity to effect concentration of analytes. The sample is contained within a lower conductivity buffer (typically 10-fold lower), relative to the higher conductivity BGE. When voltage is applied, the sample plug experiences greater electric field strength compared to the BGE. The analytes' electrophoretic velocity is increased until the boundary between the lower conductivity sample plug and the higher conductivity BGE is reached. Here, the analytes experience a significant change in electric field strength and are slowed and concentrated into a narrow plug. Although this is one of the simplest techniques to employ, enhancement is only about 10- to 20-fold.

Field-amplified sample injection (FASI) (Figure 4.2) operates similarly to FASS. In FASI, the sample is prepared in a low conductivity buffer and is electrokinetically injected

into the capillary. The low conductivity of the sample creates a point of higher electric field strength and more analytes are injected than would be with hydrodynamic injection. Typically a short plug of water is hydrodynamically injected before the sample to ensure that field-amplified stacking conditions exist. Much larger increases in enhancement are observed in FASI compared to FASS (100- to 1000-fold increases or more), but analyte bias can occur due to electrokinetic injection.

Micellar electrokinetic chromatography (MEKC) was first demonstrated by Terabe and co-workers in 1984 and was initially developed as a means to separate neutral analytes in CE (Figure 4.3).[15, 29] MEKC involves using surfactant micelles in the BGE to create a pseudostationary phase. The analytes reversibly complex with the micelles, and can be separated according to their differential affinity. This technique can also be used to resolve charged species that co-elute, and can increase the resolution of chiral separations. Enhancement can range from several-fold to 20-fold.

A dynamic pH junction (Figure 4.4) manipulates the charge state of the analytes to enhance separation. The capillary is filled with high pH BGE and a large plug of low pH sample is injected. When voltage is applied, a dynamic pH boundary moves through the sample zone. Analytes, depending on their pK_as, are converted from one charge state to another and their net migration velocities change. This leads to a net focusing of the analyte bands within the capillary. One hundred- to two hundred-fold enhancements have been reported for this technique.

Another technique that manipulates pH and conductivity is pH-mediated sample stacking (Figure 4.5). It involves titrating a high conductivity sample to lower conductivity, which creates concentrated bands of analytes. The charge of the analytes determines whether “acid stacking” (cations) or “base stacking” (anions) is used. Samples are injected electrokinetically, and sample ions are replaced by “titrable” BGE ions. The sample plug is followed immediately by an electrokinetic injection of either acid or base, depending on whether “acid stacking” or “base stacking” is employed, respectively. The BGE ions are titrated by the acid or base, creating a zone of low conductivity where field amplification can occur. Enhancements of up to 200-fold have been demonstrated for pH-mediated

sample stacking. A limitation of this technique is that a significant portion of the separation capillary is used for the stacking process, leaving little capillary available for separation of analytes.

The instrument used for these analyses employs a label-free native laser-induced fluorescence detector system that has been optimized for detection of indolamines (detailed in Chapter 3). Briefly, a 224 nm HeAg hollow cathode ion laser is combined with a sheath-flow cuvette; the fluorescence emission is collected and measured using three photomultiplier tubes (dichroic beamsplitters select the appropriate wavelength range for each detector). This detector, when combined with a capillary electrophoresis system, allows unambiguous identification of indolamines based on each peaks' unique fluorescence emission profile and migration time. The ability to efficiently concentrate, separate, and detect serotonin and its catabolites under biological conditions are highlighted. The methodology can also be applied to other biogenic amines such as catecholamines and amino acids.

4.1.2 Biological measurements of indolamines from the rat brain

The analytical measurement goals have been outlined above. The aim of this project was to determine the function of the neural projections that connect the homeostatic brain stem sites, which reports fatigue, with the suprachiasmatic nucleus (SCN), which communicates time-of-day. To do this, discrete electrical stimulation of the homeostatic sleep centers was coupled with analytical measurements of intra-SCN microdialysates in mice. The biological measurement goals were to quantitate the indolamines present in microdialysis samples. In order to measure serotonin (5-HT) and related indolamines, we used the analytical approaches described above and adapted them to work with brain dialysates. More specifically, the above techniques have been adapted and evaluated for the concentration, separation, and detection of trace indolamines within artificial cerebral spinal fluid. These techniques were also applied for the analysis of over 200 mouse microdialysis samples collected before, during, and after electrical stimulation of the homeostatic sleep centers in the brain. Over 75% of microdialysis samples had detectable levels of indolamines present, and these measurements were used to demonstrate that

acetylcholine and glutamate release at the SCN was specific to the stimulation of homeostatic sleep centers and not from nearby areas such as the serotonergic median raphe nucleus (MRN). The MRN was stimulated and the SCN dialysate was analyzed for 5-HT, acetylcholine, and glutamate (neither of which is synthesized in the MRN). As expected, stimulation of the serotonergic median raphe significantly increased 5-HT at the SCN and no significant increase in acetylcholine or glutamate was observed.

4.2 Materials and Methods

A list of abbreviations can be found in the Appendix.

4.2.1 Chemicals

Chemicals, unless otherwise noted, were from Sigma Aldrich (St. Louis, MO) and were reagent grade or higher. Citric acid sheath buffer (25 mM, pH 2.25) was made by dissolving 5.25 g of $C_6H_8O_7 \cdot H_2O$ in 1 L of ultrapure deionized water (Elga Purelab Ultra, Siemens Water Technologies, Warrendale, PA). Electrophoresis buffers were prepared as follows: (1) by using or diluting a stock solution of 50 mM borate buffer, pH 8.8, which was prepared by dissolving 9.2 g of $Na_2B_4O_7 \cdot 10H_2O$ and 3.0 g of $B(OH)_3$ in 1 L of ultrapure deionized water, (2) by using or diluting a stock solution of 50 mM phosphate buffer, pH 8.8, which was prepared by dissolving 0.07 g of NaH_2PO_4 and 7.0 g of Na_2HPO_4 in 1 L of ultrapure deionized water, (3) by dissolving an appropriate amount of sodium dodecyl sulfate (SDS) in phosphate buffer, or (4) by dissolving 31.5 g of $C_6H_8O_7 \cdot H_2O$ in 1 L of ultrapure deionized water to make 150 mM citric acid, pH 1.9. Please see Table 4.1 for more information. Serotonin (5-HT) (Alfa Aesar, Ward Hill, MA), tryptophan (Trp), N-acetylserotonin (NAS), 5-hydroxyindole-3-acetic acid (HIAA), 5-hydroxyindole thiazoladine carboxylic acid (HITCA) (National Institute of Mental Health Chemical Synthesis and Drug Supply Program), and serotonin-O-sulfate (5-HT sulfate) (National Institute of Mental Health Chemical Synthesis and Drug Supply Program) were dissolved in either 1 mM borate buffer, pH 8.8 (1:50 dilution of stock borate electrophoresis buffer) or ultrapure deionized water and 10% v/v acetone and sonicated on ice as needed for 30-60 min. Sulphorhodamine-101 (SR-101) was prepared in ultrapure deionized water. Standard stock solutions were diluted

in either 1 mM borate buffer, pH 8.8, or artificial cerebral spinal fluid (aCSF) buffer, pH 7.4, which consisted of 130 mM NaCl, 4 mM KCl, 0.75 mM NaH_2PO_4, 2 mM Na_2HPO_4, 1 mM dextrose, 2 mM $MgCl_2$, and 1.7 mM $CaCl_2$. All buffers were filtered by a 0.45 μm bottle-top filter system (Nalgene, Rochester, NY) and degassed under vacuum with stirring for 30-60 min. HCl (0.1-0.5 M) was diluted from 12 M stock in ultrapure deionized water as needed. NaOH (~0.1 M) was prepared by dissolving one pellet (~0.0025 g) in 0.025 L of ultrapure deionized water.

Buffer ionic strengths (I, M) were calculated according to $I = \frac{1}{2}\Sigma(c_i z_i)$, where c_i represents the concentration of each ionic species and z_i represents the numerical value of the charge state of each ionic species. Buffer conductivities (K, mS/cm) were experimentally determined by a conductivity meter (model 122, Thermo Scientific (Orion), Waltham, MA).

4.2.2 Animal protocols

The animal and dialysate experiments were performed within the Gillette laboratory. The male C57BL/6J mice were obtained at 5 wk of age from Jackson Laboratories (Bar Harbor, ME). Animals were housed and cared for as described in animal protocols in full compliance with NIH guidelines for the humane care and treatment of animals, approved by IACUC and supervised by the Division of Animal Resources at the University of Illinois at Urbana-Champaign.

Surgeries on mice were performed ≥ 1 wk after animals arrived (18-23 g). Mice were anesthetized with sodium pentobarbital (80 mg/kg i.p.). A microdialysis guide (CMA/7, CMA/Microdialysis, North Chelmsford, MA) was implanted in the suprachiasmatic nucleus (SCN), and a bipolar stimulating electrode (MS303/1, Plastics One, Inc., Roanoke, VA) was implanted into the laterodorsal tegmental (LDTg) nuclei, pedunculopontine tegmental (PPTg) nuclei, or median raphe nucleus (MRN) using a stereotaxic apparatus (Stoelting, Wood Dale, IL). Cannulae were secured with small machine screws (0-80 x 1/16”, Plastics One, Inc., Roanoke, VA) and cranioplastic cement (Plastics One, Inc., Roanoke, VA).

Mice were housed individually in cages (30 x 17 x 22 cm) equipped with running wheels (14.5 cm diameter) that were placed inside ventilated light-tight wooden boxes (171

x 41 x 34 cm). Wheels were locked on the first day to minimize novel wheel-induced phase shifts, which can increase the time necessary for entrainment. For light-dark cycles, lights were kept at 100 lux for 12 h, followed by 12 h of darkness, regulated by computer. Up to six mice could be housed in each box. For experimental procedures, animals were placed in light-tight circadian activity monitoring systems (CAMS) and maintained in darkness under constant conditions.

For microdialysis procedures, animals were gently restrained, a microdialysis probe (CMA/7, CMA/Microdialysis, North Chelmsford, MA) was inserted into the dialysis guide aimed at the SCN and was attached to the animal using a head-block tether system (Harvard Apparatus, Holliston, MA). Connecting cables for stimulation (305-305 TT2, Plastics One, Inc., Roanoke, VA) also were attached at this time. Animals were placed into CAMS designated for stimulation experiments, where they were attached to fluid (Instech, Harvard Apparatus, Holliston, MA) and electronic swivels (Plastics One, Inc., Roanoke, VA). Placing animals in CAMS for the duration of the experiment allowed experiments to be performed on a freely-behaving, undisturbed animal, under controlled environmental conditions.

Before each experiment, the microdialysis probe was placed in a standard solution containing 20 nM acetylcholine and 20 nM choline for 20 min to determine the recovery rate of the probe.

Probes were continuously perfused at a rate of 1 mL/min with aCSF containing 500 nM neostigmine, a cholinesterase inhibitor. Animals were allowed to equilibrate for at least 1 h before samples were collected. For experiments performed during the animal's dark period, the microdialysis probe was attached during the light period and animals were perfused with aCSF until 2 h before the first collection, at which point the perfusion fluid was switched to aCSF containing 500 nM neostigmine. This allowed all probes to be attached during the light period, while standardizing the length of time each animal was exposed to neostigmine. After ~1 h for equilibration, baseline samples were collected every 20 min for 1 h. Animals were then stimulated, and microdialysis sample collection

continued every 20 min for an additional 100 min. Samples were split for analysis, and kept at -80 °C until analysis.

4.2.3 Instrumentation

The instrument used for these analyses is the multi-channel capillary electrophoresis-laser-induced native fluorescence (MC-CE-LINF) system (Chapter 3). Deep UV radiation (224.6 nm) from a HeAg hollow cathode ion laser (HeAg70, Photon Systems Inc., Covina, CA) is directed via two UV-coated mirrors (Thorlabs, Newton, NJ) into a laboratory-built lightproof, non-conductive box and breadboard, which houses the detection optics and protects against spurious arcing. The collimated beam is nominally focused using a plano-convex lens (OptoSigma, Santa Ana, CA) to a 50 µm spot directly below the outlet of the capillary (Polymicro Technologies, Phoenix, AZ), which has been HF-etched to a cone-shaped tip and is housed in a custom-built acetal resin sheath flow cell (Delrin, E. I. duPont de Nemours & Co., Wilmington, DE). As analytes elute from the capillary they are excited by the excitation beam and emit fluorescence, which is collected and collimated by a 15x all-reflective objective (13596, Newport, Irvine, CA). The fluorescence is directed toward the three photomultiplier tube (PMT) detectors (H6780-06, Hamamatsu, Middlesex, NJ) by two dichroic mirrors (310dcxxr-haf #110258 and 400dcxru #111563, Chroma Technology, Rockingham, VT), with transition points at 310 nm and 400 nm, respectively. The first detector (PMT “blue”) measures emission from 250-310 nm, the second detector (PMT “green”) measures emission from 310-400 nm, and the third detector (PMT “red”) measures emission from 400 nm and above. The laser and PMTs are synchronized and controlled by software written in LABView and provided by Photon Systems Inc.

Negative voltage for electrophoresis is applied to the sheath flow waste by a stainless steel cylinder that is connected to a power supply (PS/MJ30N0400-11, Glassman High Voltage, High Bridge, NJ) and laboratory-built control box. Sheath buffer is gravity-driven and flow can be adjusted by a right angle switching valve (Upchurch Scientific, Oak Harbor, WA).

4.2.4 Electrophoresis

The sheath flow buffer was 25 mM citric acid buffer, pH 2.25, and the flow rate was 0.2 mm/s for all experiments. The electrophoresis buffers and sample buffers varied as stated in the text (Table 4.1 and figure captions). The voltage for all experiments was -30 kV unless otherwise stated. The typical laser pulse energy was between 1.5 μJ/pulse and 2 μJ/pulse. The capillary dimensions were 50 μm inner diameter, 360 μm outer diameter, and 71.5 cm in length.

The capillary was conditioned at the beginning of the day with 0.1 M NaOH for 15-20 min, followed by water for 5 min, and then electrophoresis buffer for a minimum of 5 min.

4.2.5 CE methods

Please see Table 4.1 for more information on buffer composition for each technique.

Hydrodynamic (HD) injection: HD injection was performed by lowering the sheath flow waste outlet by 32.5 cm for a set period of time.

Electrokinetic (EK) injection: EK injection was performed by applying voltage while the capillary inlet was submersed in a sample for a set period of time.

Field-amplified sample stacking (FASS): The sample was diluted with ultrapure deionized water + sulphorhodamine-101, used as an internal standard. The sample was introduced by either HD or EK injection.

Field-amplified sample injection (FASI): The sample was diluted with ultrapure deionized water + sulphorhodamine-101. A plug of ultrapure deionized water was HD injected into the capillary, followed by either a HD or EK injection of sample.

Micellar electrokinetic chromatography (MEKC): The sample was used without dilution and introduced into the capillary by HD injection.

Dynamic pH junction: The sample was diluted with ultrapure deionized water + sulphorhodamine-101 and introduced into the capillary by HD injection. The pH of the sample was ~7.4, and the pH of the electrophoresis buffers were 1.9, 2.4, and 8.8.

pH-mediated sample stacking: The sample was diluted with ultrapure deionized water + sulphorhodamine-101. The sample was either HD or EK injected, followed by a plug of 0.1 – 0.5 M HCl, which was also introduced to the capillary by either HD or EK injection.

These conditions were the same for all runs performed: 25 mM citric acid, pH 2.25 (sheath buffer), 3 Hz (laser repetition rate), 100 µs (laser pulse length), 8 A (laser current), 420 V (laser BUSS voltage), 470 pF (PMT gain), 64% (gain voltage), 110 µs (PMT integration time).

4.2.6 Microdialysis samples

After thawing the samples, 1 µL of the microdialysate sample was diluted with 2.5 µL of 7.5 µM sulforhodamine-101, used as an internal standard, and 6.5 µL of ultrapure deionized water for a total volume of 10 µL. The final conditions used for analyzing these samples were: 40 mM borate, pH 8.8 (electrophoresis buffer), 10x aCSF (sample buffer), 25 mM citric acid, pH 2.25 (sheath buffer), -30 kV (separation voltage), 25 µA (current), 3 Hz (laser repetition rate), 100 µs (laser pulse length), 8 A (laser current), 420 V (laser BUSS voltage), 470 pF (PMT gain), 64% (gain voltage), 110 µs (PMT integration time). The injection volume was 14.7 nL for a 30 s hydrodynamic injection, which was performed by lowering the sheath flow waste outlet by 32.5 cm. Samples were run randomly and blind to prevent any analysis bias, with the identities of the samples unblinded after measurements were completed.

4.2.7 Data analysis

Data analysis was performed in IgorPro 5.05A (WaveMetrics Inc., Lake Oswego, OR). An automated data analysis script was written that reduces the user input to a single command. Output consists of four tables of calculated values with four corresponding color-coded graphs displaying the raw data, 6-point boxcar averaged data, normalized (with respect to the laser pulse energy) data, and both normalized and boxcar averaged data. The baseline range with the lowest standard deviation is determined and used to calculate the limits of detection (LOD) for each PMT channel. Ratiometric analysis (calculating the intensity ratio between peak maxima in each of the PMT channels) is also automated to aid in analyte identification.

4.2.8 Limits of detection and quantitation

LODs and concentration of analytes were determined by generating calibration curves for each analyte under the appropriate conditions. Analyte concentrations ranged from the micromolar to the low nanomolar, within physiological limits and at maximum an order of magnitude greater than LODs. The criterion for calculating the LODs was three times the standard deviation of the baseline.

4.2.9 Statistics for biological samples

Data were analyzed with either one-way analysis of variance (ANOVA) with Tukey *post hoc* comparison, or by Student's t-test, using SigmaStat analysis software.

4.3 Results and discussion

Several different concentration techniques were applied to the analysis of trace levels of indolamines within high salt sample matrices, namely aCSF. This sample matrix has an ionic strength of 0.163M and a conductivity of 15.7 mS/cm. Although the ionic strength was comparable to the electrophoresis buffers used (Table 4.1), the buffer conductivities were significantly lower. This mismatch between conductivities can cause analyte destacking to occur during separation, which degrades resolution and signal intensity. Comparing the signal intensity and peak shape for the mixture of indolamine standards in Figure 4.6 under different conductivity pairs, it was evident that the high salt sample matrix negatively impacts detection, although using the higher conductivity phosphate buffer provides better results than borate buffer even at a lower separation voltage. The pH of both buffers was the same, pH 8.8, to ensure that differences due to electroosmotic flow (EOF) effects are minimized.

A factor that was considered was separation speed; given that a large number of samples were separated and analyzed for their indolamine content, the concentration technique needed to allow for relatively rapid separations of the analytes of interest. The EOF is maximized at pHs of 8.8 or above, leading to the separation of several common indolamines within 10 min or less. Another concern was the collection efficiency of microdialysis probes for small molecules: we have observed a 10% to 15% collection

efficiency for 5-HT, which means that the indolamine concentrations are reduced by 6.7- to 10-fold before CE analysis. Combining this with the challenges of performing efficient separations under high salt conditions, it was imperative that a sensitive and robust concentration method be used for analysis.

HD injections were also compared with EK injections. EK injections can bias sample introduction by preferentially introducing the most highly charged analytes first, making accurate quantitation within a sample difficult. If the analyte of interest is highly charged, however, EK injection can enrich the amount of that analyte within the injected sample.

FASS conditions were tested for several different combinations of buffers and aCSF dilution factors (Figures 4.7 and 4.8). Comparing borate and phosphate buffers again, phosphate buffer is unable to resolve NAS from Trp and HITCA from HIAA within a standard indolamine mixture. In borate buffer, the analyte peaks appear relatively sharp and Gaussian in shape. In Figure 4.7 (B) the net peak intensities appear lower but without band broadening compared to the same sample concentrations under ideal conditions. The relative conductivities for the sample matrix and the electrophoresis buffer in (B) are 1:10, typical for FASS. Better net signal intensity, however, is obtained for a 1:2 relative conductivity ratio, as is shown in Figure 4.8 (A).

For FASI experiments, FASS was combined with FASI to determine if the enhancement ratio would be additive. The electrophoresis buffer and sample matrix were held constant (2.4:1.5 conductivity ratio, respectively) and water plug injection lengths were varied from 20 s to 90 s. The sample injection amount and method were also held constant for several runs, to more easily calculate the enhancement factor for each run compared with a FASS control. Figure 4.9 shows the results for a variety of conditions. Based on the ratios of net intensities calculated for each analyte, little enhancement was seen for any of the combined FASS-FASI conditions. There may have been enhancement due to FASI alone if the sample matrix was not previously diluted, but based on these results it would have been equilvalent to FASS and not nearly as high as had been reported (100- to 1000-fold enhancement). Even after dilution, the sample matrix conductivity was still elevated and additional enhancement would have been beneficial.

MEKC was tested as a concentration technique for 5-HT. As shown in Figure 4.10, 5-HT did not elute under two different MEKC conditions. Once the high voltage was shut off, a syringe was attached to the capillary inlet and buffer forced through the capillary manually. The intensities in all three channels increased, and what appears to be 5-HT elutes from the capillary around 2850 s. The large difference in net intensities in the 5-HT peak in (B) and (C) could be attributed to degredation of 5-HT within the capillary due to Joule heating. The higher conductivity of the buffer in (C) (0.450 mS/cm versus 0.330 mS/cm for (B)) makes Joule heating more likely to occur and increases in current, a sign of Joule heating, were observed. Based on previous work (not shown), a possible reason for the inability of 5-HT to elute within a reasonable time frame under MEKC conditions is the composition of the sample matrix. Another possible reason was the combination of phosphate buffer with SDS; although this recipe has been used in the literature, I was unable to replicate the results. Given the results, MEKC was not further pursued as a possible technique for analysis of microdialysate samples.

Dynamic pH junction was tested on indolamine standards to determine if it was a viable concentration technique for these analytes. Figure 4.11 details the results. Compared with FASS control conditions, dynamic pH junction failed to elute analytes within a reasonable time frame and the analyte bands that did elute were very broad and misshapen. One electropherogram, (C), shows how a syringe was used to mechanically force buffer through the capillary after the high voltage was disabled. The background intensities in all three channels increase substantially, but no peaks elute and the relative increases are not consistent with signal ratios for citric acid or for indolamines. A reason for the greatly increased migration times was the reduced EOF experienced when lower pH buffers are used for separation. The peak shape and broadening could be attributed to a combination of buffer interactions and incomplete titration. Dynamic pH junction was not further investigated for enhancing the separation of indolamines.

A technique that demonstrated potential was pH-mediated sample stacking. HD and EK injection were compared for efficacy in concentrating 5-HT, shown in Figure 4.12. The sample was undiluted and phosphate buffer was used as the electrophoresis buffer. The

most successful conditions were EK injection of the sample, followed by EK injection of 0.1 M HCl. Enhancement was approximately 5-fold on average, with a high value of 11-fold enhancement. Interestingly, these experiments were repeated for borate buffer, but no enhancement was observed (data not shown). It is possible that the shorter migration time (approximately 250 s, about half of the 5-HT migration time in phosphate buffer) did not allow enough time for enhancement to occur. Figure 4.13 details different conditions for pH-mediated sample stacking.

HCl concentrations were varied from 0.1 M to 0.5 M, but enhancement ratios varied from approximately 1.5- to 8-fold and appear random (data not shown). Best results were obtained for 0.1 M HCl; however, enhancement ratios for 0.1 M HCl injections were also inconsistent across multiple separations, ranging from around 2-fold to 12.5-fold improvement in signal. Occasionally the EK injection of HCl would "fail", as the current during injection would drop rapidly to close to zero; sometimes during the separation the current would rebound and the separation would occur, and other times it remained at zero and the injection would have to be repeated. To reduce these failures, the capillary needed to be conditioned with 0.1 M NaOH between every run. Although the enhancement was greater than most of the other concentration techniques, the unpredictable nature of pH-mediated sample stacking made it unacceptable for routine use.

Post-stimulation dialysate was compared under different conditions as well, to see if the results obtained with standard indolamine mixtures were repeatable for biological samples. Undiluted and diluted samples were compared in both borate and phosphate buffers, for both HD and EK injected samples. The best results were obtained in trace (C), under FASS conditions.

Based on all of the above results, FASS using 10x diluted aCSF as the sample matrix and 40 mM borate, pH 8.8, as the electrophoresis buffer, and HD injection was chosen as the technique for analyzing microdialysis samples. Fast elution times, effective concentration of analytes, and high temporal resolution was obtained using FASS, in addition to high repeatability. The buffer concentration was lowered from 50 mM to 40 mM to reduce the likelihood of Joule heating and subsequent analyte degradation. A

representative electropherogram is shown in Figure 4.15. Two indolamines, 5-HT and Trp, are detected, identified, and quantitated within this electropherogram. Table 4.2 details the figures of merit under FASS conditions for analyte identification and the LODs, which are appropriate for trace analyte analysis.

These conditions were used to separate, concentrate, detect, identify, and quantitate trace indolamine levels in over 200 mouse microdialysis samples; greater than 75% of samples had detectable levels of indolamines. Figure 4.16 displays the statistical results of the 5-HT analysis in microdialyate samples. Electrical stimulation of the MRN resulted in increases in 5-HT release but not in acetylcholine and glutamate, which were analyzed by HPLC with electrochemical detection and CE-LIF, respectively. Mice were surgically implanted with a stimulating electrode aimed at the MRN and a microdialysis cannula aimed at the SCN. For each experiment, baseline samples were collected for 1 h, then animals were stimulated for 20 min, represented by the black square. Samples were then collected every 20 min, for 100 min following stimulation. These results indicate that 5-HT release is independent of acetylcholine and glutamate release during stimulation. These measurements demonstrate that acetylcholine and glutamate release at the SCN was specific to the stimulation of homeostatic sleep centers and not from nearby areas such as the serotonergic MRN.

4.4 Conclusions and future work

Several concentration techniques were tested for analyzing low levels of indolamines within high salt sample matrices. Only FASS was able to provide fast separation times, efficient concentration of analytes, and sufficient resolution for the analysis of over 200 mouse microdialysis samples.

Another effective concentration technique was pH-mediated sample stacking; however, the degradation of indolamines within the capillary and current stability during injection need to be addressed for biological samples before this technique can be adopted for routine use.

Future work for analyzing high salt samples could include testing base stacking in pH-mediated sample stacking, FASI combined with MEKC, MEKC using different

electrophoresis buffers and surfactants, large volume sample stacking, and reversing the pH gradient of the sample buffer and the electrophoresis buffer in dynamic pH junction.

To summarize this project, significant acetylcholine and glutamate release was found at the SCN when the homeostatic sleep centers were stimulated and, concomitantly, the behavioral circadian rhythms were reset. These results establish modes of neurochemical communication from brain regions controlling homeostatic sleep states to the SCN, with behavioral consequences. They suggest a basis for dynamic integration across brain systems that regulate vigilance states, and a potential vulnerability to altered communication in sleep disorders. This data provides a unique glimpse of dynamic neurotransmitters within the mammalian brain during sleep-wake cycling and hints how such behaviors are controlled.

4.5 Tables

buffer or solution	use	I, M	K, mS/cm
aCSF, pH 7.4	sample buffer	0.163	15.7
40 mM borate, pH 8.8	electrophoresis, FASS, FASI, dyn pH	0.207	2.38
50 mM borate, pH 8.8	electrophoresis, FASS	0.260	3.00
10 mM phosphate, pH 8.8	electrophoresis, FASS	0.060	0.97
50 mM phosphate, pH 8.8	electrophoresis, FASS, pH-med	0.300	7.33
50 mM phosphate, pH 8.8, + 30 mM SDS	electrophoresis, MEKC	0.330	9.03
50 mM phosphate, pH 8.8, + 150 mM SDS	electrophoresis, MEKC	0.450	11.5
25 mM citric acid, pH 2.4	sheath buffer, electrophoresis, dyn pH	0.025	0.67
150 mM citric acid, pH 1.9	electrophoresis, dyn pH	0.150	4.02

Table 4.1 A list of buffers and solutions, the separation mode they were used for, their ionic strengths (I), and their conductivities (K). FASS = field-amplified sample stacking, FASI = field-amplified sample injection, MEKC = micellar electrokinetic chromatography, pH-med = pH-mediated sample stacking, dyn pH = dynamic pH junction

analyte	Δt wrt SR-101, s	time, s	G/B	B/R	G/R	LOD, nM
5-HT	114	170	8.25	2.80	23.2	1.9
NAS	64	220	11.5	0.40	4.90	3.2
5-HT sulfate	42	242	5.30	1.00	5.50	0.9
Trp	27	258	9.30	0.60	5.00	2.2
SR-101	0	285	0.30	0.12	0.04	N.D.
HITCA	-56	340	8.90	3.75	33.6	6.7
HIAA	-71	355	8.20	0.80	6.50	1.6

Table 4.2 Analyte figures of merit under the final conditions selected (40 mM borate, pH 8.8 (electrophoresis buffer), 10x aCSF (sample buffer), -30 kV (separation voltage)). The column heading, Δt wrt SR-101, represents the average difference in migration time between the analyte in question and sulphorhodamine-101, an internal standard. This figure is used as additional confirmation of analyte identity. The LODs are appropriate for trace analyte analysis. Over 200 samples were analyzed, and greater than 75% of samples had detectable indolamine levels. 5-HT = serotonin, NAS = N-acetylserotonin, 5-HT sulfate = serotonin-O-sulfate, Trp = tryptophan, SR-101 = sulforhodamine-101, HITCA = 5-hydroxyindole thiazoladine carboxylic acid, HIAA = 5-hydroxyindole-3-acetic acid

4.6 Figures

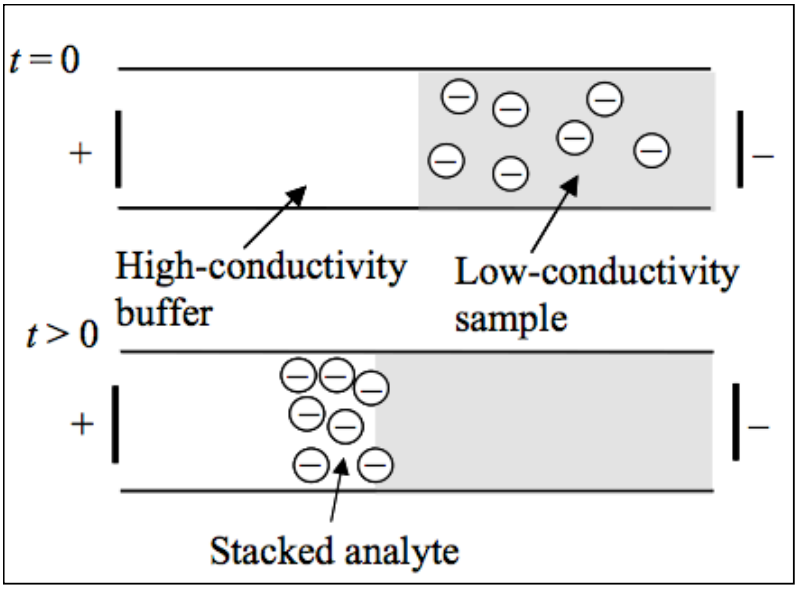

Figure 4.1 Schematic of field-amplified sample stacking (FASS). The low conductivity sample plug experiences a stronger electric field than the high conductivity background electrolyte (BGE). Once the analytes reach the boundary between the sample plug and BGE, they "stack" into a concentrated band. Adapted with permission.[30]

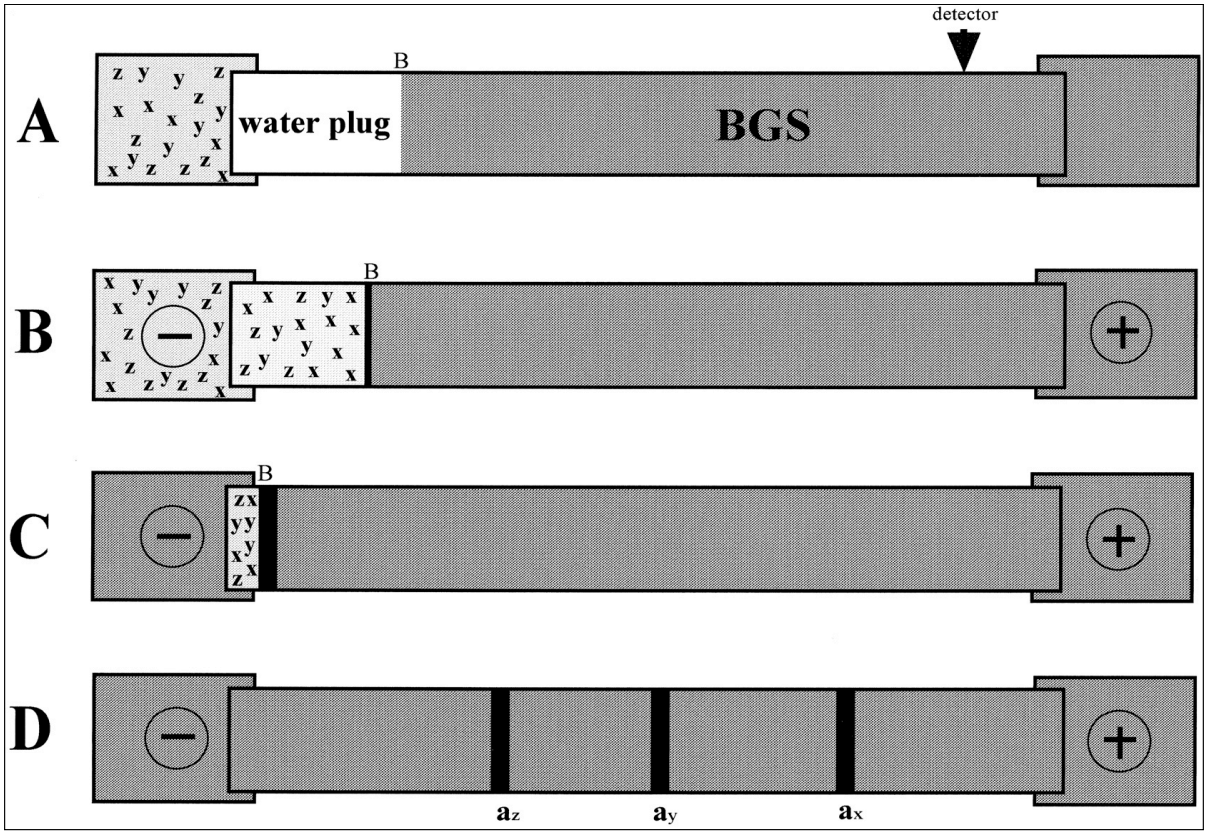

Figure 4.2 (A) Hydrodynamic injection of water after conditioning the capillary with BGE. (B) Electrokinetic injection of sample following the water plug. (C) The voltage is shut off, the sample vial is replaced by another BGE vial, and voltage is applied at negative polarity again. Analytes stack at the concentration boundary (B). (D) Focused bands separate within the capillary. Reprinted with permission from (14). Copyright 2011 American Chemical Society.

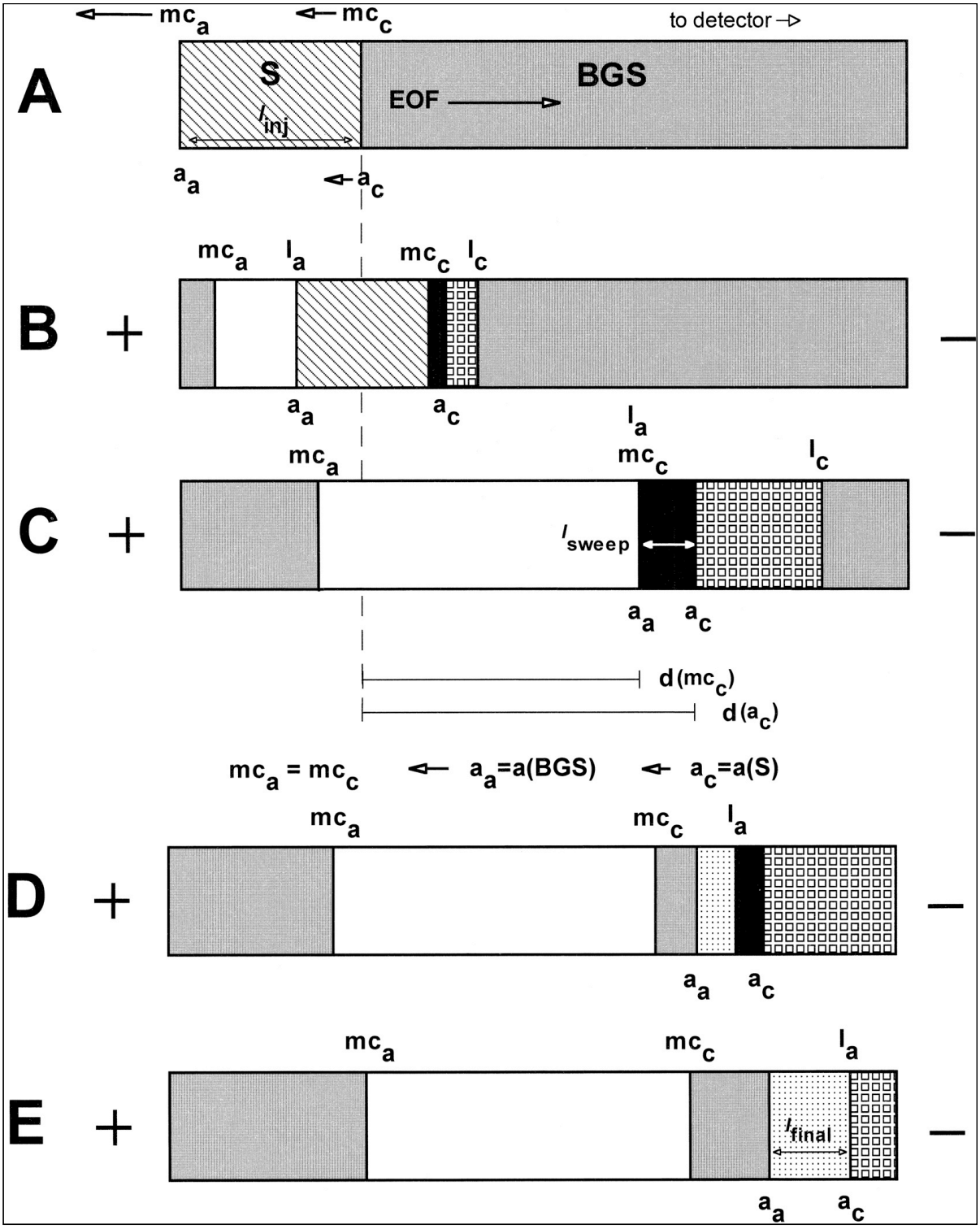

Figure 4.3 Evolution of micelles and neutral analyte molecules during sweeping in the presence of high electroosmotic flow and a high-salt- concentration matrix.

Figure 4.3 (cont.) (A) Starting situation: injection of sample S prepared in a matrix having a conductivity greater than that of the BGE; (B) application of voltage at positive polarity, micelles emanating from the cathodic side stack at the interface between S and BGE (I_c) and sweep the analyte molecules; (C) the injected analyte zone is assumed to be completely swept; (D) the stacked micelles leave the S zone and destack at (I_a) while swept analyte zones broaden; (E) swept analyte zones completely leave the S zone. Other abbreviations are: a_a: anionic analytes, a_c: cationic analytes, mc_a: micelles at the anodic end, mc_c: micelles at the cathodic end, $d(mc_c)$: distance travelled by the micelles at the cathodic end, $d(a_c)$: distance travelled by the cationic analytes. Reprinted with permission from (11). Copyright 2011 American Chemical Society.

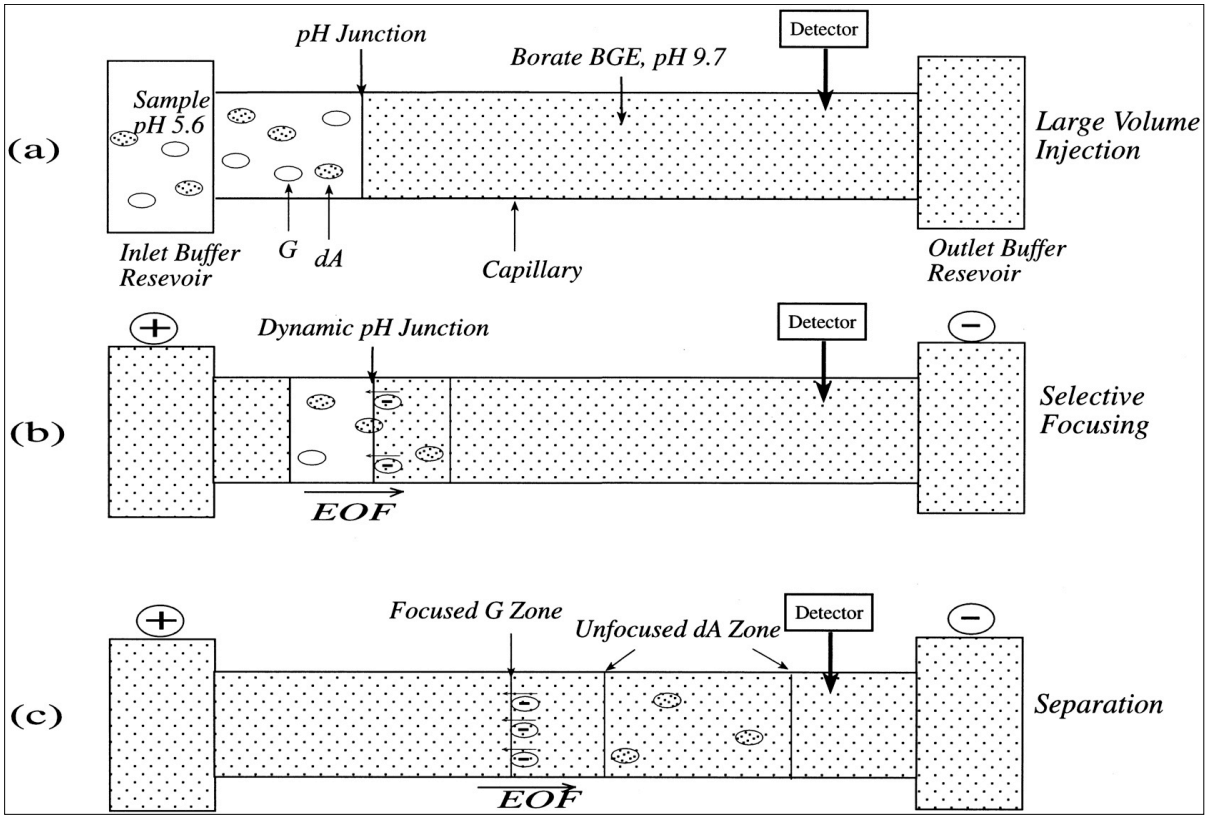

Figure 4.4 A diagram describing dynamic pH junction. (A) A large sample plug of a low-pH electrolyte is first injected into the capillary that is filled with a high-pH BGE (pH junction). (B) Focusing of some analytes occurs as a dynamic pH junction sweeps through the sample zone, whereas other analytes continue to migrate as a wide sample plug. (C) separation of the analytes by normal zone electrophoresis. Reprinted with permission from (20). Copyright 2011 American Chemical Society.

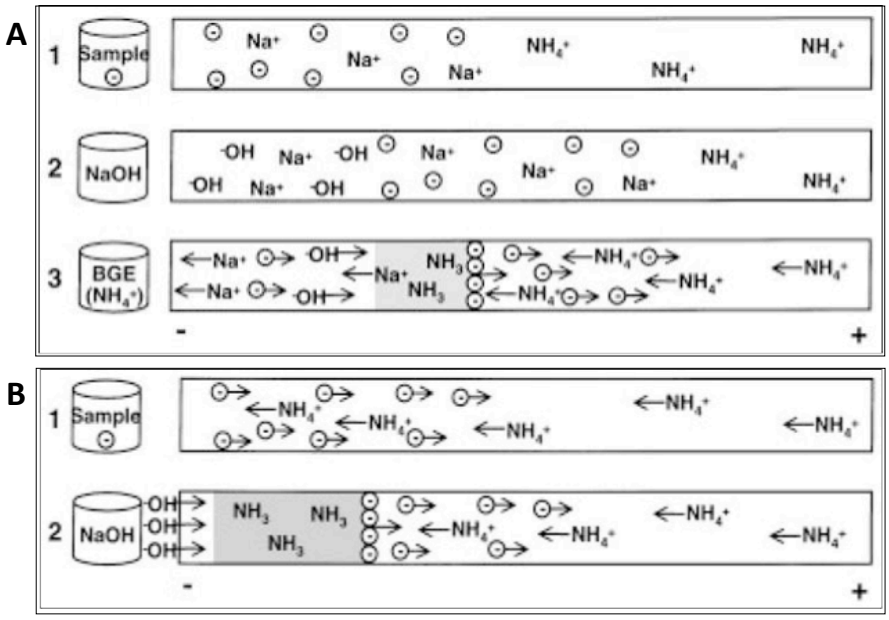

Figure 4.5 Diagrams depicting pH-mediated sample stacking. (A1) Sample is injected hydrodynamically. (A2) NaOH is injected hydrodynamically and the sample zone is pushed farther into the capillary. (A3) High voltage is applied and BGE cations replace sample cations; sample zone is titrated to low conductivity. Tailing also occurs in this mode as already described. (B1) Electrokinetic sample injection begins and anionic analytes travel towards the anode; BGE cations move toward cathode and replace sample cations. (B2) NaOH is injected electrokinetically and BGE cations in the sample zone are titrated by hydroxide ions to create a zone of low conductivity (shaded gray). Adapted and reprinted with permission from Wiley.[21]

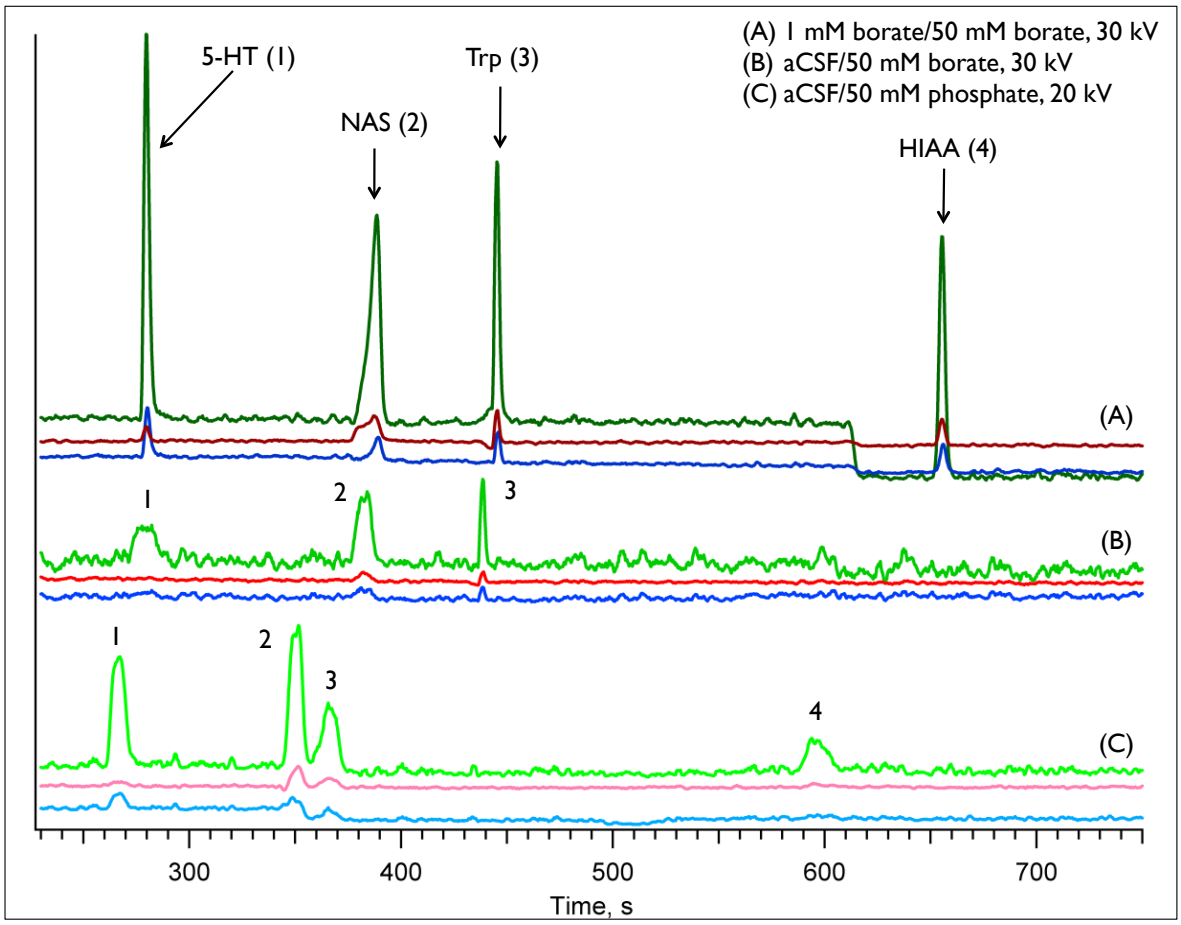

Figure 4.6 Comparing low salt and high salt matrix effects on the separation of indolamines. (A) The typical conditions used on this instrument, utilizing FASS to enhance the peaks. (B) The sample stock prepared in aCSF, a high salt matrix (see Table 4.1). (C) Same sample as (B), using a different electrophoresis buffer and voltage. [5-HT] = 734 nM, [NAS] = 792 nM, [Trp] = 340 nM, [HIAA] = 776 nM

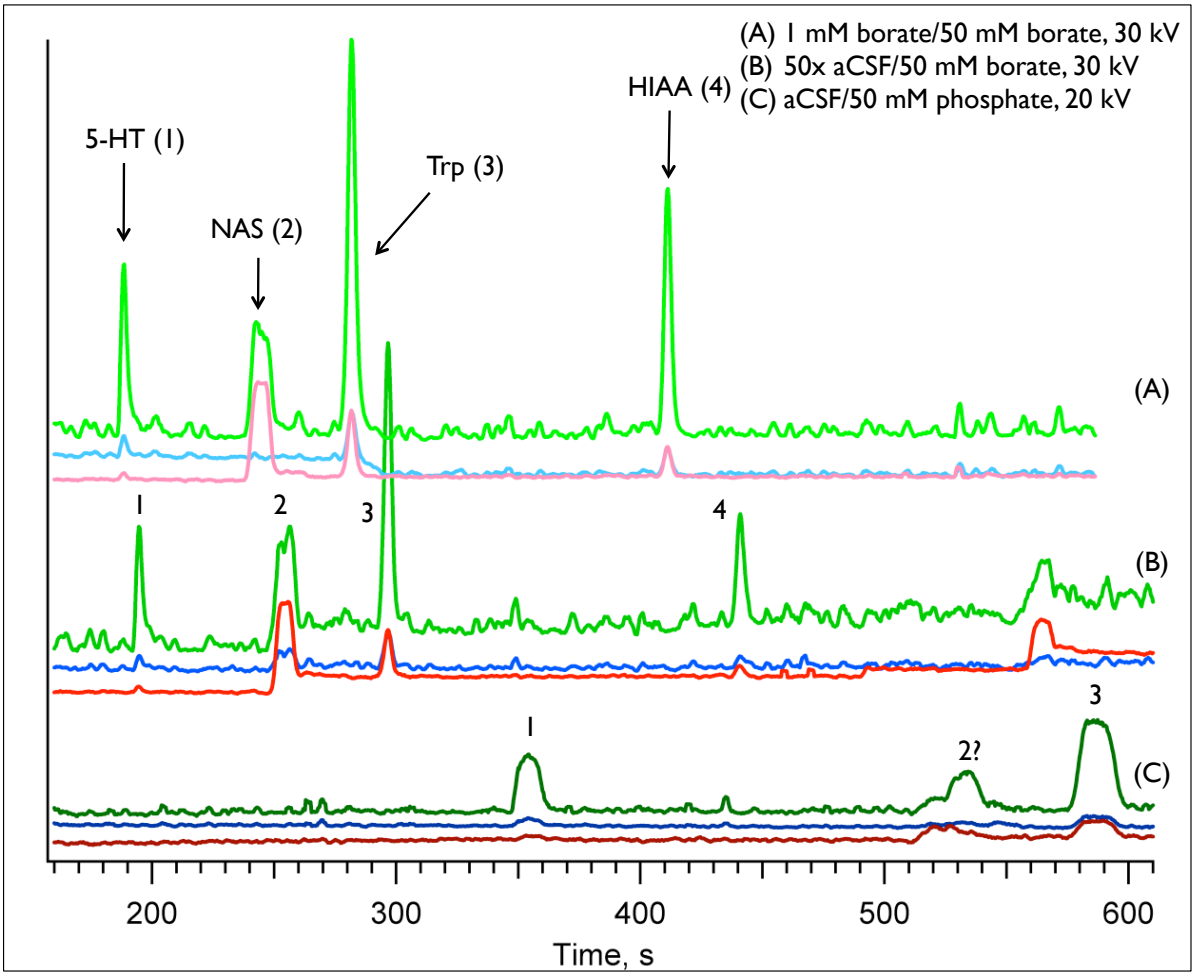

Figure 4.7 Comparing FASS conditions. (A) The optimized conditions used on this instrument for standards, which utilizes FASS and a very low salt sample matrix. (B) The sample matrix was 50-fold diluted aCSF. Note the Gaussian peak shape, but lower intensity compared with (A). (C) The sample was prepared in undiluted aCSF. Note the top hat peak shape, compared with the Gaussian-shaped peaks above. [5-HT] = 243 nM, [NAS] = 156 nM, [Trp] = 482 nM, [HIAA] = 414 nM

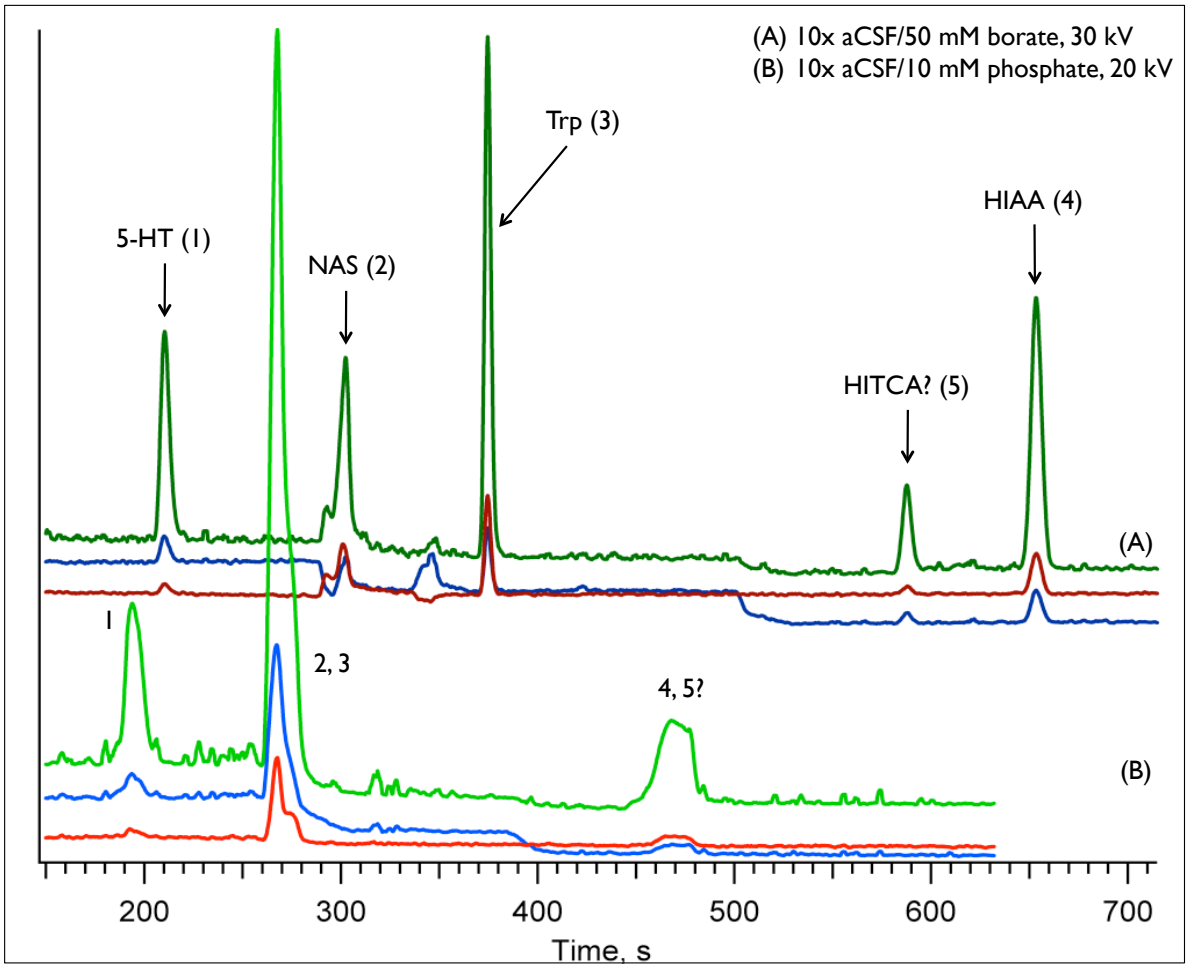

Figure 4.8 Comparing FASS conditions. The phosphate buffer concentration was reduced, to eliminate differences due to the much higher conductivity of phosphate buffer, compared to borate buffer (Table 4.1). The sample was prepared in 10-fold diluted aCSF. (A) The sample separated in borate buffer. (B) The sample separated in phosphate buffer. Note the unresolved peaks and poor peak shape for later eluents. [5-HT] = 472 nM, [NAS] = 406 nM, [Trp] = 800 nM, [HIAA] = 756 nM, [HITCA] = 350 nM

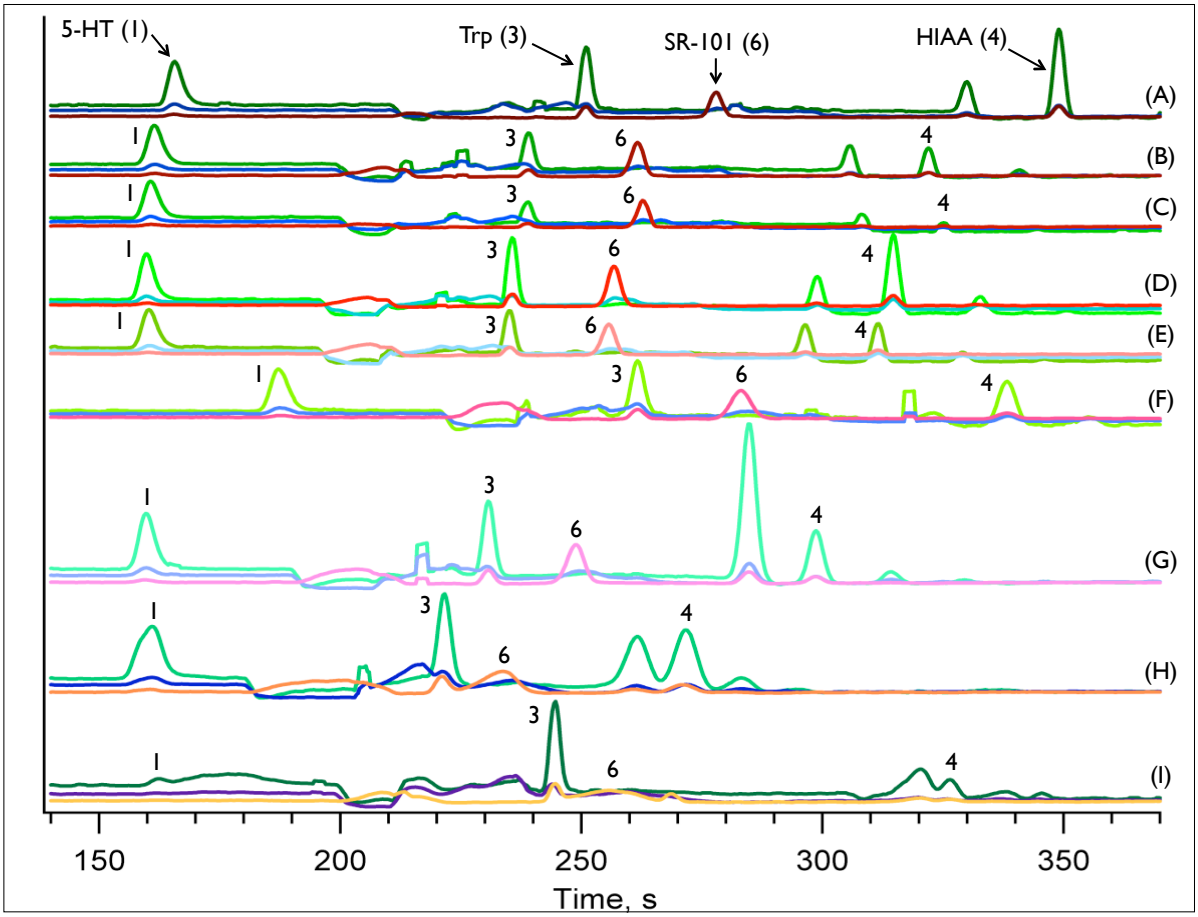

Figure 4.9 Comparing FASS-FASI conditions. The sample was prepared in 10-fold diluted aCSF and the electrophoresis buffer was 40 mM borate buffer, unless otherwise noted. The separation voltage was -30 kV. (A) Control, 30 s HD injection under FASS conditions. (B) 30 s HD injection of water, followed by 3 s EK injection of sample at -30 kV. (C) 20 s HD injection of water, followed by 3 s EK injection of sample at -30 kV. (D) 30 s HD injection of water, followed by 30 s HD injection of sample. (E) 40 s HD injection of water, followed by 3 s EK injection of sample at -30 kV. (F) 50 s HD injection of water, followed by 3 s EK injection of sample at -30 kV. (G) 60 s HD injection of water, followed by 3 s EK injection of sample at -30 kV. (H) 90 s HD injection of water, followed by 3 s EK injection of sample at -30 kV. (I) 60 s HD injection of water, followed by 3 s EK injection of undiluted aCSF sample at -30 kV. [5-HT] = 289 nM, [Trp] = 246 nM, [SR-101] = 1887 nM, [HIAA] = 398 nM

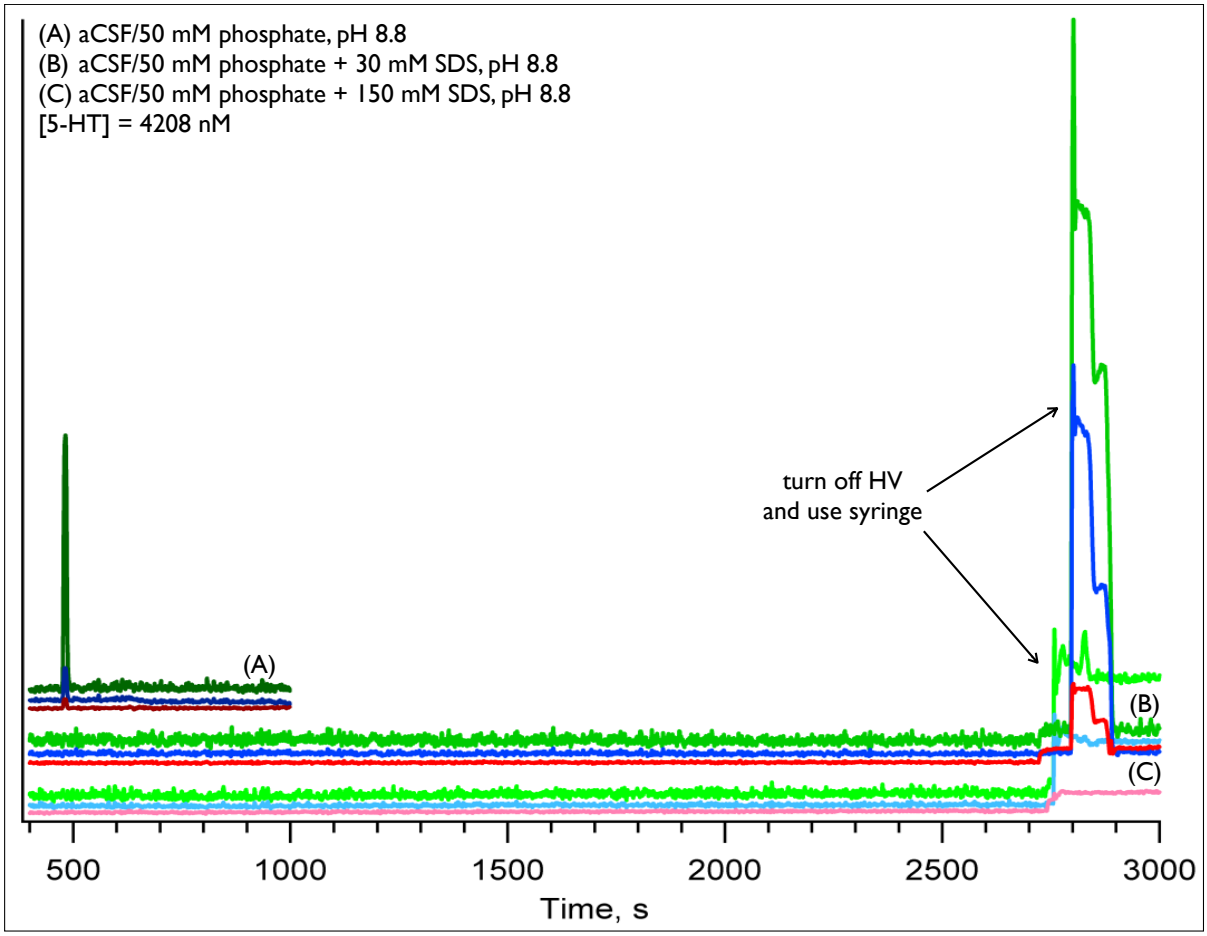

Figure 4.10 Comparing MEKC conditions. Sample (~4200 nM 5-HT) was prepared in undiluted aCSF. (A) Control conditions without surfactant in electrophoresis buffer. (B) MEKC conditions with a "low" concentration of surfactant. The intensity in all three channels peaked around 2800 – 2900 s, after the high voltage (HV) was turned off and a syringe used to mechanically force the eluent out of the capillary. (C) MEKC conditions with a "high" concentration of surfactant. The intensity in all three channels increased after the high voltage (HV) was turned off and a syringe used to mechanically force the eluent out of the capillary. A much less intense peak, compared with (B), appears around 2850 s.

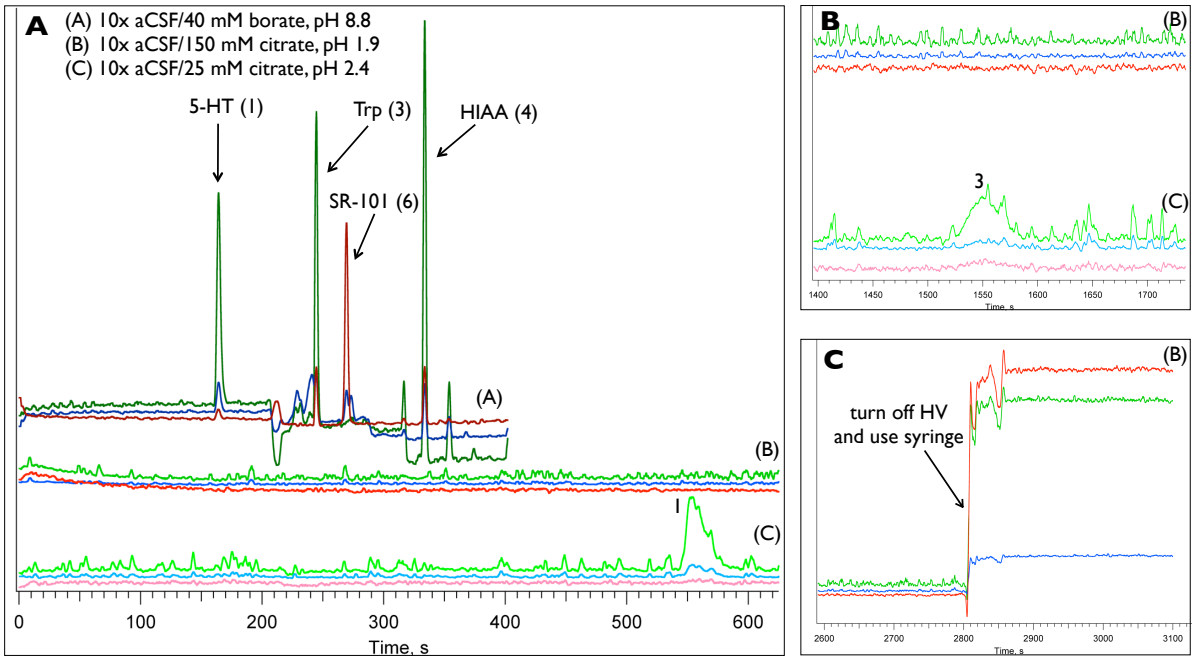

Figure 4.11 Comparing conditions for dynamic pH junction. The sample was prepared in 10-fold diluted aCSF. (AA) The sample separated in borate buffer, under FASS conditions. All the analytes elute within 400 s. (AB) The sample separation performed under dynamic pH junction conditions. No peaks eluted. (AC) The sample separated utilizing the principles of dynamic pH junction, in a higher pH, lower conductivity buffer. Note the broad peak shape, reduced intensity, and significantly increased migration time for 5-HT. (B) Traces (AB) and (AC) from 1400 s to 1700 s. (C) Trace (AB) 2600 s to 3100 s. The high voltage (HV) was turned off at ~2800 s and a syringe used to mechanically force the eluents out of the capillary. The background intensities in all three channels increase, but no peaks elute and the signal intensity does not decrease.

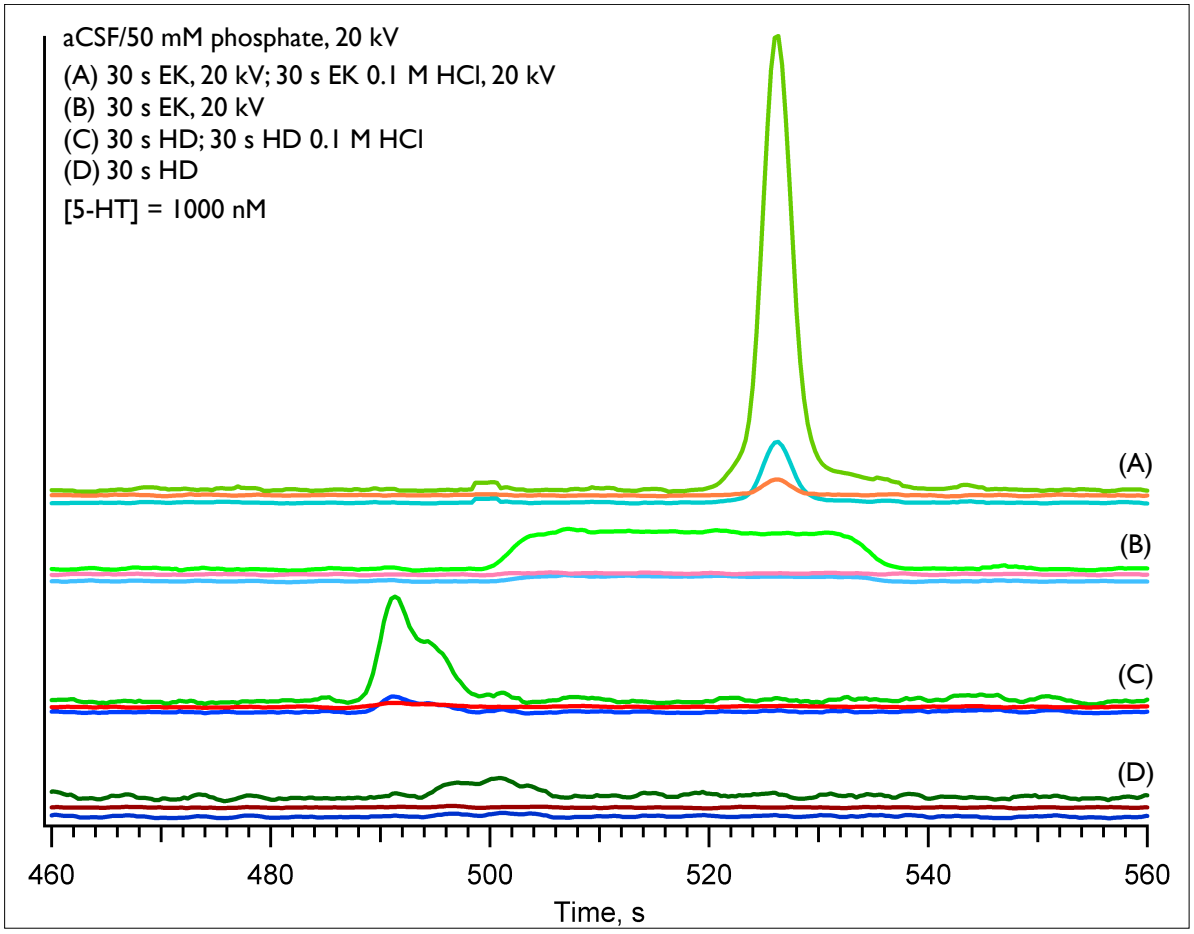

Figure 4.12 Comparing HD versus EK injection under pH-mediated sample stacking conditions. The sample (1000 nM 5-HT) was prepared in undiluted aCSF and the electrophoresis buffer was 50 mM phosphate buffer, pH 8.8. The separation voltage was -20 kV. (A) 30 s EK sample injection, followed by a 30 s EK HCl injection. Note the Gaussian peak shape and intensity. (B) 30 s EK sample injection. No focusing of the peak occurred. (C) 30 s HD sample injection, followed by a 30 s HD HCl injection. Note the partially resolved pair of peaks. (D) 30 s HD sample injection. The control sample for comparison was barely detected under these conditions without enhancement.

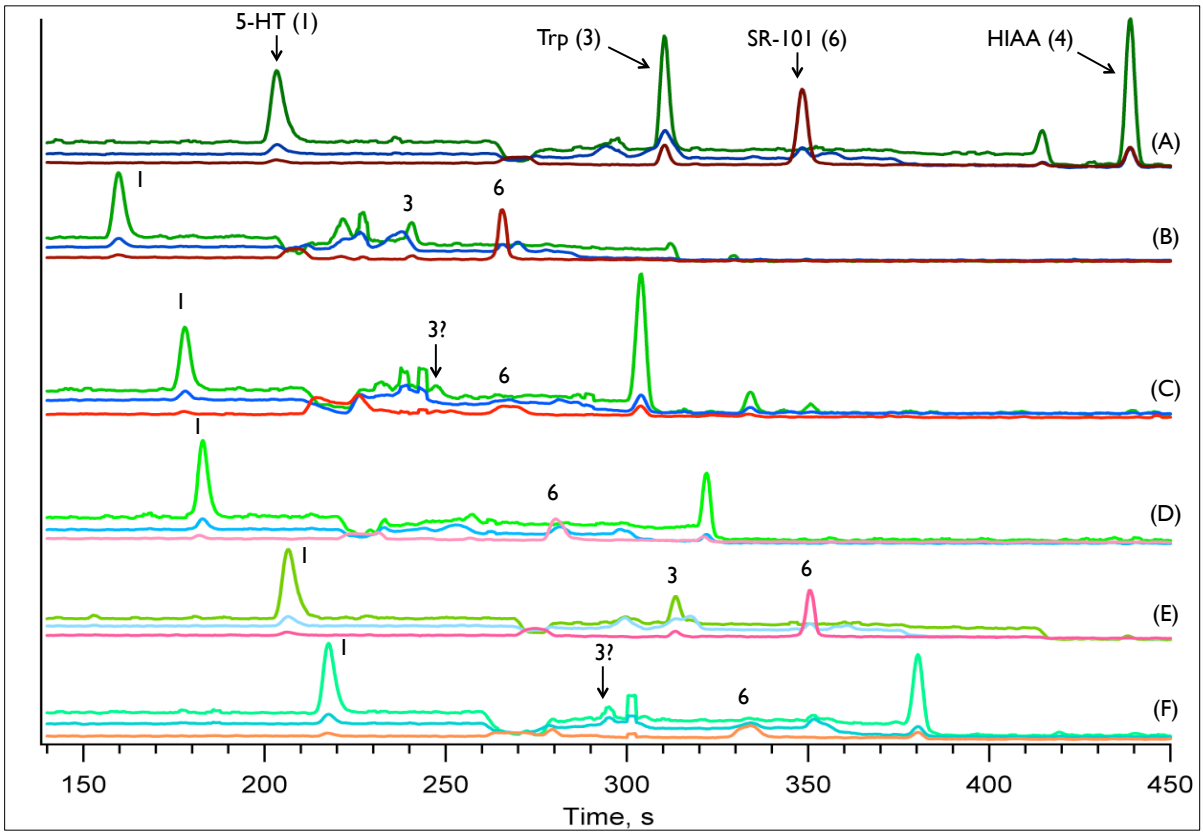

Figure 4.13 Comparing conditions for pH-mediated sample stacking. The sample was prepared in 10-fold diluted aCSF and the electrophoresis buffer was 40 mM borate buffer, pH 8.8, unless otherwise noted. The separation voltage was -30 kV. (A) Control, 30 s HD sample injection. (B) 2.5 s EK sample injection at -30 kV. (C) 2.5 s EK sample inject at -30 kV, followed by 2.5 s EK injection of 0.1 M HCl at -30 kV. (D) 2.5 s EK sample injection at -30 kV, followed by 2.5 s EK injection of 0.1 M HCl dissolved in 40 mM borate buffer, pH 8.8 at -30 kV. (E) 3 s EK sample injection at -25 kV, followed by 3 s EK injection of 0.1 M HCl at -25 kV. [5-HT] = 289 nM, [Trp] = 246 nM, [SR-101] = 1887 nM, [HIAA] = 398 nM

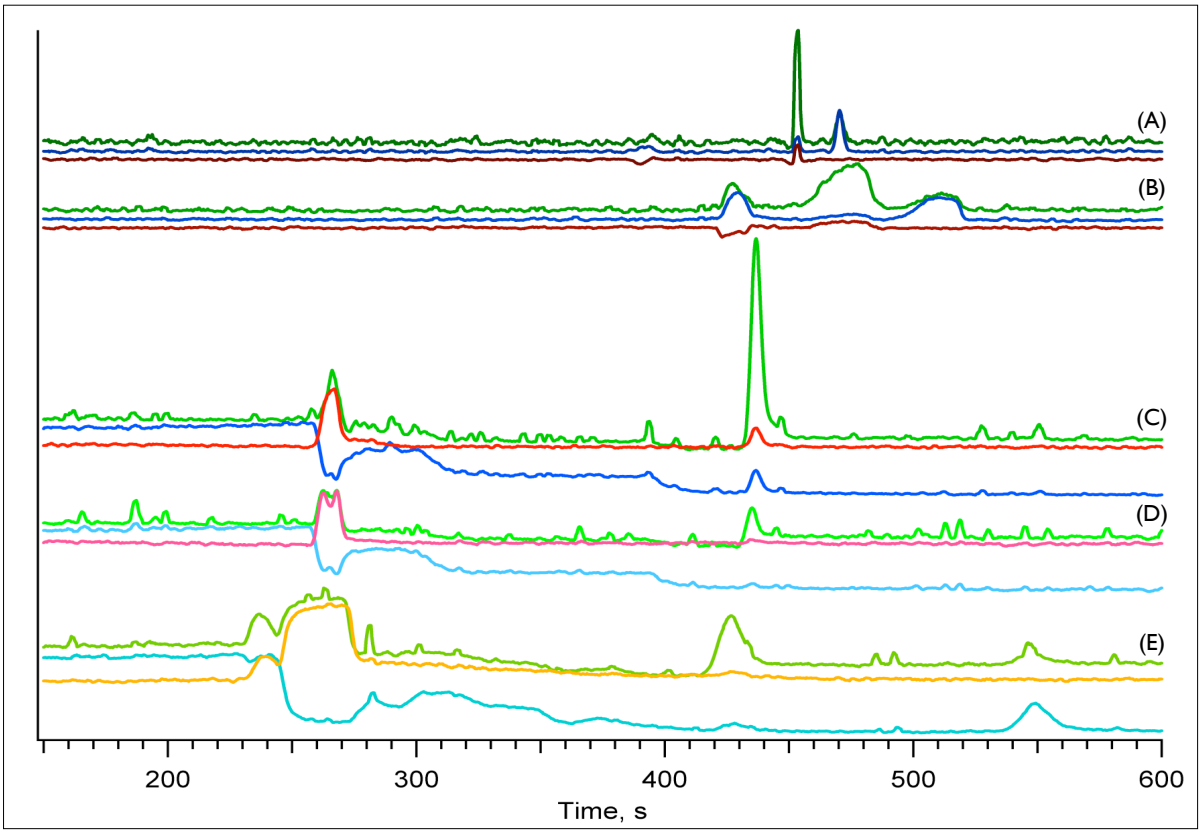

Figure 4.14 Comparing post-stimulation dialysate under different conditions. The sample was introduced into the capillary by 30 s HD injection and the separation voltage was -30 kV, unless otherwise noted. (A) The sample was prepared in undiluted aCSF and the electrophoresis buffer was 50 mM borate buffer, pH 8.8. (B) The sample was prepared in undiluted aCSF and the electrophoresis buffer was 50 mM phosphate buffer, pH 8.8. (C) The sample was diluted by 10-fold and the electrophoresis buffer was 50 mM borate, pH 8.8. (D) The sample was diluted by 100-fold and the electrophoresis buffer was 50 mM borate, pH 8.8. (E) The sample was diluted by 10-fold and the electrophoresis buffer was 50 mM borate, pH 8.8. The sample was introduced by 3 s EK injection at -30 kV.

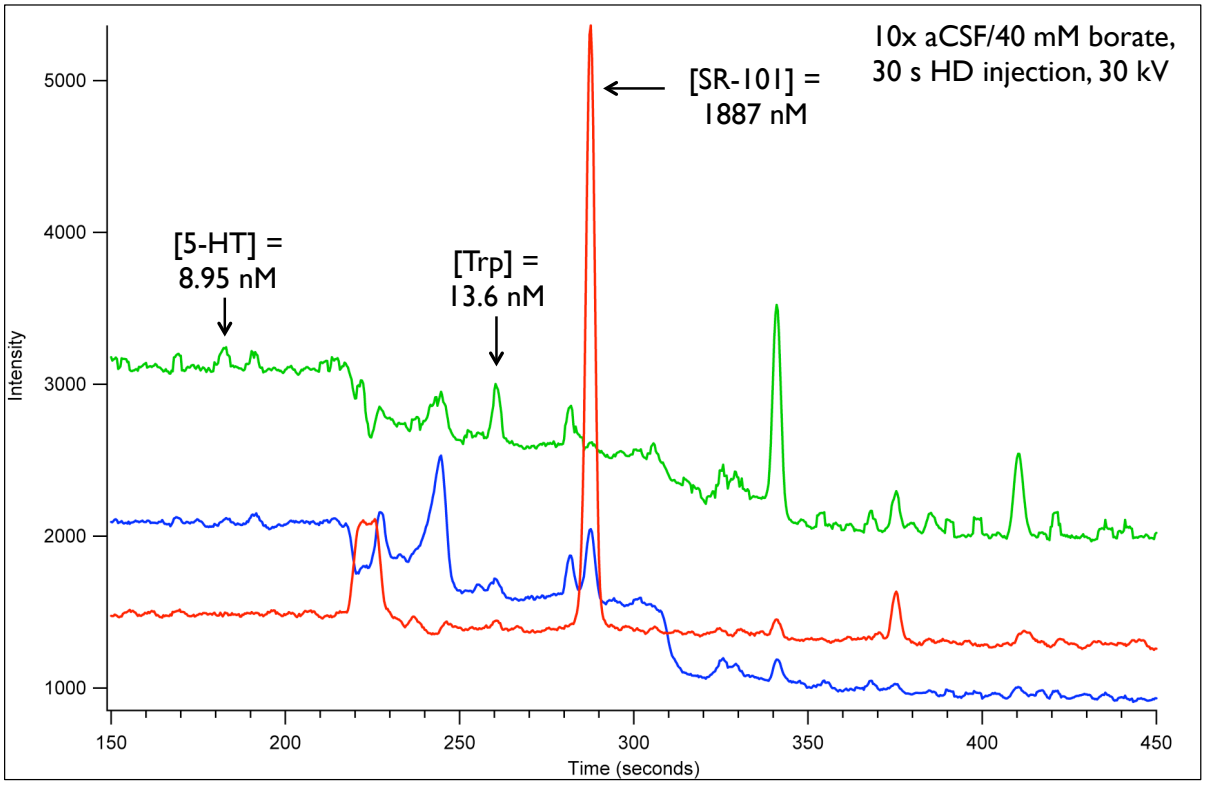

Figure 4.15 A representative microdialysis sample run. The final conditions used for analyzing these samples were: 40 mM borate, pH 8.8 (electrophoresis buffer), 10-fold diluted aCSF (sample buffer), 25 mM citric acid, -30 kV (separation voltage). Both Trp and 5-HT were detected and quantitated, along with several unidentified indolamines.

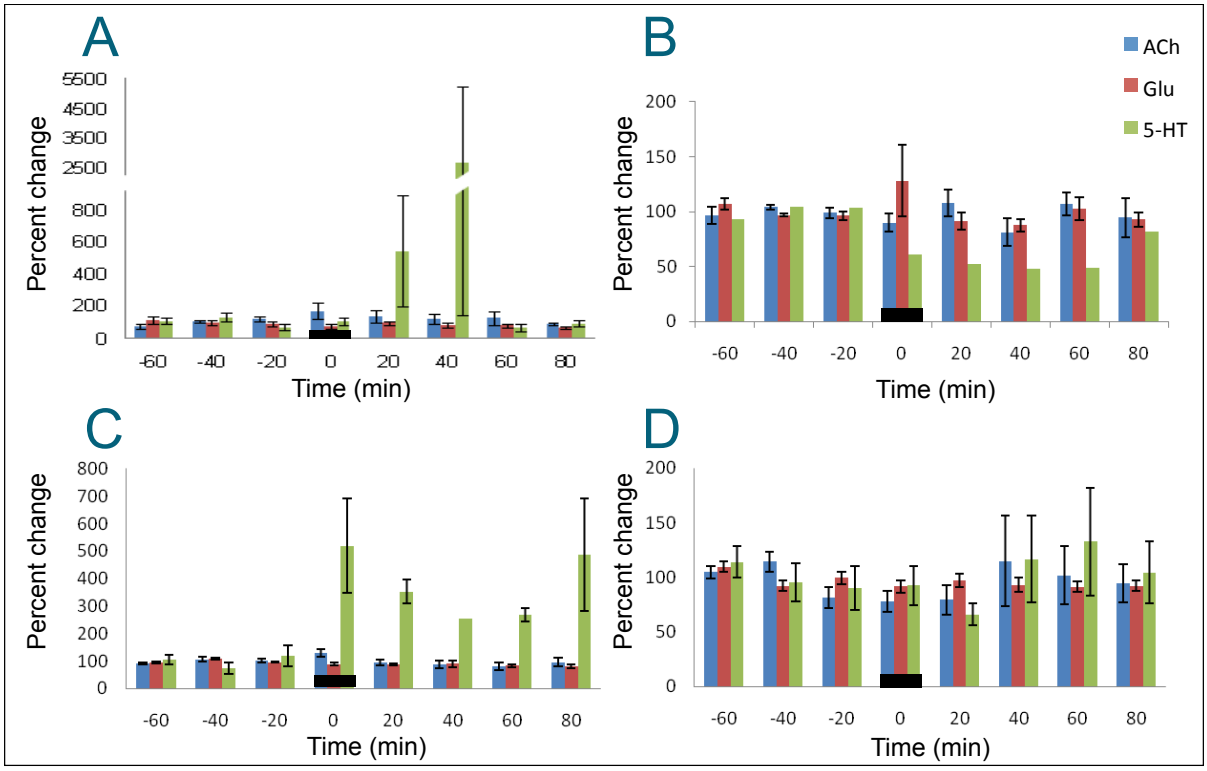

Figure 4.16 Electrical stimulation of the median Raphe nucleus (MRN) increases 5-HT release but not acetylcholine (Ach) or glutamate (Glu) release in the suprachiasmatic nucleus (SCN). (A) Parameter 1 (150 µA, 10 Hz, 2 msec pulse duration). (B) Parameter 2 (40 µA, 0.2 Hz, 0.2 msec pulse duration). (C) Parameter 3 (400 µA, 60 Hz, 0.2 msec pulse duration, applied as a 1 sec train every min). (D) Sham stimulation. Figure courtesy of Jennifer M. Arnold, Gillette group.

4.7 References

(1) Beckers, J. L.; Boček, P. *Electrophoresis*. **2000**, *21*, 2747–2767.

(2) Zhang, C.; Thormann, W. *Anal Chem*. **1996**, *68*, 2523–2532.

(3) Liu, Z.; Sam, P.; Sirimanne, S. R.; McClure, P. C.; Grainger, J.; Patterson, D. G. *J. Chrom. A*. **1994**, *673*, 125–132.

(4) Malá, Z.; Šlampová, A.; Gebauer, P.; Boček, P. *Electrophoresis*. **2009**, *30*, 215–229.

(5) Malá, Z.; Gebauer, P.; Boček, P. *Electrophoresis*. **2010**, *32*, 116–126.

(6) Britz-McKibbin, P.; Chen, D. D. Y. *Anal Chem*. **2007**, *72*, 1242–1252.

(7) Chien, R.; Burgi, D. In *Journal of Chromatography*; 1991; pp. 153–161.

(8) Zhang, L.; Sun, M. *J. Chrom. A*. **2005**, *1100*, 230–235.

(9) Wu, Y.-W.; Liu, J.-F.; Xiao, T.-X.; Han, D.-Y.; Zhang, H.-L.; Pan, J.-C. *Electrophoresis*. **2009**, *30*, 668–673.

(10) Fang, H.; Yang, F.; Sun, J.; Zeng, Z.; Xu, Y. *Electrophoresis*. **2007**, *28*, 3697–3704.

(11) Quirino, J. P.; Terabe, S.; Boček, P. *Anal Chem*. **2000**, *72*, 1934–1940.

(12) Chen, Z.; Wu, J.; Baker, G.; Parent, M.; Dovichi, N. J. *J. Chrom. A*. **2001**, *914*, 293–298.

(13) Giordano, B. C.; Copper, C.; Collins, G. E. *Electrophoresis*. **2006**, *27*, 778–786.

(14) Quirino, J. P.; Terabe, S. *Anal Chem*. **1998**, *70*, 1893–1901.

(15) Terabe, S.; Otsuka, K.; Tsuchiya, A.; Ichikawa, K.; Ando, T. *Anal Chem*. **1984**, *56*, 111-113.

(16) Terabe, S.; Miyashita, Y.; Shibata, O.; Barnhart, E.; Alexander, L.; Patterson, D.; Karger, B.; Hosoya, K.; Tanaka, N. In *Journal of Chromatography*; 1990; pp. 23–31.

(17) Giordano, B. C.; Newman, C. I. D.; Federowicz, P. M.; Collins, G. E.; Burgi, D. S. *Anal Chem*. **2007**, *79*, 6287–6294.

(18) Silva, M. *Electrophoresis*. **2009**, *30*, 50–64.

(19) Silva, M. *Electrophoresis*. **2010**, *32*, 149–165.

(20) Britz-McKibbin, P.; Bebault, G. M.; Chen, D. D. Y. *Anal Chem*. **2000**, *72*, 1729–1735.

(21) Arnett, S. D.; Lunte, C. E. *Electrophoresis*. **2003**, *24*, 1745–1752.

(22) Britz-McKibbin, P.; Terabe, S. *Chem. Record*. **2002**, *2*, 397–404.

(23) Arnett, S. D.; Lunte, C. E. *Electrophoresis*. **2007**, *28*, 3786–3793.

(24) Monton, M. R. N.; Imami, K.; Nakanishi, M.; Kim, J.; Terabe, S. *J. Chrom. A*. **2005**, *1079*, 266–273.

(25) Ptolemy, A. S.; Britz-McKibbin, P. *Analyst*. **2008**, *133*, 1643–1648.

(26) Zhao, Y.; Lunte, C. E. *Anal Chem*. **1999**, *71*, 3985–3991.

(27) Xiong, Y.; Park, S. R.; Swerdlow, H. *Anal Chem*. **1998**, *70*, 3605–3611.

(28) Hadwiger, M.; Torchia, S.; Park, S.; Biggin, M.; Lunte, C. E. *J. Chrom. B*. **1996**, *681*, 241–249.

(29) Otsuka, K.; Terabe, S.; Ando, T. *J. Chrom.* **1985**, *332*, 219–226.

(30) Bharadwaj, R.; Santiago, J. *J. Fluid Mech.* **2005**, *543*, 57–92.

5 Building and interfacing an optical trap with a capillary electrophoresis-laser-induced native fluorescence instrument for single cell sampling and analysis

Notes and Acknowledgments

I would like to acknowledge Dr. Stanislav S. Rubhakin for providing pineal samples and advice. I would like to thank Professor Jonathan V. Sweedler for support, advice, and funding, and the SCS Machine Shop for their advice and work. I would also like to acknowledge Bill Hug, Ray Reid, and Prashant Oswal at Photon Systems Inc. for providing the hollow cathode ion laser and their help with troubleshooting. This work was supported by the National Institutes of Health under award number DK070285, the National Institute of Neurological Disorders and Stroke under award number R01 NS031609, and by the National Institute of Dental and Craniofacial Researchunder award number R01 DE018866.

5.1 Introduction

Single cell analysis is becoming more routine, as cell-to-cell heterogeneity has been acknowledged even within "homogenous" cell populations.[1, 2] Cells contain hundreds of compounds spread amongst numerous analyte classes (*e.g.* amino acids, proteins, lipids), with concentrations that can span at least nine orders of magnitude. These concentrations can also vary widely depending on the time of day, the animal's satiation level, the animal's age, and the season, among other factors. When working with average values across a tissue sample or homogenate, much of this important information is lost. This prompts the use of technologies that enable single cell measurements, in order to reduce dilution of the analytes of interest and to simplify analysis. Capillary electrophoresis with laser-induced fluorescence detection (CE-LIF) is particularly appropriate for single cell analysis, as detailed in previous chapters.

While CE-LIF has the sensitivity to characterize low abundance analytes within individual cells and subcellular components, the sample handling required to isolate and inject such small samples is problematic. One way to address this issue is to interface a sampling system to enable precise, controlled manipulation and sampling of single cells.

There are numerous methods available for sampling single cells (Chapter 2), including manual[3-8] and mechanical[9-11] manipulation, microfluidics,[12, 13, 11, 14, 15] laser lysis,[16-18] and optical trapping.[19-26] Optical trapping was first demonstrated by Ashkin in 1970[27-31] and since has become an invaluable technique for studying micrometer- and nanometer-sized objects in physics, chemistry, and biology.[32-34]

Optical traps make use of radiation pressure, which is the force that is exerted by light on matter through scattering, absorption, emission, or refraction. This force may be regarded as the transfer of momentum from photons to the objects being irradiated. This force can be separated into two components, the scattering force and the gradient force. The scattering force arises from the reflection of photons off of the irradiated object and is in the direction of light propagation. In opposition to the scattering force there is the gradient force, which is due to the gradient in spatial light intensity. For a Gaussian beam, the highest intensity is in the center of the beam. As these rays are refracted and exit the object, the net force that is generated directs the object towards the beam focus. Once the object is within the beam focus, the net force is toward the lens, canceling the force due to scattering. Fluctuations in position will result in the object being directed back into the trap. Figure 5.1 contains a schematic of the gradient force acting on an object.

Optical traps were first used on single bacteria, viruses, and cells in 1987 by Ashkin[35, 36] and since then the use of optical traps for studying biological entities has grown dramatically. Optical traps have several advantages over other techniques for manipulating single biological objects. They enable fine control over the manipulation and movement of single cells,[37-40] organelles,[41, 21, 42-44, 20, 40] and even single biological molecules like DNA[45] and proteins,[46, 47] and these biological entities can be trapped without catastrophic damage. Optical traps are also considered a non-contact method, since they minimize outside interference that could affect the measurements in question, and they allow high resolution probing of the cellular microenvironment. There are also a variety of optical trap types and modifications that can be done to optimize the instrument for a particular use or sample type. The most common type of trap, the single beam optical trap, uses one laser beam and a high numerical aperture objective to form a trap at the objective's focal point. There also

exists dual beam[48-51] and ring-shaped traps,[52, 53] optical vortices,[21] and holographic traps,[54-56] to name a few, as well as the related techniques of laser microdissection/surgery,[21, 19, 44] laser ablation,[20] and catapulting.[57] Optical trap designs lend themselves to hyphenation with other technologies, such as microfluidics,[58, 59, 55, 60] and Raman[61, 62] and fluorescence spectroscopy.[63-66] Overall, optical traps are a versatile technique that can be used to study, isolate, and manipulate single cells and subcellular organelles on the micron scale with a minimum of interference.

The Sweedler group has designed, constructed, utilized, and modified a range of instruments and techniques to enable single cell analysis.[67-70, 5, 71] The efforts described here involves designing and building an optical trap and interfacing it to a laboratory-built capillary electrophoresis-laser-induced native fluorescence instrument, called the optical trap-multi-channel capillary electrophoresis with laser-induced native fluorescence detection (OT-MC-CE-LINF) system. Combining an optical trap and a CE-LIF instrument has been demonstrated previously;[72, 73] however, the combination is most often used on a microfluidic platform.[22-26] Native fluorescence detection reduces sample preparation and enables high selectivity, as well as allowing for unambiguous identification of the analytes of interest.

The OT-MC-CE-LINF instrument has several advantages. It enables single cell analysis to be performed with a minimum of sample handling and disruption, provides a separation step to reduce complexity, separate similar analytes, and potentially concentrate analytes, and utilizes native fluorescence detection optimized for catecholamines and indolamines. The optical trap is formed by tightly focusing the output of a near infrared (NIR) laser with a high numerical aperture objective. Once the cell is localized within the trap, the capillary inlet is moved adjacent to the trap using a computer-controlled micromanipulator and microscope combination. The cell is released from the trap and quickly injected into the capillary, where it is chemically lysed and its chemical components are separated and detected. The multi-channel capillary electrophoresis-laser-induced native fluorescence instrument is optimized for the native fluorescence detection of catecholamines and indolamines (Chapter 3). Briefly, a 224 nm HeAg hollow cathode ion laser is used in

combination with a sheath-flow cuvette; the fluorescence emission is collected and measured using three channel detection (each detector has its own wavelength range selected with appropriate dichroic beamsplitters). This instrument allows unambiguous identification of a variety of catecholamines and indolamines based on differences in their fluorescence emission profiles, as well as their migration times. The ability of the system to perform injections and CE-LINF separations of individual cells is highlighted, including the range of samples that the optical trap can accommodate and the CE-LINF detection performance.

5.2 Materials and methods

A list of abbreviations can be found in the Appendix.

5.2.1 Chemicals

Chemicals, unless otherwise noted, were from Sigma Aldrich (St. Louis, MO) and were reagent grade or higher. Citric acid sheath buffer (25 mM, pH 2.25) was made by dissolving 5.25 g of $C_6H_8O_7 \cdot H_2O$ in 1 L of ultrapure deionized water (Elga Purelab Ultra, Siemens Water Technologies, Warrendale, PA). Electrophoresis buffers were made by diluting a stock solution of 50 mM borate buffer, pH 8.8, which was prepared by dissolving 9.2 g of $Na_2B_4O_7 \cdot 10H_2O$ and 3.0 g of $B(OH)_3$ in 1 L of ultrapure deionized water. For surfactant-containing electrophoresis buffers, 0.72 g of sodium dodecyl sulfate (SDS) was added to 50 mL of diluted borate buffer, pH 8.8, sonicated for 2 min to dissolve, and filtered with a 0.22 µm syringe filter (Nalgene, Rochester, NY). Serotonin (5-HT) (Alfa Aesar, Ward Hill, MA) and tyrosine (Tyr) were dissolved in 2.5 mM citric acid, pH 2.5. Tryptophan (Trp), N-acetylserotonin (NAS), 5-hydroxyindole acetic acid (HIAA), melatonin (MT), 5-hydroxytryptophan (HTP), 5-methoxytryptamine (MOT) (TCI America, Portland, OR), and tryptophol (TOL) (Research Organics, Inc., Cleveland, OH) were dissolved in 2.5 mM citric acid, pH 2.5, + 10% v/v acetone and sonicated on ice for 30-60 min. Standard buffers were prepared by diluting the sheath buffer 1:10 with ultrapure deionized water. Fluorescein was prepared in ultrapure deionized water. Standard stock solutions were diluted in either 1 mM borate buffer, pH 8.8 (1:50 dilution of stock borate electrophoresis buffer) or in high

Ca^{+2}/high Mg^{+2} modified Grey's balanced salt solution (high salt mGBSS), pH 7.2, which consisted of 3.0 mM $CaCl_2$ (0.44 g), 4.9 mM KCl (0.37 g), 0.2 mM KH_2PO_4 (0.03 g), 22 mM $MgCl_2$ (4.47 g), 0.6 mM $MgSO_4$ (0.07 g), 138 mM NaCl (8.06 g), 27.7 mM $NaHCO_3$ (2.33 g), 0.8 mM Na_2HPO_4 (0.11 g), 25 mM HEPES (5.95 g), and 10 mM glucose (1.80 g) dissolved in 1 L of ultrapure deionized water. All buffers were filtered by a 0.45 µm bottle-top filter system (Nalgene, Rochester, NY) and degassed under vacuum with stirring for 30-60 min. NaOH (~0.1 M) was prepared by dissolving one pellet (~0.0025 g) in 0.025 L of ultrapure deionized water.

5.2.2 Animals

Animals were housed and cared for as described in animal protocols in full compliance with NIH guidelines for the humane care and treatment of animals, approved by IACUC and supervised by the Division of Animal Resources at the University of Illinois at Urbana-Champaign.

The pineal glands were isolated from the central nervous system of rats. Sacrifice occurred in the morning and pineal dissection and preparation was completed within 30 min. Glands were manually triturated and stored in high salt mGBSS on ice until analysis.

5.2.3 Biological samples

Human cheek, saliva, and blood samples were volunteered and obtained with full consent from myself (Christine Cecala), in accordance with the regulations outlined by the University of Illinois at Urbana-Champaign Institutional Review Board for the Protection of Human Subjects. Cheek cells were obtained by scraping the inside of the cheek, and blood samples by removing blood from a finger using a sterile disposable needle. Samples were diluted in phosphate buffered saline, pH 7.2 (BioWhittaker, Lonza, Walkersville, MD).

Rat pineal samples were split into two groups: incubated and non-incubated. Incubated samples were incubated at room temperature with a total concentration of 200 µM HTP, dissolved in high salt mGBSS, for 60 min before analysis. Non-incubated samples had an equal volume of high salt mGBSS added and were treated at room temperature for 100 min before analysis.

5.2.4 Hydrofluoric acid etching

Hydrofluoric acid (HF) etching of the capillary inlet and outlet is used to shape the ends into sharply tapered tips with a 40° angle (Figure 3.2).[74] The fused silica capillary dimensions were either 10 µm, 20 µm, or 50 µm inner diameter, 360 µm outer diameter, and 85-120 cm in length (Polymicro Technologies, Phoenix, AZ). The ends were scored and snapped to provide a relatively even surface for etching. Approximately 1 cm of the capillary's polyimide coating is burned off of each end and the tips cleaned with methanol. A container is filled to 5 mm of depth with 48% HF and covered with isooctane to prevent HF fumes from rising. The capillary tip is pushed through a FEP sleeve (Upchurch Scientific, Oak Harbor, WA) held tightly in a customized Teflon holder, which maintains the tip position during etching, until the tip touches the bottom of the container. The capillary has isooctane continuously pumped through the non-submersed end via a syringe to prevent the inner walls of the submerged end from being etched. After two hours, the etched tip is rinsed with $Na_2B_4O_7 \cdot 10H_2O$ (Borax, Henkel Corp., Billerica, MA) and water and the process is repeated for the other end.

5.2.5 Tapering capillary tips

Capillary tips were tapered using a CO_2 laser-based capillary puller (P-2000, Sutter Instrument Co., Novato, CA), which can be used on fused silica. The capillary dimensions were either 10 µm or 20 µm inner diameter, 360 µm outer diameter, and 85-120 cm in length. The ends were scored and snapped to provide a relatively even surface for etching. Approximately 1 cm of the capillary's polyimide coating is burned off of each end and the tips cleaned with methanol prior to pulling. Settings for pulling were: 400 (heat), 0 (fil), 127 (vel), 200 (del), and 150 (pull).

5.2.6 Optical trap design and construction

Unless otherwise noted, all laboratory-built and custom-built components have been designed and fabricated in-house either within the laboratory or by the SCS Machine Shop. Several optical trap designs and prototypes were built and tested. For all optical trains, the optical axis is parallel to the optical table at a height of 20 cm until the beam is

directed 90° vertically by a dichroic mirror. All optical trap optics, components, and mounts are from Thorlabs (Newton, New Jersey) and all optics are IR-coated unless otherwise specified. The NIR beam was viewed with IR viewing cards (VC-1550 and F-IRC-HP) and an IR viewer (IRV1-1700, Newport Corp., Irving, CA).

The first design (Figure 5.2A) was based off of several publications,[61, 75-77] and used a continuous wave 300 mW NIR diode (L980P300J) that emitted radiation at 980 ± 10 nm and had beam divergences of Θ(parallel) = 7° ± 3° and Θ(perpendicular) = 30° ± 5°. The diode was controlled by a driver (LDC210C) and was housed in a temperature-controlled mount (TCLDM9 and TED200C). The beam was collimated by a mounted aspheric lens (C230TME-B), which threaded into the front faceplate of the diode mount. The beam passed through a pair of plano-convex cylindrical lenses (LJ4147-B, focal length = 500 mm and LJ1695L1-B, focal length = 300 mm), mounted in kinematic mounts (KM100C)), which were used to correct astigmatism. An anamorphic prism pair (4x, PS883-B) was used to circularize the beam and was mounted using a post, clamp, bracket, and v-clamp (P12, PB4, PF175, and C1503, respectively). The beam was directed by a gold-coated mirror (PF10-03-M01) into the first of two telescope configurations created by a pair of plano-convex lenses (LA1509-B, focal length = 100 mm). The first telescope lens pair was used to expand the beam diameter to match the back aperture of the objective. The beam entered the second telescope configuration (also created with two plano-convex lenses (LA1509-B, focal length = 100 mm), used to steer and parfocalize the beam, after making a U-shaped turn with two other gold-coated mirrors (PF10-03-M01). Adjustments to one of these lenses generate corresponding movements in the laser trap. After exiting the second telescope lens pair, the beam passed through an aperture (ID12Z) and entered the epi-fluorescence port of a microscope (AxioObserver A1, Carl Zeiss, Jena, Germany), which had all of its fluorescence optics removed. The beam was directed into the back aperture of a high numerical aperture (N.A.) objective (Objective C-Apochromat 63x/1.2 W Corr, 441777-9970-000, Carl Zeiss, Jena, Germany) by a custom-coated dichroic mirror (Z900DCSP, Chroma Technology, Rockingham, VT) centered at 980 nm. The objective specifications are: 1.2 N.A., 63x

magnification, water immersion, apochromatic correction, and ~ 55% transmission at 1064 nm.

The second design (Figure 5.2B) used an Ar^+ laser (Innova 300 FrED, Coherent Inc., Santa Clara, CA) emitting 3 W of 514 nm radiation. The uncorrected beam passed through a Pellin-Broca prism (Newport Corp., Irving, CA) and was directed into a 5x beam expander (09LBX001, Melles Griot, Albuquerque, NM). The expanded beam then entered a pair of plan-convex lenses (LA1509-B, focal length = 100 mm) set up in a 1:1 telescope configuration, used to steer and parfocalize the beam. The beam was then directed into the epi-fluorescence port of the microscope and directed into the back aperture of the objective by a dichroic mirror centered at 514 nm (Z514rdc, Chroma Technology, Rockingham, VT).

The third design made use of a 540 nm HeNe laser (Electro Optics Division, Particle Measuring Systems, Boulder, CO). The beam passed through an iris, used to block satellite beams, and a pair of plano-convex lenses in a telescope configuration. The expanded beam was then directed by mirror into the epi-fluorescence port of the microscope and directed into the back aperture of the objective by a dichroic mirror centered at 514 nm (Z514rdc, Chroma Technology, Rockingham, VT).

The fourth design employed a 50 mW green laser pointer emitting 532 nm radiation from a frequency-doubled Nd:YAG crystal. The laser was mounted using the v-clamp and post system from the anamorphic prism pair and the “on” button was depressed using a zip tie and a piece of optical board to enable “continuous” emission. The beam entered a plano-convex lens pair set up in a telescopic configuration with a pinhole located at the minimum focal point. The beam was then directed into the epi-fluorescence port and directed into the back aperture of the objective by a dichroic mirror centered at 514 nm (Z514rdc, Chroma Technology, Rockingham, VT).

The fifth and final design (Figure 5.3), based on several publications,[78-80] uses a 1064 nm diode-pumped solid state Nd:YAG laser (Compass 1064-2500MN, Coherent Inc., Santa Clara, CA) with a maximum output of 2.5 W. The laser operates in TEM_{00} mode and has a wavelength stability of < 1 cm^{-1}. The beam has a nominal diameter of 0.4 mm, a divergence

of < 3.5 mrad, a pointing stability of < ± 5%, and an ellipticity of < 1.1. It is air-cooled and turn-key operated. The beam is expanded by a 20x high energy beam expander (HB-20X, Newport Corp., Irving, CA) and directed by a pair of gold-coated mirrors into a set of plano-convex lenses (SPX029, Newport Corp., Irving, CA) in a 1:1 telescope configuration, used to steer and parfocalize the beam. The beam expander is housed in a precision gimbal optic mount (605-4, Newport Corp., Irving, CA), and translated in the x-, y-, and z-directions by a translation stage (UMR12.40, Newport Corp., Irving, CA) and a heavy duty optical lab jack (L490). Plano-convex lens 1 is mounted in a 3-axis optical mount (LP-1A-XYZ, Newport Corp., Irvine, CA) located 1000 mm from the back aperture of the objective and plano-convex lens 2 is mounted in a 2-axis mount (LP-1A-XY, Newport Corp., Irvine, CA) located 500 mm from the back aperture of the objective. This set up can be generalized as the distance between the back aperture of the objective and the steering optic is equal to 4*f*, where *f* is the focal length of the lens.[81-84] In this case, the focal lengths of both of the plano-convex lenses are 250 mm. The beam was then directed into the epi-fluorescence port of the microscope and directed into the back aperture of the objective by a dichroic mirror centered at 1064 nm (950dcsp-laser, Chroma Technology, Rockingham, VT).

Polystyrene beads (1 µm (PS04N/5749) and 10 µm (PS06N/6955) diameters, Bangs Laboratories, Fishers, IN), diluted 10-fold to 100-fold in ultrapure deionized water, were used to optimize the optical trap. The beads were contained on a coverslip (2735-246, Corning Inc., Corning, NY) by a grease ring, made with vacuum grease (Silicon High Vacuum Grease, Dow Corning, Midland, MI). Laser power measurements were taken with a PM10 sensor and a LabMax-TOP meter (Coherent Inc., Santa Clara, CA).

5.2.7 Multi-channel capillary electrophoresis-laser-induced native fluorescence instrument (MC-CE-LINF) design and construction

Unless otherwise noted, all laboratory-built and custom-built components have been designed and fabricated in-house either within the laboratory or by the SCS Machine Shop. The injection port for the instrument is housed on a non-conductive breadboard platform on a microscope, contained in a clear Plexiglas box. The capillary inlet has PEEK fittings (Upchurch Scientific, Oak Harbor, WA) and a FEP sleeve (Upchurch Scientific, Oak

Harbor, WA) attached to allow for fast and easy switching between syringes and the capillary holder.

The capillary is held in place in the instrument by a custom-built acetal resin (Delrin, E. I. duPont de Nemours & Co., Wilmington, DE) sheath flow cell. It enters at the top of the cell and is held in place by liquid-tight fittings (Upchurch Scientific, Oak Harbor, WA). The sheath buffer enters the cuvette from the right side with respect to the optical table and exits from the bottom of the sheath flow cell. The quartz cuvette (Starna Cells, Atascadero, CA) used for excitation and detection of eluents is open on both ends and is attached to the top and bottom pieces of the sheath flow cell with Tra-Cast 3103 epoxy (Henkel Corp., Billerica, MA).

The current optical layout was adapted from a previous version.[85] Deep UV radiation (224.6 nm) from a HeAg hollow cathode ion laser (HeAg70, Photon Systems Inc., Covina, CA) is spectrally filtered using a four-bounce mirror configuration, attached to the front of the laser head. The beam is directed via two UV-coated mirrors (Thorlabs, Newton, New Jersey) into a laboratory-built lightproof, non-conductive box and breadboard, which houses the detection optics and protects against spurious arcing. The collimated beam is nominally focused using a plano-convex lens (OptoSigma, Santa Ana, CA) to a 50 µm spot directly below the outlet of the capillary, which has been HF-etched to a cone-shaped tip and is housed in a custom-built sheath flow cell, as described above. As analytes elute from the capillary they are excited by the focused beam and emit fluorescence, which is collected and collimated by a 15x all-reflective objective (13596, Newport Corp., Irvine, CA). The fluorescence is directed toward the three photomultiplier tube (PMT) detectors (H6780-06, Hamamatsu, Middlesex, NJ) by two dichroic mirrors (310dcxxr-haf #110258 and 400dcxru #111563, Chroma Technology, Rockingham, VT), with transition points at 310 nm and 400 nm, respectively. The first detector (PMT “blue”) measures emission from 250-310 nm, the second detector (PMT “green”) measures emission from 310-400 nm, and the third detector (PMT “red”) measures emission from 400 nm and above. The laser and PMTs are synchronized and controlled by software written in LABView and provided by Photon Systems Inc. Posts, post holders, and other optical mounts were purchased from Newport

Corp. (Irvine, CA), Melles Griot (Albuquerque, NM), or custom-built. Optical mounts for the focusing optic and the collection optic are coated in Vinyl Liquid Electric Tape (Star Brite, Ft. Lauderdale, FL) and electrical tape (Scotch Super 88 electrical tape, 3M, St. Paul, MN) to reduce arcing from the capillary outlet and tubing to the mounts.

Negative voltage for electrophoresis is applied to the sheath flow waste by a stainless steel cylinder that is connected to a power supply (PS/MJ30N0400-11, Glassman High Voltage, High Bridge, NJ) and laboratory-built control box. A 10 kΩ resistor and a digital multimeter (Fluke 76, Fluke Corp., Everett, WA) are part of the circuit and are used to measure the current across the capillary.

Sheath buffer is gravity-driven and flow can be adjusted by a right angle switching valve (Upchurch Scientific, Oak Harbor, WA). High purity Teflon PFA Plus tubing and appropriate fittings were purchased from Upchurch Scientific. All tubing is further encased within FEP-lined polyethylene tubing (McMaster-Carr, Elmhurst, IL) to reduce static attraction and arcing during electrophoresis. Tubing between the optics box and the sheath box is also surrounded by four 16 oz. polyethylene containers and electrical tape (Scotch Super 88 electrical tape, 3M, St. Paul, MN).

5.2.8 Interfacing the optical trap and MC-CE-LINF instrument

The optical trap and the MC-CE-LINF system are interfaced at the microscope stage (Figure 5.4). The trap is located at the focal point of the objective, approximately 0.28 mm from the objective surface, including the coverslip thickness (0.13-0.16 mm). The capillary inlet is controlled by a computer-controlled motorized micromanipulator (MP-285, Sutter Instrument Co., Novato, CA), which has 1” of travel in all three axes, two step sizes (coarse, 0.2 µm/step and fine, 0.04 µm/step), and a maximum speed of 2.9 mm/s. It has a tabletop controller and a rotary optical encoder for manual control. Programmable robotic control is also available. The micromanipulator is mounted on a non-conductive optical breadboard, which is stabilized by two ¼-28” tapped beams that attach to the microscope stand on either side of the stage. The capillary is held in the micromanipulator by an acetal resin cylinder, which is 6” long and has a 1/16” diameter hole drilled in the center. This holder reduces the chance of arcing to the micromanipulator motors. The clamp that came with

the micromanipulator for holding a pipette was removed and an acetal resin one machined and used in its place for holding the cylinder.

The sample is held on a coverslip holder, machined out of polycarbonate, with a lip to rest the coverslip edges on and a 30° angled oval hole for holding the electrophoresis buffer vial, which consisted of an Eppendorf tube (Hamburg, Germany) that had its top quarter removed at an angle. A platinum grounding wire (California Fine Wire Co., Grover Beach, CA) is placed in contact with the electrophoresis buffer, completing the circuit.

Trapping, manipulation, and injection were recorded by a monochrome CMOS camera (NT59-365, EO-1312M, Edmund Optics, Barrington, NJ) that is attached to the microscope housing with a 1x C-mount (Carl Zeiss, Jena, Germany).

5.2.9 Second micromanipulator and capillary

A second micromanipulator (Narishige Scientific Instrument Lab, Tokyo, Japan) was placed to the left of the microscope and a HF-etched capillary (50 µm inner diameter, 360 µm outer diameter, and ~ 50 cm in length) was held by an acetal resin cylinder, similar to the one describe above. PEEK fittings and a FEP sleeve were used to connect the capillary outlet to a syringe filled with high salt mGBSS. The pressure on the syringe was controlled by a syringe pump (model 601553, KD Scientific, Holliston, MA), located on top of the injection box.

5.2.10 Single cell injections

Single pinealocytes were injected into the capillary for analysis. A 2.5 µL droplet of sample was pipetted onto the coverslip. A cell was selected and trapped. The capillary inlet was directed into the cell's proximity by the micromanipulator, which was programmed to stop near the trap location and further position refinement was performed manually using the rotary optical encoder. Once the capillary was in place, the cell was released from the trap and hydrodynamic injection of the cell was performed by lowering the sheath waste outlet. Once injection was complete, the micromanipulator was used to bring the capillary inlet to the buffer vial, and the voltage and detectors were turned on. Injections were recorded using the CMOS camera on the microscope.

5.2.11 Electrophoresis

The sheath flow buffer was 25 mM citric acid, pH 2.25, and the flow rate was 0.2 mm/s for all experiments. The electrophoresis buffers and sample buffers varied as stated in the text and figure captions. The voltage for all experiments was -30 kV unless otherwise stated. The injection volume varies as stated, but for bulk injections the volume was 14.7 nL for a 30 s hydrodynamic injection, which was performed by lowering the sheath flow waste outlet by 32.5 cm. The typical laser pulse energy was between 1.5 μJ/pulse and 2 μJ/pulse.

The capillary was conditioned at the beginning of the day with 0.1 M NaOH for 15-20 min, followed by water for 5 min, and then electrophoresis buffer for a minimum of 5 min.

5.2.12 Data analysis

Data analysis was performed in IgorPro 5.05A (WaveMetrics Inc., Lake Oswego, OR). An automated data analysis script was written that reduces the user input to a single command. Output consists of four tables of calculated values with four corresponding color-coded graphs displaying the raw data, 6-point boxcar averaged data, normalized (with respect to the laser pulse energy) data, and both normalized and boxcar averaged data. The baseline range (30 points, 10 s) with the lowest standard deviation is determined and used to calculate the limits of detection (LOD) for each PMT channel. Ratiometric analysis (calculating the intensity ratio between peak maxima in each of the PMT channels) is also automated to aid in analyte identification.

5.2.13 Limits of detection

LODs and concentration of analytes were determined by generating calibration curves for each analyte under the appropriate conditions. Analyte concentrations ranged from the micromolar to the low nanomolar, within physiological limits and at maximum an order of magnitude greater than LODs. The criterion for calculating the LODs was three times the standard deviation of the baseline.

5.3 Results and discussion

5.3.1 Optical trap construction and performance

Several optical trap designs were designed, built, and tested. In order to successfully trap and manipulate objects, the trapping laser should have a symmetric beam profile (usually Gaussian TEM_{00}, but other spatial modes can be used), low beam divergence, low ellipticity, and high pointing stability. Many of these characteristics can be found natively in certain types of lasers (*e.g.* gas ion and diode-pumped solid state lasers), but some of these characteristics can be improved in non-ideal light sources by using optical manipulation.

The original design (Figure 5.2A) was based around a NIR diode operating at 980 nm.[61, 75-77] Diodes are inexpensive light sources that come in a wide range of wavelengths compared with traditional lasers. This wavelength was chosen based on published results demonstrating that one of the wavelength ranges for minimal damage to biological specimens was located around 980 nm.[86, 87] The NIR as a whole (from ~ 700 nm to 1300 nm) has reduced rates of damage compared with the visible and UV ranges due to the lack of NIR radiation absorption by water, but non-linear absorption by chromophores leads to some discrete wavelength ranges that are more ideal than others. The first diode tested had irregularities in the beam profile and dust inside of the window housing the diode, so it was replaced by another of the same model. This diode's beam divergences exceeded the specifications by several degrees total (Θ(parallel) = 11° and Θ(perpendicular) = 42°, calculated assuming the diode was a point source and from measurements), and it emitted non-symmetrically, which led to using a tip/tilt mount at the base of the optics holder for correction. The aspheric collimating lens was overfilled (N.A. 0.55), and this led to loss of light, beam distortions, and changes in the observed divergence angles. The appropriate N.A. lens for this system (N.A. = 0.83) was unavailable for purchased, so experiments were performed to determine whether the presence of the collimating optic was beneficial or detrimental to the trap's performance. Unfortunately, without the collimating optic, the cylindrical lenses were too small and part of the beam was cut off, also leading to loss of light and beam distortions. Another pair of cylindrical lenses were tested, without the collimating lens, and showed some success in reducing the beam's astigmatism. The

anamorphic prism pair was used to further circularize the beam by magnifying the elliptical beam in one dimension. This was also moderately successful. The beam profile remained non-symmetrical and was subject to diffraction patterns and other abnormalities that were unable to be fully corrected, even with spatial filtering. One suggestion was that dust inside of the lens' housing was causing the patterns to occur. This beam was expanded to ~ 8 mm to match the back aperture of the objective, which ensures that the steepest gradient in light intensity is achieved. A variety of optical designs were tested using these components, given the unusual nature of the beam, and the beam was aligned with the objective and focused. Despite this, no trapping was observed under any circumstances with the diode laser. In addition to all of the challenges that arose with the diode, the initial power was not great enough to overcome the light loss at each optical interface. Although it has been reported that one can trap biological specimens with as little as 5 mW of incident power, this has not been the case with any of the objects I have trapped.

The second design (Figure 5.2B) employed a gas ion laser that emitted at 514 nm. This laser had many of the necessary characteristics for use as a trapping laser: low beam divergence, a TEM_{00} profile, sufficient pointing stability, and relatively low ellipticity. The wavelength is non-ideal for biological specimens, as 514 nm is within the range of the strongest absorption by a variety of biochemicals and other cellular constituents, but the visible wavelength is beneficial for alignment. This optical train was composed of optical elements already present in our laboratory, including the laser. Satellite beams were present in the main output beam, so a Pellin-Broca prism was used to further disperse the wavelengths. Far-field diffraction patterns and multiple beams were observed exiting the plano-convex telescope, due to the IR anti-reflective coating. Uncoated plano-convex lenses were found and used, which reduced these issues. Unfortunately, the laser was retired before trapping was tested.

The third and fourth designs were both based off of the previous design using the Ar^+ laser and created using components already present in the laboratory. The green HeNe laser had an unusual beam profile that may have been composed of multiple higher-order modes, but it was symmetrical and the beam shape was circular. Satellite beams were

observed and blocked by an iris before the beam entered the plano-convex telescope. Weak trapping was observed for 1 μm and 10 μm polystyrene beads, where the beads would congregate in a particular location but not remain within the trap. The frequency-doubled Nd:YAG laser pointer has a greater power output than the HeNe laser, which should enable a stronger trap to exist. One concern was that the laser pointer emission is pulsed, which would lead to fluctuations in trap strength and potentially releasing the object of interest. Another concern was the mounting, which was unstable for long-term (*i.e.* > 1-3 h) use. Multiple beams were observed, so a pinhole was used to spatially filter the emission. The power output fluctuated greatly, from μW to mW. No trapping was observed likely due to the combined instabilities in mounting, continuous operation, and power.

Based on these previous experiences, the fifth and final design (Figure 5.3) was created and constructed.[78-80] An Nd:YAG laser with 1064 nm emission was selected, which fulfilled the ideal requirements for a trapping laser. No beam correction was needed, and the beam was expanded by a factor of 20 to 8 mm, to fill the back aperture of the objective. The 1:1 telescope configuration was set up with the steering optic (plano-convex lens 1) located at a distance of 4*f* (1000 mm) from the back aperture, and all other optics were located with respect to that figure.[81-84] Translations in this lens correspond to movements in the trap location, which can be used to direct trapped objects to specific locations. The optical throughput of this system was experimentally determined to be 32% of the initial power, with the highest loss occurring at the objective. To initially demonstrate trapping and locate the trap on camera, the initial power was set to 1.5 W (incident power = ~ 500 mW) and the sample was 100-fold diluted 10 μm polystyrene beads. Beads began moving quickly off camera, indicating that the trap was located outside the field of view of the camera and not along the optical axis. Using this, the trap's location and alignment could be further refined and centered in the field of view. Once this was done, the initial power used to trap 10 μm polystyrene beads in water was typically 90 mW (incident power = ~ 30 mW, power density = ~ 6.5 x 10^6 W/cm^2 for a trap size of 1 μm). It is easy to distinguish whether a bead is trapped, as its focal position changes with respect to untrapped beads (Figure 5.5). This may seem counterintuitive, since the objective is used simultaneously for magnifying

the sample and creating the trap, but it can be understood as the trap existing as a continuum within an area instead of as a point. The bead is resting in a location of minimal energy with maximum stability under the conditions of trapping. This location is "above" the focal point of the objective, where the trap occupies a larger area than at the focal point but the trap is also weaker since the power density is lower. For objects that are larger than the trap (*e.g.*, a 10 μm bead) a weaker trap across a larger area is more stable than a stronger trap across a smaller area. This phenomenon is not observed with 1 μm beads, where the trap size and the bead size are essentially identical.

The next experiment determined how to translate a trapped object. Originally, the trap was designed to be moveable by adjusting the position of the steering lens (plano-convex lens 1). While this works, there are two disadvantages: it is difficult to reach the lens controls in the current optical set up, and the distances that the trap can be moved are limited. These challenges were easily overcome by gently translating the microscope stage, although the trapped object is subject to being prematurely ejected from the trap due to the variable nature of the movement. A motorized stage would greatly reduce this likelihood, if the step size and speed were sufficiently low. It is also interesting to note that optical alignment prior to the objective is noticeably skewed when the trap appears centered in the objective.

5.3.2 Trapping cells

Biological samples were next tested to see how they respond to trapping, manipulation, and interacting with the capillary. Cheek cells, obtained by scraping, and saliva were first tested. The cheek cells adhered to the slide, and trapping was unsuccessful. Saliva did not possess enough material for trapping. Red and white blood cells were tested next. Dilution in phosphate buffered saline was necessary to successfully trap and move cells, as the cell density was too high otherwise. Higher powers were also used with biological samples as the trap appeared to be weaker compared to the bead work. This could be attributed to the slightly higher refractive index of the saline solution (n ~ 1.34 to 1.37)[88, 89] compared to water (n = 1.33), and also the lower refractive index of cells (n ~ 1.39 to 1.40)[90, 91] compared to beads (n = 1.57). Larger refractive index differences lead to

stronger traps, as the gradient force generated depends on the amount of refraction that the beam experiences. Although this is a gross simplification, cells are mostly salt and water, and do best in an environment that is also composed of salt and water, leading to a smaller refractive index change when the beam travels from the solution to the cell.

Cells could also be translated while in the trap by using the microscope stage. No damage was observed during any of the trapping experiments, including cells that were contained within the trap for 5-10 min. The changes in focal position observed for trapped beads was not as obvious for trapped cells, although it was still detectable. This may be due to the smaller size of the cells compared to the beads (4-7 μm versus 10 μm, respectively). Interestingly, red blood cells, when contained in the trap, turn 90° and remain in that position until they are released from the trap. Red blood cells have a biconcave shape and look discoid. The dimensions for red blood cells in mammals are typically 5-7 μm in diameter and 2-3 μm in thickness. The lowest energy position with the greatest stability is along the long axis for red blood cells, making it easy to tell when one is trapped since, when free in solution, the cells settle with their long axis facing the coverslip.

5.3.3 Interfacing the optical trap and the MC-CE-LINF instrument

The MC-CE-LINF possesses a unique combination of elements (deep UV excitation, wavelength-resolved detection, post-column detection, the ability to independently optimize separation and detection conditions, and an sharply tapered inlet and outlet) that make it compatible with detecting low abundance analytes within single cells. Hyphenating this instrument to an optical trap increases its abilities to sample from single cells, and enables smaller cells to be effectively studied on a single cell level.

Experiments were performed to first determine the ideal conditions for introducing the capillary to trapped objects. To test the interaction between the trapped bead and the capillary, the capillary was controlled by the micromanipulator using the rotary optical encoder with both coarse and fine step sizes. The initial powers used were 130 mW, 320 mW, and 1300 mW (corresponding to incident powers of 42 mW, 102 mW, and 416 mW and power densities ranging from 10^6 W/cm^2 to 10^7 W/cm^2). Electrostatic attraction was observed between the beads and the capillary. The trap with an initial power of 1300 mW

was able to contain the bead while the capillary was moved into position adjacent to the bead. The trapped bead was able to withstand both in-flow and out-flow from the capillary (created by lowering or raising the sheath waste reservoir, respectively), even when untrapped beads collided with the trapped bead as they entered the capillary. When untrapped beads exited the capillary during out-flow, the trapped bead could be released from the trap prematurely if the untrapped beads collided with it. The lower powers were able to trap beads but were less successful in preventing premature release of the beads within the trap while the capillary was moving within the sample droplet. At an initial power of 130 mW, it was difficult to trap an object that was near the capillary tip, once the capillary was in place adjacent to the trap. Results were improved when the micromanipulator was programmed to approach the trap location, as opposed to manually directed.

Introducing the capillary to a trapped blood cell was less successful than to introducing it to a trapped bead. Many of the untrapped cells adhered to the capillary, and the trapped cell was easily damaged if the capillary came into contact with it. Higher initial powers were also necessary to prevent the cell from being ejected from the trap when the capillary was being moved into position.

These observations led to modifications to the trapping procedure designed for single cell trapping and injection: the cell would have to be released before injection, adding another step and potentially complicating the process. On a positive note, other cells and cellular debris could be “removed” from the vicinity of the trapped cell by using capillary out-flow to clear a path for injection, provided that the buffer in the capillary is compatible with the cellular environment.

Different capillary inner diameters were also tested, since the inner diameter of the capillary dictates the size of the cells that can be injected, the likelihood of injecting multiple cells simultaneously, and also how much dilution occurs after lysis. The outer diameter was held constant, to prevent changing the fitting assemblies on the instrument and in the capillary holder for the micromanipulator. With smaller inner diameters, the LODs are expected to increase, but the mass amounts that are detected should decrease. There were

challenges with aligning the detection optics with both the 20 µm and 10 µm inner diameter capillaries; the 20 µm inner diameter capillary could be aligned after much adjustment but the 10 µm inner diameter was unable to be successfully integrated into the instrument. There were issues with clogging within the capillaries and also with continuous, steady flow eluting from the outlet when syringes were used, making alignment and conditioning for routine use difficult. Figure 5.6 shows the differences in the electropherograms obtained when using the 20 µm inner diameter capillary and the typical 50 µm inner diameter capillary. Although the injection volumes are different (1.9 nL versus 14.7 nL, respectively, which is a 7.7-fold difference), the number of moles of serotonin detected were 6.6 fmol in the 20 µm inner diameter capillary and 51 fmol in the 50 µm inner diameter capillary, also a 7.7-fold difference, which is expected. The LODs for these measurements were 111 nM in the 20 µm inner diameter capillary and an average of 3.3 nM in the 50 µm inner diameter capillary, a 34-fold difference. Experiments were also performed with 300 s injections in the 20 µm inner diameter capillary, and the average LOD for those measurements was 58 nM for 5-HT, an 18-fold difference, with the lowest LOD measured equal to 32 nM for an individual experiment. These discrepancies in the LODs between 20 µm and 50 µm inner diameter capillaries are only partially explained by the lower mass amounts and by peak broadening, which is minimized by the use of field-amplified sample stacking, a technique that concentrates the analyte band within the capillary. The full width at half maximum intensity is 4 s on average for all of the 20 µm inner diameter capillary measurements, and is 5 s on average for the 50 µm inner diameter capillary measurements. The baseline values were similar for all electropherograms as well. Based on these results and observations, the 50 µm inner diameter capillary was used for all further experiments.

HF-etched capillary tips were also compared with pulled tips for use as the capillary inlet (Figure 5.7). A tapered inlet tip is necessary to reach the trapped sample, since the capillary is held at 35° to 45° in the micromanipulator. A flat tip, when the outer diameter is 360 µm and it is held in the micromanipulator, does not allow the capillary opening to get close enough to the trap to sample effectively. Moving the trap axially can alleviate some of this, but the distance between the trap and the opening is still too large.

Both etching and pulling have advantages and disadvantages. HF etching is time-consuming (4 h for both ends to be etched, plus set up and clean up) and potentially hazardous, but HF-etched tips preserve the inner diameter of the capillary and are relatively robust. Pulling fused silica requires the use of a laser-based capillary puller and is quick (5 min total for preparation and pulling), but there are more parameters to adjust and it does not preserve the capillary inner diameter. Pulled tips, due to their much smaller dimensions and elongated tip, are less robust and require gentle handling to avoid snapping them. Interfacing a pulled tip with the MC-CE-LINF was attempted using two different unions, one of which was a "zero-dead volume" union, in order to merge a new inlet with an existing capillary outlet that was aligned with the detection optics. This process would have allowed the capillary inlet to be easily changed when damaged without requiring extensive realignment of the optics. Fluid flow was observed for two short capillary pieces that were connected by a union. On a larger scale, when voltage was applied across the instrument capillary while a union was in use, the current was 5- to 6-fold lower than it was without the union. Also, a continuous stream of fluorescein was used to determine if there was flow between the capillary inlet, the union, and the outlet aligned to the detection optics; no fluorescein was observed exiting the capillary by eye and no fluorescence was observed with the detectors. It is possible that the smaller dimensions of the pulled tip prevented the capillary from filling within a reasonable amount of time.

Another concern about pulled tips is that the change in inner diameter results in a change in electric field strength along that portion of the capillary, which may affect the injection and separation of samples, especially if electrokinetic injection is used to introduce samples into the capillary. Parabolic flow profiles are also possible due to the change in diameter, instead of the plug flow profile that is inherent to capillary electrophoresis, which would lead to band broadening and poorer LODs. Given these difficulties, pulled tips and unions were not further investigated. A modified HF etching procedure was developed to etch the capillary inlet within the injection box, which prevents having to realign the MC-CE-LINF instrument each time the capillary tip snaps.

5.3.4 Sampling from single cells

Figure 5.8 is an electropherogram of a single pinealocyte that has been incubated in 5-hydroxytryptophan, the precursor to serotonin. Pinealocytes are the cells of the pineal gland, which is involved in circadian rhythm and reproduction. The mammalian pineal gland is known to contain several indolamines, including serotonin and melatonin, in high concentrations.[92-94] The cells were incubated with non-physiological amounts of 5-hydroxytryptophan to increase production of indolmines within the cells. This ensures that the sample preparation and handling steps do not damage the cells or prevent the cells from synthesizing the analytes of interest. Several peaks were detected in the single cell, including serotonin and tryptophan, and the serotonin concentration (~ 3300 nM) was elevated by approximately a factor of 10 compared with the native levels detected in non-incubated samples (data not shown). Multiple single cell experiments can be performed in a single day, allowing for day-to-day variations to be determined.

Challenges that arose during single pinealocyte trapping and injection include adhesion to the coverslip and multiple cells and/or debris entering the capillary simultaneously. Adhesion will be covered in Chapter 6, as the degree to which it occurred appears to be unique to pinealocytes. Multiple cells or debris entering the capillary can be prevented by using capillary out-flow (to push the untrapped objects away from the capillary inlet), but only when the buffer is compatible with the sample. Typically the electrophoresis buffer used for these experiments contains a surfactant to lyse the cell once it is within the capillary. Using capillary out-flow under these conditions lyses all of the cells in the vicinity, including the trapped cell. Results from injecting a lysed cell and the solution around it were not positive.

A potential solution to this is to use a second capillary, housed in and controlled by a second micromanipulator to flush the area before injection (Figure 5.9). The second micromanipulator was manually adjusted and the second capillary's outlet was fitted to a syringe filled with high salt mGBSS and placed in a syringe pump. This worked under ideal conditions, although the movements of the second capillary were not smooth and the capillary experienced vibration and delayed movement, which made trapping more difficult.

The flow from the syringe pump on the lowest setting was fast enough to push the trapped cell out of the trap at times. More optimization is needed before this can be used as a solution.

5.4 Conclusions and future work

Multiple optical trap designs were built, tested, and optimized, both non-biological and biological samples were trapped and manipulated, and hyphenation was successful. Single cells were trapped, isolated, and injected into the capillary and analyzed; analytes from single pinealocytes were detected, identified, and quantified. A number of improvements can be made to the hyphenated instrument, including better optical alignment for the optical trap, more testing of smaller inner diameter capillaries, and refining the second micromanipulator/capillary combination. Better optical alignment will enable lower powers to be used for trapping. Using smaller inner diameter capillaries will reduce the likelihood of injecting multiple cells or debris simultaneously and greatly reduce dilution, enabling lower concentrations to be detected. Using a second micromanipulator and capillary to clear the area around a trapped cell can ensure that a single cell is injected for analysis. All of these factors are important for improving the instrumentation so that more difficult analyses (lower abundance analytes, smaller cells) can be routinely performed.

5.5 Figures

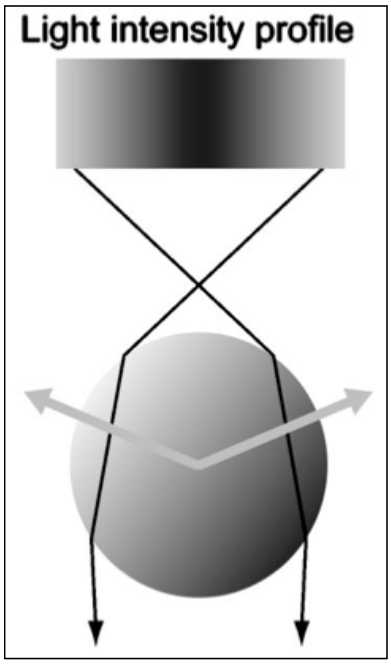

Figure 5.1 A diagram of the gradient forces acting on the irradiated object. The gradient force in the z-direction directs the object towards the beam focus along the optical axis. The gradient force in the x- and y-directions directs the object towards the center of the beam focus, where the highest intensity is located. The net force is toward the beam focus, in opposition to the scattering force. Adapted with permission from (79). Copyright 2011 American Institute of Physics.

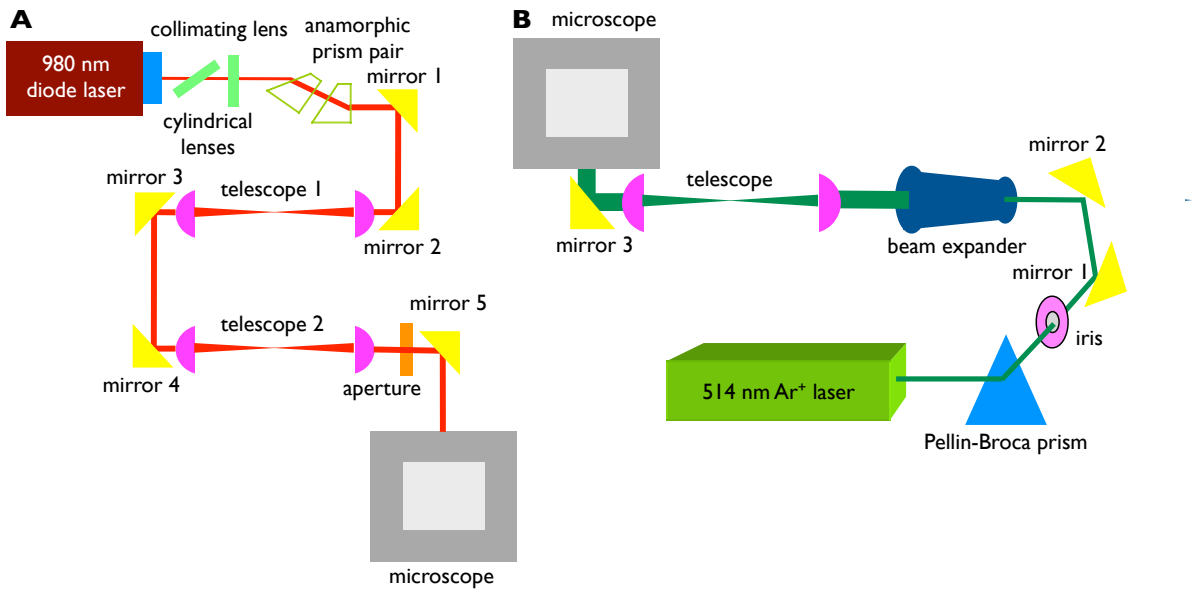

Figure 5.2 Schematics of two optical trap prototypes. (A) A NIR diode laser is used as the trapping laser. The beam is collimated, circularized, and expanded before entering the epi-fluorescence port of the microscope. (B) A gas ion laser is used as the trapping laser. The beam does not require correction and is expanded before entering the epi-fluorescence port.

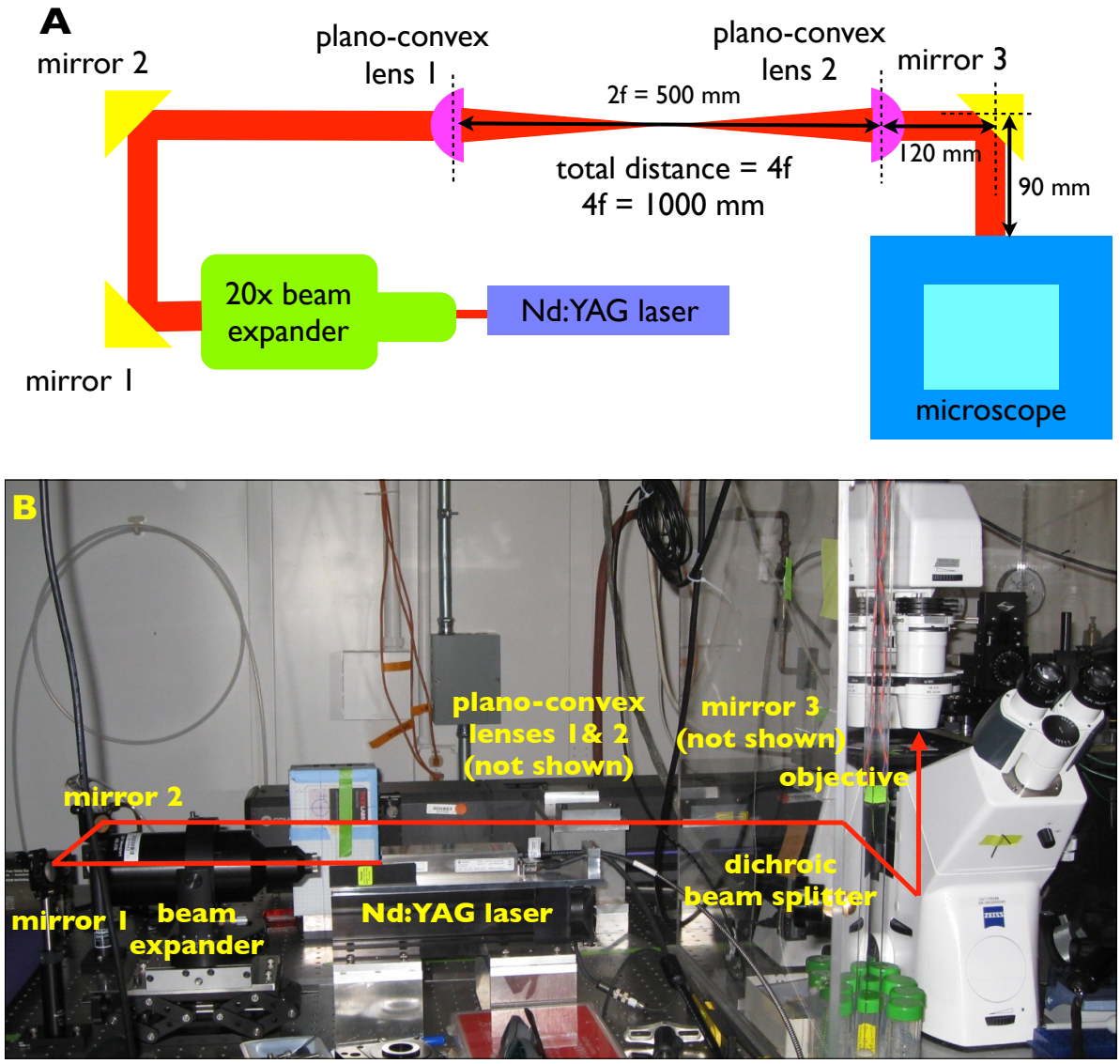

Figure 5.3 (A) A schematic of the final optical trap design. The beam is expanded 20x (to 8 mm nominally) before entering the telescope configuration. (B) A picture of the optical train.

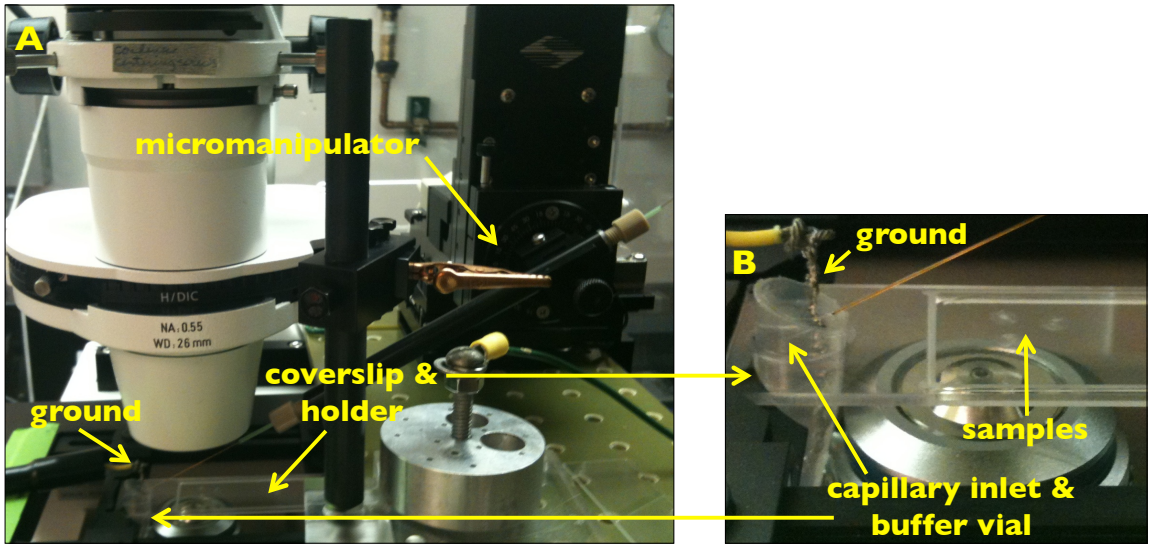

Figure 5.4 Interfacing the optical trap and the MC-CE-LINF instrument. (A) An overview of the micromanipulator holding the capillary in position in the buffer vial. (B) A close up view of the sample holder.

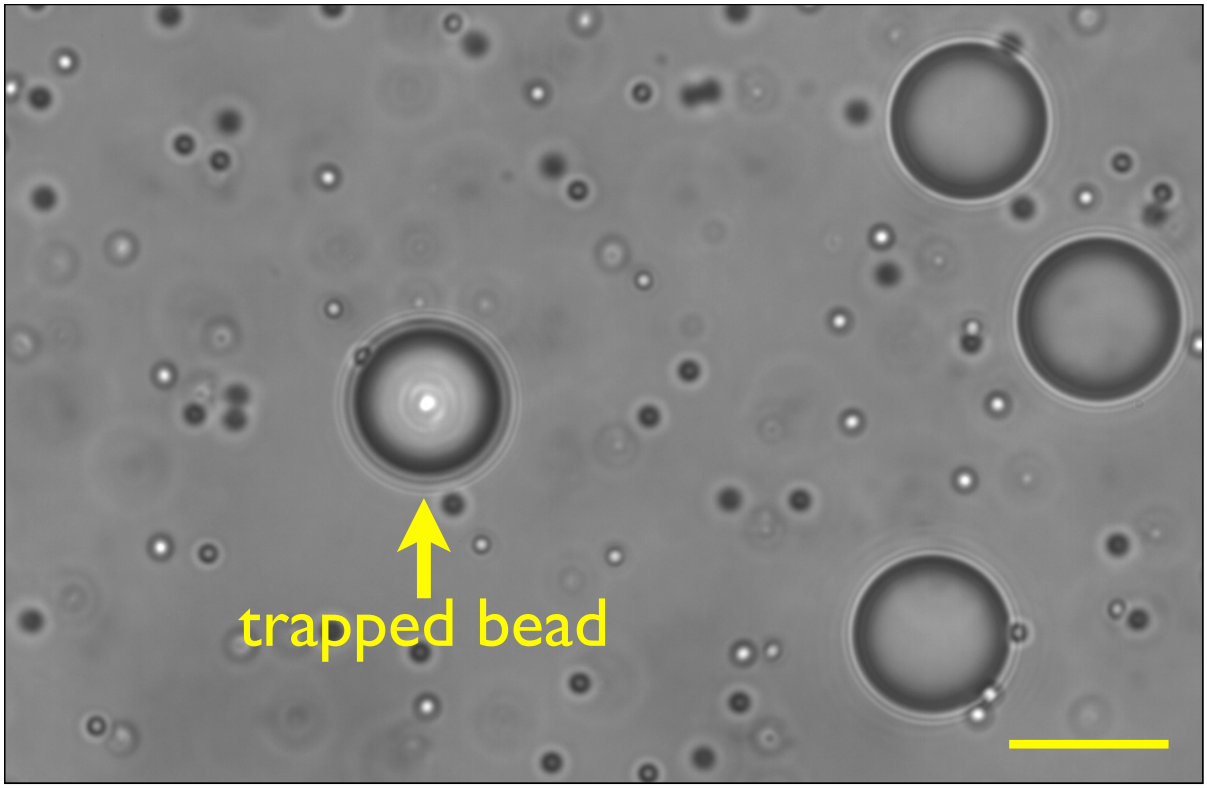

Figure 5.5 Comparing trapped and untrapped beads. Scale bar is 10 µm.

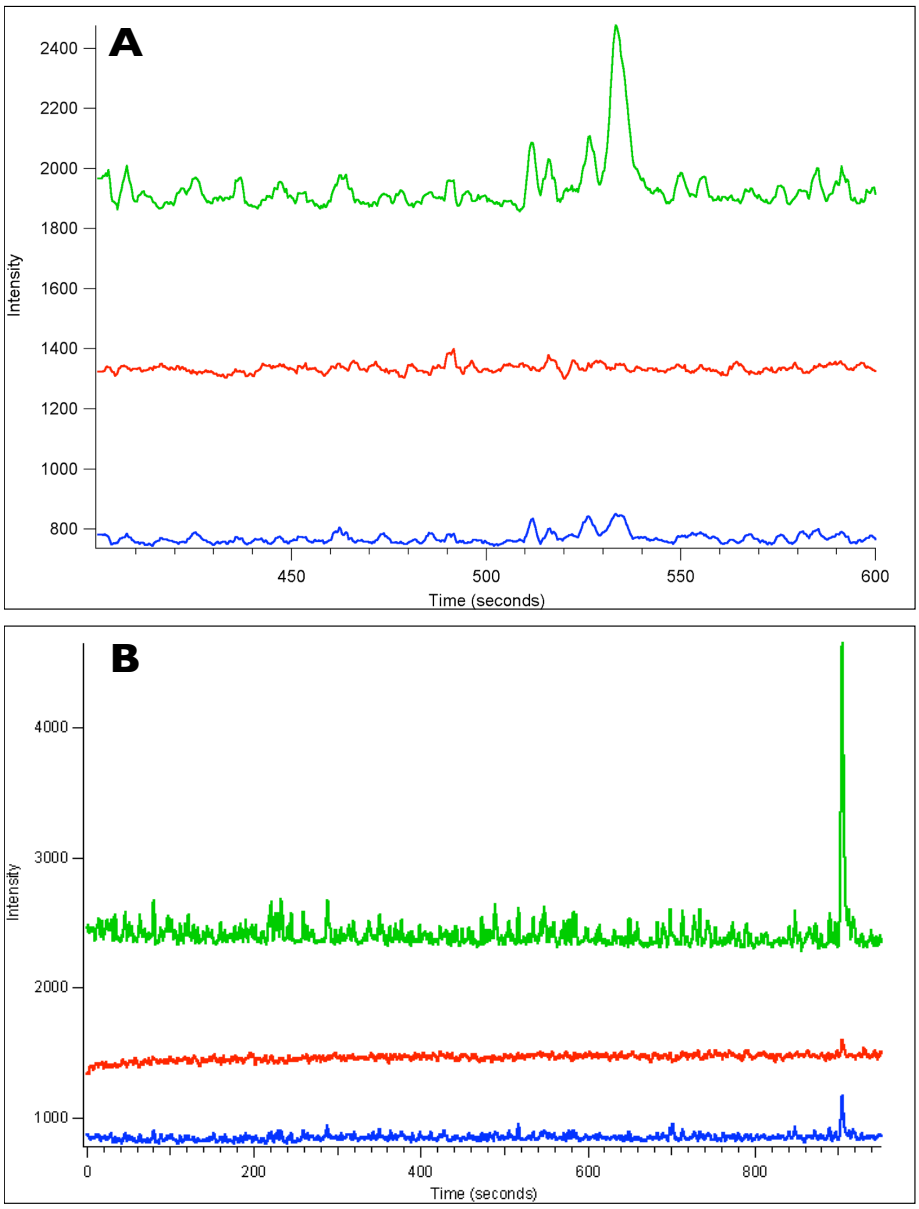

Figure 5.6 (A) An electropherogram obtained using a 20 µm inner diameter capillary. Figures of merit are: 3.5 µM serotonin, 150 s hydrodynamic injection. (B) An electropherogram obtained using a 50 µm inner diameter capillary. Figures of merit are: 3.5 µM serotonin, 30 s hydrodynamic injection. Conditions for both experiments are: 50 mM borate buffer, pH 8.8 (electrophoresis buffer), 1 mM borate buffer, pH 8.8 (sample buffer), 25 mM citric acid buffer, pH 2.25 (sheath buffer), -30 kV (separation voltage), 3 Hz (laser repetition rate), 100 µs (laser pulse length), 8 A (laser current), 420 V (laser BUSS voltage), 470 pF (PMT gain), 64% (gain voltage), 110 µs (PMT integration time).

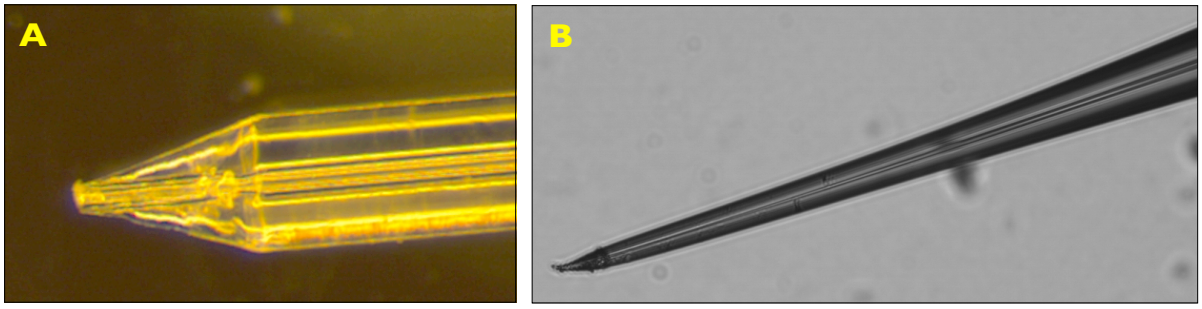

Figure 5.7 (A) A HF-etched capillary tip. Inner diameter is 50 µm and outer diameter at the non-etched portion is 360 µm. (B) A pulled capillary tip. Original dimensions were 20 µm inner diameter and 360 µm outer diameter. Notice how the inner diameter is not preserved.

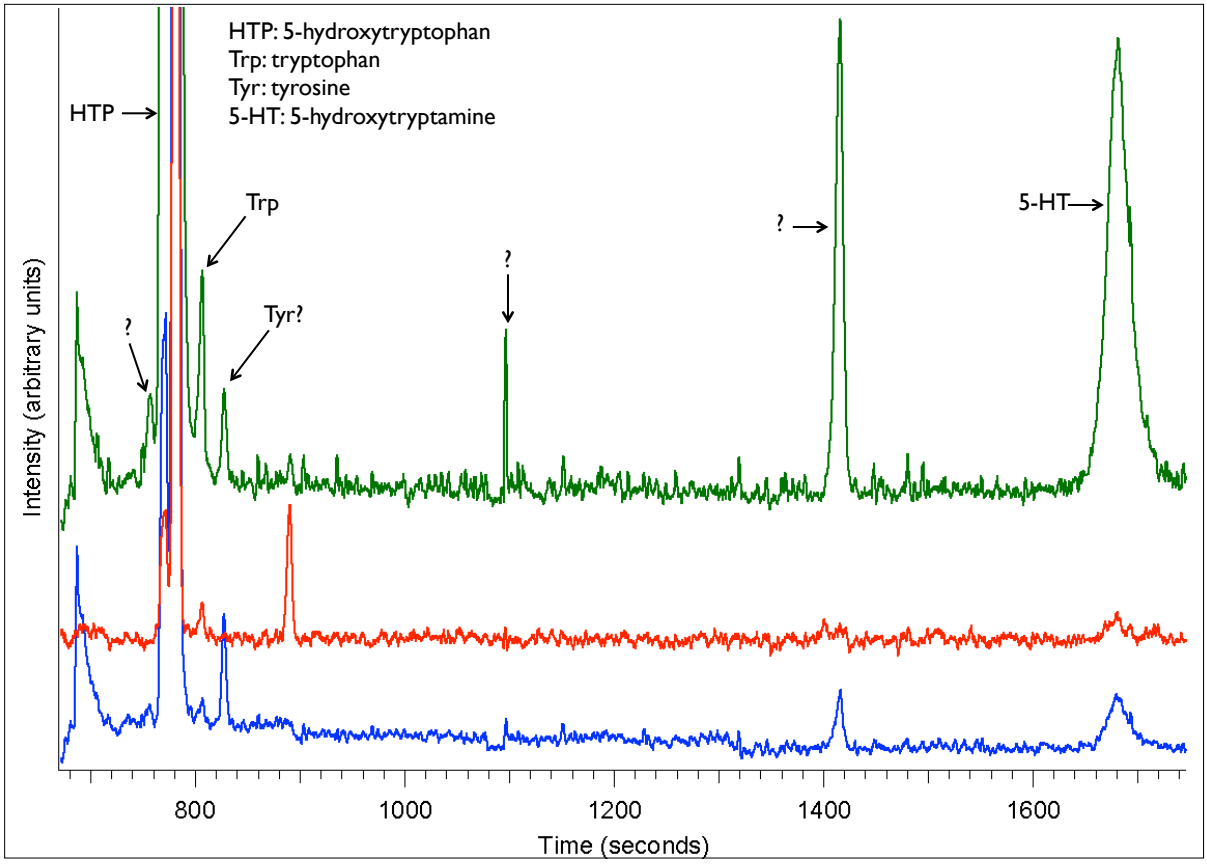

Figure 5.8 An electropherogram of a single pinealocyte that has been incubated in 5-hydroxytryptophan, showing all three channels. Conditions are: 20 mM borate buffer, pH 8.8, + 50 mM SDS (electrophoresis buffer), high salt mGBSS (sample buffer), 25 mM citric acid buffer, pH 2.25 (sheath buffer), -30 kV (separation voltage), 3 Hz (laser repetition rate), 100 µs (laser pulse length), 8 A (laser current), 420 V (laser BUSS voltage), 470 pF (PMT gain), 64% (gain voltage), 110 µs (PMT integration time).

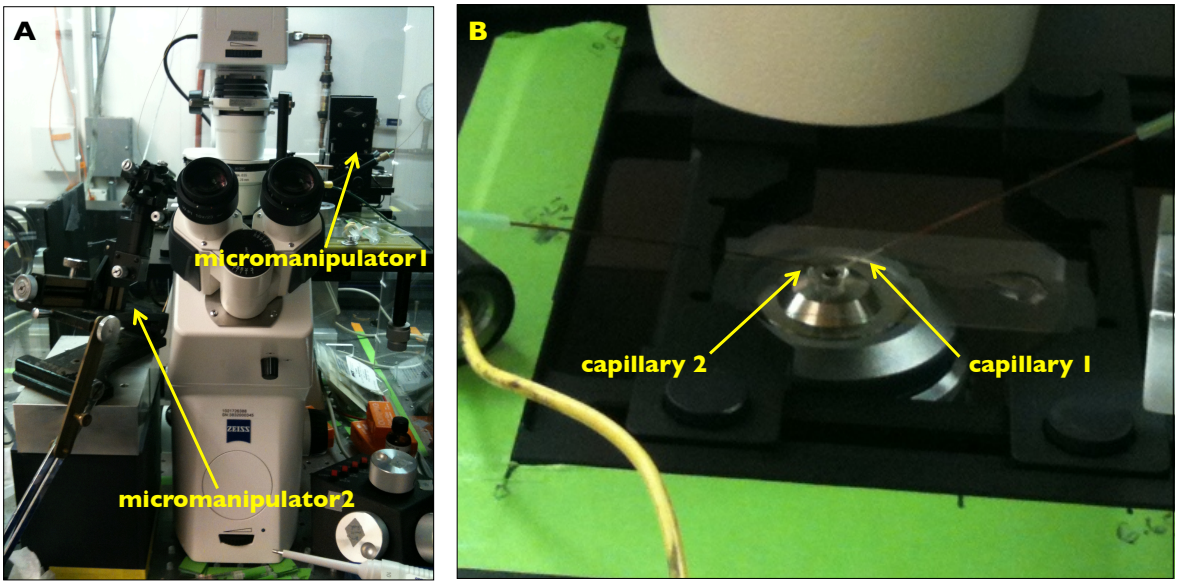

Figure 5.9 (A) The location of the two micromanipulators with respect to the microscope. (B) The two capillaries; capillary 1 is used for injection and capillary 2 is used for removing nearby cells and debris.

5.6 References

(1) Lapainis, T.; Sweedler, J. V. *J. Chrom. A*. **2008**, *1184*, 144–158.

(2) Li, G.-W.; Xie, X. S. *Nature*. **2011**, *475*, 308–315.

(3) Anderson, B. B.; Ewing, A. G. *J Pharm Biomed Anal*. **1999**, *19*, 15–32.

(4) Nemes, P.; Knolhoff, A. M.; Rubakhin, S. S.; Sweedler, J. V. *Anal Chem*. **2011**, *83*, 6810–6817.

(5) Lapainis, T.; Rubahkin, S. S.; Sweedler, J. V. *Anal Chem*. **2009**, *81*, 5858–5864.

(6) Gunasekera, N.; Olson, K. J.; Musier-Forsyth, K.; Arriaga, E. A. *Anal Chem*. **2004**, *76*, 655–662.

(7) Johnson, R. D.; Navratil, M.; Poe, B. G.; Xiong, G.; Olson, K. J.; Ahmadzadeh, H.; Andreyev, D.; Duffy, C. F.; Arriaga, E. A. *Anal Bioanal Chem*. **2007**, *387*, 107–118.

(8) Ewing, A. *J. Neurosci. Methods*. **1993**, *48*, 215–224.

(9) Boardman, A.; Chang, T.; Folch, A.; Dovichi, N. J. *Anal Chem*. **2010**, *82*, 9959–9961.

(10) Marc, P. J.; Sims, C. E.; Bachman, M.; Li, G. P.; Allbritton, N. L. *Lab Chip*. **2008**, *8*, 710.

(11) Mellors, J. S.; Jorabchi, K.; Smith, L. M.; Ramsey, J. M. *Anal Chem*. **2010**, *82*, 967–973.

(12) Chueh, B.-H.; Li, C.-W.; Wu, H.; Davison, M.; Wei, H.; Bhaya, D.; Zare, R. N. *Anal Biochem*. **2011**, *411*, 64–70.

(13) Omiatek, D. M.; Santillo, M. F.; Heien, M. L.; Ewing, A. G. *Anal Chem*. **2009**, *81*, 2294–2302.

(14) Dishinger, J. F.; Reid, K. R.; Kennedy, R. T. *Anal Chem*. **2009**, *81*, 3119–3127.

(15) Xu, C.-X.; Yin, X.-F. *J. Chrom. A*. **2011**, *1218*, 726–732.

(16) Allen, P. B.; Doepker, B. R.; Chiu, D. T. *Anal Chem*. **2009**, *81*, 3784–3791.

(17) Brown, R. B.; Hewel, J. A.; Emili, A.; Audet, J. *Cytometry*. **2010**, *77A*, 347–355.

(18) Jiang, D.; Sims, C. E.; Allbritton, N. L. *Electrophoresis*. **2010**, *31*, 2558–2565.

(19) Ando, J.; Bautista, G.; Smith, N.; Fujita, K.; Daria, V. R. *Rev. Sci. Instrum.* **2008**, *79*, 103705.

(20) Maghelli, N.; Tolić-Nørrelykke, I. M. *Methods in Cell Biology: Volume 95*. **2010**, *97*,

173–183.

(21) Jeffries, G. D. M.; Edgar, J. S.; Zhao, Y.; Shelby, J. P.; Fong, C.; Chiu, D. T. *Nano Lett.* **2007**, *7*, 415–420.

(22) Ros, A.; Hellmich, W.; Regtmeier, J.; Duong, T. T.; Anselmetti, D. *Electrophoresis*. **2006**, *27*, 2651–2658.

(23) Hellmich, W.; Pelargus, C.; Leffhalm, K.; Ros, A.; Anselmetti, D. *Electrophoresis*. **2005**, *26*, 3689–3696.

(24) Munce, N. R.; Li, J.; Herman, P. R.; Lilge, L. *Anal Chem*. **2004**, *76*, 4983–4989.

(25) Valley, J. K.; Ohta, A. T.; Hsan-Yin Hsu; Neale, S. L.; Jamshidi, A.; Wu, M. C. *IEEE Trans. Biomed. Circuits Syst.* **2009**, *3*, 424–431.

(26) Wu, H.; Wheeler, A.; Zare, R. N. *Proc Natl Acad Sci USA*. **2004**, *101*, 12809–12813.

(27) Ashkin, A. *Phys Rev Lett*. **1970**, *24*, 156–159.

(28) Ashkin, A.; Dziedzic, J. M. *App. Phys. Lett.* **1971**, *19*, 283–285.

(29) Ashkin, A.; Dziedzic, J. M. *App. Phys. Lett.* **1974**, *24*, 586–588.

(30) Ashkin, A. *Opt. Lett.* **1984**, *9*, 454–456.

(31) Ashkin, A.; Dziedzic, J. M.; Bjorkholm, J. E.; Chu, S. *Opt. Lett.* **1986**, *11*, 288–290.

(32) Ashkin, A. *IEEE JOURNAL ON SELECTED TOPICS IN QUANTUM ELECTRONICS*. **2001**, *6*, 841–856.

(33) Dholakia, K.; Čižmár, T. *Nature Photonics*. **2011**, *5*, 335–342.

(34) Block, S. M. *Nature*. **1992**, *360*, 493–495.

(35) Ashkin, A.; Dziedzic, J. M.; Yamane, T. *Nature*. **1987**, *330*, 769–771.

(36) Ashkin, A.; Dziedzic, J. M. *Science*. **1987**, *235*, 1517–1520.

(37) Dharmadhikari, J.; D'Souza, J.; Gudipati, M.; Dharmadhikari, A.; Rao, B.; Mathur, D. *Sensor Actuat B-Chem*. **2006**, *115*, 439–443.

(38) Doornbos, R.; Schaeffer, M.; Hoekstra, A.; Sloot, P.; de Grooth, B. G.; Greve, J. *App. Optics*. **1996**, *35*, 729–734.

(39) Steubing, R.; Cheng, S.; Wright, W.; Numajiri, Y.; Berns, M. In *Laser-Tissue Interaction, SPIE*; 1990; pp. 272–280.

(40) Hawes, C.; Osterrieder, A.; Sparkes, I. A.; Ketelaar, T. *Current Opinion in Plant Biology*. **2010**, *13*, 731–735.

(41) Hansen, P. M.; Oddershede, L. B. *Proc. SPIE (Optical Trapping and Optical Micromanipulation II)*. **2005**, *5930*, 593003–1 – 593003–9.

(42) Gross, S. *Method Enzymol*. **2003**, *361*, 162–174.

(43) Sacconi, L.; Tolic-Norrelykke, I.; Stringari, C.; Antolini, R.; Pavone, F. *App. Optics*. **2005**, *44*, 2001–2007.

(44) Sacconi, L.; Tolic-Norrelykke, I.; Antolini, R.; Pavone, F. In *Imaging, Manipulation, and Analysis of Biomolecules and Cells: Fundamentals and Applications III*; 2005; pp. 313–324.

(45) Comstock, M. J.; Ha, T.; Chemla, Y. R. *Nat Methods*. **2011**, *8*, 335–340.

(46) Mónico, C.; Belcastro, G.; Capitanio, M.; Vanzi, F. *2011 International Workshop on Biophotonics, BIOPHOTONICS 2011*.

(47) Rezaei, N.; Downing, B. P. B.; Wieczorek, A.; Chan, C. K. Y.; Welch, R. L.; Forde, N. R. In *Proc. SPIE (Photonics North 2011)*; SPIE, 2011; pp. 80070K1–80070K–10.

(48) Lautenschlaeger, F.; Guck, J. *Optomechatronic Technologies*. **2009**.

(49) Lai, C.; Hsiung, S.; Yeh, C.; Chiou, A.; Lee, G. *Sensor Actuat B-Chem*. **2008**, *135*, 388–397.

(50) Whyte, G.; Lautenschlager, F.; Kreysing, M.; Boyde, L.; Ekpenyong, A.; Delabre, U.; Chalut, K.; Franze, K.; Guck, J. In *Optical Trapping and Optical Micromanipulation VII*; SPIE, 2010; pp. 77620G–1–77620G–6.

(51) Hosokawa, Y.; Masuhara, H.; Matsumoto, Y.; Sato, S. *Proc. SPIE*. **2002**, *4622*, 138–142.

(52) Shi, L.; Shao, B.; Chen, T.; Berns, M. *J. Biophoton.* **2009**, *2*, 167–177.

(53) Shao, B.; Shi, L. Z.; Nascimento, J. M.; Botvinick, E. L.; Ozkan, M.; Berns, M. W.; Esener, S. C. *Biomed Microdevices*. **2007**, *9*, 361–369.

(54) Lin, H.-C.; Hsu, L. *Proc. SPIE*. **2005**, *5930*, 59301V–1–59301V–8.

(55) Eriksson, E.; Scrimgeour, J.; Enger, J. In *Proceedings of SPIE*; 2007; pp. 65920P–1–65920P–9.

(56) Uhrig, K.; Kurre, R.; Schmitz, C.; Curtis, J. E.; Haraszti, T.; Clemen, A. E. M.; Spatz, J. P. *Lab Chip*. **2009**, *9*, 661.

(57) Clement-Sengewald, A.; Buchholz, T.; Schutze, K.; Berg, U.; Berg, F. *J Assist Reprod Gen*. **2002**, *19*, 183–194.

(58) Nève, N.; Kohles, S. S.; Winn, S. R.; Tretheway, D. C. *Cel. Mol. Bioeng.* **2010**, *3*, 213–228.

(59) Murata, M.; Okamoto, Y.; Park, Y.-S.; Kaji, N.; Tokeshi, M.; Baba, Y. *Anal Bioanal Chem*. **2009**, 1–7.

(60) Applegate, R.; Squier, J.; Vestad, T.; Oakey, J.; Marr, D. *Optics Express*. **2004**, *12*, 4390–4398.

(61) Alexander, T.; Pellegrino, P.; Gillespie, J. *App. Spec.* **2003**, *57*, 1340–1345.

(62) Bankapur, A.; Zachariah, E.; Chidangil, S.; Valiathan, M.; Mathur, D. *PLoS ONE*. **2010**, *5*, e10427.

(63) Liu, Y.; Sonek, G. J.; Berns, M. W.; Konig, K.; Tromberg, B. J. *Opt. Lett.* **1995**, *20*, 2246.

(64) Kühn, S.; Phillips, B. S.; Lunt, E. J.; Hawkins, A. R.; Schmidt, H. *Lab Chip*. **2009**, *10*, 189.

(65) Konig, K.; Liu, Y.; Sonek, G.; Berns, M.; Tromberg, B. *Photochem. Photobiol.* **1995**, *62*, 830–835.

(66) Snijder-Van As, M. I.; Rieger, B.; Joosten, B.; Subramaniam, V.; Figdor, C. G.; Kanger, J. S. *J Microsc*. **2009**, *233*, 84–92.

(67) Fuller, R. R.; Moroz, L. L.; Gillette, R.; Sweedler, J. V. *Neuron*. **1998**, *20*, 173–181.

(68) Dahlgren, R. L.; Page, J.; Sweedler, J. V. *Anal Chim Acta*. **1999**, *400*, 13–26.

(69) Miao, H.; Rubahkin, S. S.; Sweedler, J. V. *Anal Bioanal Chem*. **2003**, *377*, 1007–1013.

(70) Ye, X.; Rubahkin, S. S.; Sweedler, J. V. *Analyst*. **2008**, *133*, 423–433.

(71) Cruz, L.; Moroz, L. L.; Gillette, R.; Sweedler, J. V. *J Neurochem*. **1997**, *69*, 110–115.

(72) Chiu, D. T.; Hsiao, A.; Gaggar, A.; Garza-Lopez, R.; Orwar, O.; Zare, R. N. *Anal Chem*. **1997**, *69*, 1801–1807.

(73) Chiu, D. T.; Lillard, S. J.; Scheller, R. H.; Zare, R. N.; Rodriguez-Cruz, S. E.; Williams, E. R.; Orwar, O.; Sandberg, M.; Lundquist, J. A. *Science*. **1998**, *279*, 1190–1193.

(74) Hoffmann, P.; Dutoit, B.; Salathe, R. P. *Ultramicroscopy*. **1995**, *61*, 165–170.

(75) Grego, S.; Arimondo, E.; Frediani, C. *J Biomed Opt*. **1997**, *2*, 332–339.

(76) Frediani, C.; Grego, S.; Guidoni, L.; Arimondo, E. *SPIE*. **1996**, *2696*, 56–61.

(77) Maghelli, N.; Tolić-Nørrelykke, I. M. *J. Biophoton.* **2008**, *1*, 299–309.

(78) Svoboda, K.; Block, S. M. *Annu. Rev. Biophys. Biomolec. Struct.* **1994**, *23*, 247–285.

(79) Neuman, K. C.; Block, S. M. *Rev. Sci. Instrum.* **2004**, *75*, 2787–2809.

(80) Block, S. In *Cells: A Laboratory Manual Volume 2: Light Microscopy and Cell Structure*; Spector, D.; Goldman, R.; Leinwand, L., Eds. Cold Spring Harbor Laboratory Press, 1998; pp. 1–11.

(81) Reicherter, M. **2004**, *5462*, 68–78.

(82) MacDonald, M.; Neale, S.; Paterson, L.; Riches, A. In *Proceedings of …*; 2004.

(83) Fallman, E.; Axner, O. *App. Optics*. **1997**, *36*, 2107–2113.

(84) Fallman, E.; Andersson, M.; Axner, O. *Proc. of SPIE (Imaging, Manipulation, and Analysis of Biomolecules, Cells, and Tissues IV)*. **2006**, *6088*, 1–12.

(85) Lapainis, T.; Scanlan, C.; Rubahkin, S. S., Sweedler, J. V. *Anal Bioanal Chem*. **2007**, *387*, 97–105.

(86) Mirsaidov, U.; Timp, W.; Timp, K.; Mir, M.; Matsudaira, P.; Timp, G. *Phys. Rev. E*. **2008**, *78*, 1–7.

(87) Neuman, K. C.; Chadd, E. H.; Liou, G. F.; Bergman, K.; Block, S. M. *Biophys. J.* **1999**, *77*, 2856–2863.

(88) Aly, K.; Esmail, E. *Optical Materials*. **1993**, *2*, 195–199.

(89) Querry, M.; Holland, W.; Waring, R.; Earls, L.; Querry, M. *Journal of Geophysical Research*. **1977**, *82*.

(90) Jin, W.; Wang, Y.; Ren, N.; Bu, M.; Shang, X.; Xu, Y.; Chen, Y. *Optics and Lasers in Engineering*. **2011**, 1–5.

(91) Takagi, M.; Kitabayashi, T.; Ito, S.; Fujiwara, M.; Tokuda, A. *J Biomed Opt*. **2007**, *12*, 054010–.

(92) Sugden, D. *Experientia*. **1989**, *45*, 922–932.

(93) Goto, M.; Oshima, I.; Tomita, T.; Ebihara, S. *J Pineal Res*. **1989**, *7*, 195–204.

(94) Ganguly, S.; Coon, S.; Klein, D. *Cell and Tissue Research*. **2002**, *309*, 127–137.

6 Analyzing single pinealocytes for indolamine content using an optical trap-capillary electrophoresis-laser-induced native fluorescence instrument

Notes and Acknowledgments

I would like to acknowledge Dr. Stanislav S. Rubhakin for performing pineal dissections and isolations and providing advice, and Jennifer M. Arnold, Dr. Jennifer Miller, and Prof. Martha U. Gillette for providing animals, advice, and a place to perform dissections under red light. I would like to thank Prof. Jonathan V. Sweedler for support, advice, and funding, and the SCS Machine Shop for their advice and work. I would also like to acknowledge Bill Hug, Ray Reid, and Prashant Oswal at Photon Systems Inc. for providing the hollow cathode ion laser and their help with troubleshooting. This work was supported by the National Institute of Neurological Disorders and Stroke under award number R01 NS031609 and by the National Institute of Dental and Craniofacial Research under award number R01 DE018866.

6.1 Introduction

The pineal gland has been known since the early Greeks, and was largely thought of a brain region without much function until the discovery of melatonin in the pineal gland in 1958.[1] Melatonin is an indolamine hormone that is most often associated with sleep and circadian rhythm,[2-7] but has other physiological functions including regulating seasonal reproduction[8-11] and acting as an anti-oxidant and protective chemical within the immune system.[12-17] Most of the melatonin present in the body is synthesized in and secreted from the pineal gland, which in humans is located in a central position between the cerebral hemispheres. The precursor to melatonin is tryptophan, which is converted to serotonin in two steps (Figure 6.1). Serotonin is N-acetylated to form N-acetylserotonin, which is then O-methylated to form melatonin. The formation of melatonin follows a unique pattern, in that it only occurs at night during darkness (Figure 6.2).[18-20] At night the suprachiasmatic nucleus signals the postganglionic neurons in the pineal gland to release norepinephrine, which mediates a cascade of signal transduction events that culminate in the conversion of serotonin to melatonin. Melatonin is secreted by the pineal gland into the blood and

cerebral spinal fluid and circulates throughout the body for a period of time determined by the length of darkness. If light exposure occurs, melatonin levels can drop rapidly and synthesis can be disrupted.

The pineal gland is composed of pinealocytes, which are neuroendocrine cells, and interstitial glial cells that may assist with the secretion of melatonin into the blood stream. Rat pinealocytes are 10 µm to 15 µm in diameter, which corresponds to picoliter volumes, and spherical in shape.[21-23] There is some evidence that pinealocytes display heterogeneity in their morphology or even their synthesis and secretion of melatonin,[24-30] but little is known about variations in analyte concentration across cell types within the pineal gland. An interesting facet of this is the number of indolamine products that can be produced within the pineal gland.[31] Furthermore, although the role, synthesis, and secretion of melatonin are widely conserved within multiple phyla, it is known that the onset of N-acetylserotonin and melatonin production varies by species and breed (Figure 6.3).[18, 5] It has also been shown that different breeds of mice and rats can have widely varying levels of pineal indolamines.[32-35] In humans and other animals melatonin levels are known to decrease with age,[36-40] which can be related to insomnia and other disorders in older adults.[41-43] These variations in pineal indolamines have been well studied on a bulk level,[31, 6, 44] but there is a dearth of research on single cell indolamine concentrations. Understanding pinealocyte heterogeneity will provide a deeper understanding of indolamine synthesis and secretion, provide insight into indolamine-related dysfunctions, and pave the way for indolamine-based treatments, several of which are already in use.[45-49]

Successfully performing single cell analysis requires instrumentation that is amenable to volume-limited samples, compatible with biological conditions, possesses a sensitive detection method, and is able to perform low volume sampling. Capillary electrophoresis with laser-induced fluorescence detection (CE-LIF) is particularly appropriate for single cell and subcellular analysis, as it possesses three of the conditions listed.[50-56] Sample injection is typically in the low nanoliter to picoliter range, relatively rapid high resolution separations are possible, and there are numerous methods available to separate a wide variety of analyte types. Fluorescence detection is often used for single cell

analysis due its sensitivity, selectivity, versatility, and low limits of detection appropriate for trace analyte analysis in single cells.

While CE-LIF has the sensitivity to characterize low abundance analytes within individual cells and subcellular components, the sample handling required to isolate and inject such small samples is challenging. One way to address this issue is to interface a sampling system to enable precise, controlled manipulation and sampling of single cells.

Optical traps make use of radiation pressure, which may be regarded as the transfer of momentum from photons to the objects being irradiated. Ashkin published experimental results from optical traps in the 1970s,[57-60] and their use for trapping and manipulating biological entities was first reported for single bacteria, viruses, and cells in 1987.[61, 62] There are several advantages to using optical traps. They enable fine control over the manipulation and movement of single cells,[63-65] organelles,[66-70] and even single biological molecules[71-73] and these biological entities can be trapped without catastrophic damage. Optical traps are also considered a non-contact method and they allow high resolution probing of the cellular microenvironment. Overall, optical traps are a versatile technique that can be used to study, isolate, and manipulate single cells and subcellular organelles on the micron scale with a minimum of interference.

To enable single cell analysis, a hyphenated optical trap-capillary electrophoresis-laser-induced native fluorescence (OT-MC-CE-LINF) instrument was designed and constructed (Chapter 5). It enables single cell analysis to be performed with a minimum of sample handling and disruption, provides a separation step to reduce complexity, separate similar analytes, and potentially concentrate analytes, and utilizes native fluorescence detection optimized for catecholamines and indolamines. The optical trap is formed by tightly focusing the output of a near infrared (NIR) laser with a high numerical aperture objective. Once the cell is localized within the trap, the capillary inlet is moved adjacent to the trap using a computer-controlled micromanipulator and microscope combination. The cell is released from the trap and quickly injected into the capillary, where it is chemically lysed and its chemical components are separated and detected. The multi-channel capillary electrophoresis-laser-induced native fluorescence instrument is optimized for the native

fluorescence detection of catecholamines and indolamines (Chapter 3). Briefly, a 224 nm HeAg hollow cathode ion laser is used in combination with a sheath-flow cuvette; the fluorescence emission is collected and measured using three channel detection (each detector has its own wavelength range selected with appropriate dichroic beamsplitters). This instrument allows unambiguous identification of a variety of catecholamines and indolamines based on differences in their fluorescence emission profiles, as well as their migration times.

This instrument has been used to identify and quantitate indolamines, including serotonin, N-acetylserotonin, and melatonin, in single pinealocytes from rats. Comparisons between day and night levels and incubation versus native levels are made. Incubation is used to ensure the viability of samples, by forcing non-physiological amounts of indolamines to be synthesized from excess precursor compounds that are added to the cell suspensions. Incubation also provides information on enzymatic pathways in the pineal gland, detailed in Figure 6.1. A number of unusual indolamines such as substituted tryptophols and O-methylated versions of the more common indolamines were identified within single pinealocytes and also in multiple cell experiments, under both incubated and untreated conditions. The concentration range that was measured for the common indolamines (*e.g.* serotonin, N-acetylserotonin, 5-hydroxytryptophol) in single pinealocytes alone was mM; however, given the volume of a single pinealocyte, mM concentrations correspond to fmol to amol levels of analytes. The lower level indolamines (including the rare indolamines listed above, but also 5-hydroxyindole-3-acetic acid) were present in µM levels in single pinealocytes. The chemical profiles of incubated and untreated samples are also compared, as well as day versus night differences in profiles. Overall, few day and night differences in chemical profile are observed incubated samples; however, in untreated samples there appears to be distinct differences between the chemical profiles of single pinealocytes collected during the day versus ones collected at night.

6.2 Materials and methods

A list of abbreviations can be found in the Appendix.

6.2.1 Chemicals

Chemicals, unless otherwise noted, were from Sigma Aldrich (St. Louis, MO) and were reagent grade or higher. Citric acid sheath buffer (25 mM, pH 2.25) was made by dissolving 5.25 g of $C_6H_8O_7 \cdot H_2O$ in 1 L of ultrapure deionized water (Elga Purelab Ultra, Siemens Water Technologies, Warrendale, PA). Electrophoresis buffers were made by diluting a stock solution of 50 mM borate buffer, pH 8.8, which was prepared by dissolving 9.2 g of $Na_2B_4O_7 \cdot 10H_2O$ and 3.0 g of $B(OH)_3$ in 1 L of ultrapure deionized water. For surfactant-containing electrophoresis buffers, sodium dodecyl sulfate (SDS) was added to 50 mL of diluted borate buffer, pH 8.8, sonicated for 2 min to dissolve, and filtered with a 0.22 µm syringe filter (Nalgene, Rochester, NY). Serotonin (5-HT) (Alfa Aesar, Ward Hill, MA), dopamine (DA), tyrosine (Tyr), norepinephrine (NE), and epinephrine (E) were dissolved in 2.5 mM citric acid, pH 2.5, and sonicated on ice for 30 min if needed. Tryptophan (Trp), N-acetyl serotonin (NAS), 5-hydroxyindole acetic acid (HIAA), melatonin (MT), 5-hydroxytryptophan (HTP), 5-methoxytrytophol (MTOL), 5-methoxytryptamine (MOT) (TCI America, Portland, OR), tryptophol (TOL) (Research Organics, Inc., Cleveland, OH), 5-methoxyindole acetic acid (MIAA) (Gold Biotechnology, St. Louis, MO), and 5-hydroxytryptophol (HTOL) (Gold Biotechnology, St. Louis, MO) were dissolved in 2.5 mM citric acid, pH 2.5, + 10% v/v acetone and sonicated on ice for 30-60 min. Standard buffers were prepared by diluting the sheath buffer 1:10 with ultrapure deionized water. Fluorescein was prepared in ultrapure deionized water. Standard stock solutions were diluted in Ca^{+2}-free modified Grey's balanced salt solution (Ca^{+2}-free mGBSS), pH 7.2, modified Grey's balanced salt solution (mGBSS),pH 7.2, or in high Ca^{+2}/high Mg^{+2} modified Grey's balanced salt solution (high salt mGBSS), pH 7.2. The solutions were prepared by dissolving the appropriate salts and other compounds in 1 L of ultrapure deionized water (Table 6.1). Glycerol solutions were prepared by adding the appropriate volume of glycerol to mGBSS. All buffers were filtered by a 0.45 µm bottle-top filter system (Nalgene, Rochester, NY) and degassed under vacuum with stirring for 30-60 min. NaOH (~0.1 M) was prepared by dissolving one pellet (~0.0025 g) in 0.025 L of ultrapure deionized water. NaOH (10 M) was prepared by dissolving 20 g of pellets in 0.05 L of ultrapure deionized water.

6.2.2 Animals

Animals were housed and cared for as described in animal protocols in full compliance with NIH guidelines for the humane care and treatment of animals, approved by IACUC and supervised by the Division of Animal Resources at the University of Illinois at Urbana-Champaign.

The pineal glands were isolated from the central nervous system of Long Evans/Blugill rats, which were demonstrated to be genetically homogeneous by high density genome scan. Sacrifice occurred during the day (CT 3:00 or CT 5:00) or during the night (CT 20:00 or 22:00) and pineal dissection and preparation was completed within 30 min. Glands were manually triturated and stored in Ca^{+2}-free mGBSS, mGBSS, mGBSS + glycerol, or high salt mGBSS on ice until analysis. Samples isolated under red light (during the night) were analyzed in the dark.

The olfactory bulb and cerebellum were isolated from the central nervous system of rats. Sacrifice occurred during the day (CT 3:00) and dissection and preparation was completed within 30 min. Manual trituration was used to separate the cells from the connective tissue. Samples were stored in mGBSS on ice until analysis.

6.2.3 Biological samples

Daytime pineal samples were split into two groups: HTP-incubated and non-incubated. Incubated samples were incubated at room temperature with a total concentration of 200 µM HTP, dissolved in high salt mGBSS, for 60 min before analysis. Non-incubated samples had an equal volume of high salt mGBSS added and were treated at room temperature for 60 min before analysis.

Nighttime pineal samples were split into three groups: HTP-incubated, 5-HT-incubated, and non-incubated. Incubated samples were incubated at room temperature with a total concentration of 200 µM HTP or 200 µM 5-HT, dissolved in high salt mGBSS, for 60 min before analysis. Non-incubated samples had an equal volume of high salt mGBSS added and were treated at room temperature for 60 min before analysis.

6.2.4 Hydrofluoric acid etching

Hydrofluoric acid (HF) etching of the capillary inlet and outlet is used to shape the ends into sharply tapered tips with a 40° angle (Figure 3.2).[74] The fused silica capillary dimensions were either 10 µm, 20 µm, or 50 µm inner diameter, 360 µm outer diameter, and 85-120 cm in length (Polymicro Technologies, Phoenix, AZ). The ends were scored and snapped to provide a relatively even surface for etching. Approximately 1 cm of the capillary's polyimide coating is burned off of each end and the tips cleaned with methanol. A container is filled to 5 mm of depth with 48% HF and covered with isooctane to prevent HF fumes from rising. The capillary tip is pushed through a FEP sleeve (Upchurch Scientific, Oak Harbor, WA) held tightly in a customized Teflon holder, which maintains the tip position during etching, until the tip touches the bottom of the container. The capillary has isooctane continuously pumped through the non-submersed end via a syringe to prevent the inner walls of the submerged end from being etched. After two hours, the etched tip is rinsed with $Na_2B_4O_7 \cdot 10H_2O$ (Borax, Henkel Corp., Billerica, MA) and water and the process is repeated for the other end.

6.2.5 Optical trap design and construction

Unless otherwise noted, all laboratory-built and custom-built components have been designed and fabricated in-house either within the laboratory or by the SCS Machine Shop. The trapping laser is a 1064 nm diode-pumped solid state Nd:YAG laser (Compass 1064-2500MN, Coherent Inc., Santa Clara, CA) with a maximum output of 2.5 W. The beam is expanded by a 20x high energy beam expander (HB-20X, Newport Corp., Irving, CA) and directed by a pair of gold-coated mirrors into a set of plano-convex lenses (SPX029, Newport Corp., Irving, CA) in a 1:1 telescope configuration, used to steer and parfocalize the beam. Plano-convex lens 1 is mounted in a 3-axis optical mount (LP-1A-XYZ, Newport Corp., Irvine, CA) located 1000 mm from the back aperture of the objective and plano-convex lens 2 is mounted in a 2-axis mount (LP-1A-XY, Newport Corp., Irvine, CA) located 500 mm from the back aperture of the objective (Objective C-Apochromat 63x/1.2 W Corr, 441777-9970-000, Carl Zeiss, Jena, Germany). The beam was then directed into the epi-fluorescence port of the microscope (AxioObserver A1, Carl Zeiss, Jena, Germany) and directed into the back

aperture of the objective by a dichroic mirror centered at 1064 nm (950dcsp-laser, Chroma Technology, Rockingham, VT). More details on the optical trap design and construction can be found in Chapter 5.

Polystyrene beads (10 µm (PS06N/6955) diameter, Bangs Laboratories, Fishers, IN), diluted 100-fold in ultrapure deionized water, were used to optimize the optical trap daily for experiments.

6.2.6 Multi-channel capillary electrophoresis-laser-induced native fluorescence instrument (MC-CE-LINF) design and construction

The injection port for bulk analysis is housed on a non-conductive breadboard platform on a microscope contained in a clear Plexiglas box. The bulk injection port consists of a stainless steel disk with bored holes to hold the microvials used for sample injection and the buffer vials used for electrophoresis. This disk is mounted to the breadboard platform on a T-shaped Plexiglas holder with a 2.5", ¼"-20 screw that connects the disk and holder to the platform. The capillary is held in place during electrophoresis by a capillary holder which consists of an alligator clip mounted in an acetal resin block (Delrin, E. I. duPont de Nemours & Co., Wilmington, DE) which is held in place by a U-shaped slot with set screws for manipulation. The capillary is held in place in the instrument by a custom-built acetal resin sheath flow cell. It enters at the top of the cell and is held in place by liquid-tight fittings (Upchurch Scientific, Oak Harbor, WA).

The current optical layout was adapted from a previous version.[75] Deep UV radiation (224.6 nm) from a HeAg hollow cathode ion laser (HeAg70, Photon Systems Inc., Covina, CA) is directed via two UV-coated mirrors (Thorlabs, Newton, New Jersey) into a laboratory-built lightproof, non-conductive box and breadboard, which houses the detection optics and protects against spurious arcing. The collimated beam is nominally focused using a plano-convex lens (OptoSigma, Santa Ana, CA) to a 50 µm spot directly below the outlet of the capillary, which has been HF-etched to a cone-shaped tip and is housed in a custom-built sheath flow cell, as described above. As analytes elute from the capillary they are excited by the focused beam and emit fluorescence, which is collected and collimated by a 15x all-reflective objective (13596, Newport Corp., Irvine, CA). The fluorescence is directed toward

the three photomultiplier tube (PMT) detectors (H6780-06, Hamamatsu, Middlesex, NJ) by two dichroic mirrors (310dcxxr-haf #110258 and 400dcxru #111563, Chroma Technology, Rockingham, VT), with transition points at 310 nm and 400 nm, respectively. The first detector (PMT "blue") measures emission from 250-310 nm, the second detector (PMT "green") measures emission from 310-400 nm, and the third detector (PMT "red") measures emission from 400 nm and above. The laser and PMTs are synchronized and controlled by software written in LABView and provided by Photon Systems Inc.

Negative voltage for electrophoresis is applied to the sheath flow waste by a stainless steel cylinder that is connected to a power supply (PS/MJ30N0400-11, Glassman High Voltage, High Bridge, NJ) and laboratory-built control box. A 10 kΩ resistor and a digital multimeter (Fluke 76, Fluke Corp., Everett, WA) are part of the circuit and are used to measure the current across the capillary. Sheath buffer is gravity-driven and flow can be adjusted by a right angle switching valve (Upchurch Scientific, Oak Harbor, WA). More information about this instrument can be found in Chapter 3.

6.2.7 Interfacing the optical trap and MC-CE-LINF instrument

The optical trap and the MC-CE-LINF system are interfaced at the microscope stage. The trap is located at the focal point of the objective approximately 0.28 mm from the objective surface, including the coverslip thickness (0.13-0.16 mm). The capillary inlet is controlled by a computer-controlled motorized micromanipulator (MP-285, Sutter Instrument Co., Novato, CA). The micromanipulator is mounted on a non-conductive optical breadboard, which is stabilized by two ¼-28" tapped beams that attach to the microscope stand on either side of the stage. The capillary is held in the micromanipulator by an acetal resin cylinder, which is 6" long and has a 1/16" diameter hole drilled in the center.

The sample is held on a coverslip holder, machined out of polycarbonate, with a lip to rest the coverslip edges on and a 30° angled oval hole for holding the electrophoresis buffer vial, which consisted of an Eppendorf tube (Hamburg, Germany) that had its top quarter removed at an angle. A platinum grounding wire (California Fine Wire Co., Grover Beach, CA) is placed in contact with the electrophoresis buffer, completing the circuit.

Trapping, manipulation, and injection were recorded by a monochrome CMOS camera (NT59-365, EO-1312M, Edmund Optics, Barrington, NJ) that is attached to the microscope housing with a 1x C-mount (Carl Zeiss, Jena, Germany).

6.2.8 Coverslip coatings and additives

Glass coverslips (2735-246, Corning Inc., Corning, NY) were used for all experiments except where noted. Several coatings and additives were tested to reduce adhesion of cells to the coverslip surface. Treated coverslips were stored at ambient temperature and humidity in Parafilm M (Pechiney Plastic Packaging Inc., Chicago, IL)-covered glass dishes, unless otherwise noted, until use.

Tests were performed by pipetting 2.5 µL to 5 µL of cell suspension (pinealocytes, olfactory bulb cells, or cerebellum cells) in mGBSS onto the treated coverslip or pipetting the additive solution into an aliquot of the cell suspension and transferring that onto a coverslip. The optical trap was operated at 1.3 W to 1.5 W initial power, and the capillary was controlled by the micromanipulator (MP-285, Sutter Instrument Co., Novato, CA). Video was recorded for all tests using a monochrome CMOS camera (NT59-365, EO-1312M, Edmund Optics, Barrington, NJ).

Bovine serum albumin (BSA): (1) Coverslips were sonicated with isopropyl alcohol for 10 min, rinsed with ultrapure deionized water, and dried. BSA was dissolved in phosphate buffered saline (BioWhittaker, Lonza, Walkersville, MD) (0.01 g/mL). Coverslips were soaked in BSA solution for 10 min. Excess BSA was rinsed off with phosphate buffered saline and the coverslip dried using compressed air. (2) Coverslips were sonicated in 25% w/v NaOH (200 mL) + 95% ethanol (600 mL) for 10 min, rinsed by dipping into five individual containers of ultrapure deionized water, and dried in a 45°C oven. BSA (10 mg/mL) was dissolved in 80 mM PIPES (piperazine-N,N'-bis(2-ethanesulfonic acid), 6.05 g dissolved in 250 mL ultrapure deionized water, titrated to pH 6.8 with 10 M NaOH) and filtered by a 0.22 µm syringe filter (Nalgene, Rochester, NY). The coverslips were coated with the BSA solution and immediately rinsed by dipping into five individual containers of ultrapure deionized water.

Parafilm M: Coverslips were washed with Alconox, rinsed with ultrapure deionized water and methanol, and dried. Parafilm M (Pechiney Plastic Packaging Inc., Chicago, IL) was stretched over the surface of the coverslip.

Plastic coverslips: Plastic coverslips were used without cleaning or treatment.

Glass Free: Coverslips were washed with Alconox (Powdered Precision Cleaner, Alconox Inc., White Plains, NY), rinsed with ultrapure deionized water and methanol, and dried. Coverslips were submerged in Glass Free (National Diagnostics, Atlanta, GA) for 5 min in a ventilation hood, then rinsed with toluene followed by methanol. The coverslips were gently buffed with a paper towel until dry and stored in a plastic bag, interleaved with paper until use.

Poly(2-hydroxyethyl methacrylate) (pHEMA): Coverslips were washed with Alconox, rinsed with ultrapure deionized water and methanol, and dried. pHEMA solution (2.5 % w/v) was prepared by dissolving 6 g of pHEMA in 50 mL of 95% ethanol, stirred overnight at 37°C, and filtered by a 0.22 µm syringe filter (Nalgene, Rochester, NY) before use. pHEMA solution was pipetted onto coverslips and allowed to evaporate to dryness.

Sigmacote: Coverslips were washed with Alconox, rinsed with ultrapure deionized water and methanol, and dried. Sigmacote (Sigma-Aldrich, St. Louis, MO) was applied to the coverslips and allowed to dry. Dried coverslips were rinsed with ultrapure deionized water before use.

Ethylenediaminetetraacetic acid (EDTA): EDTA solution (5 mM) was prepared by dissolving 0.018 g EDTA in 10 mL mGBSS. The final concentration of EDTA in the cell suspensions was 2.5 mM.

Nanodiamonds: Nanodiamond (ND98, Dynalene Inc., Whitehall, PA) suspensions were prepared by adding 5% w/v of nanodiamonds to 1 mL of mGBSS and sonicating for 60 min. The final concentration of nanodiamonds in cell suspensions was 2.5% w/v.

Ethylene glycol: Ethylene glycol solution (~10% v/v) was prepared by adding 1 mL of ethylene glycol to 9.5 mL of mGBSS. The final concentration of ethylene glycol in cell suspensions was 5% v/v.

6.2.9 Single cell injections

Single pinealocytes were injected into the capillary for analysis. A 2.5 µL droplet of sample was pipetted onto the coverslip. A cell was selected and trapped using 1.3 W of initial power (incident power ~ 433 mW). The capillary inlet was directed into the cell's proximity by the micromanipulator, which was programmed to stop near the trap location and further position refinement was performed manually using the rotary optical encoder. Once the capillary was in place, the cell was released from the trap and hydrodynamic injection of the cell was performed by lowering the sheath waste outlet. Once injection was complete, the micromanipulator was used to bring the capillary inlet to the buffer vial, and the voltage and detectors were turned on. Injections were recorded using the CMOS camera on the microscope.

6.2.10 Electrophoresis

The sheath flow buffer was 25 mM citric acid, pH 2.25, and the flow rate was 0.2 mm/s for all experiments. The electrophoresis buffers and sample buffers varied as stated in the text and figure captions. The voltage for all experiments was -30 kV unless otherwise stated. The injection volume varies as stated, but for bulk injections the volume was 14.7 nL for a 30 s hydrodynamic injection, which was performed by lowering the sheath flow waste outlet by 32.5 cm. The typical laser pulse energy was between 1.5 µJ/pulse and 2 µJ/pulse.

The capillary was conditioned at the beginning of the day with 0.1 M NaOH for 15-20 min, followed by water for 5 min, and then electrophoresis buffer for a minimum of 5 min.

6.2.11 Data analysis

Data analysis was performed in IgorPro 5.05A (WaveMetrics Inc., Lake Oswego, OR). An automated data analysis script was written that reduces the user input to a single command. Output consists of four tables of calculated values with four corresponding color-coded graphs displaying the raw data, 6-point boxcar averaged data, normalized (with respect to the laser pulse energy) data, and both normalized and boxcar averaged data. The baseline range (30 points, 10 s) with the lowest standard deviation is determined and used to calculate the limits of detection (LOD) for each PMT channel. Ratiometric analysis

(calculating the intensity ratio between peak maxima in each of the PMT channels) is also automated to aid in analyte identification.

Single cell analyte concentrations were calculated as follows: the ratio of the injection lengths between a sample analyzed under cell lysing conditions and the same sample analyzed under non-cell lysing conditions was used to normalize the analyte concentrations in the non-cell lysing conditions. These normalized values were used to calculate equivalent background concentrations, which were subtracted from the concentrations calculated under cell lysing conditions. These values were then adjusted based on an assumed cell volume of 4 pL to represent the concentration within the cell.

6.2.12 Limits of detection

LODs and concentration of analytes were determined by generating calibration curves for each analyte under the appropriate conditions. Analyte concentrations to generate calibration curves ranged from the micromolar to the low nanomolar, within physiological limits and at maximum an order of magnitude greater than LODs. The criterion for calculating the LODs was three times the standard deviation of the baseline.

6.3 Results and discussion

This section covers experiments performed to reduce pinealocyte adhesion and to optimize conditions for trapping, separation, and detection. Multiple cell injections (referred to throughout the text as “bulk”) and single cell injections and experiments are also discussed.

6.3.1 Coverslip coatings and additives to reduce cell adhesion

Pinealocytes can adhere to the surface of the glass coverslip within 3 min or less, which makes selecting and trapping a cell for injection time-sensitive and wastes valuable sample. Once the cells are adhered, trapping is ineffective and moving the cells is difficult, even when using the capillary inlet to “push” them around the surface. Pinealocytes are robust and adhesion is strong; typically pinealocytes do not lyse when they forcefully come into contact with the capillary inlet. Several coverslip coatings and solution additives were

tested with pinealocytes to determine the best method to reduce adhesion. Efficacy was determined by three figures of merit: how easily a cell could be trapped and manipulated, and how long it took for cells to adhere to the coverslip.

Bovine serum albumin (BSA) was first tested as a coverslip coating, using two different preparation methods. BSA is commonly used as an all-purpose 'blocking' agent; it is used to occupy the majority of sites that other proteins and molecules would bind to on a surface, preventing cellular adhesion. Pinealocyte adhesion was tested, and BSA-coated coverslips were found to be ineffective. Cells could be loosened more easily using the capillary inlet on BSA-coated coverslips, but pinealocytes still adhered within a few minutes and trapping was unable to be performed.

Diluting the pinealocyte suspension by a factor of two with mGBSS did not lessen the adhesion, reinforcing the fact that it was due to the covalent interaction of the cells' membrane proteins with the glass surface. Plastic coverslips were used to see if the covalent interactions would be lessened; this was not the case. Parafilm M was also tested, and it was effective in eliminating pinealocyte adhesion; however, the film interfered with the use of the optical trap.

Since pinealocytes were not responding to any of the above methods to reduce adhesion, cells from two other brain regions were also tested to determine if the degree of adhesion observed with pineal cells was unique or common to brain cells, since previous experiments with blood cells did not display this behavior (Chapter 5). Cerebellum cells (*e.g.* Purjinke cells, glia, granular cells) and olfactory bulb cells (*e.g.* mitral cells, periglomerular cells, granular cells) were used for comparison, and cells from all three brain regions were exposed to a variety of coatings and additives. Olfactory bulb and cerebellum cells were first monitored on untreated glass coverslips; both exhibited little to no response to the optical trap or the capillary inlet within minutes of exposure to the surface. Cerebellum cells were slightly more responsive to capillary in-flow and out-flow after adhesion than olfactory bulb cells and pinealocytes.

Silicon-based solutions were tested next. Glass Free, a silanizing agent, is typically used to coat glass casting plates for easy release of polyacrylamide gels. Sigmacote is a

silicone solution in heptane that readily forms a covalent, microscopically thin film on glass and is used to prevent clotting of blood plasma on surfaces and is water repellent. Glass Free was mildly effective in reducing adhesion of olfactory bulb cells and pinealocytes but not cerebellum cells; trapping and manipulation was still challenging. Sigmacote noticeably reduced adhesion for olfactory bulb and cerebellum cells and both of these samples could be trapped and manipulated for several minutes. Pinealocyte adhesion appeared reduced, but not as much as for the other brain regions' cells and pinealocytes demonstrated little response to the optical trap.

pHEMA is a polymer that is used in soft contact lens, forms a hydrogel in water, and has been shown to reduce adhesion of brain cells on glass surfaces.[76] The response to pHEMA-coated coverslips was positive; all three brain regions' cells displayed reduced adhesion and were able to be trapped and manipulated for several minutes. Pinealocytes were the most affected, demonstrating greater mobility compared to olfactory bulb and cerebellum cells.

Several different additives were tested, which included ETDA, a nanodiamond suspension, and ethylene glycol. These additives were tested on untreated coverslips and pHEMA-coated coverslips. EDTA is a chelating agent and is used in tissue culture for, among other actions, detaching adherent cells for passaging. EDTA had no effect on pinealocyte adhesion but it was very effective in eliminating adhesion of cerebellum and olfactory bulb cells to uncoated coverslips. Olfactory bulb cells in particular were easy to trap and manipulate. The nanodiamond suspension consisted of 5 nm nanodiamonds (potentially carbon nanotubes) in powered form, and according to the manufacturer's website its uses range from drug delivery to separations to biologically-resistant coatings. Pinealocyte adhesion was slightly improved and some response to the trap was observed on uncoated coverslips; reduced adhesion was observed for the other cell types and trapping and manipulation could be performed. On pHEMA-coated coverslips, the nanodiamond suspension reduced adhesion for all cell types, and, interestingly, clustering was observed for pinealocytes. Trapping and manipulation could be performed on all cells.

Ethylene glycol can be used as an alternative to formaldehyde for preserving samples and may reduce interactions between cells and surfaces. It had very little effect on pinealocytes, and no effect on cerebellum or olfactory bulb cells on untreated coverslips; however on pHEMA-coated coverslips, ethylene glycol reduced adhesion noticeably for all cells and made trapping and manipulation possible. Part of this response (and the responses observed in previous additive experiments) may be due to reduced viscosity, as it is easier to trap objects in less viscous solutions, although this was not observed for diluted pinealocytes on untreated coverslips. To further explore this phenomenon, suspensions of olfactory bulb and cerebellum cells were 2-fold diluted with mGBSS and mGBSS + 5 mM EDTA and observed on uncoated coverslips and pHEMA-coated coverslips. Cells that were diluted with mGBSS were easier to trap and manipulate on pHEMA-coated coverslips compared with undiluted suspensions, and mGBSS + EDTA-diluted suspensions on pHEMA-coated coverslips were actually a little more difficult to trap but still improved compared with undiluted suspensions. Diluted suspensions on uncoated coverslips were easier to trap and manipulate compared with undiluted suspensions on uncoated coverslips as well. This discrepancy in behavior between pinealocytes and other brain cells is only partially explained by viscosity, since pinealocyte suspensions exhibit low viscosity compared with olfactory bulb and cerebellum cell suspensions but still adhere strongly to untreated and treated coverslips, regardless of dilution.

Based on the results of the above experiments, pHEMA-coated coverslips were subsequently used for experiments.

6.3.2 Buffers for prolonging sample viability

Different buffers were tested to prolong sample viability for multi-day testing. mGBSS was the basis for all buffers used. Glycerol is a common component in buffers for biological samples, since it stabilizes cell membrane proteins and can prevent breakdown of tissue. Pinealocyte viability was tested by triturating glands in mGBSS, mGBSS + 5% v/v glycerol, or mGBSS + 33% v/v glycerol and determining the number of cells in suspension and trapping efficiency over a period of two days. Cells in 33% v/v glycerol buffer were unable to be trapped at any power (the maximum initial power tested was 2 W). No

clustering or manipulation was observed. The refractive index of water-glycerol solution is 1.34 for 6% w/w glycerol (equivalent to 5% v/v glycerol) and 1.39 for 42% w/w glycerol (equivalent to 33% v/v glycerol).[77] Given that the refractive index of saline (or mGBSS) is similar to water,[78, 79] these values can be used as approximations for the refractive index of the mGBSS-glycerol solutions. Since the approximate refractive index of a cell is 1.39 to 1.40,[80, 81] and the difference in refractive indicies between the object and its surround medium is what allows for trapping, it is understandable that the 33% v/v glycerol sample buffer was not compatible with trapping.

Cells in the 5% v/v glycerol buffer could be trapped with an initial power of 1.6 W, compared with 1 W to 1.3 W for cells in mGBSS alone. The increase in trapping power can be explained by the change in viscosity. The viscosity of 6% w/w glycerol (equivalent to 5% v/v glycerol) is ~ 1.15 mPa•s at 20°C,[82] compared with 0.890 mPa•s for water at 20°C[83] and 0.903 mPa•s for 143.5 mM NaCl at 20°C[84] (the main component in mGBSS is NaCl, with a concentration of 138 mM). The relatively large change in viscosity between water or mGBSS and 5% glycerol buffer could negatively affect trapping, since it would take a stronger trap to hold and manipulate objects in a higher viscosity solution. To compare, the viscosity of 42% w/w glycerol (equivalent to 33% v/v glycerol) is ~ 4.17 mPa•s at 20°C.[82] The 0.3 W to 0.6 W increase in trapping power necessary to hold and manipulate pinealocytes in 5% v/v glycerol buffer could potentially lead to a loss of cell viability and damage. The cells appeared equally viable in mGBSS and in mGBSS + 5% v/v glycerol, and glycerol can negatively affect separations even at low concentrations. For these reasons, mGBSS + 5% v/v glycerol was not used further as a sample buffer.

Buffers of varying salt concentrations were tested next. Ca^{+2}-free mGBSS, which has 2 mM of EGTA added to chelate any trace levels of Ca^{+2}, was selected since Ca^{+2} can induce release of neurochemicals from some cell types,[85-89] which would reduce or eliminate the amount of indolamines within the pinealocytes and prevent accurate quantitation of the levels present within individual cells. High Ca^{+2}/high Mg^{+2} mGBSS (referred to as high salt mGBSS) was selected because high Ca^{+2} and Mg^{+2} levels can also inhibit release in certain cell types.[90-96] It was unknown which would be effective for pinealocytes, so both extremes

were tested. Bulk pinealocyte samples were analyzed under Ca^{+2}-free and high salt conditions over the course of three days (day 0, 1, 2). Indolamine levels were compared as a function of sample buffer composition and time, under both cell lysing (micellar electrokinetic chromatography) and non-cell lysing (traditional CE) conditions which are detailed below.

Analytes identified in the bulk pineal samples include 5-hydroxytryptophan (HTP), serotonin (5-HT), 5-hydroxyindole-3-acetic acid (HIAA), tryptophan (Trp) and possibly N-acetylserotonin (NAS). Concentrations of 5-HT were 148% higher in high salt mGBSS compared with Ca^{+2}-free mGBSS, regardless of which day was compared. HIAA, an enzymatic product of 5-HT, was only observed on days 1 and 2 and a concentration decrease of 54% was seen in high salt mGBSS. This inverse in concentration levels seen for 5-HT and HIAA could be due to the production of HIAA from 5-HT under conditions that promote cell release or lysis, in this case Ca^{+2}-free mGBSS. HTP is the precursor to 5-HT and several other indolamines, and it was measured on all days. In high salt mGBSS, HTP levels also decreased by 54% compared with Ca^{+2}-free mGBSS. NAS levels did not change between the two conditions, and Trp levels decreased by 24% in high salt mGBSS. Although several indolamines showed decreases under high salt mGBSS, 5-HT was noticeably higher and NAS levels remained the same under both conditions. Since 5-HT and NAS are both part of the enzymatic pathway that produces melatonin (MT), conditions that are optimal for their preservation take precedence over other indolamines. Given this, high salt mGBSS was used as the sample buffer for single cell experiments and for subsequent bulk sample analyses.

6.3.3 Pineal analysis

Single pinealocyte analysis was performed using the OT-MC-CE-LINF system, and bulk cell suspension was analyzed by the MC-CE-LINF without use of the optical trap (detailed in Chapter 3). As mentioned above, two different CE conditions were used for analysis: micellar electrokinetic chromatography (MEKC) and traditional CE. MEKC involves using surfactant micelles (SDS in this case) in the electrophoresis buffer to create a pseudostationary phase. The analytes reversibly complex with the micelles, and can be separated according to their differential affinity. This technique can be used to resolve

charged species that co-elute, increase the resolution of chiral separations, and separate neutral analytes. There are benefits to using two different modes of CE. One is that the MEKC electrophoresis buffer also acts as the cell lysing solution, which simplifies the injection process since a plug of lysing solution does not need to be injected before or after the sample. Several of the indolamines of interest, under the traditional CE conditions described, co-elute; MEKC allows confirmation of identity since it is able to separate the co-eluting species. Another benefit is that identification of analytes is doubly confirmed, since the two separation modes operate under different principles. The migration times and fluorescence ratios differ under both conditions, so independent verification of analytes can be accomplished. Finally, using both MEKC and traditional CE methods allows for the quantification of analytes present within single cells, since the traditional CE method provides the analyte levels present in the media alone, regardless of whether a cell is injected or not since no lysing solution is present under those conditions.

Several buffer systems were tested for MEKC and traditional CE,[97-103] and based on resolution and separation time two set of buffers were selected: 20 mM borate buffer, pH 8.8 + 50 mM SDS for MEKC and 40 mM borate buffer, pH 8.8 as the CE buffer, or 15 mM borate buffer, pH 8.8 + 37.7 mM SDS for MEKC and 30 mM borate buffer, pH 8.8 as the CE buffer. The conductivities of the each buffer pair were matched (~ 2.8 mS/cm for the first pair and ~ 2.2 mS/cm for the second pair) to prevent large changes in current when switching between electrophoresis buffers throughout the day. The capillary was replaced between experiments and the buffer system had to be re-optimized, which is why there are two sets of electrophoresis buffers used. LODs did not significantly change between buffer sets (data not shown).

To ensure that the samples were viable after preparation and transport, suspensions were split into two or three aliquots and incubated with either HTP, 5-HT, or high salt mGBSS. Incubation with non-physiological amounts of HTP or 5-HT promotes cellular uptake and synthesis of detectable amounts of indolamines.[104] If other indolamines are not produced, it may mean that the cells were damaged and are not viable for analysis. It also provides information on day/night differences in indolamine production, since it is well

known that NAS and MT levels increase dramatically at night, but less is known about the lower abundance indolamines that are produced in the pineal gland, such as the tryptophols. Since these analytes may be present in single cells at levels that are below the instrument detection limits (Table 6.2), incubation can provide information and further confirm identification. Incubation can also provide insight into enzymatic pathways and kinetics of indolamine production in the pineal gland.

A set of images of the capillary tip approaching and injecting a pinealocyte is shown in Figure 6.4; the capillary inner diameter is comparable to the diameter of the pinealocyte. Injections can be a short as 2 s, corresponding to 1.15 nL. The volume of an average pinealocyte, assuming a 10 μm diameter,[21-23] is 4 pL, which is approximately a 280-fold dilution. Most single cell injections range from 2 s to 15 s.

Example electropherograms from single pinealocytes and bulk injections from HTP-incubated samples and untreated samples from a rat sacrificed at night are shown in Figures 6.5 and 6.6, respectively. HTP (4.6 mM), 5-HT (9.3 mM), NAS, and Trp (77 μM) were observed in the HTP-treated single cell, compared with 5-HT (970 μM), HIAA, Trp, and Tyr (1.5 mM) observed in the untreated single cell, which was from the same animal and analyzed on the same day. NAS, HIAA, and Trp were unable to be definitively quantitated within the cells shown here because their concentrations were higher in the media, determined under non-cell lysing conditions; the concentration of NAS measured was 76 nM within 300 pL and the concentrations of HIAA and Trp were 116 nM and 246 nM within 12.6 nL, respectively, under cell lysing conditions. This situation is common for HIAA and NAS; when samples are analyzed under non-cell lysing conditions, it is typically several hours or more after incubation was initiated. Both of these analytes are 5-HT enzymatic products, so incubation with non-physiological amounts of HTP or 5-HT could increase their production by enzymes free in solution, which would skew the amounts measured over time. A way to solve this in future work would be to analyze samples under non-cell lysing conditions soon after incubation.

Bulk sample analysis further confirms the single cell measurements (Figures 6.5B and 6.6B). In HTP-incubated samples, two analytes are potentially observed that are not

seen in single cell analysis: 5-methoxytryptophan (MTrp) and MT. MTrp is the O-methylated analogue to HTP and is synthesized from HTP by the enzyme hydroxyindole-O-methyltransferase (*himot*) (Figure 6.1). This enzyme is used in a number of indolamine reactions within the pineal gland, including the conversion of NAS to MT. The net concentration of MTrp (the difference between the concentration under cell lysing conditions and the concentration under non-cell lysing conditions for bulk analyses) is 1.7 μM, which means that MTrp is being synthesized within pinealocytes as opposed to in free solution by enzymes from lysed cells or through non-enzymatic means.

MT is expected in this sample, since this animal was sacrificed at night (CT 20:00); however, it is not confirmed in this sample or in any of the other samples for several reasons. The possible MT peak co-elutes with a series of broad peaks, making it challenging to calculate the fluorescence ratio accurately. Additionally, the peak is usually low intensity, so fluorescence ratios are unable to be calculated at times. It is also difficult to confirm MT using the non-cell lysing conditions, since it co-elutes with NAS under traditional CE conditions; since NAS is the precursor to MT, any samples run under non-cell lysing conditions should have both analytes present. The net concentration of MT is unable to be calculated for this sample since the concentration is higher in media (similar to NAS and HIAA, as mentioned previously), which may point to production in free solution and not within pinealocytes, if this peak is identified as MT. Any one of these reasons alone would not prevent identification, but taken together it is challenging to unambiguously identify MT in these samples. From a biological standpoint it is unusual since MT should be present in sufficiently high concentrations that it can be detected on a single cell level.

Figures 6.7 and 6.8 detail the analyte concentrations measured in single pinealocytes and bulk pinealocyte suspensions, respectively, as a function of time of sacrifice (day versus night) and treatment (HTP-incubated, 5-HT incubated, and untreated). Table 6.3 displays the number of single pinealocytes injected and analyzed under the described conditions.

In single pinealocytes, HTP- and 5-HT-incubation results in significant increases in 5-HT, as expected. Bulk samples show a similar trend, but there is no significant difference observed between bulk untreated day and night samples.

HIAA, which is the enzymatic degradation product of 5-HT, is seen in relatively low levels compared to 5-HT, and only in HTP-incubated single cell samples. Although only a few measurements have been performed, levels of HIAA appear to be higher at night. This may indicate greater activity by monoamine oxidase (*mao*) and aldehyde dehydrogenase (*ad*), the enzymes involved in the conversion of 5-HT to HIAA, at night (Table 6.1). In bulk samples, as mentioned previously, some of the net concentrations are negative, indicating that media levels were higher than the amount lysed from cells due to the offset in analysis time versus incubation initiation.

5-Hyroxytryptophol (HTOL), an uncommon indolamine, is seen in single cells and in bulk measurements under incubation. It has only been observed under cell lysing conditions, which indicates that it is only produced within pinealocytes and not freely in solution.

HTP is only observed in HTP-incubated single cells, but is observed in all sample categories in bulk measurements. HTP is synthesized from Trp (Table 6.1).

5-Methoxyindole-3-acetic acid (MIAA) is the O-methylated version of HIAA. It was identified in one single pinealocyte sample (5 μM), but was observed in a few bulk samples with nM concentrations including in one untreated sample. MIAA is produced directly from HIAA by *hiomt* or from a multistep enzymatic degradation of MTrp or 5-methoxytryptamine (MOT) (Table 6.1). Different enzymes are used in all of these reactions; however, given the prosaic nature of HIAA and the less common occurrences of MTrp and MOT, the majority of MIAA identifications occur when HIAA is present (data not shown).

MOT was only confidently identified once in all of the samples under non-cell lysing conditions; it is synthesized by *hiomt* from 5-HT (Table 6.1). The sample was from an animal sacrificed during the day. It was present in an untreated sample, which is somewhat surprising since one would expect to see uncommon indolamines under incubation conditions in addition to untreated samples.

MT was potentially identified in two single cell samples; both were collected on the same day, but from two different animals. Several potential identifications were made in

bulk night samples, as well, with values ranging widely. It is difficult to know if these identifications are correct, given the challenges mentioned before.

5-Methoxytryptopol (MTOL) and MTrp were not identified in single pinealocytes, but were each confirmed once in HTP-incubated, bulk night samples under non-lysing conditions in the tens of nM range. MTOL is produced from HTOL by *hiomt*, and MTrp is produced from HTP by *hiomt* (Table 6.1). Both are O-methylated versions of the original compounds.

NAS was identified in HTP-incubated single cells and in bulk samples. Surprisingly, it was identified multiple times during the day in single cells, but not in bulk samples. The enzyme that synthesizes NAS from 5-HT, N-acetyltransfersase, is 15- to 100-fold higher during the night and is 180° out of phase with the 5-HT rhythm.[105, 20, 106] Furthermore, during the day this enzyme is folded into an inactive form in pinealocytes, so that NAS synthesis is curtailed until signals from the suprachiasmatic nucleus indicate that night had fallen.

Tryptophol (TOL) was only detected twice, in an untreated single pinealocyte and a bulk sample from animals sacrificed during the day. It was only observed under cell lysing conditions, similarly to HTOL, supporting the idea that it is only produced within pinealocytes and not in solution.

Trp and Tyr are both ubiquitous, as expected, with levels measured in the mM range for single pinealocytes.

Table 6.4 compares estimated concentrations obtained in this work with literature values for a variety of indolamines found in the pineal gland. The estimation was performed by multiplying the experimentally determined number of pinealocytes present in a rat pineal gland (2.4×10^{-6} cells/mm^3; volume of the rat pineal gland experimentally determined to be approximately 1 mm^3)[107] by the number of mol of analyte present in a single pinealocyte under untreated conditions and from samples collected at night. The literature values are from rat pineal glands (Mills *et al.* do not specify the breed used for their analyses, but the other two columns of data are from Wistar rats) that were homogenized and extracted using perchloric acid. Mills *et al.* collected their samples two h

after dark and after stressing the rats, Beck *et al.* collected their samples in the morning, and Chen *et al.* do not specify what time the samples were collected. Both Mills *et al.* and Chen *et al.* stored the samples at -80 °C until analysis, which in the case of Mills *et al.* was 18 mo after collection. Despite all of these variables, the measurements in the literature for concentrations of indolamines in the pineal gland are at least three orders of magnitude lower than that estimated from single pinealocytes in this work. Several factors may contribute to this disparity. One is the assumption of pinealocyte size (10 µm) used in this work, based on literature measurements and also estimated roughly by sight. Measuring the diameter of each pinealocyte injected for analysis could potentially reduce some of the variability in concentrations; this can be done after the fact since all of the single pinealocyte injections are recorded. This assumption, however, does not account for all of the differences between the values measured in this work and the literature. The different rat breeds and collection times used could account for some of the differences as well, although not for orders of magnitude differences in all analytes measured. Storage conditions likely play a role, since dissolved oxygen in solution can still oxidize indolamines at subzero temperatures, leading to inaccurate measurements in terms of physiological relevance.[108] It is likely that much of the difference can be attributed to partial extraction of analytes compared with values determined from direct injection of single cells. In order to directly compare these values, an extraction from a rat pineal homogenate should be analyzed using the MC-CE-LINF.

6.4 Conclusions and future work

The OT-MC-CE-LINF instrument was used to analyze single pinealocytes and bulk samples. Quantitation was performed, and several uncommon indolamines, in addition to common ones, were identified within both single cell and bulk measurements. MT was not unambiguously identified, due to a variety of factors. Its potentially low levels are surprising, given the large increase in MT concentration at night that has been reported since it was discovered in the 1950s; however, MT production begins approximately 60 min after the 5-HT surge at night.[18] The timing of this surge varies based on differences at the individual, breed, and species level. It is likely that the appropriate sacrifice time has not

been found for the breed of rats used for the night experiments, although a puzzling factor is that once MT synthesis begins, it continues for several hours. Given the sacrifice times selected (n = 2 for CT 20:00 (7 h after darkness onset) and n = 1 for CT 22:00 (9 h after darkness onset)), it was expected that MT would be present regardless of the timing of the 5-HT surge since that typically occurs earlier in the night. More samples are needed overall and more sacrifice times need to be sampled to verify this, possibly by microdialysis sampling over the course of several days and nights.

It is also possible, since the rat breed used in these analyses is not well characterized in terms of pineal indolamine concentrations, that this breed produces low amounts of MT relative to other rat breeds; this is well documented in inbred mice strains although it has not been reported for rats. Given that the only synthesis pathway for MT in the pineal gland is from NAS via the enzyme *hiomt*, it is possible that this breed has low levels of *hiomt*; however, many of the unusual indolamines can be produced via *hiomt* as well as by other enzyme pathways. It is interesting to speculate whether *hiomt* is actively produced other indolamines instead MT at night or that *hiomt* has low activity and the other indolamines are produced by the other pathways described in Table 6.1. This could explain the challenges in detecting MT in these samples. It is also possible that the enzyme that synthesizes NAS from 5-HT is present in lower than expected levels; this is less likely as NAS is unambiguously detected under a variety of conditions. Future work can focus on identifying MT in pineal samples, both in single cells and in bulk. Capillary electrophoresis with mass spectrometric detection can be used to verify the identity of MT in pineal sample, as well as further strengthen the identities of the unusual indolamines.

The identification and quantitation of uncommon indolamines (HTOL, MTOL, TOL, MOT, MTrp, and MIAA) in both single cells and in bulk samples, under both incubated and untreated conditions, is interesting. Most of these analytes are produced from HTP, if not directly, then over multiple steps and they all can use the enzyme *hiomt* as part of the synthesis, although there are multiple pathways present to produce these compounds. These analytes have been identified before in pineal samples.[103, 109, 31, 44, 6] The O-methylated idolamines display antioxidant properties, which may suggest an

immunoprotective role,[110-114] and have effects on reproduction.[115-119] These roles are also performed by melatonin in the body, so it is unsurprising that closely related methoxyindoles also have similar functions. The sporadic detection of these compounds is likely due to their low abundance in pinealocytes; typically it is probably below the detection level, except in rare cases. More experiments need to be performed to further understand the day and night differences in these compounds.

Both single cell and bulk concentrations can vary widely for many of the analytes detected. This variability could be due to individual biological differences or unanticipated differences in sample preparation, among other possibilities. As more experiments are performed, variability may decrease. Future experiments should include homogenate analysis to verify that the variability measured is due to cell-to-cell differences and not bulk biological variability. Extracts from homogenates should also be analyzed, to determine why such large differences exist between the values determined here and the literature.

6.5 Tables

component	Ca^{+2}-free mGBSS, mM	mGBSS, mM	high salt mGBSS, mM
$CaCl_2$	0	1.5	3
KCl	4.9	4.9	4.9
KH_2PO_4	0.2	0.2	0.2
$MgCl_2$	11	11	22
$MgSO_4$	0.3	0.3	0.6
NaCl	138	138	138
$NaHCO_3$	27.7	27.7	27.7
Na_2HPO_4	0.8	0.8	0.8
HEPES	25	25	25
glucose	10	10	10
EGTA	2	0	0

Table 6.1 Concentrations of components used to make the sample buffers. HEPES = 4-(2-hydroxyethyl)-1-piperazineethanesulfonic acid, EGTA = ethylene glycol tetraacetic acid

analyte	MEKC conditions, nM	CE conditions, nM
5-hydroxyindole-3-acetic acid, HIAA	3.5	2.8
5-hydroxytryptophan, HTP	5.4	1.6
5-hydroxtryptophol, HTOL	2.6	6.7
5-methoxyindole-3-acetic acid, MIAA	3.4	2.0
5-methoxytryptamine, MOT	14	9.5
5-methoxytryptophan, MTrp	NA	1.3
5-methoxytryptophol, MTOL	3.5	3.0
melatonin, MT	14	2.8
N-acetylserotonin, NAS	5.1	3.7
serotonin, 5-HT	14	14
tyrosine, Tyr	39	17
tryptophan, Trp	6.0	1.6
tryptophol, TOL	2.5	2.6

Table 6.2 Limits of detection (LODs) for indolamines and tyrosine under micellar electrokinetic chromatography (MEKC, 20 mM borate buffer, pH 8.8 + 50 mM SDS or 15 mM borate buffer, pH 8.8 + 37.7 mM SDS) and traditional CE (40 mM borate, pH 8.8 or 30 mM borate, pH 8.8) conditions.

n = number of single cells analyzed	HTP-incubated	5-HT-incubated	untreated
day	n = 9*	N.A.	n = 4
night	n = 13	n = 14	n = 11

Table 6.3 Table showing the number of single cells analyzed under different treatments and time of sacrifice. The asterisk (*) represents several multiple cell injections where the number of cells injected is known and the average concentrations from these measurements were used for analysis.

analyte	untreated, estimated nmol/gland	Mills *et al.*, pmol/gland[31]	Beck *et al.*, pmol/gland[44]	Chen *et al.*, pmol/gland[99]
5-HT	10	40 ± 0.10	N.D.	73
HIAA	N.D.	7.5 ± 0.16	N.D.	N.D.
HTOL	N.D.	0.73 ± 0.22	N.D.	N.D.
HTP	N.D.	0.28 ± 0.39	N.D.	7.7
MIAA	0.05	0.63 ± 0.36	N.D.	N.D.
MOT	N.D.	0.45 ± 0.48	0.04	N.D.
MT	5.0 ± 5.0	0.94 ± 0.14	0.61	8.2
MTOL	N.D.	0.64 ± 0.31	N.D.	N.D.
MTrp	N.D.	N.D.	N.D.	N.D.
NAS	1.0	N.D.	N.D.	N.D.
TOL	N.D.	0.68 ± 0.62	N.D.	N.D.
Trp	0.30	11 ± 0.11	N.D.	14
Tyr	10 ± 2.5	37 ± 0.19	N.D.	N.D.

Table 6.4 A comparison of literature values for analytes detected in the pineal gland. The column labeled "untreated, estimated nmol/gland" is data collected in this work and represents estimated values from analytes identified in single pinealocytes from samples collected at night under untreated conditions, as described in the text. The other three columns represent values reported in the literature for homogenated pineal glands extracted with perchloric acid. The error is standard error of the mean for all columns.

6.6 Figures

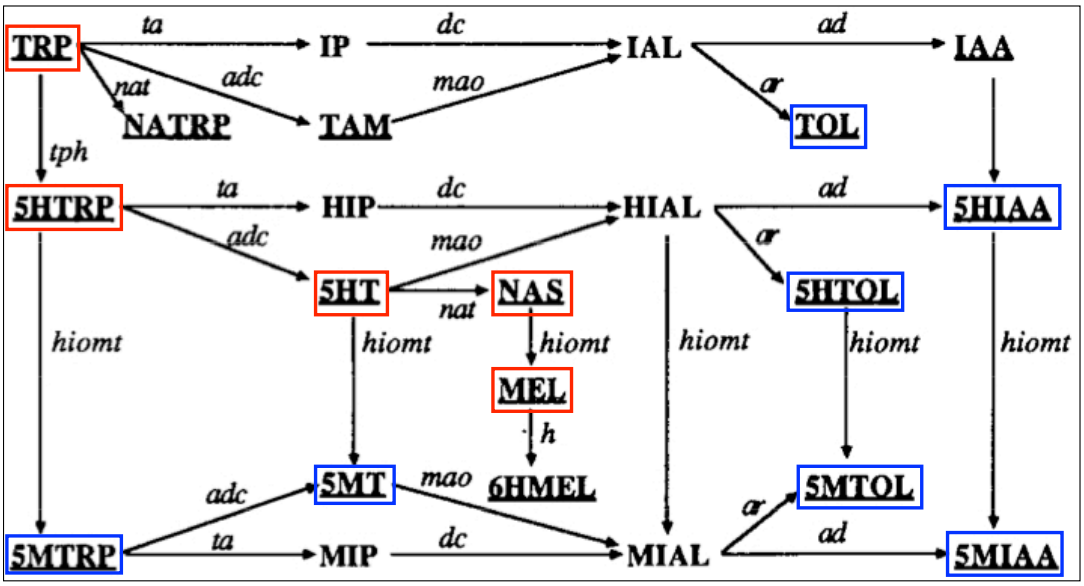

Figure 6.1 Indolamine synthesis pathways in the pineal gland. The melatonin synthesis pathway is boxed in red. Tryptophan (TRP) is converted to 5-hydroxytryptophan (5HTRP) by tryptophan hydroxylase (*tph*), and serotonin (5HT) is produced from 5HTP by L-aromatic amino acid decarboxylase (*adc*). 5HT is converted to N-acetyl serotonin (NAS), the precursor to melatonin (MEL), by N-acetyltransferase (*nat*). MEL is formed from of NAS by hydroxyindole-O-methyltransferase (*hiomt*). Other analytes detected are boxed in blue. Enzyme abbreviations: *ad* = aldehyde dehydrogenase, *adc* = L-aromatic amino acid decarboxylase, *ar* = aldehyde reductase, *dc* = decarboxylase, *h* = hydroxylase, *hiomt* = hydroxyindole-O-methyltransferase, *mao* = monoamine oxidase, *nat* = N-acetyltransferase, *ta* = transaminase, *tph* = tryptophan hydroxylase; compound abbreviations: 5HIAA = 5-hydroxyindole-3-acetic acid, 6HMEL = 6-hydroxymelatonin, 5HT = 5-hydroxytryptamine, 5HTOL = 5-hydroxtryptophol, 5HTRP = 5-hydroxytryptophan, 5MIAA = 5-methoxyindole-3-acetic acid, 5MT = 5-methoxytryptamine, 5MTOL = 5-methoxytryptophol, 5MTRP = 5-methoxytryptophan, HIAL = 5-hydroxyindole-3-acetaldehyde, HIP = 5-hydroxyindole-3-pyruvic acid, IAA = indole-3-acetic acid, IAL =indole-3-acetaldehyde, IP = indole-3-pyruvic acid, MIAL = 3-methoxy-4-hydroxymandelic aldehyde, MIP = 5-methoxyindole-3-pyruvic acid, NAS = N-acetylserotonin, NATRP = N-acetyltryptophan, TAM = tryptamine, TOL = tryptophol, TRP = tryptophan. Adapted from (31) with permission from Elsevier.

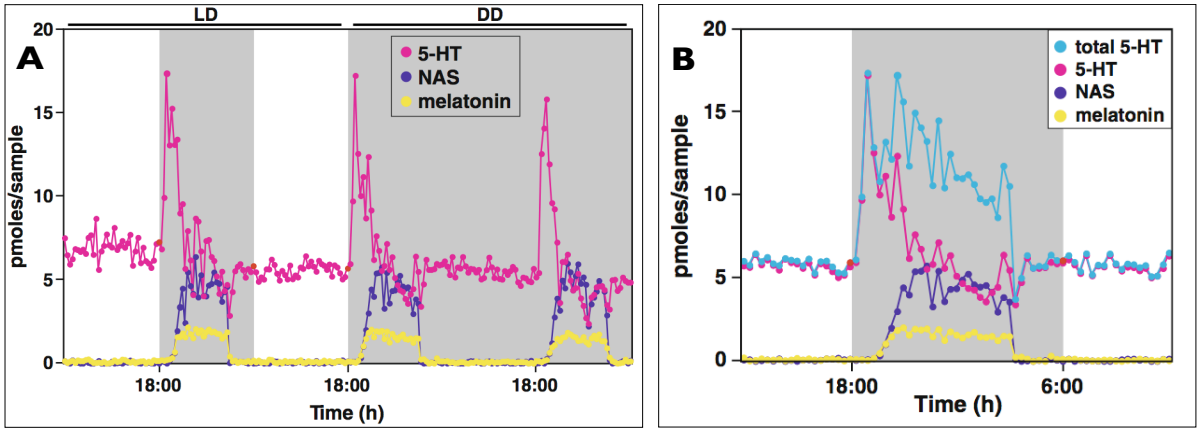

Figure 6.2 (A) Secretion profiles of serotonin (5-HT), N-acetylserotonin (NAS), and melatonin from pineal microdialysis of a rat. All three compounds display marked circadian rhythms in both light and dark (LD) and constant dark (DD) conditions with nocturnal increase in secretion. (B) The total 5-HT output displays marked circadian rhythm with high levels at night. The total 5-HT is calculated as the sum of 5-HT, NAS, and melatonin. Adapted with kind permission from Springer Science + Business Media from (5).

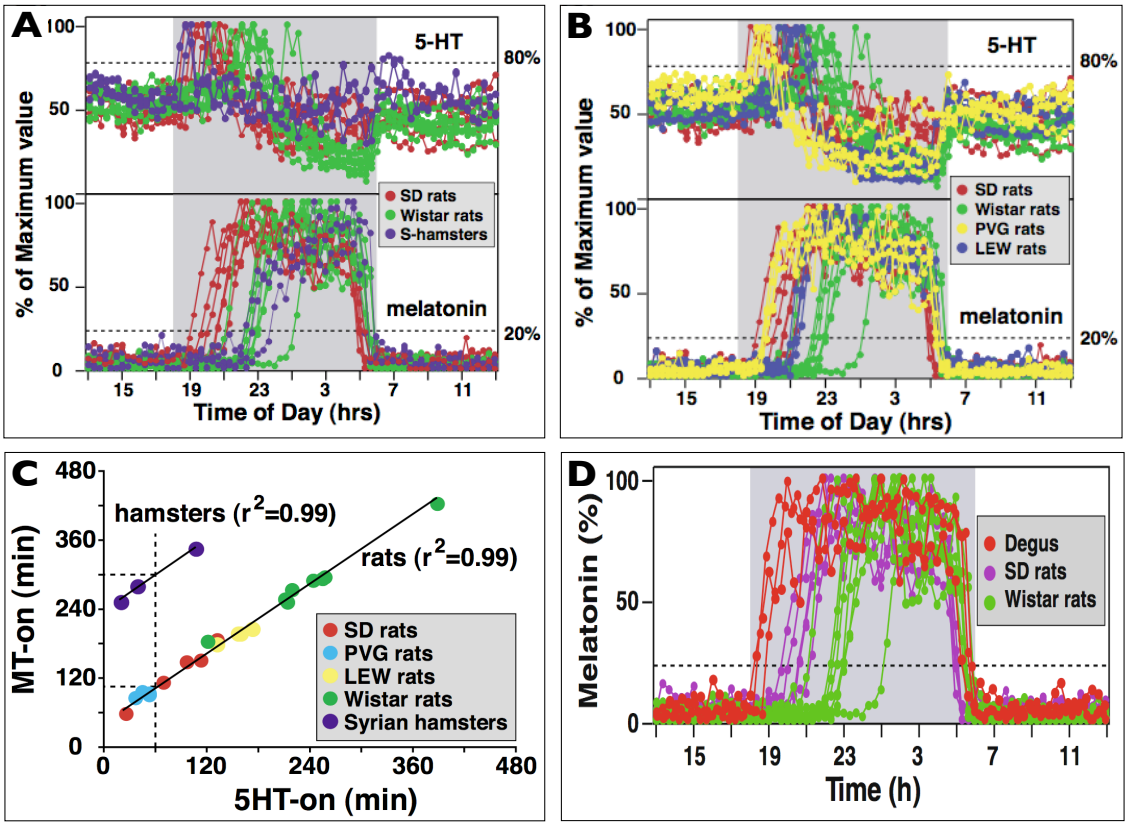

Figure 6.3 (A) Comparison of serotonin (5-HT) (upper panel) and melatonin (lower panel) secretion profiles from outbred animals. Data from Sprague Dawley (SD) rats (red), Wistar rats (green), and hamsters (blue) are superimposed to show the relative timing of 5-HT and melatonin secretion. (B) Comparison of serotonin (5-HT) (upper panel) and melatonin (lower panel) secretion profiles from four strains of rats: Sprague-Dawley (SD) (red), Wistar (green), PVG (yellow), and Lewis (LEW) (blue) rats. (C) Comparison of the relative timing of serotonin onset (5HT-on) and melatonin onset (MT-on). The 5HT-on represents the intervals between the dark onset and the early 5-HT surge at 80% of the nocturnal maximum levels. The MT-on indicates the time interval between the dark onset and the melatonin onset at 20% of the nocturnal maximum levels. (D) Inter-individual and inter-species variation of melatonin onset timing. Three Degus rats (red dots), 5 Sprague Dawley (SD) rats (purple dots), and 7 Wistar rats (green dots) are shown. The onset timing is defined as when melatonin reaches 20% of daily maximum level, which is marked by the dashed line. Adapted with kind permission from Springer Science + Business Media from (5). Adapted with permission from (18).

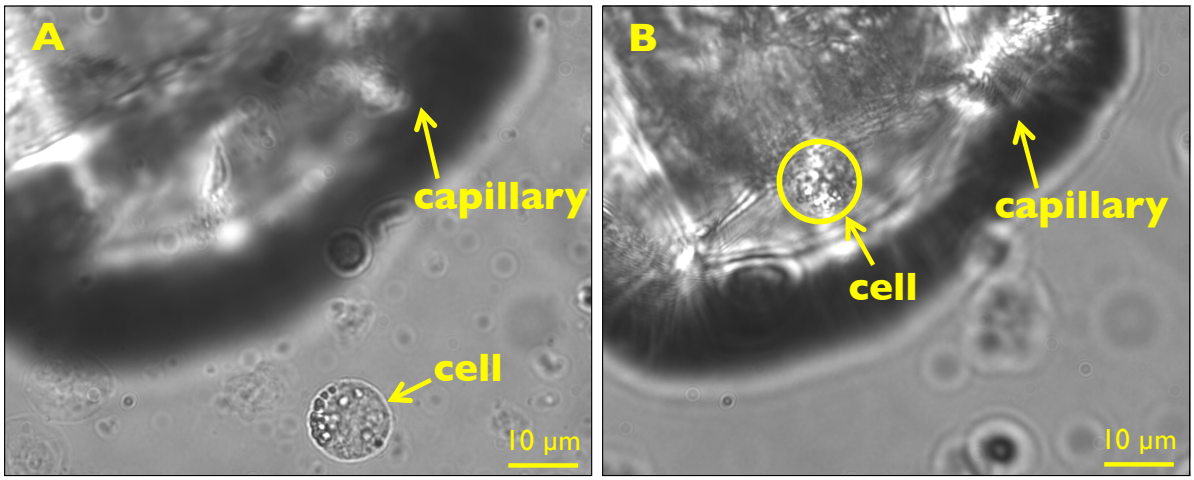

Figure 6.4 (A) The capillary inlet approaches a single pinealocyte. (B) The pinealocyte is injected hydrodynamically into the capillary for analysis.

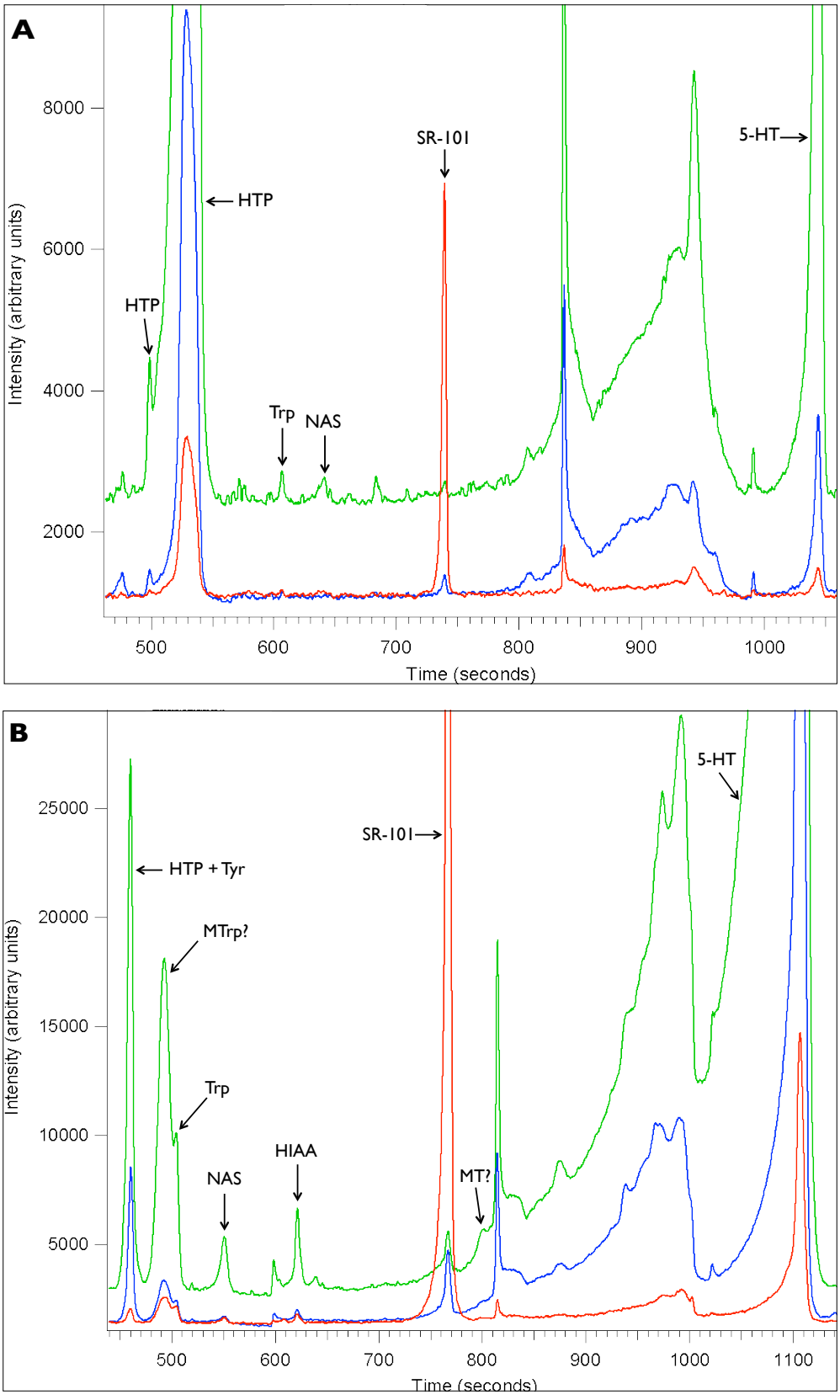
A
8000
6000
4000
2000
Intensity (arbitrary units)
HTP
HTP
Trp
NAS
SR-101
5-HT
500
600
700
800
900
1000
Time (seconds)
B
25000
20000
15000
10000
5000
Intensity (arbitrary units)
HTP + Tyr
MTrp?
Trp
NAS
HIAA
SR-101
MT?
5-HT
500
600
700
800
900
1000
1100
Time (seconds)

Figure 6.5

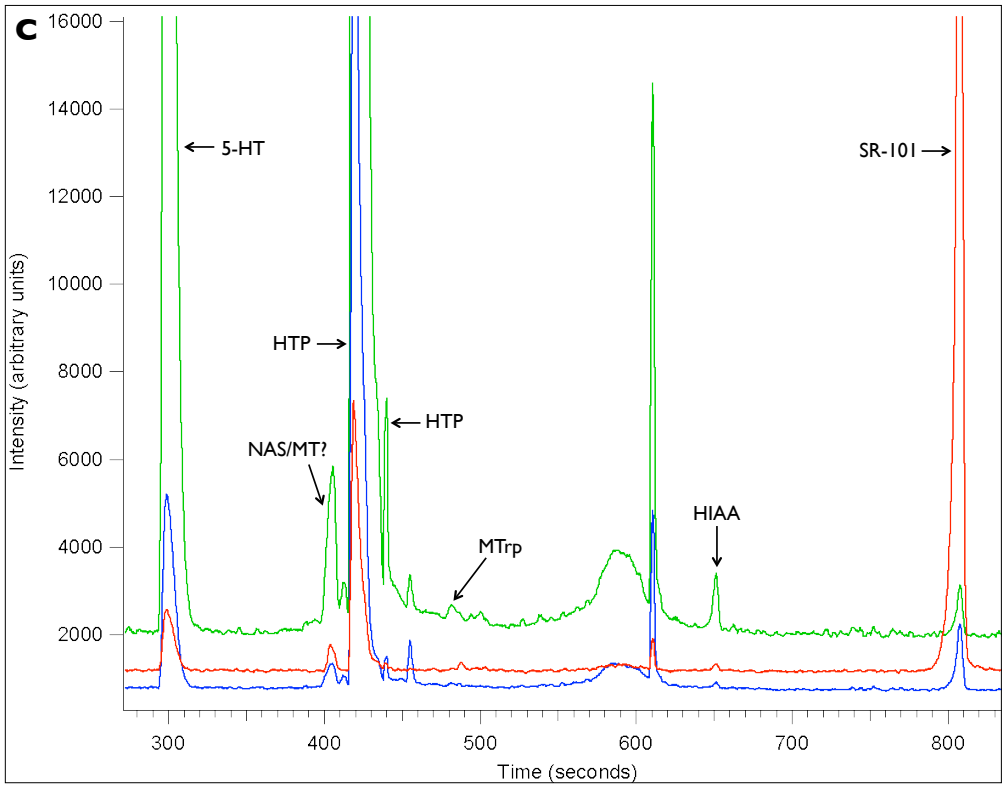

Figure 6.5 (cont.) Electropherograms from HTP-incubated pinealocytes. (A) A single pinealocyte analyzed under cell lysing (MEKC) conditions. (B) A bulk sample (14.7 nL) analyzed under cell lysing (MEKC) conditions. (C) A 5 nL sample analyzed under non-cell lysing (traditional CE) conditions. Conditions for (A) and (B) are: 15 mM borate buffer, pH 8.8 + 37.4 mM SDS (electrophoresis buffer); conditions for (C) are 30 mM borate buffer, pH 8.8 (electrophoresis buffer). Conditions common to all samples are: high salt mGBSS (sample buffer), 25 mM citric acid buffer, pH 2.25 (sheath buffer), -30 kV (separation voltage), 3 Hz (laser repetition rate), 100 µs (laser pulse length), 8 A (laser current), 420 V (laser BUSS voltage), 470 pF (PMT gain), 64% (gain voltage), 110 µs (PMT integration time). 5-HT = serotonin, HIAA = 5-hydroxyindole-3-acetic acid, HTP = 5-hydroxytryptophan, MT = melatonin, MTrp = 5-methoxytryptophan, NAS = N-acetylserotonin, SR-101 = sulforhodamine-101 (internal standard), Trp = tryptophan, Tyr = tyrosine

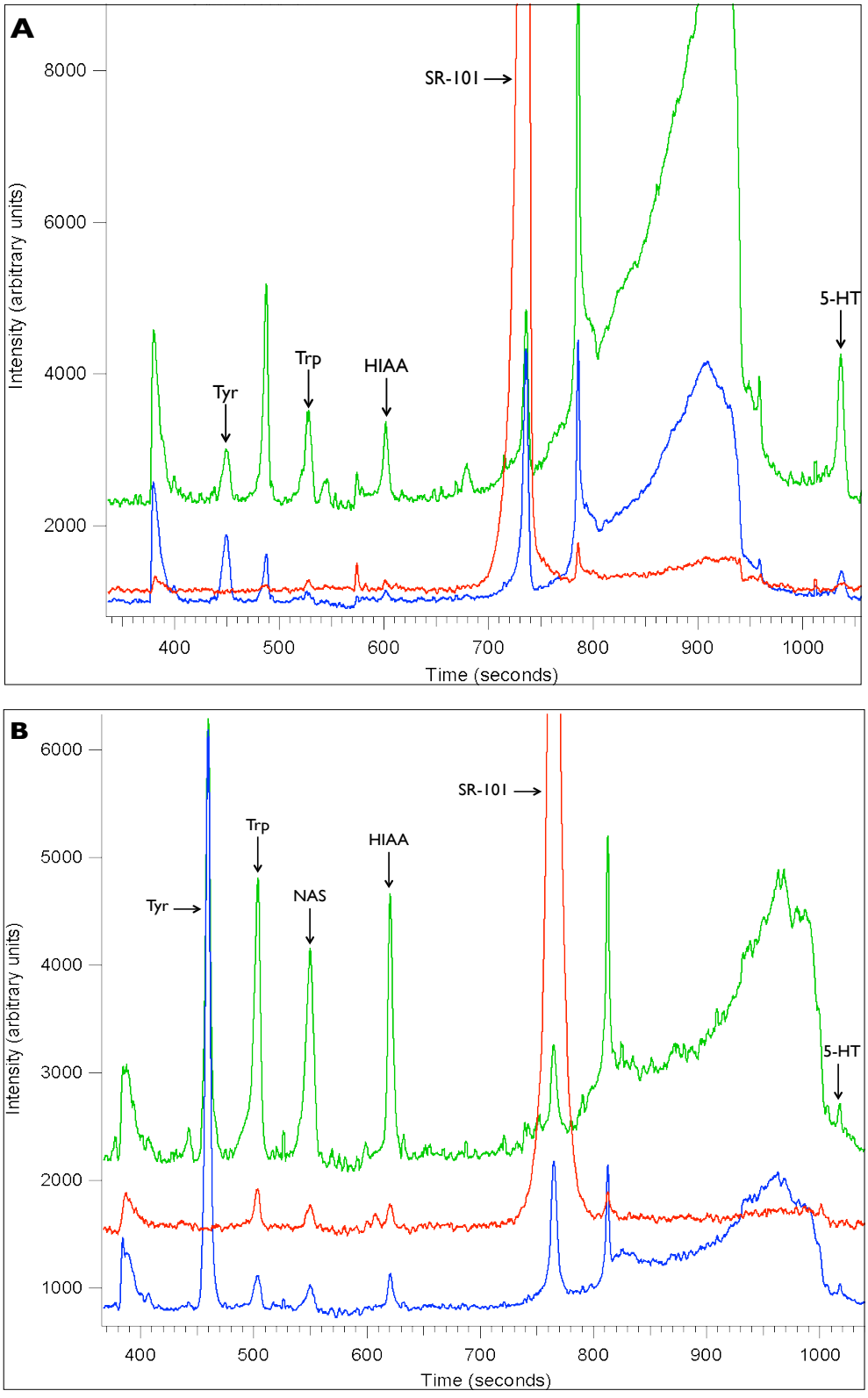
A
8000
6000
4000
2000
Intensity (arbitrary units)
SR-101
Tyr
Trp
HIAA
5-HT
400
500
600
700
800
900
1000
Time (seconds)
B
6000
5000
4000
3000
2000
1000
Intensity (arbitrary units)
SR-101
Trp
HIAA
Tyr
NAS
5-HT
400
500
600
700
800
900
1000
Time (seconds)

Figure 6.6

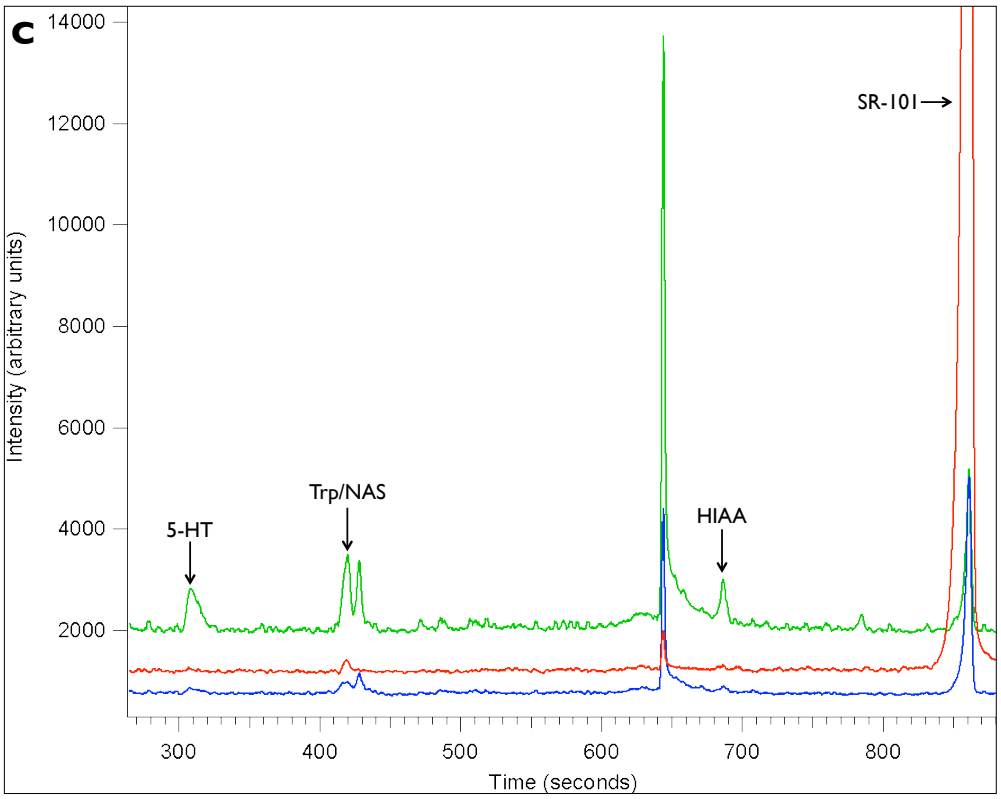

Figure 6.6 (cont.) Electropherograms from untreated pinealocytes. (A) A single pinealocyte analyzed under cell lysing (MEKC) conditions. (B) A bulk sample (14.7 nL) analyzed under cell lysing (MEKC) conditions. (C) A 5 nL sample analyzed under non-cell lysing (traditional CE) conditions. Conditions for (A) and (B) are: 15 mM borate buffer, pH 8.8 + 37.4 mM SDS (electrophoresis buffer); conditions for (C) are 30 mM borate buffer, pH 8.8 (electrophoresis buffer). Conditions common to all samples are: high salt mGBSS (sample buffer), 25 mM citric acid buffer, pH 2.25 (sheath buffer), -30 kV (separation voltage), 3 Hz (laser repetition rate), 100 µs (laser pulse length), 8 A (laser current), 420 V (laser BUSS voltage), 470 pF (PMT gain), 64% (gain voltage), 110 µs (PMT integration time). 5-HT = serotonin, HIAA = 5-hydroxyindole-3-acetic acid, HTP = 5-hydroxytryptophan, NAS = N-acetylserotonin, SR-101 = sulforhodamine-101 (internal standard), Trp = tryptophan, Tyr = tyrosine

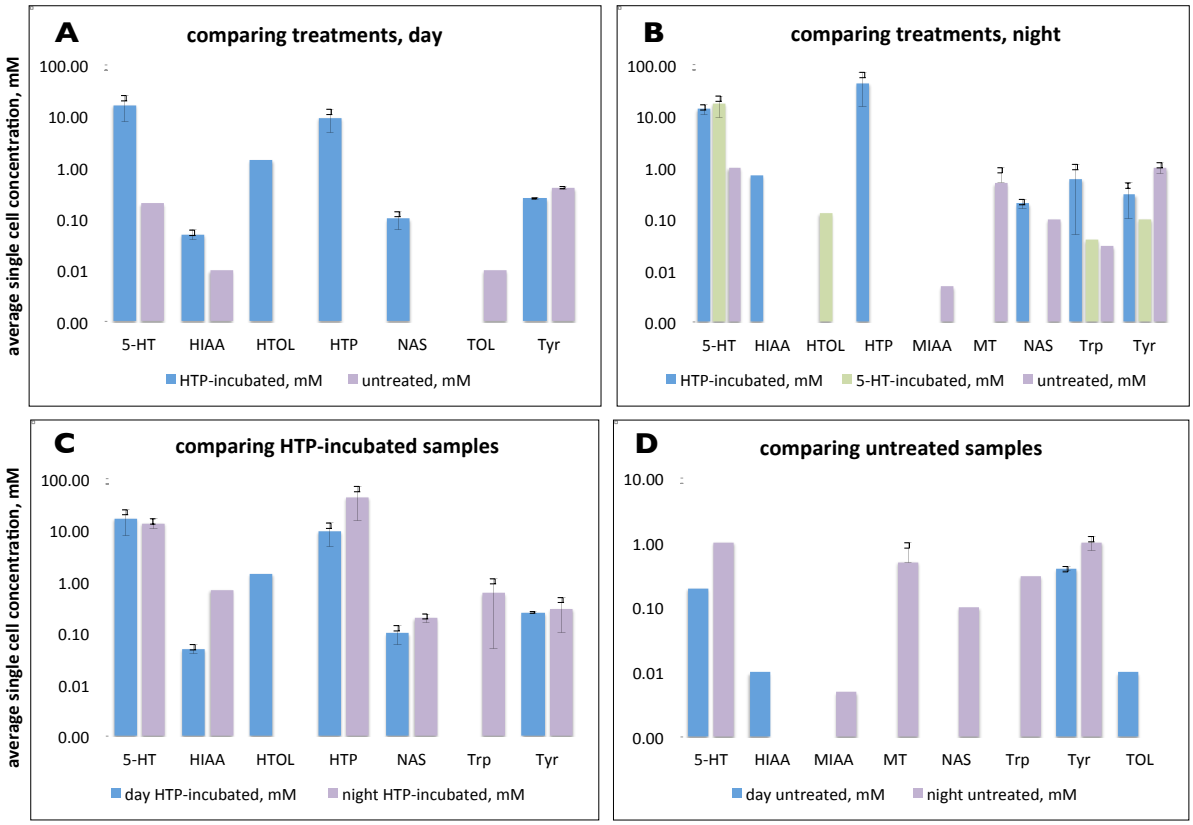

Figure 6.7 Histograms comparing the average concentrations of analytes observed in single pinealocytes as a function of treatment (A, B) and time of sacrifice (C, D). All concentration units are mM and error bars are standard error of the mean. Columns without error bars represent measurements that were only made once for a given analyte under the conditions listed. The y-axis is logarithmic to more easily show the differences in concentration between analytes. n = 5 for night sacrifice, n = 2 for day sacrifice; 5-HT = serotonin, HIAA = 5-hydroxyindole-3-acetic acid, HTOL = 5-hydroxtryptophol, HTP = 5-hydroxytryptophan, MIAA = 5-methoxyindole-3-acetic acid, MOT = 5-methoxytryptamine, MTOL = 5-methoxytryptophol, MTrp = 5-methoxytryptophan, NAS = N-acetylserotonin, TOL = tryptophol, Trp = tryptophan, Tyr = tyrosine

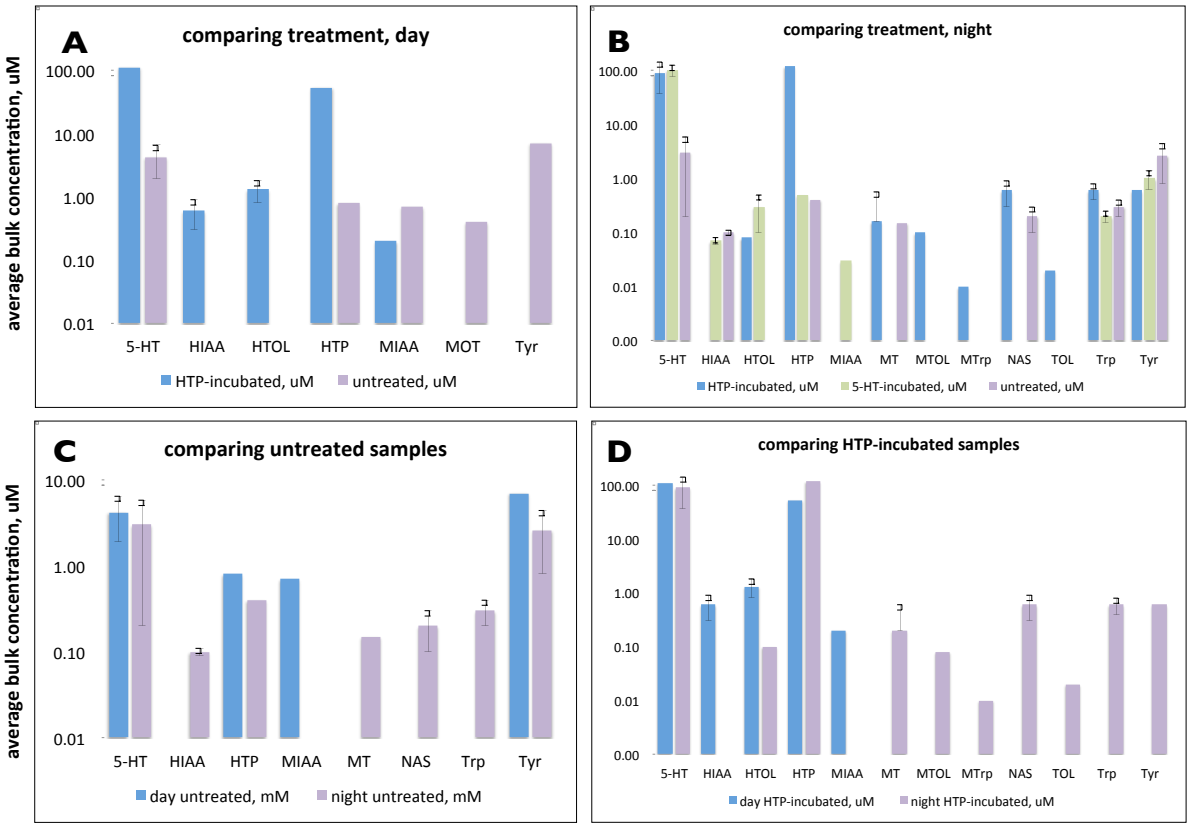

Figure 6.8 Histograms comparing the average concentrations of analytes observed in bulk cell suspension measurements from pinealocytes as a function of treatment (A, B) and time of sacrifice (C, D). All concentration units are µM and error bars are standard error of the mean. Columns without error bars represent measurements that were only made once for a given analyte under the conditions listed. The y-axis is logarithmic to more easily show the differences in concentration between analytes. n = 5 for night sacrifice, n = 2 for day sacrifice; 5-HT = serotonin, HIAA = 5-hydroxyindole-3-acetic acid, HTOL = 5-hydroxtryptophol, HTP = 5-hydroxytryptophan, MIAA = 5-methoxyindole-3-acetic acid, MOT = 5-methoxytryptamine, MTOL = 5-methoxytryptophol, MTrp = 5-methoxytryptophan, NAS = N-acetylserotonin, TOL = tryptophol, Trp = tryptophan, Tyr = tyrosine

6.7 References

(1) Lerner, AB; Case, J.; Takahashi, Y.; Lee, T.; Mori, W. *J Am Chem Soc*. **1958**, *80*, 2587–2587.

(2) Bondarenko, L. *B Exp Biol Med*. **1985**, *100*, 1001–1003.

(3) Zawilska, J. B.; Skene, D. J.; Arendt, J. *Pharmacol Rep*. **2009**, *61*, 383–410.

(4) Hardeland, R. *Cell Mol Life Sci*. **2008**, *65*, 2001–2018.

(5) Chattoraj, A.; Liu, T.; Zhang, L. S.; Huang, Z.; Borjigin, J. *Rev Endocr Metab Disord*. **2009**, *10*, 237–243.

(6) Conti, A.; Maestroni, G. *J Pineal Res*. **1996**, *20*, 138–144.

(7) Kennaway, D.; Voultsios, A.; Varcoe, T.; Moyer, R. *Am J Physiol-Reg I*. **2002**, *282*, R358–R365.

(8) McGuire, N. L.; Kangas, K.; Bentley, G. E. *Endocrinology*. **2011**, *152*, 3461–3470.

(9) Fenn, A. M.; Fonken, L. K.; Nelson, R. J. *J Pineal Res*. **2011**, *51*, 180–186.

(10) Sawalha, M. N.; Kridli, R. T.; Jawasreh, K. I.; Meza-Herrera, C. A. *Trop Anim Health Prod*. **2011**, *43*, 1345–1350.

(11) Ikegami, K.; Yoshimura, T. *Mol Cell Endocrinol*. **2011**, 1–6.

(12) Srinivasan, V.; Kaur, C.; Pandi-Perumal, S.; Brown, G. M.; Cardinali, D. P. *International Journal of Alzheimer's Disease*. **2011**, *2011*, 1–15.

(13) Sirajudeen, M.; Gopi, K.; Tyagi, J. S.; Moudgal, R. P.; Mohan, J.; Singh, R. *Environ. Toxicol.* **2011**, *26*, 153–160.

(14) Motilva, V.; García-Mauriño, S.; Talero, E.; Illanes, M. *J Pineal Res*. **2011**, *51*, 44–60.

(15) Espino, J.; Bejarano, I.; Paredes, S. D.; Barriga, C.; Rodríguez, A. B.; Pariente, J. A. *J Pineal Res*. **2011**, *51*, 195–206.

(16) Conti, A.; Maestroni, G. *Ann Ny Acad Sci*. **1998**, *840*, 395–410.

(17) Radogna, F.; Diederich, M.; Ghibelli, L. *Biochem. Pharmacol.* **2010**, *80*, 1844–1852.

(18) Liu, T.; Borjigin, J. *J Circad Rhythms*. **2006**, *4*, 12.

(19) Quay, W. *Neurochem Res*. **1989**, *14*, 957–961.

(20) Roseboom, P. H. *Endocrinology*. **1996**, *137*, 3033–3045.

(21) Castellano, A.; Lopez-Barneo, J.; Armstrong, C. *Pflug Arch Eur J Phy*. **1989**, *413*, 644–650.

(22) Aguayo, L. *J Physiol-London*. **1989**, *414*, 283–300.

(23) Aguayo, L.; Weight, F. *J Physiol-London*. **1988**, *405*, 397–419.

(24) Cozzi, B. *Anat Rec*. **1986**, *216*, 165–174.

(25) Wicht, H.; Korf, H. W.; Schaad, N. C. *J Pineal Res*. **1993**, *14*, 128–137.

(26) Redecker, P. *J. Neurocytol.* **1993**, *22*, 572–581.

(27) Sato, T.; Kaneko, M.; Fujieda, H.; Deguchi, T.; Wake, K. *Cell and Tissue Research*. **1994**, *277*, 201–209.

(28) Schomerus, C.; Laedtke, E.; Korf, H. W. *Neurochem Int*. **1995**, *27*, 163–175.

(29) Pevet, P. *J Neural Transm*. **1977**, *40*, 289–304.

(30) Schaad, N.; Parfitt, A.; Russel, J.; Schaffner, A.; Korf, H.; Klein, D. *Brain Res*. **1993**, *614*, 251–256.

(31) Mills, M. H.; Finlay, D. C.; Haddad, P. R. *J. Chrom.* **1991**, *564*, 93–102.

(32) Goto, M.; Oshima, I.; Tomita, T.; Ebihara, S. *J Pineal Res*. **1989**, *7*, 195–204.

(33) Ebihara, S.; MARKS, T.; HUDSON, D.; MENAKER, M. *Science*. **1986**, *231*, 491–493.

(34) Vivien-Roels, B.; Malan, A.; Rettori, M.-C.; Delagrange, P.; Jeanniot, J.-P.; Pevet, P. *Journal of Biological Rhythms*. **1998**, *13*, 403–409.

(35) Stehle, J. X. R.; Gall, von, C.; Korf, H.-W. *Cell and Tissue Research*. **2002**, *309*, 173–182.

(36) Iguichi, H.; Kato, K. I.; Ibayashi, H. *J. Clin. Endocrinol. Metab.* **1982**, *55*, 27–29.

(37) Touitou, Y. In *Experimental Gerontology*; 2001; pp. 1083–1100.

(38) Czeisler, C. A.; Dumont, M.; Duffy, J. F.; Steinberg, J. D.; Richardson, G. S.; Brown, E. N.; Sánchez, R.; Ríos, C. D.; Ronda, J. M. *Lancet*. **1992**, *340*, 933–936.

(39) Ferrari, E.; Arcaini, A.; Gornati, R.; Pelanconi, L.; Cravello, L.; Fioravanti, M.; Solerte, S. B.; Magri, F. *Exp. Gerontol.* **2000**, *35*, 1239–1250.

(40) Miguez, J.; Recio, J.; Sanchez-Barcelo, E.; Aldegunde, M. *J Pineal Res*. **1998**, *25*, 106–115.

(41) Djeridane, Y.; Charbuy, H.; Touitou, Y. *Exp. Gerontol.* **2005**, *40*, 403–408.

(42) Srinivasan, V.; Maestroni, G.; Cardinali, D.; Esquifino, A.; Perumal, S. P.; Miller, S. *Immunity & Ageing*. **2005**, *2*, 17.

(43) Waldhauser, F.; Kovács, J.; Reiter, E. *Exp. Gerontol.* **1998**, *33*, 759–772.

(44) Beck, O.; Jonsson, G.; Lundman, A. *N-S Arch Pharmacol*. **1981**, *318*, 49–55.

(45) Zhdanova, I. V.; WURTMAN, R.; Regan, M.; Tayler, J.; Shi, J.; Leclair, O. *J. Clin. Endocrinol. Metab.* **2001**, *86*, 4727–4730.

(46) Gooneratne, N. S.; Gehrman, P.; Gurubhagavatula, I.; Al-Shehabi, E.; Marie, E.; Schwab, R. *J Clin Sleep Med*. **2010**, *6*, 572–580.

(47) Baskett, J. J.; Broad, J. B.; Wood, P. C.; Duncan, J. R.; Pledger, M. J.; English, J.; Arendt, J. *Age Ageing*. **2003**, *32*, 164–170.

(48) Arendt, J.; Skene, D. J. *Sleep Medicine Reviews*. **2005**, *9*, 25–39.

(49) Wade, A. G.; Ford, I.; Crawford, G.; McConnachie, A.; Nir, T.; Laudon, M.; Zisapel, N. *BMC Med*. **2010**, *8*, 51.

(50) Oates, M. D.; Cooper, B. R.; Jorgenson, J. W. *Anal Chem*. **1990**, *62*, 1573–1577.

(51) Kennedy, R. T.; Oates, M. D.; Cooper, B. R.; Nickerson, B.; Jorgenson, J. W. *Science*. **1989**, *246*, 57–63.

(52) Ge, S.; Koseoglu, S.; Haynes, C. L. *Anal Bioanal Chem*. **2010**, *397*, 3281–3304.

(53) Arcibal, I. G.; Santillo, M. F.; Ewing, A. G. *Anal Bioanal Chem*. **2007**, *387*, 51–57.

(54) Chen, Y.; Xiong, G.; Arriaga, E. A. *Electrophoresis*. **2007**, *28*, 2406–2415.

(55) Huang, W.; Ai, F.; Wang, Z.; Cheng, J. *Journal of Chromatography B*. **2008**, *866*, 104–122.

(56) Olson, K. J.; Ahmadzadeh, H.; Arriaga, E. A. *Anal Bioanal Chem*. **2005**, *382*, 906–917.

(57) Ashkin, A. *Phys Rev Lett*. **1970**, *24*, 156–159.

(58) Ashkin, A.; Dziedzic, J. M. *App. Phys. Lett.* **1971**, *19*, 283–285.

(59) Ashkin, A.; Dziedzic, J. M. *App. Phys. Lett.* **1974**, *24*, 586–588.

(60) Ashkin, A. *Phys Rev Lett*. **1978**, *40*, 729–732.

(61) Ashkin, A.; Dziedzic, J. M.; Yamane, T. *Nature*. **1987**, *330*, 769–771.

(62) Ashkin, A.; Dziedzic, J. M. *Science*. **1987**, *235*, 1517–1520.

(63) Dharmadhikari, J.; D'Souza, J.; Gudipati, M.; Dharmadhikari, A.; Rao, B.; Mathur, D. *Sensor Actuat B-Chem*. **2006**, *115*, 439–443.

(64) Doornbos, R.; Schaeffer, M.; Hoekstra, A.; Sloot, P.; de Grooth, B. G.; Greve, J. *App. Optics*. **1996**, *35*, 729–734.

(65) Steubing, R.; Cheng, S.; Wright, W.; Numajiri, Y.; Berns, M. In *Laser-Tissue Interaction, SPIE*; 1990; pp. 272–280.

(66) Hawes, C.; Osterrieder, A.; Sparkes, I. A.; Ketelaar, T. *Current Opinion in Plant Biology*. **2010**, *13*, 731–735.

(67) Hansen, P. M.; Oddershede, L. B. *Proc. SPIE (Optical Trapping and Optical Micromanipulation II)*. **2005**, *5930*, 593003–1 – 593003–9.

(68) Gross, S. *Method Enzymol*. **2003**, *361*, 162–174.

(69) Sacconi, L.; Tolic-Norrelykke, I.; Antolini, R.; Pavone, F. In *Imaging, Manipulation, and Analysis of Biomolecules and Cells: Fundamentals and Applications III*; 2005; pp. 313–324.

(70) Sacconi, L.; Tolic-Norrelykke, I.; Stringari, C.; Antolini, R.; Pavone, F. *App. Optics*. **2005**, *44*, 2001–2007.

(71) Comstock, M. J.; Ha, T.; Chemla, Y. R. *Nat Methods*. **2011**, *8*, 335–340.

(72) Mónico, C.; Belcastro, G.; Capitanio, M.; Vanzi, F. *2011 International Workshop on Biophotonics, BIOPHOTONICS 2011*.

(73) Rezaei, N.; Downing, B. P. B.; Wieczorek, A.; Chan, C. K. Y.; Welch, R. L.; Forde, N. R. In *Proc. SPIE (Photonics North 2011)*; SPIE, 2011; pp. 80070K1–80070K–10.

(74) Hoffmann, P.; Dutoit, B.; Salathe, R. P. *Ultramicroscopy*. **1995**, *61*, 165–170.

(75) Lapainis, T.; Scanlan, C.; Rubahkin, S. S.; Sweedler, J. V. *Anal Bioanal Chem*. **2007**, *387*, 97–105.

(76) Pine, J.; Chow, G. *Ieee T Bio-Med Eng*. **2009**, *56*, 1184–1188.

(77) Dow Chemical Company *http://www.dow.com/safechem/optim/optim-advantage/physical-properties/refractive.htm*. **1999**.

(78) Aly, K.; Esmail, E. *Optical Materials*. **1993**, *2*, 195–199.

(79) Querry, M.; Holland, W.; Waring, R.; Earls, L.; Querry, M. *Journal of Geophysical Research*. **1977**, *82*.

(80) Jin, W.; Wang, Y.; Ren, N.; Bu, M.; Shang, X.; Xu, Y.; Chen, Y. *Optics and Lasers in Engineering*. **2011**, 1–5.

(81) Takagi, M.; Kitabayashi, T.; Ito, S.; Fujiwara, M.; Tokuda, A. *J Biomed Opt*. **2007**, *12*, 054010–.

(82) Dow Chemical Company *http://www.dow.com/safechem/optim/optim-advantage/physical-properties/viscosity.htm*. **1999**.

(83) Korson, L.; Drost-Hansen, W.; Millero, F. *The Journal of Physical Chemistry*. **1969**, *37*, 34–39.

(84) Zhang, H.; Han, S. *J Chem Eng Data*. **1996**, *41*, 516–520.

(85) Zucker, R. *J Physiology-Paris*. **1993**, *87*, 25–36.

(86) Xu, J.; He, L.; Wu, L.-G. *Current Opinion in Neurobiology*. **2007**, *17*, 352–359.

(87) Gilmanov, I. R.; Samigullin, D. V.; Vyskočil, F.; Nikolsky, E. E.; Bukharaeva, E. A. *J Comput Neurosci*. **2008**, *25*, 296–307.

(88) Kanthasamy, A. G.; Maduh, E. U.; Peoples, R. W.; Borowitz, J. L.; Isom, G. E. *Toxicol. Appl. Pharmacol.* **1991**, *110*, 275–282.

(89) Theoharides, T. C.; Betchaku, T.; Douglas, W. W. *Eur J Pharmacol*. **1981**, *69*, 127–137.

(90) Meissner, G.; Rios, E.; Tripathy, A.; Pasek, D. *J Biol Chem*. **1997**, *272*, 1628–1638.

(91) Shankar, V.; Bax, C.; Bax, B.; Alam, A.; Moonga, B.; Simon, B.; Pazianas, M.; Huang, C.; Zaidi, M. *J Cell Physiol*. **1993**, *155*, 120–129.

(92) Sánchez-Olea, R.; Pasantes-Morales, H.; Schousboe, A. *Neurochem Res*. **1993**, *18*, 147–152.

(93) Krieger-Brauer, H. I.; Gratzl, M. *J Neurochem*. **1983**, *41*, 1269–1276.

(94) Meissl, H.; Yáñez, J.; Ekström, P.; Grossmann, E. *J Pineal Res*. **1994**, *17*, 69–78.

(95) Kume-Kick, J.; Rice, M. E. *J. Neurosci. Methods*. **1998**, *84*, 55–62.

(96) Dizhoor, A. M.; Olshevskaya, E. V.; Peshenko, I. V.

(97) Cartoni, G.; Coccioli, F.; Jasionowska, R.; Masci, M. *Chromatographia*. **2000**, *52*, 603–606.

(98) Chan, K.; Muschik, G.; Issaq, H. *J. Chrom. A*. **1995**, *718*, 203–210.

(99) Chen, G.; Cheng, J.; Ye, J. *Fresen J Anal Chem*. **2001**, *370*, 930–934.

(100) Hevia, D.; Botas, C.; Sainz, R. M.; Quiros, I.; Blanco, D.; Tan, D. X.; Gomez-Cordoves, C.; Mayo, J. C. *J. Chrom. A*. **2010**, *1217*, 1368–1374.

(101) Musijowski, J.; Pobozy, E.; Trojanowicz, M. *J. Chrom. A*. **2006**, *1104*, 337–345.

(102) Pucci, V.; Ferranti, A.; Mandrioli, R.; Raggi, M. *Anal Chim Acta*. **2003**, *488*, 97–105.

(103) Wu, X.; Wu, W.; Zhang, L.; Xie, Z.; Qiu, B.; Chen, G. *Electrophoresis*. **2006**, *27*, 4230–4239.

(104) Squires, L. N.; Jakubowski, J.; Stuart, J. N.; Rubahkin, S. S.; Hatcher, N. G.; Kim, W.-S.; Chen, K.; Shih, J.; Seif, I.; Sweedler, J. V. *J Biol Chem*. **2006**, *281*, 13463–13470.

(105) Ganguly, S.; Coon, S.; Klein, D. *Cell and Tissue Research*. **2002**, *309*, 127–137.

(106) Klein, D. C.; Weller, J. L. *Science*. **1970**, *169*, 1093–1095.

(107) Ferreira-Medeiros, M.; Mandarim-de-Lacerda, C. A.; Correa-Gillieron, E. M. *Anatom Histol Embryol*. **2007**, *36*, 284–289.

(108) Zhang, X.; Fuller, R. R.; Dahlgren, R. L.; Potgieter, K.; Gillette, R.; Sweedler, J. V. *Fresen J Anal Chem*. **2001**, *369*, 206–211.

(109) Wilson, B.; Lynch, H.; Ozaki, Y. *Life Sci*. **1978**, *23*, 1019–1024.

(110) Zawilska, J. *General and Comparative Endocrinology*. **2003**, *134*, 296–302.

(111) Millán-Plano, S.; Piedrafita, E.; Miana-Mena, F. J.; Fuentes-Broto, L.; Martínez-Ballarín, E.; López-Pingarrón, L.; Sáenz, M. A.; García, J. J. *Int J Mol Sci*. **2010**, *11*, 312–328.

(112) Ceinos, R. M.; Rábade, S.; Soengas, J. L.; Míguez, J. M. *General and Comparative Endocrinology*. **2005**, *144*, 67–77.

(113) Ng, T.; Liu, F. *J Neural Transm*. **2000**, *107*, 1243–1251.

(114) Wang, H. X.; Liu, F.; Ng, T. B. *Comp. Biochem. Physiol. C Toxicol. Pharmacol.* **2001**, *130*, 379–388.

(115) Pevet, P.; Roels, B. V.; Masson-Pevet, M.; Steinlechner, S.; Skene, D.; Canguilhem, B.

J Pineal Res. **1989**, *6*, 233–242.

(116) Petterborg, L. J.; Reiter, R. J. *J Neural Transm*. **1982**, *55*, 149–155.

(117) van Benthem, J.; Steinen, A. C.; Sommer, M. C.; De Koning, J.; Ebels, I.; Balemans, M. G. *J Neural Transm*. **1989**, *78*, 145–158.

(118) Glass, J. *Domestic Animal Endocrinology*. **1984**, *1*, 105–119.

(119) Ocal-Irez, T.; Durmus, G.; Sekerkiran, Y.; Peker, C.; Uygur, G. *Brain Res*. **1989**, *493*, 1–7.

Appendix

Abbreviations

5-HT = serotonin

5-HT sulfate = serotonin-O-sulfate

aCSF = artificial cerebral spinal fluid

BGE = background electrolyte

CE = capillary electrophoresis

CE-LIF = capillary electrophoresis-laser-induced fluorescence

CE-LINF = capillary electrophoresis-laser-induced native fluorescence

HD = hydrodynamic

dyn pH = dynamic pH junction

EK = electrokinetic

EOF = electroosmotic flow

FASI = field-amplified sample injection

FASS = field-amplified sample stacking

HF = hydrofluoric acid

HIAA = 5-hydroxyindole-3-acetic acid

HITCA = 5-hydroxyindole thiazoladine carboxylic acid

HTOL = 5-hydroxtryptophol

HTP = 5-hydroxytryptophan

LIF = laser-induced fluorescence

LINF = capillary electrophoresis-laser-induced native fluorescence

LOD = limit of detection

MC-CE-LINF = multichannel capillary electrophoresis-laser-induced native fluorescence

MEKC = micellar electrokinetic chromatography

MIAA = 5-methoxyindole-3-acetic acid

MOT = 5-methoxytryptamine

MRN = median raphe nucleus

MTOL = 5-methoxytryptophol

MTrp = 5-methoxytryptophan

NAS = N-acetylserotonin

OT-MC-CE-LINF = optical trap-multichannel capillary electrophoresis-laser-induced native fluorescence

pH-med = pH-mediated sample stacking

SCN = suprachiasmatic nucleus

SDS = sodium dodecyl sulfate

SR-101 = sulforhodamine-101

TOL = tryptophol

Trp = tryptophan

Tyr = tyrosine